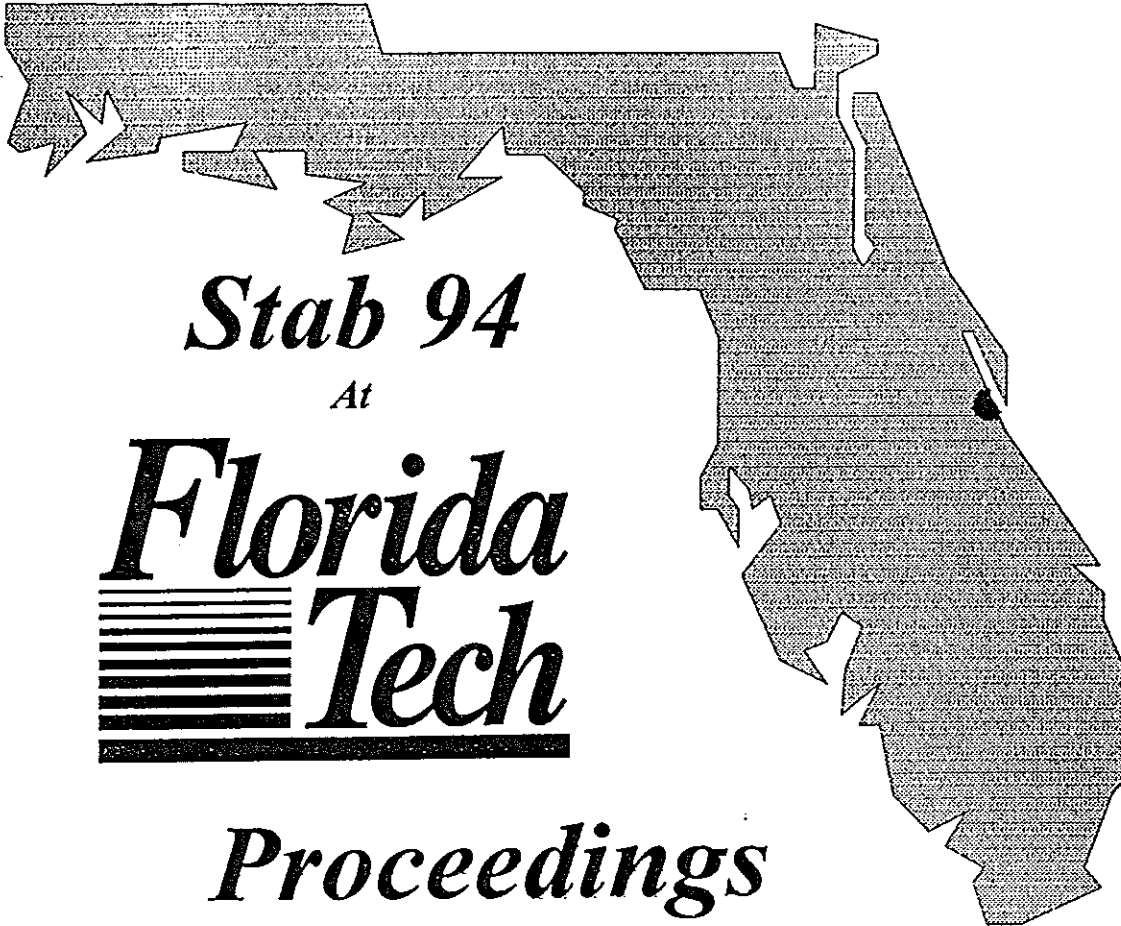


FIFTH INTERNATIONAL CONFERENCE ON STABILITY
OF
SHIPS AND OCEAN VEHICLES

NOVEMBER 7-11, 1994



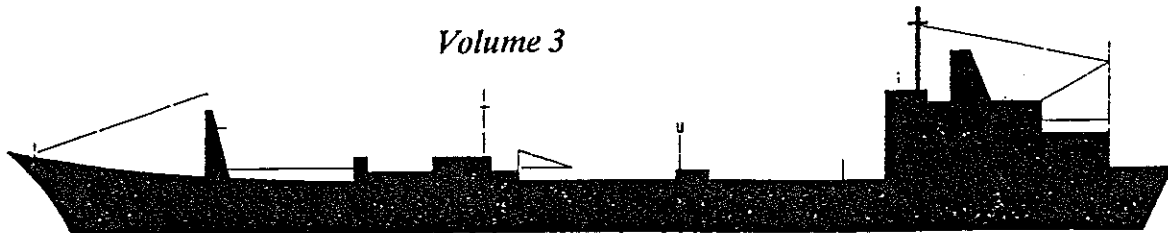
Stab 94

At

**Florida
Tech**

Proceedings

Volume 3



150 W. UNIVERSITY BLVD.
MELBOURNE, FL 32901-6988

FLORIDA INSTITUTE OF TECHNOLOGY

LYNN E. WEAVER, Ph.D. - PRESIDENT

**COLLEGE OF ENGINEERING
ROBERT L. SULLIVAN, Ph.D. - DEAN**

**DIVISION OF MARINE AND ENVIRONMENTAL SYSTEMS
GEORGE A. MAUL, Ph.D. - DIRECTOR**

**OCEAN ENGINEERING PROGRAM
ANDREW ZBOROWSKI, Ph.D. - CHAIRMAN**

WILLIAM R. DALLY, Ph.D.

GRAEME RAE, Ph.D.

GEOFFREY W. J. SWAIN, Ph.D.

LEE HARRIS - ASSOCIATE PROFESSOR

W. A. CLEARY, JR. - ADJUNCT PROFESSOR

PURPOSE OF STAB 94

STAB 94 had been offered to promote a full exchange of ideas and methodologies regarding STABILITY OF SHIPS AND OCEAN VEHICLES and to provide an opportunity to professional naval architects, capsizing prevention researcher, regulatory agencies, inspection and certifying authorities, ship owners, consultants and ship operators to present, discuss and listen to improvements in capsizing prevention for all types and sizes of ships.

SPONSORS

The Society of Naval Architects and Marine Engineers
The Royal Institution of Naval Architects

STAB 94**TABLE OF CONTENTS****VOLUME NO. 1**

Monday 7 November
Papers Sessions - 1, 2, 3, 4

VOLUME NO. 2

Tuesday 8 November
Papers Sessions - 5, 6, 7, 8

VOLUME NO. 3

Wednesday 9 November
Papers Sessions - 9, 10, 11, 12

VOLUME NO. 4

Thursday 10 November
Papers Sessions - 13, 14, 15, 16

VOLUME NO. 5

Friday 11 November
Papers Sessions - 17, 18, 19

**SUPPLEMENT TO
NO. 5**

Executive Summaries of workshops
1 through 7 by workshop moderator
(To be mailed to all registrants after
conference completion.)

WEDNESDAY 9 NOVEMBER

GLEASON AUDITORIUM

PAPERS SESSION 9

Moderator: Prof. M. PAWLOWSKI
Ship Research Institute
Gdansk, Poland

0900-0925

Comparative Model Tests on Capsizing of Ships
in Quartering Seas

Authors: M. Kan T. Saruta H. Taguchi

0930-0955

Some Observations on Experimental Techniques
for Modelling Ship Stability in Wind and Waves

Authors: J. Shaughnessy B. Nehrling
R. Compton

1000-1025

Damage Scenario Analysis: A Tool for Damage
Survivability of Passenger Ships

Authors: O. Turan, D. Vassalos

A. M. BREAK

PAPERS SESSION 10

Moderator: Dr. M. KAN
Ship Research Institute, - Tokyo

1035-1100

Stability Criteria Development on a First
Principles Methodology

Author: W. Buckley

1105-1130

Methodology of the Development of Stability on the
Basis of Risk Evaluation

Author: L. Kobylinski

1135-1200

Operational Stability and On Board Computer

Authors: V. Ljps S. Palekhov V. Peresypln

LUNCH - DELEGATES LOUNGE

PAPERS SESSION 11

Moderator: Prof. P. CASSELLA
University Federico II, Naples

1330-1355

Broaching of a Fishing Vessel in Following and
Quartering Seas: Nonlinear Dynamical System Approach

Authors: N. Umeda M. Renilson

1400-1425

Parametric Stability of Fishing Vessels

Authors: M. Neves L. Valerio

1430-1455

The Capsizing of the Fishing Vessel - "STRAITS PRIDE II"

Authors: D. Bass C. Weng

P. M. BREAK

PAPERS SESSION 12

Moderator: Prof. M. NEVES
Universidade Federal-Rio de Janeiro

1515-1540

Safety for Fishing Vessels in the Hauling Course

Authors: Tie Cheng Feng Y. Tao

1545-1610

Nonlinear Dynamics and Capsizing of Small Fishing Vessels

Authors: C. Jlang A. Troesch S. Shaw

1615-1640

On the Practical Evaluation of Shallow Water Effect

In Large Inclinations for Small Fishing Boats

Authors: K. Amagal N. Kinura K. Ueno

CENTRAL BAPTIST AUDITORIUM

SAFETY CASE WORKSHOP

Moderator: Prof. Chengl KUO
University of Strathclyde

"MANAGING STABILITY USING THE SAFETY CASE CONCEPT"

0900-0930 Introduction to the Safety case
Concept

0930-1000 General Debate on the
Concept's Applicability to Stability

1000-1100 Exercise by Participants
(in groups of 3 or 4)

NO BREAK - Refreshments available
during exercise

SAFETY CASE WORKSHOP

(continued)

1000-1100 Exercise - continued

1100-1145 Group Presentations

1145-1215 Discussions & Conclusions

LUNCH - DELEGATES LOUNGE

WORKSHOP / PANEL

Moderator: Prof. N. H. RAKHMANIN
Krylov Shipbuilding Research
Institute

INFORMATION TO THE MASTER

P. M. BREAK

INFORMATION TO THE MASTER

(continued)

and

(concluded)

Comparative Model Tests on Capsizing of Ships in Quartering Seas

M.Kan, T.Saruta and H.Taguchi
Ship Research Institute, Ministry of Transport
6-38-1, Shinkawa, Mitaka, Tokyo 181, Japan

Abstract

Comparative model tests on capsizing of container ships were performed in quartering waves by using two different hull forms. One had a large stability variation in waves and another had a small one. The model tests were carried out for both irregular and regular waves in the 80m square basin of the Ship Research Institute. The encounter angle was varied precisely every 10 degrees by using the autopilot steering device in order to specify the dangerous range. Among the total 1643 runs, 490 capsizings were observed. From these results the following three characteristic features were confirmed to be common for the two different hull forms. Firstly, the most dangerous encounter angle is 20~40 or 50deg, and the dangerous range extends to 0~60deg as the ship speed increases. Secondly, as the ship speed decreases, the capsizing also decreases, and there exists a critical ship speed below which the capsizing never occurs. Thirdly, the direction of capsizing is always to the leeward. Although these results are almost the same as the authors' previous model tests, the model used in that previous tests proved to have an extraordinary tendency of inward heel in turning motion. Therefore it has been considered necessary to reconfirm the above features by supplementary tests for more general hull forms. A previously proposed hypothetical explanation on the mechanism of capsizing in quartering waves can also explain the present results. The capsizing due to the parametric rolling, which has been considered to be one of the typical modes of dynamical capsizing, were not observed for both hull forms. Instead, a new mode of dynamical capsizing accompanied with the period bifurcation phenomenon, which is regarded as a precursor of the chaos, was also reconfirmed.

1. Introduction

The danger of capsizing of a ship running in quartering seas has been internationally recognized through the experimental studies, for instance, the pioneering experiments in San Francisco Bay by Paulling and his colleagues [1], and also other laborious experiments by Yamakoshi et al. [2], Grochowalski [3], and authors [4]. The safety measures to avoid the capsizing in quartering seas, such as a revision

of stability regulations [5] or an establishment of operational guidance [6] have been discussed in IMO. However it doesn't seem that the mechanism of capsizing in quartering seas has been clarified completely.

At the last Stability Conference (STAB'90), the authors reported the results of the model tests on capsizing of a container ship running in quartering waves, and clarified the following characteristic features [4]. That is, the most dangerous encounter angle was 20~40deg, and extended to 0~50deg in high speed running. Capsizing never occurred at lower speed, and the direction of capsizing was always to the leeside. A hypothetical explanation for such capsizing was also proposed. However the hull form of the container ship model (model G) of that experiment was designed to have the minimum stability variations in waves, and had the V-shaped cross sections even at the midship. This kind of hull form proved to have an extraordinary tendency of inward heel during the steady turning motion, while an ordinary ship usually has the outward heel. Since it is not appropriate to draw the general conclusion from the experiment for only such an extreme hull form, it has been considered necessary to perform the similar capsizing experiment for more general hull forms. Therefore the capsizing tests for another container ship model (model F) was planned on almost the same scale as for the model G. The present hull form (model F) was designed to have the maximum stability variations in waves, and had the U-shaped cross sections at and near the midship and the usual outward heel during the turning motion, and therefore could be regarded as an ordinary hull form.

From the present supplementary experiment for the model F, it seems that the characteristic features on capsizing in quartering waves described in the previous paper [4] can be generalized as common features to any hull forms.

In the previous experiment, a new type of capsizing accompanied with the period bifurcation phenomenon, which is regarded as a precursor of the chaos, was often observed, while the capsizing due to the parametric rolling was not observed [4]. These were also reconfirmed again with the present experiment.

Although in this paper the results for the model F should be mainly described, the previous results for the model G are reproduced and referred for the purpose of convenient comparison.

2. Description of models and experimental method

2.1 Models and heel in turning

The model used in the present supplementary experiment was

designed to have the large stability variations between the wave crest and the wave trough amidship and named "model F", while the model used in the previous experiment was designed to have the small stability variations and named "model G". Both models were imaginary container ships designed by HSVA (Hamburgische Schiffbau-Versuchsanstalt) [9]. Fig.1 shows the body plans, shapes of bow and stern, and principal particulars of both models. The model F has an ordinary U-shaped cross section with the vertical side at the midship, while the model G has a V-shaped cross section with the inclined side upto the upper deck even at the midship. Fig.2 shows the stability curves of both models for tested 4 cases of GM, at the wave crest amidship for the wave length to ship length ratio $\lambda/L=1.0$, the wave height to wave length ratio $h/\lambda=1/15$, and the encounter angle $\chi=0$, as well as in the still water.

The GM values for both models were selected by trial runs so that the capsizing occurred in the given irregular sea state, which was equivalent to the experiments in HSVA [9]. Therefore the GM values for both models had not any exact corresponding meaning. The C value of the Japanese stability criterion, which means the ratio of the residual dynamic stability to the work by beam sea and wind and is almost equivalent to the IMO weather criterion A.562, was calculated as $C=1.9$ for $GM=3.87\text{cm}$ of the model F, and $C=2.2$ for the $GM=1.98\text{cm}$ of the model G, by taking the vanishing angle as the flooding angle. This is an example to show that even if the ships have similar stability qualities, the GM values are sometimes largely different according to the hull form.

Although the models had the watertight hatches on the upper deck and the watertight superstructure aft on the upper deck to install the steering gear, these hatches and superstructure were not taken into consideration in stability calculations in Fig.2. The models had also the watertight box high above the upper deck to house a directional gyro as a sensor for the autopilot device. This box was mounted on so high position that it did not prevent capsizing. However, after the model capsized, this box acted very successfully as an automatic restoring device by the successive wave attack, especially for the model G (see Photo 1).

The natural roll period $T\phi$ was obtained by the free roll test as $T\phi=2.6\text{sec}$ for $GM=3.87\text{cm}$ of the model F, and $T\phi=3.4\text{sec}$ for $GM=1.98\text{cm}$ of the model G.

Fig.3 shows the experimental results of the heel in turning motion as well as the steady turning ability (L/R , where R is the radius of steady turning circle) together with the drift angle β . Although the

both models F and G have the same tendency of the initial inward heel just after the steering action and the model F has the outward heel in the following turning motion, which is typical for an ordinary ship, the model G has the peculiar tendency of the inward heel at a large rudder angle. As a matter fact, the model G for the minimum GM ($GM=1.98\text{cm}$) did not capsize even at full speed ($Fn=0.34$) with large rudder angle ($\delta=\pm 35\text{deg}$), while the model F for the minimum GM ($GM=3.87\text{cm}$) capsized at the same running condition ($Fn=0.34$ and $\delta=\pm 35\text{deg}$). This is the reason why the results of the model F are shown for lower speed ($Fn=0.30$) in Fig.3. Since the similar tendencies for both models were also obtained for larger GM values, the extraordinary inward heel in steady turning of the model G was confirmed to be independent on the GM value.

2.2 Experimental method

The capsizing model tests for the model F were carried out by the same method as the previous tests for the model G by using the radio controlled free running model in the 80m square basin of the Ship Research Institute. The encounter angle to wave (χ) was varied precisely every 10 degrees from $\chi=0$ (pure following wave) to $\chi=90\text{deg}$ (pure beam wave) by using an autopilot steering device, and the number of propeller revolution was varied every 1rps by the motor controller, so that the critical running condition for capsizing was obtained. The gain of the autopilot device was set as $a=1.25$ and $b=0$, which means the rudder responds by 1.25deg against to the deviation of heading angle of 1deg, but doesn't respond to the yaw rate. However for the model F, which had a usual outward heel in turning, some supplementary runs with $a=2.5$ (double rudder response angle) were added, because the effect of steering on capsizing could be expected.

The items of measurement were roll angle, pitch angle, yaw angle, yaw rate, rudder angle, number of propeller revolution, and trajectory of model (model speed and course angle).

In case of the tests in irregular waves, runs were repeated 10 to 20 times at most under the same condition to obtain the capsizing rate. However, the timing to encounter the wave train was not random, but was handled to meet the almost same wave group, which was the recent practice in HSVA [7]~[9]. Therefore the obtained capsizing rate does not mean the probability of capsizing, but only means a certain index of danger of capsizing. The Pierson-Moskowitz type wave spectrum used in the tests for both models is shown in Fig.4. This wave corresponds to very rough sea with the significant wave height of 10m and the peak period of 13.6sec in full scale. In order to obtain the

critical value of GM for this wave, the height of center of gravity was also varied. The number of propeller revolution was varied 1rps at most depending on the encounter angle to keep approximately the average speed referred in the related figures.

In case of the experiments in regular waves, runs were limited to once for the same condition in principle. However, sometimes runs were repeated twice or three times in the marginal cases to the critical condition of capsizing. The value of GM for both models was respectively fixed to one case through the experiment in regular waves, namely GM=3.87cm for the model F and GM=1.98cm for the model G. The wave length to ship length ratio λ/L was varied from 0.5 to 2.25 at an interval of 0.25, and the wave height to wave length ratio was selected from 1/20, 1/15, 1/12, 1/10. The number of propeller revolution was not varied depending on the encounter angle, but kept constant equal to the still water value.

3. Results of Experiments

3.1 Capsizing in irregular waves

Fig.5 shows the results of all experiments in irregular waves as the total capsizing rate versus the encounter angle. The occurrence of capsizing is confined to $\chi=10\sim60\text{deg}$ for the model F and $10\sim50\text{deg}$ for the model G. Although there is no exact corresponding relation between the tested GM condition of both models, the most dangerous range can be regarded as $\chi=20\sim40\text{deg}$. The number of runs for the beam wave ranges $\chi=80\sim90\text{deg}$ was limited to a small number, because the firm conviction was obtained intuitively from the observation that the capsizing would never occur no matter how many times runs were repeated.

Fig.6 shows the effect of the ship speed on the capsizing rate in case of the minimum GM value. It is shown that the range of dangerous encounter angle extends to $\chi=10\sim50$ or 60deg in higher ship speed, and that the capsizing decreases as the ship speed decreases until the capsizing vanishes at slower speed than some critical value, in this case $Fn \leq 0.26$. Although the corresponding GM values are largely different between both models, the tendencies of capsizing rate are very similar. In the same figure, the non-capsizing cases with large roll angle ($\phi_{\max} \geq 40\text{deg}$ for the model F, $\phi_{\max} \geq 50\text{deg}$ for the model G) are added.

Fig.7 shows the effect of the GM value on the capsizing. From this figure the critical ship condition for this wave can be estimated as GM=4.6cm (1.77m in full scale) for the model F, and GM=2.7cm (1.04m in full scale) for the model G.

The total number of capsizing in the irregular waves are 130 cases among 483 runs for the model F, and 126 cases among 418 runs for the model G. All these capsizings occurred to the leeward side only without exception. Although most runs were performed in the waves from the starboard side, some runs were supplemented in the waves from the port side ($\chi = -30^\circ$ for the model F, and $\chi = -20^\circ$ for the model G), but there was no meaningful difference between the results in the waves from the starboard side and the port side for both models.

3.2 Capsizing in regular waves

From the experiments in irregular waves for the model F, the characteristic features of capsizing in quartering waves, which were obtained by the the previous experiments for the model G [4], seems to be common for any type of ships. However, in order to examine this in more detail, the experiments in regular waves were also performed. The results are summarized in Table 1 for the model F, together with Table 2 for the model G. In these tables, \circ means the non-capsizing case, \times means the capsizing case, Δ means the non-capsizing case with the maximum roll angle over 40° , and \square (only for the model F) means the non-capsizing case with the maximum roll angle of $30 \sim 40^\circ$. The meaning of the abbreviation marks in these tables are as follows. L means the capsizing due to the pure loss of stability at the wave crest, P means the capsizing accompanied with the period bifurcation phenomenon, B means the capsizing due to the broaching-to, and BT means broaching-to tendency. P, B and BT are annotated for the non-capsizing cases where such phenomena were observed. The characteristics of each classified capsizing mode and their typical time histories and course trajectories of the model were described and exemplified in the previous paper [4].

Although the detailed comparison between the model F and G is not significant because there is not any exact corresponding relation between the conditions of both models, some tendencies can be drawn from these tables. For short waves such as $\lambda/L = 0.5$, any danger was not observed for the present model F, while some danger was observed at $\chi = 40^\circ$ for the previous model G. For $\lambda/L = 0.75$ the range of dangerous encounter angle of the model F seems to be somewhat larger than that of the model G, while the critical speed for capsizing of the model F seems to be higher than that of the model G. For longer waves than $\lambda/L = 1.0$, it is clear that the range of dangerous encounter angle of the model F is wider than that of the model G, and the capsizing at $\chi = 50 \sim 60^\circ$ was observed frequently for the model F, which was scarcely observed for the model G. This tendency is not so

significant, because the capsizing occurs easily as the center of gravity goes up higher and there is not any exact corresponding relation between the GM values of both models, but consistent with the difference of C values of the tested conditions (C=1.9 for the model F, and C=2.2 for the model G), and also with the difference of the stability decrease at the wave crest amidship (the stability decrease of the model F is larger than that of the model G, see Fig.2).

It has been said that the most dangerous wave length is $\lambda/L=1.0$. However it is obvious from these tables that many capsizings were observed in longer waves such as $\lambda/L=1.25\sim 1.75$ for both models as pointed out previously for the model G [4]. Therefore we should recognize that the most dangerous wave length is not restricted to $\lambda/L=1.0$, but extended to longer waves like $\lambda/L=1.0\sim 1.75$.

For much longer waves such as $\lambda/L=2.0\sim 2.25$, the capsizing seems to decrease for both models, and therefore it may be considered that the capsizing decreases for longer waves than $\lambda/L>2.0$. In case of the capsizing in irregular waves, much difference was not recognized between both models (see Fig.5). This may be explained by the fact that the irregular waves used in the experiment has peak period $T_p=2.16$ sec, which corresponds to $\lambda/L=2$ of the regular wave where much difference between the model F and G was not observed (see corresponding parts of Table 1 and Table 2).

For the experiments of the model F, some supplementary runs were added to examine the effect of steering on capsizing by doubling the gain of autopilot device ($a=2.5$, $b=0$). From the results, which are shown in the lower columns of Table 1 for $\lambda/L=1.75\sim 2.25$, it is obvious that the range of capsizing extends. This suggests that the steering will have a bad influence on the capsizing for the ordinary ship which has the outward heel in turning.

In the regular waves, total capsizings amount to 135 cases among 397 runs for the model F, and 99 cases among 345 runs for the model G. The distribution of the capsizing rate and the classification of the capsizing mode versus encounter angle are shown in Fig.8. Although the range of capsizing of the model F extends more widely than that of the model G as described above, the following common features are drawn from this figure for both models. Namely the most dangerous encounter angle is regarded as 30deg, the capsizing due to broaching-to is restricted to $\chi \leq 20$ deg, and the capsizing is not observed in beam waves. As for the capsizing mode, the capsizing due to the pure loss of stability is 77% for the model F and 64% for the model G, the capsizing accompanied with the period bifurcation phenomenon is 13% for the model F, and 26% for the model G, and the capsizing due to the

broaching-to is 10% for the both models.

The period doubling phenomenon in roll motion is such a phenomenon that the ship does not respond regularly to every one encounter wave, in spite of running in the regular wave, but repeats the large and small roll responses to every two encounter waves by turns, or to every n waves. Fig.9 exemplifies some time histories, with (a) and (b) for the period doubling bifurcation, and (c) for the period tripling bifurcation. However, this new mode of capsizing accompanied with the period bifurcation phenomenon should be supposed to be caused fundamentally by the pure loss of stability in waves, and to be observed when the conditions such as the wave condition, the running condition or the ship condition, are close to the critical condition of capsizing. This supposition has been confirmed by a series of numerical studies [11]~[12], as the fact that the occurrence of the capsizing through the chaos including a successive cascade of the period bifurcations is limited very small range of parameters, and that beyond the small range only a simple mode of capsizing is observed. In other words, The period bifurcation is not a cause of capsizing but a mode of rolling as a warning sign of capsizing. Therefore as for the cause of capsizing, it should be correct that the capsizing due to the pure loss of stability is 90% and the capsizing due to the broaching-to is 10%. Namely it can be said that most capsizings in quartering waves are caused by the pure loss of stability.

The capsizing due to the parametric rolling was not observed at all for both models. The possible reason for this will be described later in 4.2.

The direction of capsizing is almost to the leeside with only one exception among 135 capsizings for the model F and also one exception among 99 capsizings for the model G.

4. Discussions on experimental results

4.1 On mechanism of capsizing

Judging from above experiments in irregular and regular waves for two hull forms having extremely different characteristics on stability variations, the following three features seem to be common for any hull forms on capsizing in quartering waves.

(a) The dangerous encounter angle is $\chi=20\sim40$ or 50deg , and extends to $\chi=0\sim60\text{deg}$ at higher ship speed.

(b) The danger of capsizing increases as the ship speed increases, while it decreases as the ship speed decreases until it vanishes at slower speed than some critical one.

(c) The capsizing occurs to the leeside.

As for the existence of the dangerous encounter angle $\chi=20\sim40$, or 50deg, the following qualitative explanation described in the previous paper [4] seems to be still valid. That is to say, in the range of dangerous encounter angle, the maximum value of the capsizing moment by waves (or amplitude of roll exciting moment) M_r is greater than the maximum value of the reduced restoring moment at the wave crest $W \cdot GZ_{\max(\text{crest})}$ as shown in Fig.10. This figure is calculated for the same wave condition and for the tested ship condition, and shows that the dangerous zone of the model F is wider and thicker than that of the model G. This is consistent with the experimental results described in 3.2. Although this explanation is not accurate, because the maximum capsizing moment is calculated at the point of maximum wave slope amidship, while the restoring moment is calculated at the wave crest amidship, it seems to give an intuitively understandable explanation. In order to give a complete explanation, more accurate numerical simulations such as attempted by de Kat [13], and Hamamoto [14], should be pursued.

As regards the danger at high speed running and the capsizing to the leeside, the previous explanations [4] are also considered valid. Namely, when the ship speed approaches the wave speed, an asymmetric large surging motion with the longer encounter period develops and the dangerous condition of staying at the upper down slope near the wave crest, where the capsizing moment overcomes the reduced restoring moment, continues for longer duration. If this duration is long enough to cause the capsizing, the ship will capsize to the leeside, because the capsizing moment acts to the direction of leeside down as proved in [4].

4.2 On parametric rolling

Although the capsizing due to the parametric rolling has been regarded as one of the main causes or modes of capsizing, such a capsizing mode was not observed at all in our experiments for both models. The parametric rolling here is defined as the rolling motion which occurs in the Mathieu's first unstable region where the encounter frequency nondimensionalized by the natural rolling frequency Ω is approximately 2, and performs one cycle of roll motion for every two encounter waves. Figure 11 shows the distribution of capsizings as well as the total runs against Ω . As suggested by this figure, the possible reason why the parametric rolling was not observed may be a very small number of experimental runs in the Mathieu's first unstable region $\Omega=1.6\sim2.0$. However, although some

additional runs for the model F, which had large stability variation, were tested by selecting $\Omega=1.6\sim 2.0$, which was realized only in combination of short wave, low speed and near beam wave, such parametric rolling was not observed too. These additional runs are not listed in Table 1.

4.3 Comparison with German results on critical GM

The same hulls with larger 5m length were tested at HSVA by Blume [9] to determine the critical GM values between safe and unsafe for the same irregular wave concerning the form factor which modifies the IMO stability criterion A.168 [9]. The Blume's method to determine the critical GM utilizes the residual dynamic stability E_r over the maximum rolling angle during a noncapsizing run, and repeats 10~20 runs with the same condition to get the mean value \bar{E}_r and the standard variation σ of the residual dynamic stability E_r . By repeating the similar experiments for several GM values, the critical GM is obtained by interpolation as a value corresponding to $\bar{E}_r - 3\sigma = 0$. The critical value by the present experiments was obtained by more direct capsized runs and was estimated from Fig.7 as described in 3.1. Fig.12 shows the comparison of the critical GM obtained by such different methods of HSVA and SRI for the scale of 3.5m model. The agreement for the model F is fairly good after some possible correction to the HSVA's results, and very good for the model G without any correction. It can be said that the Blume's method to determine the critical GM is largely timesaving and effective, and also that the selection of $\chi=30\text{deg}$ as a basis of the proposed criterion is appropriate, because $\chi=30\text{deg}$ has been confirmed to be most dangerous and should be adopted as a representative case for the criterion.

5. Concluding Remarks

The capsizing experiments were performed in both irregular and regular quartering waves using the free running models of extremely different two container ships. Among the total 1643 runs, 490 capsizings were observed. From these results the following three characteristic features can be considered to be common for any hull forms.

(a) The dangerous encounter angle is $\chi=20\sim 40$ or 50deg , and extends to $\chi=0\sim 60\text{deg}$ in higher ship speed.

(b) The danger of capsizing increases as the ship speed increases, while it decreases as the ship speed decreases until it vanishes at slower speed than some critical one.

(c) The capsizing occurs to the leeward side.

Most of the observed capsizings were caused by the pure loss of stability at wave crest (90%), and the remainders were caused by the broaching-to (10%). The capsizing due to the parametric rolling was not observed, probably because only a few runs were tested in the Mathieu's first unstable region.

Although a new mode of capsizing accompanied with the period bifurcation phenomenon was reconfirmed to exist, it should be noted that such phenomenon appears as a mode of rolling and that the cause of such capsizing is fundamentally the pure loss of stability at wave crest.

Principal mechanism of capsizing in quartering waves has been proposed that the capsizing moment by waves approaches or overcomes the reduced restoring moment in waves at the range of encounter angle $\chi=20\sim40$ or 50deg, and that the capsizing occurs if this dangerous situation continues for a long time enough to cause the capsizing. The inevitable leeside capsizing is explained by the fact that the capsizing moment acts to the leeside at the downslope of wave, where the ship stays for a longer duration when running with high speed comparable to the wave speed. Although these explanations were already proposed in the previous paper [4], they were reconfirmed by the present experiments.

6. Acknowledgement

The authors would like to express their sincere appreciation to Prof.O.Krappinger and Dr.H.Payer, the former directors of HSVA, Dr.P.Blume, the head of seakeeping division of HSVA, Dr.K.Sugai, the former director of SRI, and Dr.Y.Takaishi, the former deputy director of SRI, for their guidance and encouragement on the cooperative model tests between Germany and Japan, and also Prof.S.Motora and Prof.M.Fujino of University of Tokyo, Prof M.Hamamoto of Osaka University, and other members of Regulation Research Panel 24 of the Shipbuilding Research Association of Japan for their valuable discussions and encouragement.

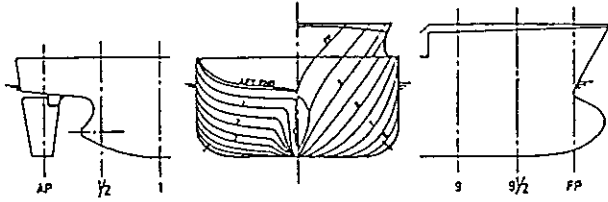
References

- [1] Paulling, J.R., Oakley, O.H. and Wood, P.D. ; Ship capsizing in heavy seas, Proceedings of the International Conference on Stability of Ships and Ocean Vehicles, Glasgow, 1975.3.
- [2] Yamakoshi, Y., Takaishi, Y., Kan, M., Yoshino, T. and Tsuchiya, T. ; Model experiments on capsizing of fishing boats in waves, Proceedings of the Second International Conference on Stability of Ships and Ocean Vehicles (STABILITY'82), Tokyo, 1982.10, pp.199-214.

- [3] Grochowalski, S. ; Investigation into the physics of ship capsizing by combined captive and free-running model tests, SNAME Transactions, Vol.97, 1989, pp.169-212.
- [4] Kan, M., Saruta, T., Taguchi, H., Yasuno, M. and Takaishi, Y. ; Model tests on capsizing of a ship in quartering waves, Proceedings of the Fourth International Conference on Stability of Ships and Ocean Vehicles (STAB'90), Naples, Vol.1, 1990.9, pp.109-116.
- [5] Germany ; Improved stability criteria, IMO, SLF 35/3/2, and SLF 35/3/3, 1990.11
- [6] Japan ; Guidance to the master for avoiding dangerous situations in following and quartering seas, IMO, SLF 38/3/5, 1993.12, and SLF 38/INF.10, 1994.1
- [7] Blume, P. and Hattendorff, H.G. ; An investigation on intact stability of fast cargo liners, Proceedings of the Second International Conference on Stability of Ships and Ocean Vehicles (STABILITY'82), Tokyo, 1982.10, pp.171-183.
- [8] Blume, P. ; The safety against capsizing in relation to seaway properties in model tests, Proceedings of the Third International Conference on Stability of Ships and Ocean Vehicles (STAB'86), Gdansk, Vol.1, 1986.9, pp.83-91.
- [9] Blume, P. ; On the influence of the variation of righting levers in waves on stability requirements, Proceedings of the Fourth International Conference on Stability of Ships and Ocean Vehicles (STAB'90), Naples, Vol.2, 1990.9, pp.452-459.
- [10] Hamamoto, M. ; Transverse stability of ships in quartering sea, Proceedings of the Third International Conference on Stability of Ships and Ocean Vehicles (STAB'86), Gdansk, Vol.1, 1986.9, pp.7-13.
- [11] Kan, M. and Taguchi, H. ; Chaos and fractal in capsizing of a ship, International Symposium on Hydro- and Aerodynamics in Marine Engineering (HADMAR'91), Varna, Bulgaria, Vol.1, 1991.10, pp.8.1-8.8.
- [12] Kan, M. ; Chaotic capsizing ; Proceedings of ITTC.SKC-KFR Osaka Meeting, 1992.9, pp.155-180.
- [13] de Kat, J.O. and Paulling, J.R. ; The simulation of ship motions and capsizing in severe seas, SNAME Transactions, Vol.97, 1989, pp.139-168.
- [14] Hamamoto, M., Fujino, M. and Kim, Y.S. ; Dynamic stability of a ship in quartering seas, to be submitted to Fifth International Conference on Stability of Ships and Ocean Vehicles (STAB'94), Melbourne, Florida, 1994.11

MODEL F

Item	Ship	Model
Length $L_{pp}(m)$	135.0	3.50
Breadth $B(m)$	23.0	0.596
Depth $D(m)$	11.5	0.298
Draught $d(m)$	8.37	0.217
Block Coeffl. C_b	0.589	0.589
Disp. Vol. $\nabla(m^3)$	15307	0.267



MODEL G

Item	Ship	Model
Length $L_{pp}(m)$	135.0	3.50
Breadth $B(m)$	24.3	0.630
Depth $D(m)$	11.5	0.298
Draught $d(m)$	8.37	0.217
Block Coeffl. C_b	0.570	0.570
Disp. Vol. $\nabla(m^3)$	15652	0.273

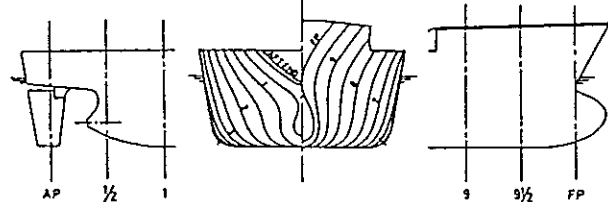


Fig.1 Body plans, shapes of bow and stern, and principal particulars

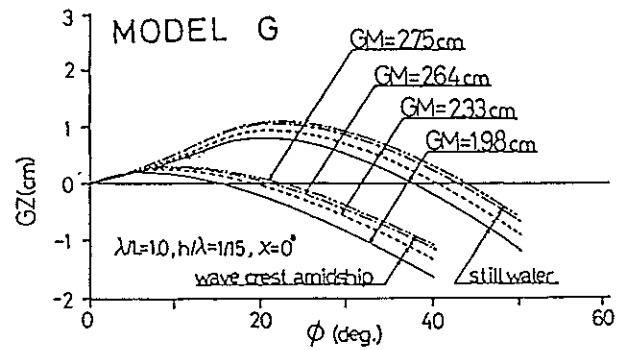
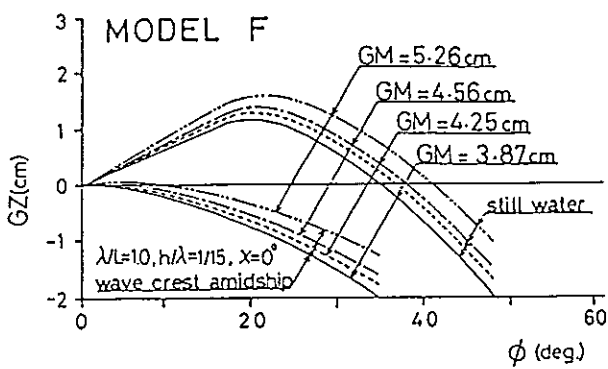


Fig.2 Stability curves in still water and in wave crest amidship

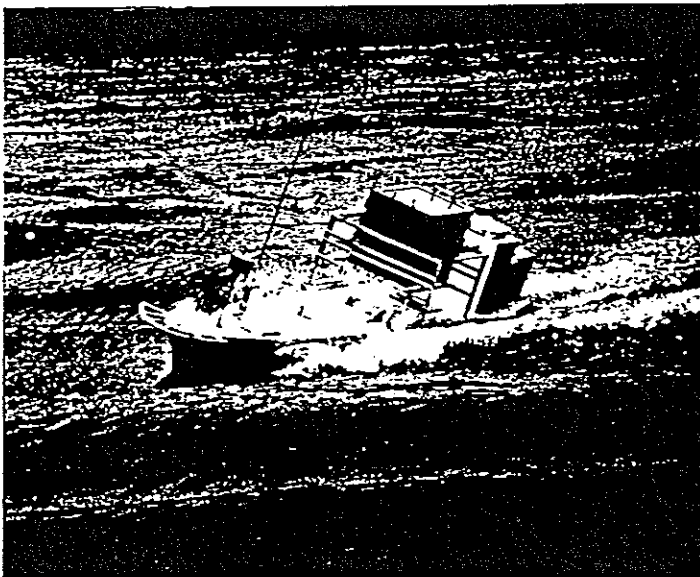


Photo 1 Scene of capsizing test

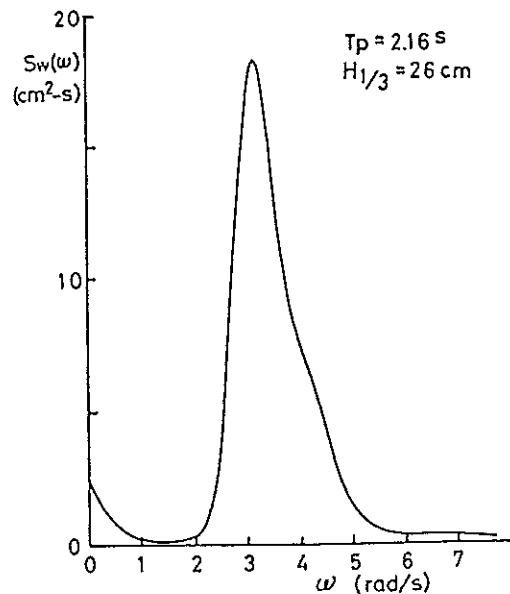
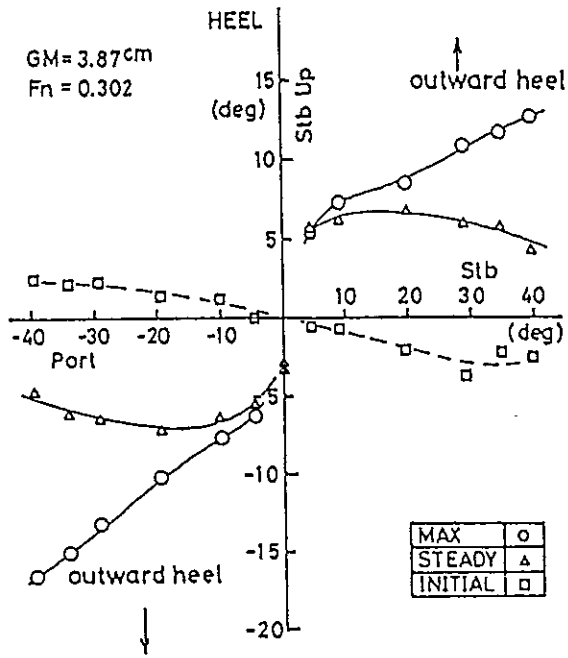


Fig.4 Spectrum of irregular wave

MODEL F



MODEL G

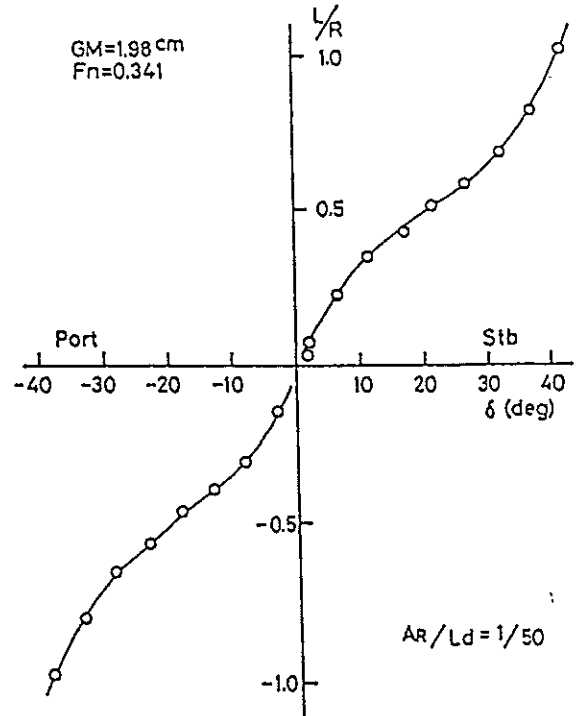
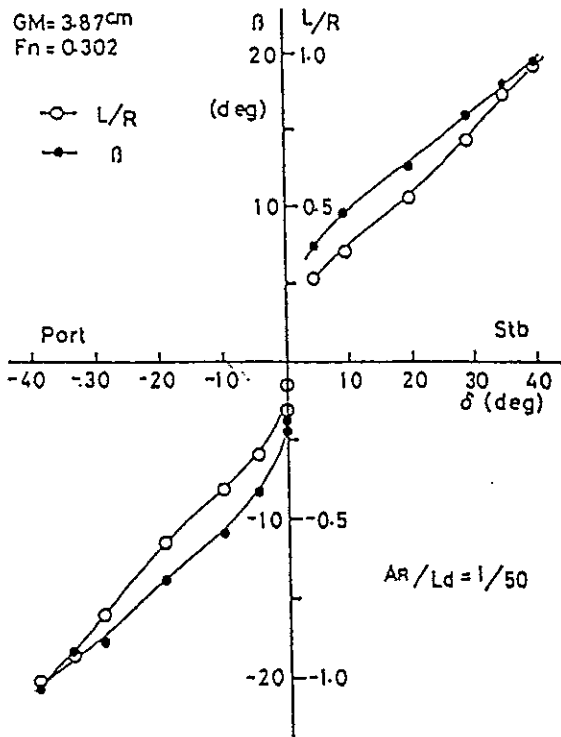
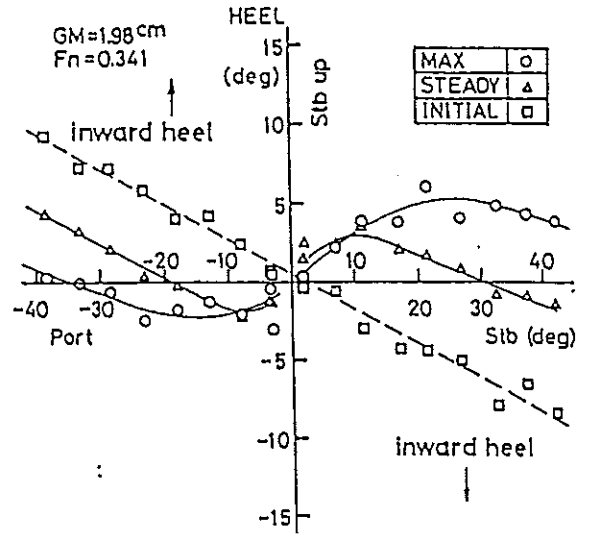


Fig.3 Turning rate and heel in turning

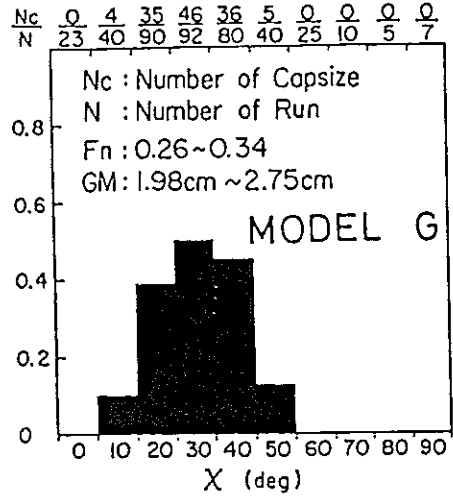
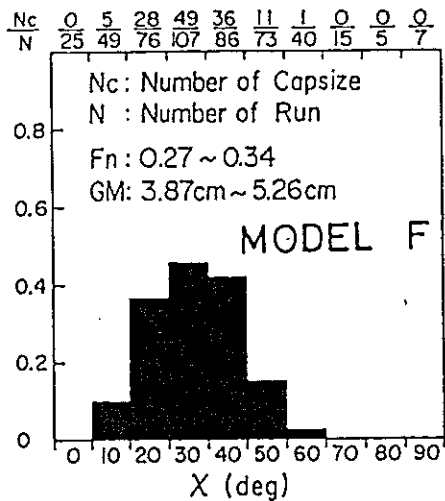


Fig.5 Total capsizing rate in irregular wave

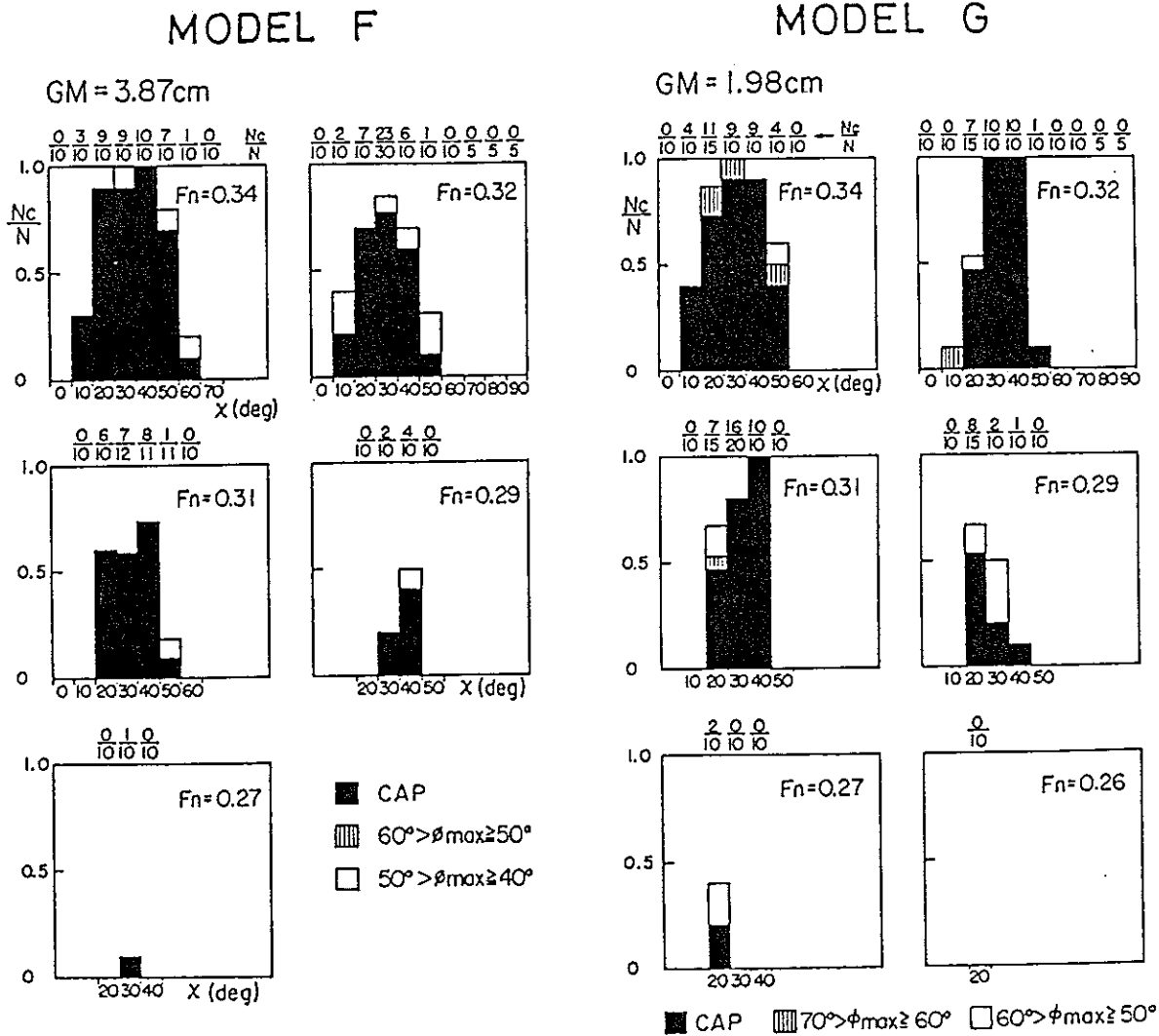


Fig.6 Effect of ship speed on capsizing rate

MODEL F

MODEL G

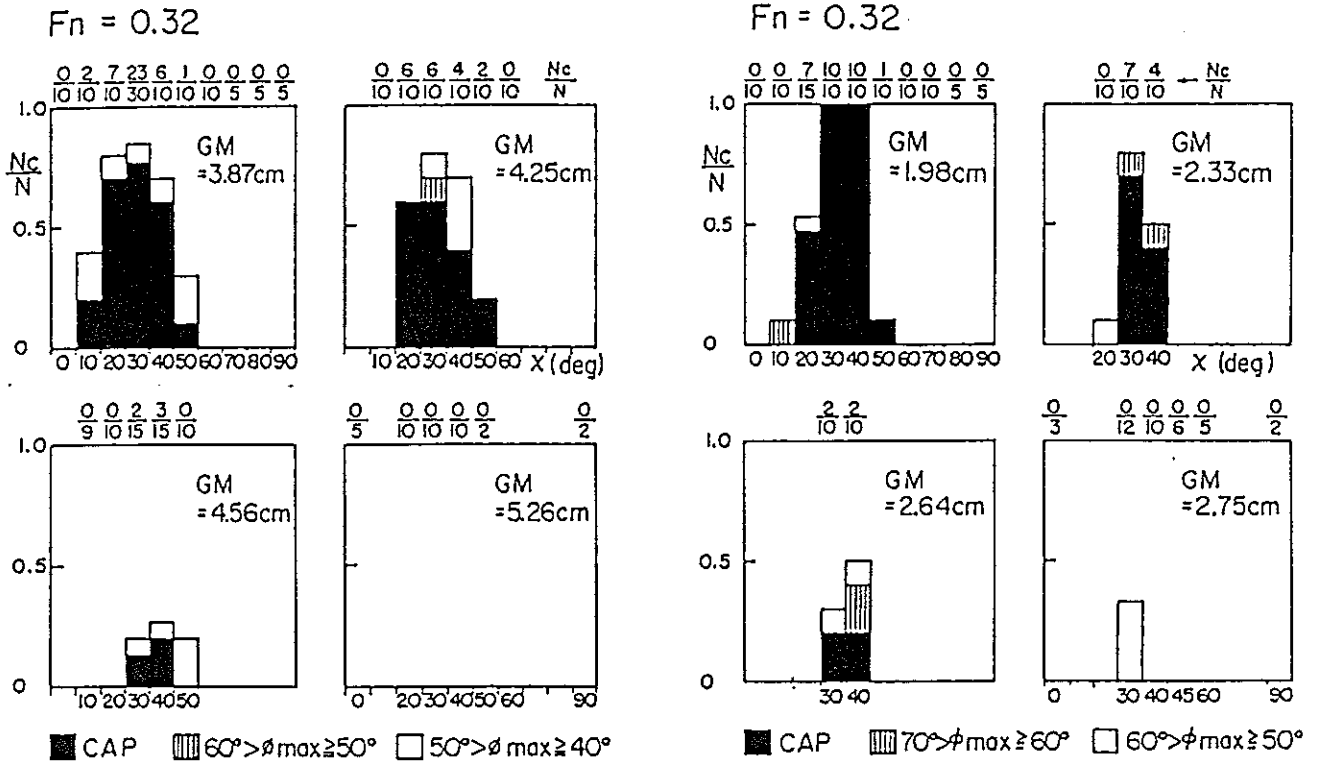


Fig. 7 Effect of GM on capsizing rate

MODEL F

MODEL G

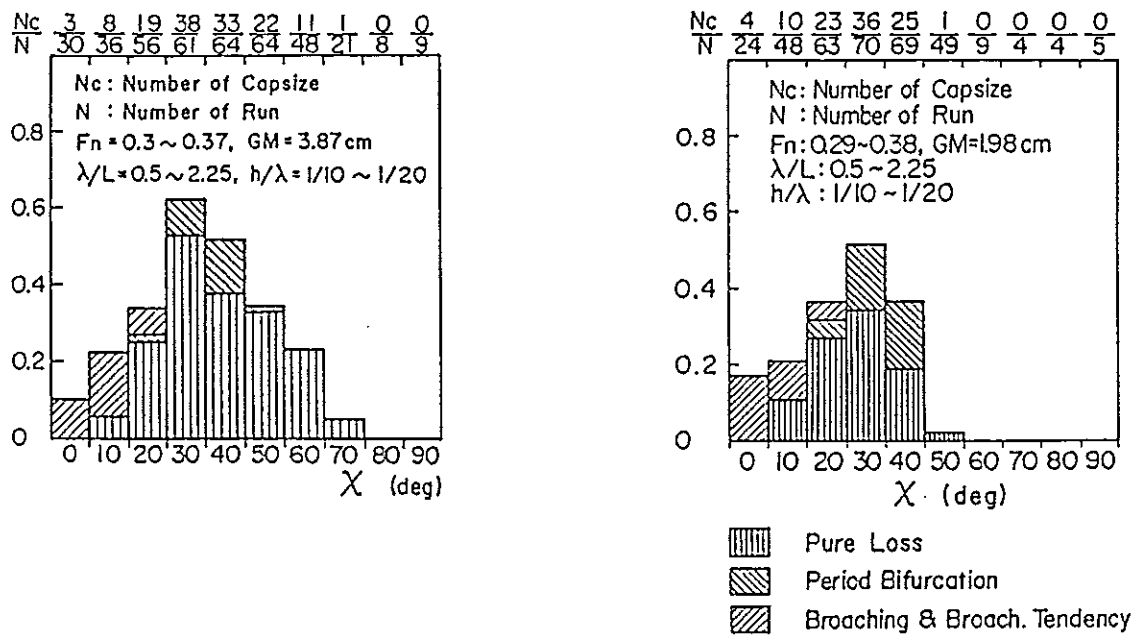


Fig. 8 Total rate of capsizing and classified modes in regular waves

λ/L	h/λ	F_n	X (deg)									
			0	10	20	30	40	50	60	70	80	90
0.5	$1/20$	0.36	MODEL F									
		0.37	MODEL F									
	$1/10$	0.30				O	O	O	O	O	O	O
		0.32										
		0.34	O	O	O	O	O	O	O	O	O	O
		0.36				O	O	O	O	O	O	O
		0.37										

λ/L	h/λ	F_n	X (deg)									
			0	10	20	30	40	50	60	70	80	90
1.50	$1/20$	0.28	MODEL F									
		0.30			O	O	O	O				
		0.32			O	X	X	OP	O			
		0.34		O	O	X	X	OP	OP	O		
		0.36	O	O	X	X	X	X	X	X	O	
	$1/15$	0.28	MODEL F									
		0.30			OP	OP	O	O	O			
		0.32		O	X	X	X	X	X	O		
		0.34	O	OP	X	X	X	X	X	OP		
		0.36	O	X	X	X	X	X	X	OP		

λ/L	h/λ	F_n	X (deg)										
			0	10	20	30	40	50	60	70	80	90	
0.75	$1/20$	0.32	MODEL F										
		0.34	MODEL F										
		0.36			OBT	O	O	OP	O	O			
		0.37			OBT	O	O	O	O				
		0.38			OBT	O	O	O	O				
	$1/15$	0.34	O	O	OBT	O	OP	O	O				
		0.37	O	O	O	X	X	O	O				
		0.32											
		0.34	O	O	O	O	OP	O	O				
	$1/12$	0.36	O	O	X	X	OP	O	O				
		0.37	O	O	X	X	OP	OP	O				
		0.38	O	O	X	X	OP	OP	O				
	$1/10$	0.32											
		0.34										O	
		0.36			OBT	X	X	OP	O				

λ/L	h/λ	F_n	X (deg)									
			0	10	20	30	40	50	60	70	80	90
1.75	$1/20$	0.28	MODEL F									
		0.30			O	O	OP	O				
		0.32			O	O	OP	OP	OP	O		
		0.34		O	OP	X	X	O	O			
		0.36	O	O	X	X	X	X	X	O		

λ/L	h/λ	F_n	X (deg)									
			0	10	20	30	40	50	60	70	80	90
1.0	$1/20$	0.32	MODEL F									
		0.34	O	O	O	OP	OP	X				
		0.36	O	OBT	O	OP	OP	X	O			
		0.37	O	X	X	X	X	X	O			
		0.38	O	X	X	X	X	X	O			
	$1/15$	0.30			O	O	O					
		0.32			O	OP	OP					
		0.34	O	O	O	X	OP	O	O	O	O	O
		0.36	O	X	X	X	X	OP				
	$1/12$	0.37	OBT	OB	X	X	X	X	O			
		0.30										
		0.32	O	O	O	OP	OP					

λ/L	h/λ	F_n	X (deg)									
			0	10	20	30	40	50	60	70	80	90
2.0	$1/20$	0.28	MODEL F									
		0.30										
		0.32			O	O	OP	OP				
		0.34		O	OP	X	X	OP	OP	O		
		0.36	O	O	O	X	X	OP	OP	O	O	O

λ/L	h/λ	F_n	X (deg)										
			0	10	20	30	40	50	60	70	80	90	
1.25	$1/20$	0.30	MODEL F										
		0.32	MODEL F										
		0.34			O	O	OP	OP	O	O			
		0.36	O	O	O	X	X	O	O				
		0.37	O	O	O	X	X	X	O				
	$1/15$	0.28	MODEL F										
		0.30			OP	OP	OP	O	O				
		0.32	O	O	O	X	X	X	X	O			
		0.34	O	O	X	X	X	OP	OP	O			
		0.36	O	X	X	X	X	X	X	OP			

λ/L	h/λ	F_n	X (deg)										
			0	10	20	30	40	50	60	70	80	90	
225	$1/20$	0.28	MODEL F										
		0.30	MODEL F										
		0.32											
		0.34			O	O	O	O	O	O			
		0.36			O	O	O	O	O	O	O	O	O

O: Non Capsize
 Δ: $\Phi_{max} > 40^\circ$, □: $30^\circ \leq \Phi_{max} \leq 40^\circ$
 X: Capsize
 L: Pure Loss
 P: Period Bifurcation
 B: Broaching
 BT: Broaching Tendency

Table 1 Results in regular waves (model F)

λ/L	h/λ	F_n	χ (deg)									
			0	10	20	30	40	50	60	70	80	90
0.5	1/10	0.31	MODEL G							GM=1.98 cm a=1.25, b=0		
		0.32										
		0.34				O	ΔP	O	OP			
		0.36	O	O	O	O	ΔP	O	O	O	O	O
		0.37				O	OP	O	O			

λ/L	h/λ	F_n	χ (deg)									
			0	10	20	30	40	50	60	70	80	90
1.50	1/20	0.31	MODEL G							GM=1.98 cm a=1.25, b=0		
		0.32		O	O	OP	ΔP					
		0.34			Δ	ΔP	OP					
		0.36		O	O	O	Δ	ΔP	O			
		0.37		O	Δ	ΔP	ΔP	O				
	1/15	0.31		Δ	ΔP	OP	Δ	MODEL G				
		0.32		O	Δ	ΔP	ΔP	OP				
		0.36	O	O	Δ	ΔP	ΔP	OP				
		0.37	O	Δ	ΔP	ΔP	OP					
		0.37	O	Δ	ΔP	ΔP	ΔP	O				

λ/L	h/λ	F_n	χ (deg)									
			0	10	20	30	40	50	60	70	80	90
0.75	1/20	0.36			O	O	ΔP	O	GM=1.98 cm a=1.25, b=0			
		0.37			O	Δ	O					
	1/15	0.31			O	ΔP	O					
		0.32			O	Δ	OP	O				
		0.34			O	Δ	Δ	O				
	1/12	0.36	O	O	O	Δ	Δ	O	MODEL G			
		0.37	O	OB	CBT	Δ	Δ	O				
		0.31	O	O	O	O	O	O				
	1/10	0.32		O	O	ΔP	O					
		0.34	O	O	O	ΔP	ΔP	O				
		0.36	O	OB	O	Δ	Δ	O	O			
	1/10	0.37	O	OB	CBT	Δ	Δ	O	O			
		0.29				OP	OP					
		0.36		O	O	ΔP	ΔP	OP				

λ/L	h/λ	F_n	χ (deg)									
			0	10	20	30	40	50	60	70	80	90
1.75	1/20	0.31	MODEL G							GM=1.98 cm a=1.25, b=0		
		0.32			O	ΔP	O					
		0.34			O	ΔP	Δ					
		0.36		O	O	OP	ΔP	O	MODEL G			
		0.37		O	O	Δ	Δ	O				

λ/L	h/λ	F_n	χ (deg)									
			0	10	20	30	40	50	60	70	80	90
2.0	1/20	0.31	MODEL G							GM=1.98 cm a=1.25, b=0		
		0.32			O	OP	O					
		0.34			O	Δ	ΔP	O				
		0.36	O	O	O	Δ	Δ	O	O	O	O	
		0.37	O	O	O	Δ	Δ	O	MODEL G			

λ/L	h/λ	F_n	χ (deg)									
			0	10	20	30	40	50	60	70	80	90
1.0	1/20	0.32	MODEL G							GM=1.98 cm a=1.25, b=0		
		0.34										
		0.36		O	O	ΔP	O					
		0.37		O	O	Δ	O					
		0.38		OB	Δ	Δ	O					
	1/15	0.31	O	ΔP	O	O	MODEL G					
		0.32	O	O	Δ	O						
		0.34	O	Δ	Δ	Δ	O					
		0.36	OB	Δ	Δ	ΔP	O					
	1/12	0.37	OB	Δ	Δ	Δ	O					
		0.31	O	O	O	O	OP	O				
		0.32	O	Δ	ΔP	OP	Δ	O				
		0.34	O	O	Δ	Δ	O	O				
	1/10	0.36	O	Δ	Δ	Δ	Δ	O	O	O	O	
		0.37	OB	Δ	Δ	Δ	Δ	ΔP				

λ/L	h/λ	F_n	χ (deg)									
			0	10	20	30	40	50	60	70	80	90
2.25	1/20	0.31	MODEL G							GM=1.98 cm a=1.25, b=0		
		0.32										
		0.34			O	Δ	O					
		0.36	O	O	O	Δ	Δ	O	MODEL G			
		0.37	O	O	O	Δ	Δ	OP				

λ/L	h/λ	F_n	χ (deg)									
			0	10	20	30	40	50	60	70	80	90
1.25	1/20	0.31	MODEL G							GM=1.98 cm a=1.25, b=0		
		0.32			O	ΔP	O					
		0.34			ΔP	ΔP	OP					
		0.36		O	O	Δ	OP					
		0.37		O	Δ	Δ	OP					
	1/15	0.31	O	O	Δ	O	O	O	MODEL G			
		0.32	O	O	Δ	ΔP	OP	O				
		0.34	O	Δ	ΔP	ΔP	ΔP	O				
		0.36	O	Δ	ΔP	ΔP	Δ	O				
	1/12	0.37	OB	Δ	Δ	Δ	Δ	O				
		0.31		O	OP	O	O					
		0.32	O	O	Δ	Δ	O					
		0.34	O	ΔP	ΔP	ΔP	O					
	1/10	0.36	Δ	Δ	Δ	Δ	ΔP	ΔP				
		0.37	Δ	Δ	Δ	Δ	ΔP	ΔP	O	O	O	

O : Non Capsize
 Δ : $\Phi_{max} > 40^\circ$
 X : Capsize
 L : Pure Loss
 P : Period Bifurcation
 B : Broaching
 BT : Broaching Tendency

Table 2 Results in regular waves (model G)

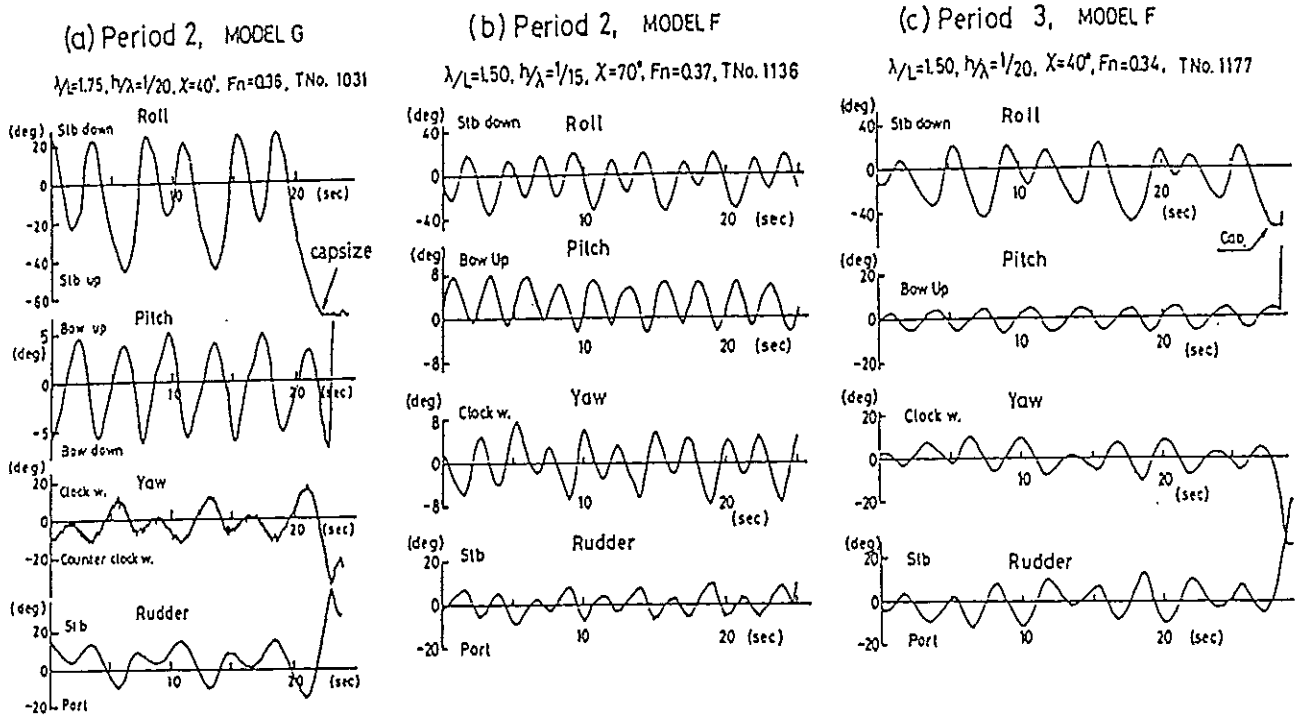


Fig.9 Examples of period bifurcation of roll

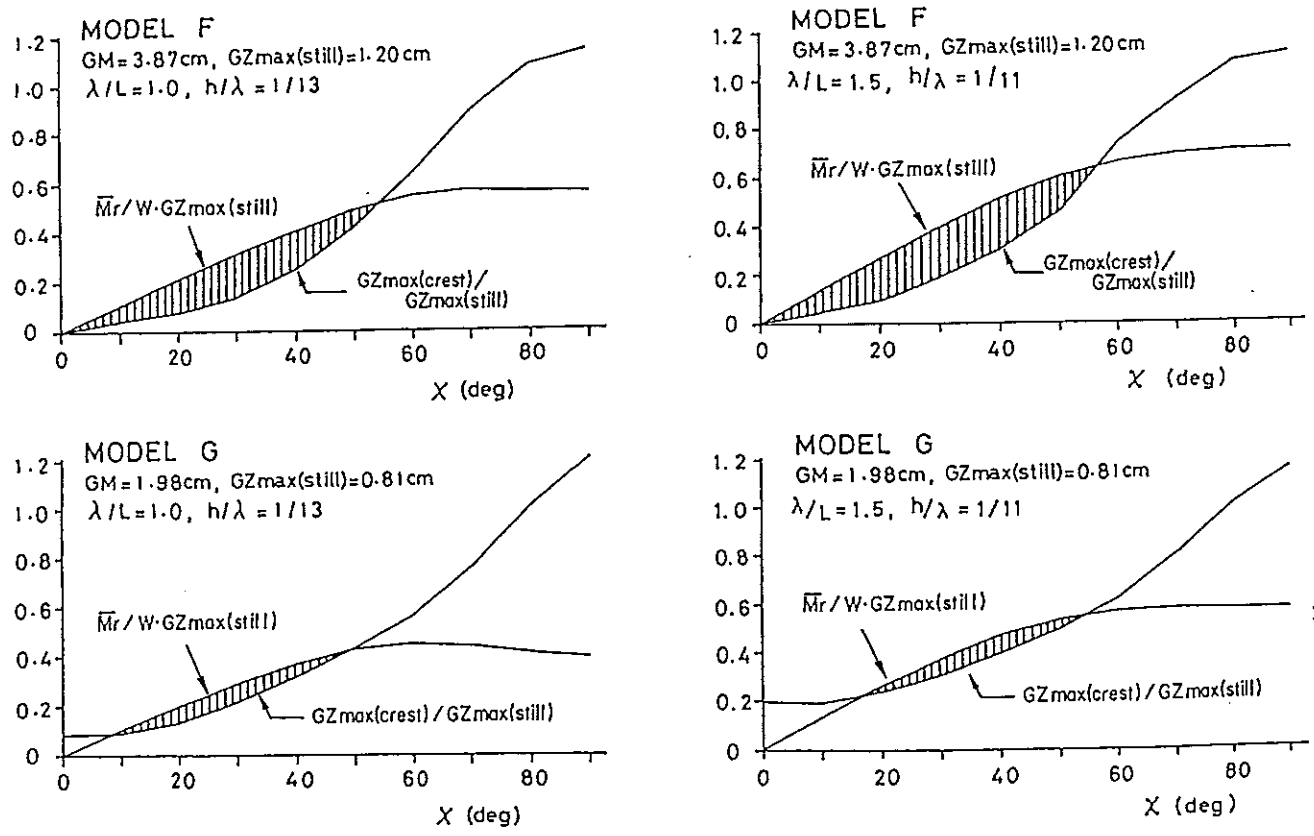


Fig.10 Comparison of capsizing moment and restoring moment

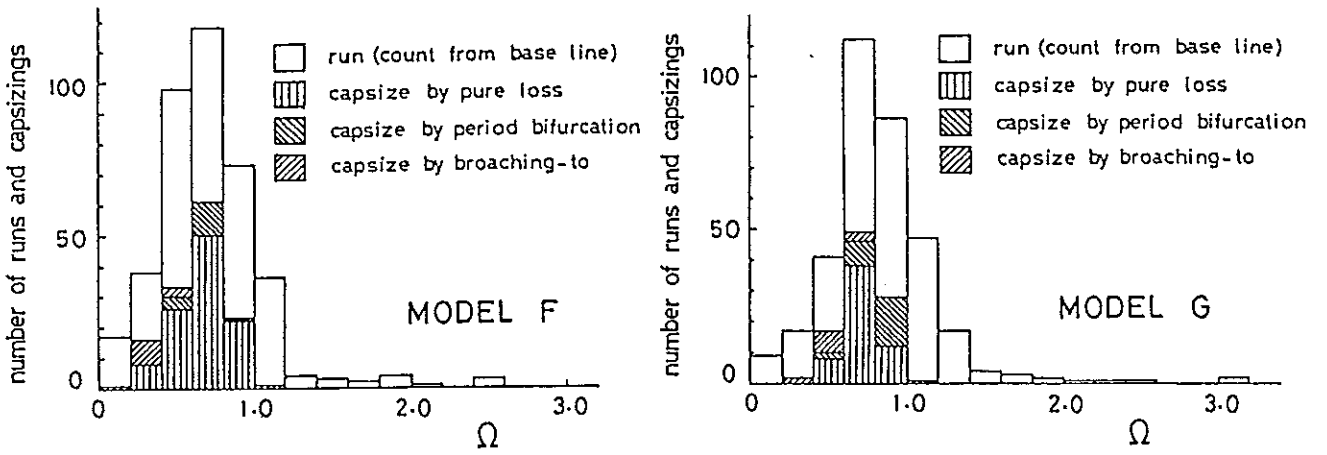


Fig.11 Histogram of experimental runs and classified capsizing modes

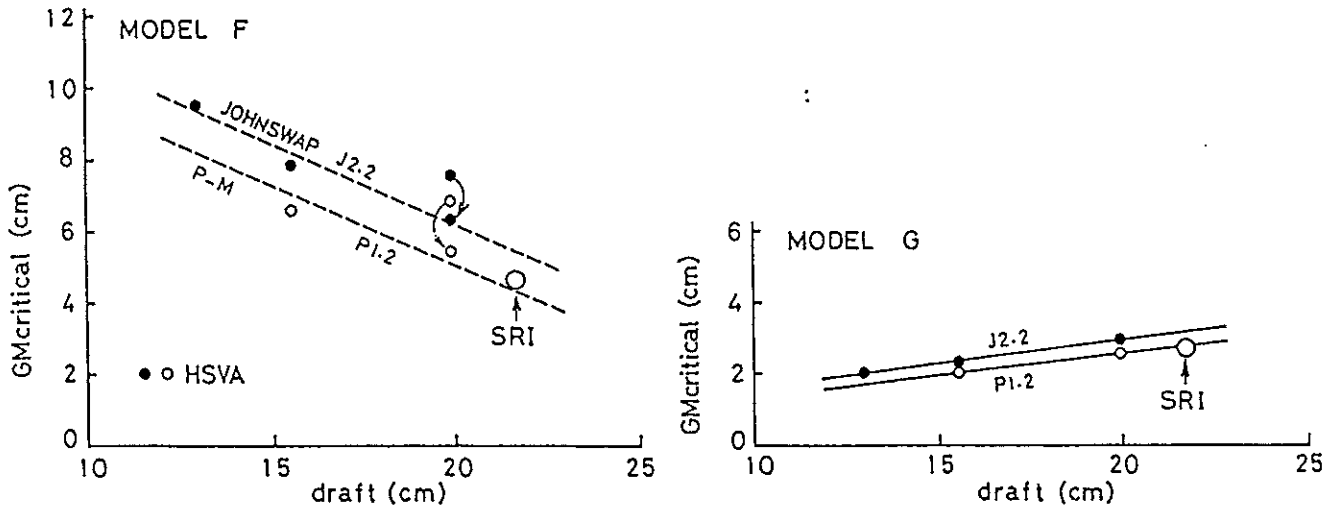


Fig.12 Comparison of critical value of GM between HSVA and SRI

SOME OBSERVATIONS ON EXPERIMENTAL TECHNIQUES FOR MODELING SHIP STABILITY IN WIND AND WAVES

James Shaughnessy ¹
Bruce C. Nehrling ²
Roger H. Compton ³

ABSTRACT

A series of experiments for measuring the intact and damaged stability characteristics of scale ship models in wind and waves have recently been conducted at the United States Naval Academy's Hydromechanics Laboratory. The equipment which was developed for these experiments, the pros and cons of the various modeling techniques which were investigated, and some general conclusions and observations about these experiments are described in this paper.

The generation, measurement, and behavior of the wind field is discussed. The wind field was generated by sets of centrifugal fans spanning the width of the Academy's larger towing tank. The wind field was mapped by using electro-mechanical anemometers. The behavior of a wind field in an enclosed towing tank places special requirements on the size and position of the ship model, its restraint system, and on the subsequent analysis of the acquired data. Model tethering considerations are addressed. The influence of a simplified 2D superstructure versus a more realistic but costly 3D superstructure is discussed.

Experiences gained with the use of a non-intrusive system to video tape the model's motions and the subsequent computer analysis of this time history are described. The relative influences that wind only, waves only, and wind and waves have on a model's behavior are compared.

INTRODUCTION

This paper addresses some of the pragmatic aspects associated with subjecting a scale model hull, tethered in a traditional towing tank, to relatively severe wind and wave action. The intent, of such a set of experiments, is to help devise better ways to predict a ship's stability characteristics.

Stability testing in wind and waves is relatively uncommon. Consequently, appropriate apparatus, instrumentation, and software need

to be developed. In addition, significant questions exist concerning the physical phenomena involved, interpreting the experimental results, and making rational full scale performance predictions. These questions must be carefully resolved.

ENVIRONMENTAL SIMULATION

WAVES

All of the experiments described in this report were conducted in the 380 foot towing tank at the Naval Academy Hydromechanics Laboratory (NAHL). A sketch showing the major dimensions of this towing tank is given in Figure 1. Waves were generated

¹ Naval Architect, NAHL, U.S. Naval Academy

² Professor of Naval Architecture, U.S. Naval Academy

³ Professor of Naval Architecture, NAHL Director, U.S. Naval Academy

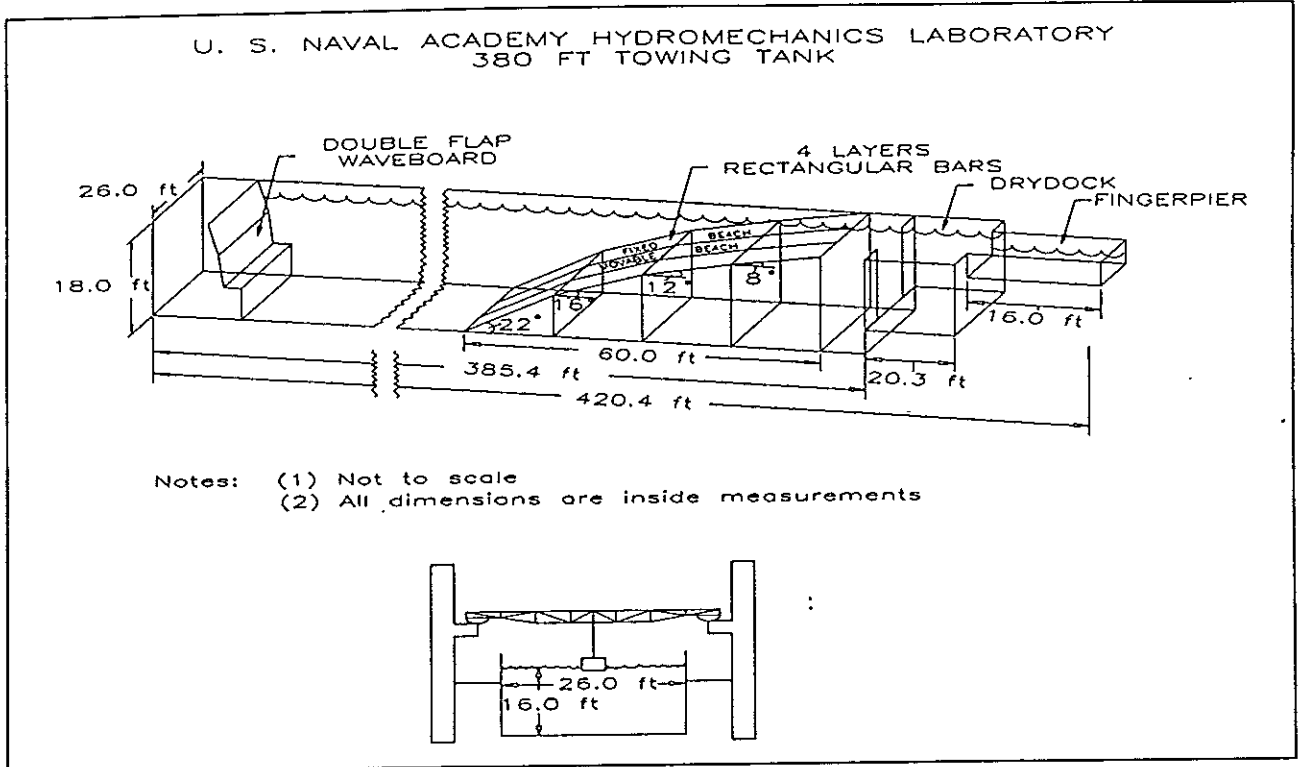


FIGURE 1: 380 FOOT TOWING TANK AT NAHL

using a dual flap, electro-hydraulically activated wavemaker. Only long crested waves can be generated, but either regular or irregular (pseudo-random) wave systems are possible. For these tests, irregular waves described by a particular energy spectrum which, in turn, was specified by a significant wave height and modal period, were developed. These wave systems were generated and their energy content measured in calm air without any model being present.

Each wave system was developed in the following way:

- (1) Given the agreed upon spectral shape, significant wave height ($H_{1/3}$), and modal period, a relatively brief initial wavemaker drive signal was developed consisting of several sinusoidal components having random relative phases.
- (2) The wave time history, as acquired by a stationary resistance wire wave probe,

was used as feedback to adjust the wavemaker drive signal to match the desired wave spectrum more closely. Thus, the wavemaker control transfer function was developed through an iterative process. Normally, three to four iterations were necessary to achieve a reasonable agreement with the desired wave system.

- (3) To create a composite non-repeating irregular wave system which would represent a reasonable full scale time period, a series of independent wave systems, having the same $H_{1/3}$ and modal period, but with different stationary time histories, were strung together. This concatenation was accomplished by changing the relative phasing among component sinusoidal waves for each subsequent independent wave system.

Table I is a summary of the model wave conditions used in the

various test programs discussed in this report.

Ship Model	A	B			C		D	
Wave Type	irregular	irregular			irregular		irregular	
Spectral Form	Modified ITTC	Bretschneider			JONSWAP		JONSWAP	
≈ Sea State	8	5	6	7	6	7	6	7
H _{1/3} (ft) #	1.05	0.45	0.67	0.99	1.14	1.36	0.89	1.07
Modal Frequency (Hz)	0.37	0.51	0.40	0.33	0.42	0.30	0.48	0.34
Typical Wave Duration (sec)	600	600			480		420	

Significant peak-to-trough wave heights are based on an assumed Rayleigh distribution of the wave's energy spectrum.

TABLE I: REPRESENTATIVE WAVE SYSTEMS

WIND

Figures 2 and 3 show the basic wind generation and measurement system which was developed for the 380 foot towing tank at the NAHL. The wind generation system consists of four fan assemblies. Each fan assembly, which is 8 feet long and contains three centrifugal fans operating on a common shaft, is driven by a separately controlled 15 horsepower AC motor. Each fan assembly has a maximum rated output velocity of 4,100 ft/min and a maximum rated capacity of 23,800 ft³/min. The vertical discharge of each fan is vectored by means of adjustable vanes. The discharge is throttled using adjustable internal baffles. Pairs of fan assemblies are attached to sets of trusses resting on the walls of the tank. The fan assemblies can be butted together at the tank's centerline or spread apart. If desired, three fans can be mounted on one set of trusses. While the trusses can be positioned anywhere along the length of the tank, a nominal distance of 85 feet from the wavemaker has been adopted in order to allow the wavemaker's waves to fully develop before entering the wind field. The fan assemblies are usually

positioned with their discharge openings approximately 30 inches above the calm water level.

The wind velocity is measured by using miniature electro-mechanical vane anemometers. Prior to being used, each anemometer is calibrated individually in a small wind tunnel. The towing tank's wind field is calibrated longitudinally, vertically, and transversely by systematically relocating an array of anemometers. Thus a matrix of discrete wind velocities, for a given fan configuration, is developed. Plots of the wind field are developed and interpolated to obtain the nominal distance, from the front set of fans, at which the model should be tethered. Figure 4 contains typical wind gradient plots for the fan configuration depicted in Figure 2. This figure shows a plot of the wind profile measured on the tank's centerline and approximately 24 feet down wind from the face of the front fan assembly with no waves or ship model present. The raw data for this plot were obtained by positioning anemometers in a vertical array configured to measure the wind at various heights above the calm water level. This vertical array was then positioned

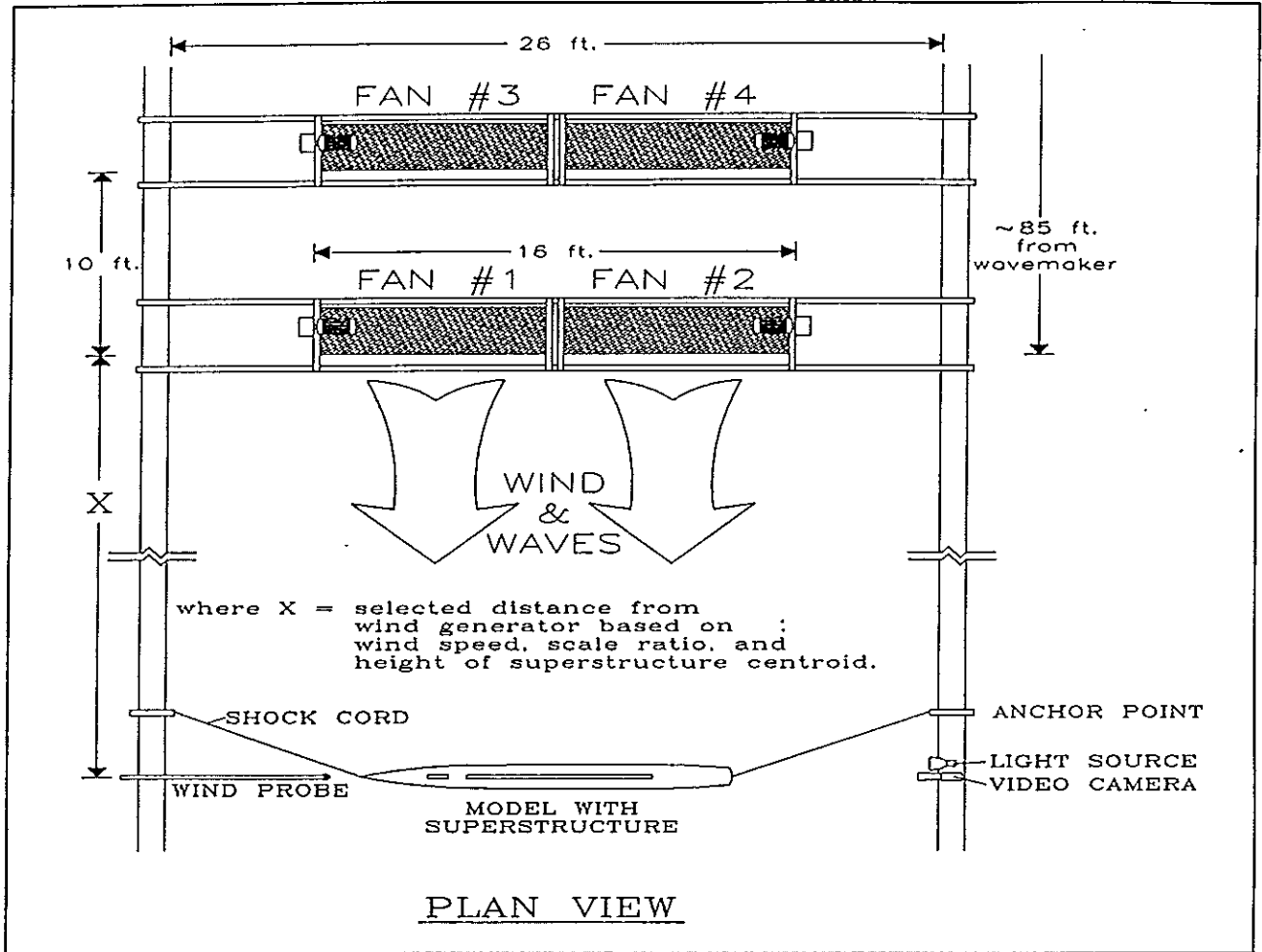


FIGURE 2: NAHL WIND SYSTEM - TYPICAL CONFIGURATION

at several locations away from the tank's centerline. Data obtained in this fashion enable a plan view of the wind distribution at a given vertical location to be plotted. By cross plotting the acquired data, a three dimensional map of the wind field can be created. Interpolating within this map permits the experimenter to select a nominal tethering location which will have the required wind velocity occurring at a stipulated elevation.

OBSERVATIONS

The wind system responded very quickly. Probes placed roughly 10

feet from the fans indicated that a wind velocity in excess of 1,800 ft/min could be achieved in less than 2 seconds. The anemometers, however, had a response time of about 5 seconds. Consequently, to measure and observe the initial development of the wind's gradient more accurately, an analog tap was installed to count blade pulses. The fans also stopped very quickly. By rapidly cycling the fans on and off, it was possible to generate severe wind gusts which were capable of capsizing some of the models tested. To date, no quantitative analysis of these wind gusts has been made.

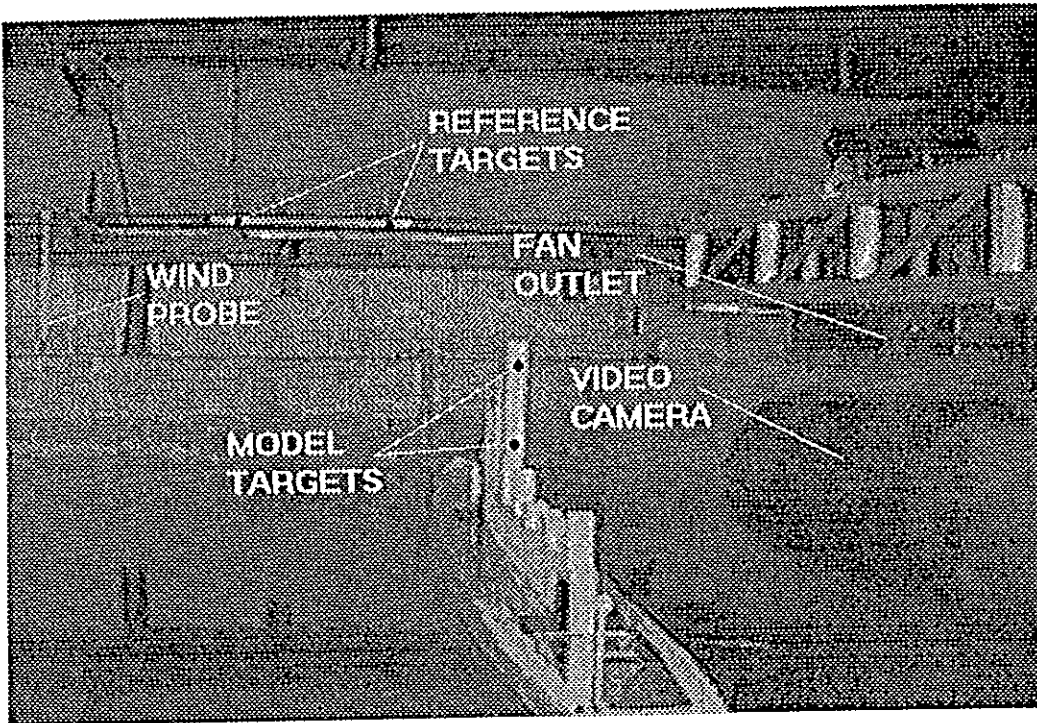


FIGURE 3: NAHL WIND GENERATION AND MEASUREMENT SYSTEM - PHOTO

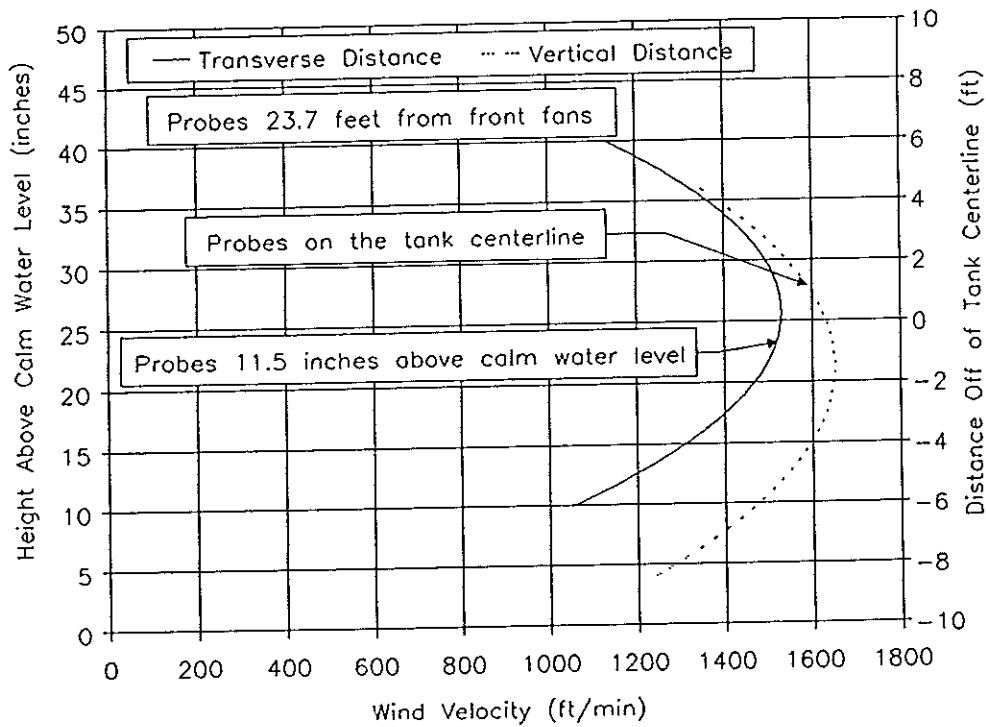


FIGURE 4: TYPICAL WIND DISTRIBUTION WITHIN THE 380 FOOT TOWING TANK AT NAHL

After the wind generation system was turned on, capillary waves quickly formed in a fan like shape on the water's surface. These wind generated waves became fully developed about 30 feet from the fans. The length of the "footprint" for reasonably consistent wind generated waves was about 40 feet. Of course, wind and water motion immediately adjacent to the tank's walls was adversely influenced by these boundaries.

Representative steady state wind fields were developed by allowing the fans to run for 30

seconds and then measuring the wind field for 120 seconds. Table II shows some typical wind statistics gathered during testing by a single probe mounted 2 feet off of the tank's centerline and 24 inches above the calm water level. It can be seen from these data that the wind field weakens and becomes confused as it moves away from the fans. Thus, a finite usable length exists to the wind field which limits the positioning of a model relative to the fans for a specific wind velocity and wind quality.

		Nominal Distance from Fans (ft)					
		35	40	45	50	55	60
Average Wind Velocity	ft/min	1519	1458	1362	1161	1048	613
Standard Deviation	ft/min	52.8	59.9	69.8	80.2	95.3	227.8

Note: 2' off of the tank's centerline and 24" above the calm water level

TABLE II: REPRESENTATIVE WIND MEASUREMENTS

Table III shows the influence of steady state wind conditions on both calm water and waveboard generated waves. In this table, the relative energy spectra for the "wave only", "wind only", and "combined wind and wave" conditions were computed from wave time histories acquired using a stationary resistance wave wire without a model being present.

Relative energy is based on the ratio of the areas under the respective spectral curves. These spectra were normalized using the "wave only" energy spectrum as the reference value. In the "combined wind and wave" condition, it was apparent to observers that the wind caused some wave energy to be dissipated through wave breaking and spray formation.

	Wind Only	Waves Only	Wind and Waves
$H_{1/3}$ (in) #	2.43	10.21	10.12
Modal Frequency (Hz)	1.95	0.42	0.39
Relative Energy Spectra	0.05	1.00	0.95
Typical Wind Duration (sec)	120	NA	120

Significant peak-to-trough wave heights are based on an assumed Rayleigh distribution of the wave's energy spectrum.

TABLE III: REPRESENTATIVE INFLUENCE OF WIND ON WAVES

MODEL CONSIDERATIONS

MODELS

The experimental testing and observations described in this paper pertain to four different models. Selected characteristics of these four models are listed in Table IV. All four models were "fully

appended" (i.e., geometrically scaled bilge keels, sonar domes, exposed shafts and struts, and rudders, as appropriate, were fitted). Scaled plexiglas disks were used to represent the ship's propellers. The models were modified slightly at the bow and stern to accept the tethers that were necessary to keep the models properly positioned during testing.

PARAMETER	UNITS	MODEL HULL			
		A	B	C	D
LBP	ft	11.33	8.27	17.66	18.99
Beam @ waterline	ft	1.27	1.57	2.63	2.28
Displacement	lbs	191.6	177.0	1320.2	1108.1
Mean Draft (reference)	in	5.37	4.98	11.49	9.82
Trim (+ stern)	in	0.0	0.73	0.37	0.38
Heel (+ port)	deg	0.0	0.0	0.0	0.0
KG	in	6.34	7.56	14.06	11.48
GM _T	in	1.04	2.47	2.39	1.83
Roll Period	secs	1.85	1.61	2.83	2.71
Pitch gyradius as a percent of LBP	%	26.4	NA	24.0	23.8
Projected sail area	in ²	1,553	1,185	5,251	4,609
Center of Pressure (above BL)	in	12.52	11.95	26.29	21.64

TABLE IV: SELECTED MODEL CHARACTERISTICS

SCALE CONSIDERATIONS

The scale factor associated with any towing tank model being considered for wind and wave testing should be carefully selected. If the selected scale factor (λ), defined as $(L_{\text{ship}}/L_{\text{model}})$, is too small, then the model, when positioned for beam winds, will experience strong and consistent winds near amidships but weak and erratic winds near the bow and stern. This towing tank related phenomenon is shown graphically in Figure 5. In a head or following orientation, a long model will experience rapidly diminishing wind velocities along its length. A shorter model, which would tend to avoid these two problems, might need

to be tethered far away from the fans where the wind field tends to be very inconsistent with eddies, pockets of stagnant air, and reversals in the direction of air flow. At this stage, we are assuming that Froude scaling would provide for a corresponding wind velocity between the model and the full scale ship.

BALLASTING CONSIDERATIONS

In order to do an effective job of model testing in wind and waves, the model must be ballasted to the required displacement (or draft), trim, vertical center of gravity (KG), natural roll period, and pitch gyradius. A conventional

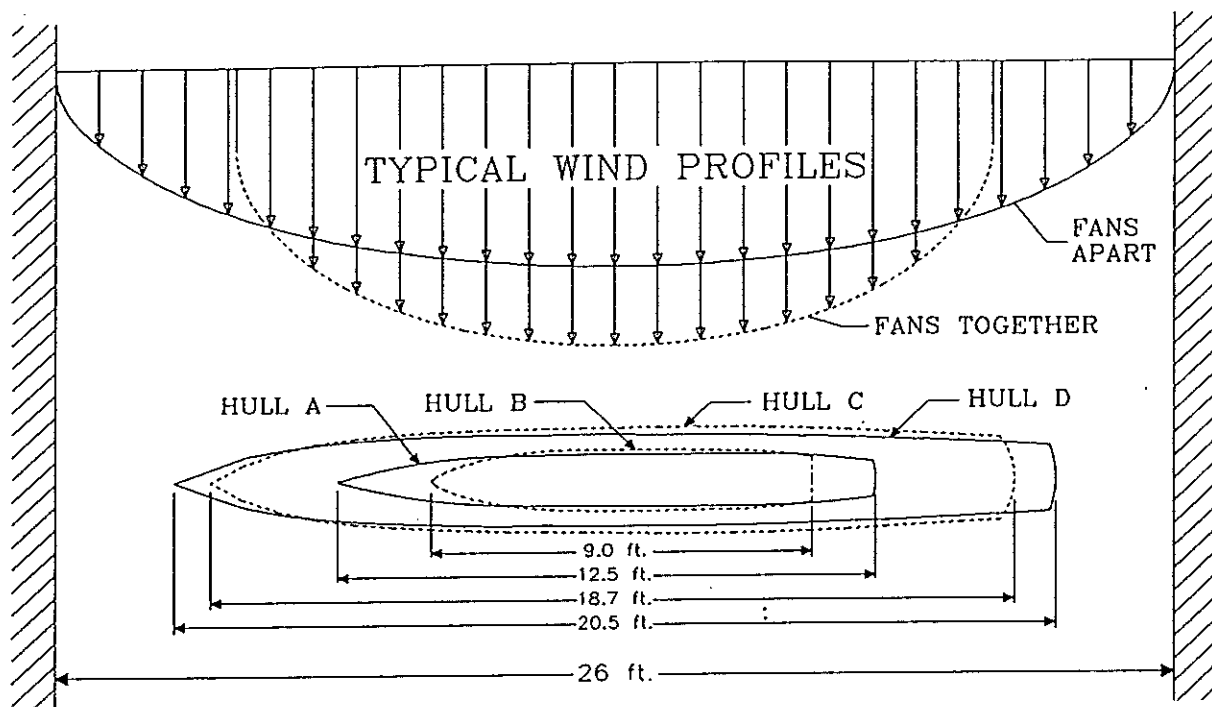


FIGURE 5: RELATIONSHIP BETWEEN WIND FIELD WIDTH AND MODEL LENGTH

inclining experiment, in conjunction with vertical weight adjustments, can be performed in order to set the required KG. The desired roll period can be achieved by shifting appropriate ballast weights equidistantly port and starboard and/or up and down and then tallying the model. On the assumption that the pitch gyradius is approximately equal to the yaw gyradius, the model can be hung and swung in bifilar suspension in order to determine the yaw gyradius. Equal onboard weights can be shifted equidistantly from the longitudinal center of gravity until the desired value for the pitch gyradius, typically about 25% of LBP, is obtained.

TETHERING CONSIDERATIONS

The model must be tethered in order to conduct these wind and wave

experiments. Otherwise, it will quickly re-position itself and be blown out of the usable wind field. For wind and wave experiments on relatively large models, a bungee chord arrangement appears to be a satisfactory method for gently constraining the model. Therefore, a "soft" restraint system was devised to keep the model at a specific distance from the fans and to maintain its desired nominal heading relative to the wind and wave direction while minimizing the influence of the restraint system on the environmentally induced motions of the model. This was accomplished by using an appropriate length of elastic chord in each mooring line, and by keeping the forces applied by the restraint system at or near the waterline and as horizontal as possible. The shore end of each tether was either secured in place or held by an experimenter. The other end was secured at either the model's current waterline or at a

height equal to one half of the draft. At times, the forces in these lines became fairly large. For oblique headings, the experimenter would need to make periodic adjustments in order to maintain the model's nominal heading. Assorted trials were conducted to investigate the influence of these various tethering techniques. The results of some of these trials are summarized in Table V. Schematic drawings of typical tethering configurations are shown in Figures 6 and 7. It appears that the tethering scheme does not have a significant impact on the motions of a relatively large model.

SUPERSTRUCTURE CONSIDERATIONS

Both two dimensional and three dimensional superstructures were modeled. Two dimensional centerline profiles representing superstructure shapes were fabricated out of both braced aluminum sheet and stiffened 2" thick closed cell foam. In addition, three dimensional high-density closed cell foam superstructures were also constructed. These superstructure configurations were intended to adequately represent the general characteristics of the ship's superstructure without dwelling on

CONFIGURATION		NATURAL ROLL PERIOD
Attachment Point	Tethering Lines	(seconds)
@ LWL	Slack	2.99
@ LWL	Normal	3.00
@ LWL	Taught	2.99

Notes: Nominal total length of the unloaded tether: 3½ ft
 ¼ inch diameter bungee chord formed into a loop
 Nominal length of the slack bungee chord loop: 2 ft
 Model D ($\Delta = 1034.9$ lbs, $GM_T = 1.50"$ $T_{roll} = 3.00$ secs)

TABLE V: INFLUENCE OF TETHERING ON ROLL PERIOD

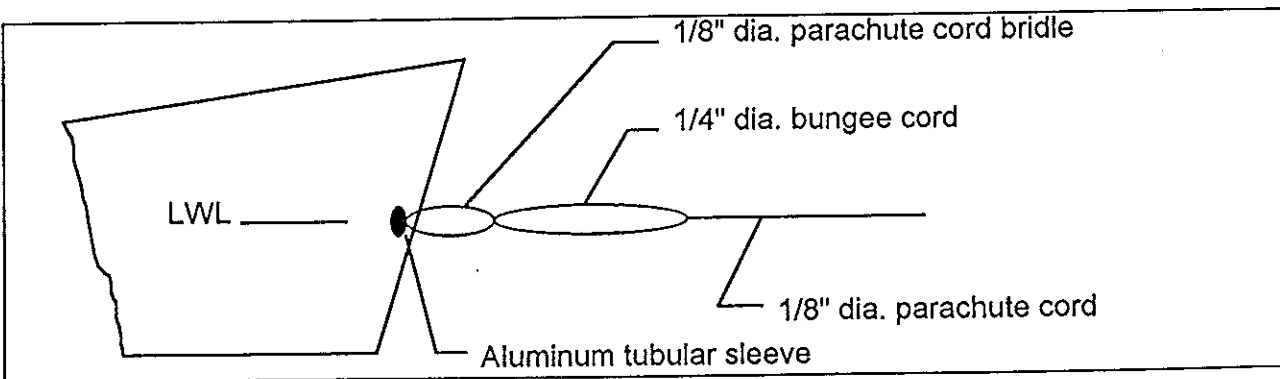


FIGURE 6: TYPICAL TETHERING SCHEMATIC

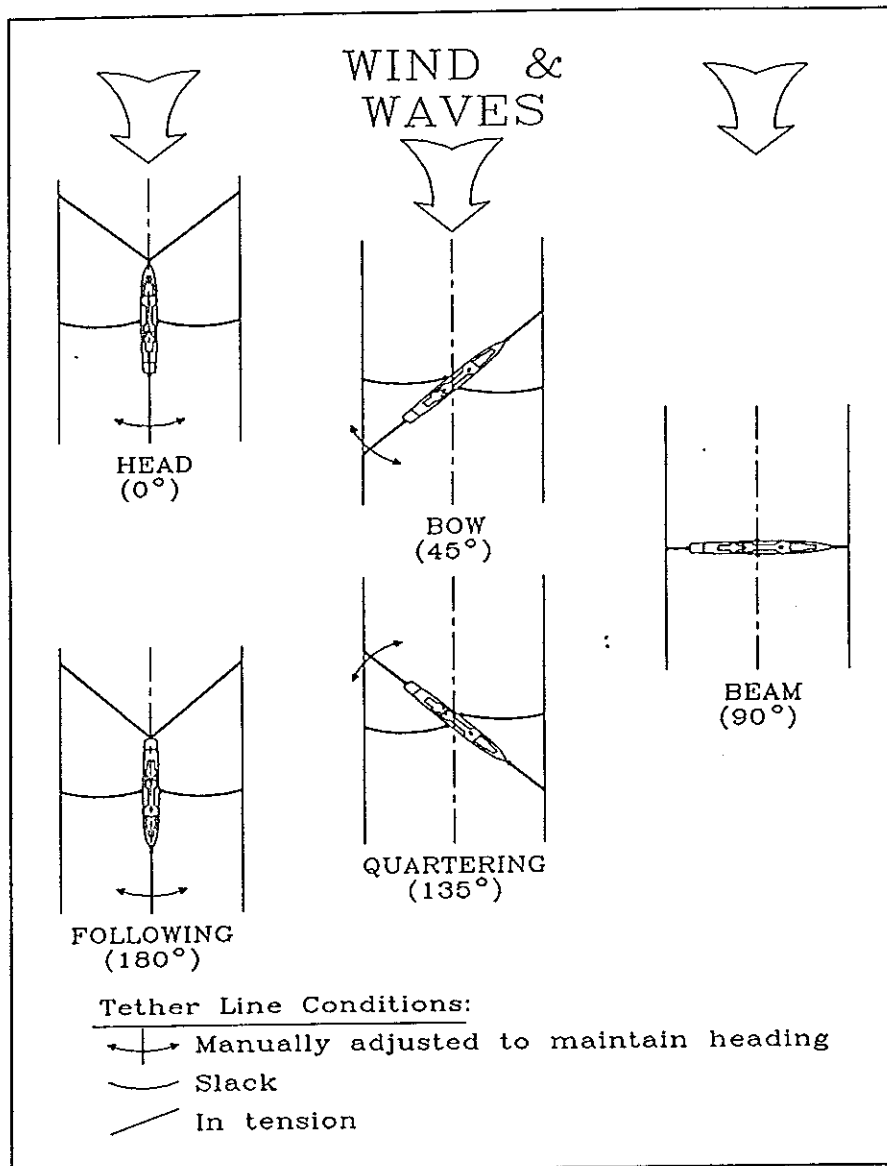


FIGURE 7: REPRESENTATIVE TETHERING RELATIONSHIPS

excessive detail. The goal was to model, with reasonable accuracy, the desired center of pressure and projected lateral area. Table VI contains a summary of the performance of one model in the same beam winds with both a two dimensional and a three dimensional superstructure. It would seem that modeling the superstructure two dimensionally is sufficient for beam

conditions and low angles of heel. However, for head, following, or oblique orientations, as well as large angles of heel, a three dimensional configuration is necessary. It should be noted that the three dimensional configuration was approximately six times more expensive to fabricate than the two dimension version.

Super-structure	Sample Time (minutes)	Average Heel (deg)	Std. Dev. of Roll (deg)	Min. Roll Amplitude (deg)	Max. Roll Amplitude (deg)
2-D	3	-7.84	2.34	+0.88	13.95
3-D	3	-6.07	2.72	-3.48	14.27

- Notes:
1. Model A, intact, tethered @ LWL, bow and stern
 2. Extreme beam winds
 3. - angle indicates roll to leeward

TABLE VI: ROLL STATISTICS FOR TWO SUPERSTRUCTURE CONFIGURATIONS

DATA ACQUISITION

MOTION ANALYSIS SYSTEM

In most cases, the wind and wave induced motions of the model in a transverse plane were measured in an innovative and non-intrusive way. Pairs of small circular targets made of retro-reflective tape were attached, a known distance apart and on a common plane, to the superstructure of the model and also to a parallel reference plane on some convenient but stationary tank structure. To record the model's roll motions during beam wind and waves, a video camera, mounted on the side wall of the towing tank and pointing perpendicular to the targets on the model's superstructure, was used. During an experiment, the motions of these targets relative to each other provided the necessary spatial data for the Motion Analysis System (MAS) to calculate the model's inplane motions. The fixed targets provided a stationary reference to true vertical in order to make any corrections for the camera not being perfectly level. Other wind and wave induced motions such as heave, sway, or pitch could be determined by attaching targets to a different set of parallel reference planes, re-positioning, if necessary, the video camera, and recording data.

The MAS provided an integrated method for acquiring and analyzing

the wind and wave induced motions of the model. As shown in Figure 8, the MAS system itself is made up of five essential subsystems:

- Video camera
- Video recorder and monitor
- Video processor
- Desktop computer with a hard drive, and
- Printer

During a given experiment, for instance, beam wind and waves, the roll motions of the model (more precisely, the relative bearing changes of the two targets) were captured by the video camera which relayed these images to the video recorder. As the motions of the targets were being recorded, it was essential to ensure that the targets' images were kept within the viewing window on the monitor and that the resolution of the targets was not diminished by extraneous light sources, reflections, parallax, or lens distortion. This was accomplished by keeping the test area as dark as possible, painting the upper surfaces of the model with non-reflective paint, and locating the center focus of the camera near the expected position that the restrained model would drift to under the influence of the beam wind and waves. The target motions, which were recorded on tape by the video recorder, were processed after the completion of each test run.

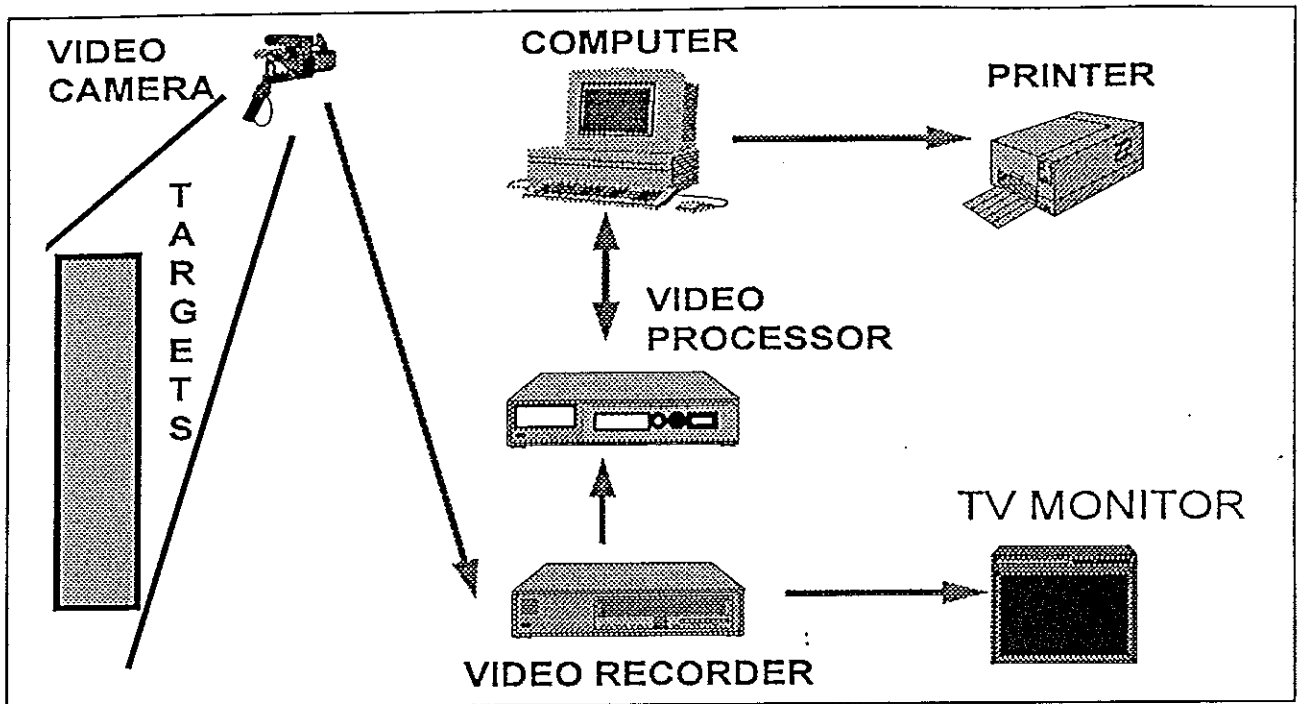


FIGURE 8: MOTION ANALYSIS SYSTEM (MAS) COMPONENTS

In processing the data, the tape was played back and the raw images were converted by the video processor into digital outlines which were saved on the computer's hard drive. The conversion of the images to outlines helped to reduce the considerable amount of disk space taken up by the data. Using the MAS software, the centroids of these outlines were calculated and stored. The path traced by the movement of these centroids was then analyzed to obtain the necessary relative bearings and, using the established reflective target geometry, the model's roll time history.

The MAS software could only accept 3000 frames at a time; at a frame rate of 15Hz, this corresponds to only 3 minutes and 20 seconds of test data. A frame rate of 15Hz was chosen because it provided the best resolution while keeping the processing time and computer memory size requirements to reasonable levels. Since data acquisition periods of up to 12 minutes were

desired, the software was modified to automatically generate the necessary sequential roll time history files required for each test condition. These time history files were stored as ASCII files and imported into Quattro Pro in order to perform the required statistical analysis. Since the MAS is a non-intrusive and sensitive way of obtaining roll time histories, it was also used to acquire data during some of the tethered and untethered sailing experiments, including experiments, and roll gyradius trials.

To investigate the effect of windowing and frame size on the analysis of the MAS data, a power spectral analysis was conducted on the acquired roll time histories. Windowing results in smoother spectral curves (intuitively more representative of the real physical phenomena). This smoothing effect can be seen by comparing the spectra shown in Figures 9 and 10, which are based on a common frame size of 512, with Figure 10 having a Hanning window with a 50% taper. As can be

seen in Figures 11 and 12, the roll spectra becomes increasingly more jagged as frame size is increased. Although the graphical appearance of the distribution of roll energy, as a function of both windowing and frame size, varies greatly, the total energy, as measured by the area under the spectral curves, is amazingly consistent. Table VII summarizes the relatively small effects that frame size and windowing have on the calculated roll spectral energy while also showing that severe beam winds strongly dampen roll motion.

Test	Frame Size	No Window	Hanning Window (50% taper)	% Diff.
Waves Only	512	98.59	99.25	0.67
	1024	99.19	104.34	5.18
	4096	99.20	105.14	5.98
Wind and Waves	512	51.48	48.45	-5.87
	1024	51.63	55.77	8.01
	4096	51.68	49.33	-4.55

TABLE VII: SPECTRAL ENERGY COMPARISONS (MODEL A)

TRANSDUCERS

The need to actively handle the soft tethers in oblique headings, meant that it was only possible to maintain a nominal orientation. Thus, it was difficult to use the MAS since this system requires that the video camera be as perpendicular as possible to the parallel planes of the active and reference targets. Consequently, an intrusive system consisting of duplicate transducers was mounted in two of the models to measure their pitch and roll motions. These small, light weight, two-axis transducers were mounted on the

centerline plane at the approximate location of the model's center of gravity. Signal wires were passed through the top of the superstructure. In order to keep the wires slack, so as not to affect the model's motions, the signal wire bundle had to be supported from above and its position, relative to the model, actively monitored during testing.

MODEL BEHAVIOR

HEADINGS

Selected experimental data obtained for model D is listed in Table VIII and shown in Figure 13. To properly position the model, an average wind velocity, which was required to occur at a prescribed height above the water (i.e., at the vertical center of pressure of the ship's projected lateral area), was chosen. The corresponding experimental wind velocity at the vertical center of pressure of the model's projected lateral area (h) was computed using Froude scaling and the standard meteorological assumption that the wind velocity (U_h) at a distance h above the still water level equals the nominal wind velocity at 10 meters (U_{10}) times (h/10) raised to the 1/7th power.

$$U_h = U_{10} * (h/10)^{1/7}$$

Using this value of U_h and faired wind calibration plots derived from the measured wind distribution data as represented by Figure 4, a nominal tethering location for the model, with respect to the fans, was determined. During testing, the tethering lines had to be periodically tended in order to keep the model's center of gravity at approximately this location.

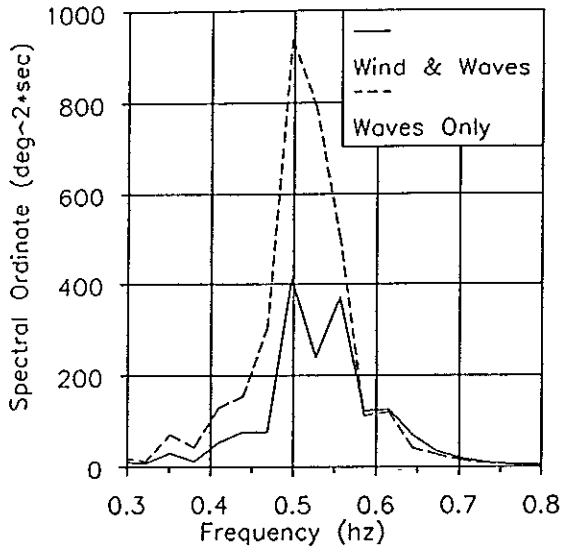


FIGURE 9: COMPARATIVE MODEL ROLL SPECTRA IN SEA STATE 8, WITHOUT WINDOWING, FRAME SIZE 512, MODEL D

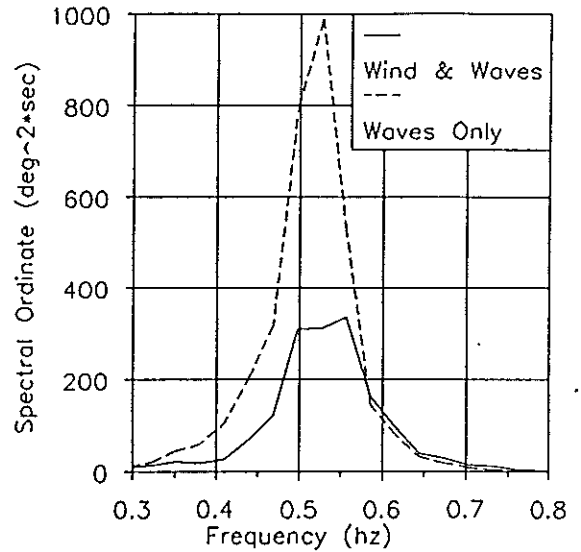


FIGURE 10: COMPARATIVE MODEL ROLL SPECTRA IN SEA STATE 8, WITH HANNING WINDOWING, FRAME SIZE 512, MODEL D

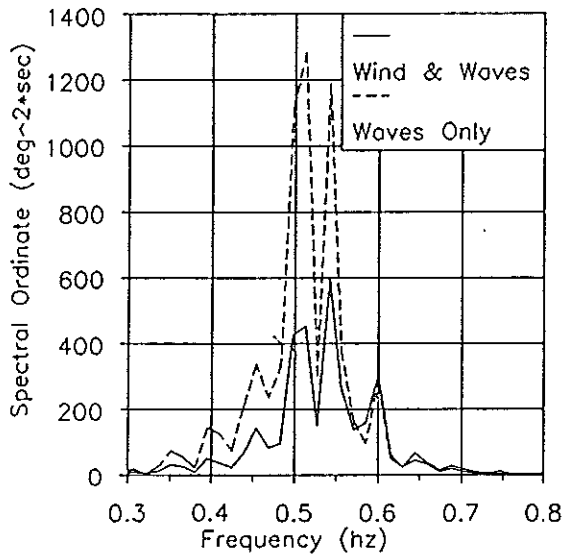


FIGURE 11: COMPARATIVE MODEL ROLL SPECTRA IN SEA STATE 8, WITHOUT WINDOWING, FRAME SIZE 1024, MODEL D

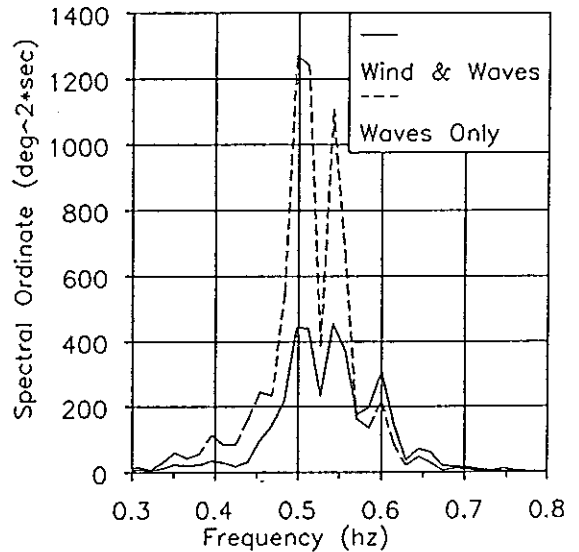


FIGURE 12: COMPARATIVE MODEL ROLL SPECTRA IN SEA STATE 8, WITH HANNING WINDOWING, FRAME SIZE 1024, MODEL D

NOMINAL HEADING	AVERAGE HEADING	WIND ONLY				
		Roll				Pitch
		mean	standard deviation			std dev
HEAD	0					
BOW	45	-0.644	0.496			0.032
BEAM	90	-1.616	0.632			0.029
QUARTERING	135	-0.722	0.594			0.034
FOLLOWING	180					
		WAVES ONLY				
		Roll				Pitch
		mean	standard deviation			std dev
HEAD	0	-0.030	0.559			1.841
BOW	45	-0.496	4.540			1.582
BEAM	90	-0.222	5.669			0.163
QUARTERING	135	-0.357	5.064			1.582
FOLLOWING	180	+0.027	0.405			1.853
		WIND AND WAVES				
		Roll				Pitch
		mean	std dev	max to lee	max to wind	std dev
HEAD	0	-0.364	0.850	-2.73	2.29	1.850
BOW	45	-1.139	4.230	-12.16	9.98	1.510
BEAM	90	-1.593	4.607	-14.35	10.39	0.117
QUARTERING	135	-1.102	4.739	-14.95	10.86	1.530
FOLLOWING	180	+0.378	0.834	-2.22	2.59	1.784

Notes: Model D (Table IV) in sea state 7 (Table I)
Average wind velocity at center of pressure: \approx 1305 ft/min
Average sampling time for wind and waves: \approx 8.6 minutes
All angles are in degrees
Roll angles are negative to leeward
Mean pitch angles are negligibly small (< 0.1 deg)

TABLE VIII: REPRESENTATIVE MODEL BEHAVIOR

LESSONS LEARNED

The physical testing of scale ship models in wind and waves remains an evolving developmental effort. As techniques are developed, exercised, and refined, observations of the physical phenomena often reinforce engineering intuition, but sometimes raise troublesome questions regarding experimental equipment and procedures. Several general non-ship specific conclusions can be drawn from the experimental programs already undertaken.

- (1) Tethering is necessary. Fortunately, softly tethering the model at the waterline during wind and wave experiments appears to have only a negligible effect on damping.
- (2) The sensitive and non-intrusive Motion Analysis System (MAS) has proven to be an extremely viable method for developing time histories of model motions (in any one plane, at present) without requiring mechanical or electrical connections to the model. For stability studies involving damaged hulls, this

- system promises to be very useful.
- (3) Considering the current state-of-the-art of model testing in winds, it is not considered cost-effective to require three-dimensional modeling of the superstructure for just beam winds. If other headings are to be investigated, then the added effort and expense of developing a nominal three-dimensional superstructure is warranted.

- (4) The shape of the three dimensional wind field developed in an enclosed towing tank does not correspond very well with the wind pattern that a ship in the open ocean would experience. Consequently, it is important to carefully select the model size relative to both the width of the tank and the three-dimensional shape of the mechanically produced wind field.

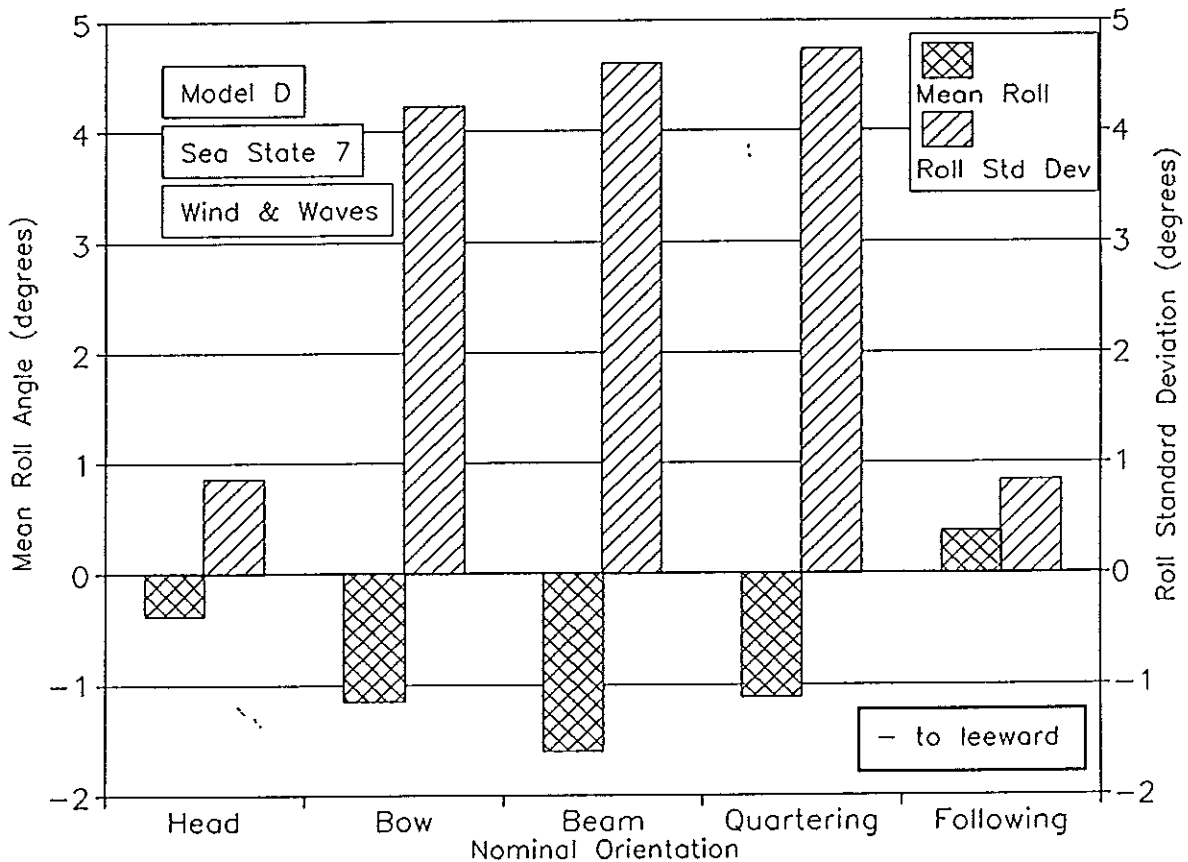


FIGURE 13: REPRESENTATIVE ROLL MOTION AMPLITUDES

- (5) Froude scaling of wind speed appears to be reasonable and practical.
- (6) The strong damping influence a beam wind has on a model's wave induced roll motions has been demonstrated and partially quantified.
- (7) The mathematical analyses performed routinely on time series data to generate wave or wave-induced response spectra produce widely varying graphical images. Nevertheless, statistical predictions of spectral energy

are very consistent
irrespective of the windowing
or frame size selected.

- (8) The influence of the duration and fetch of the mechanically produced wind on the wavemaker produced waves needs to be further quantified.
- (9) The amount of wave reflection which will develop over time must be considered when establishing the duration of each test run.
- (10) There are several inherent differences between the model testing environment and the real world. These differences (i.e., wind field pattern, tethering, etc.) are difficult to quantify in an absolute

sense. Consequently, the statistical interpretation of the experimental data is most applicable to comparative testing. For example, comparing model variations or model to ship behavior patterns.

ACKNOWLEDGMENTS

The authors wish to thank the entire staff of the Naval Academy Hydromechanics Laboratory. We especially appreciated the support and contributions provided to us by Donald Bunker, Stephen Enzinger, and Norman Tyson.



DAMAGE SCENARIO ANALYSIS: A TOOL FOR ASSESSING THE DAMAGE SURVIVABILITY OF PASSENGER SHIPS

by

D Vassalos* and O Turan**

*Department of Ship and Marine Technology, University of Strathclyde, Scotland, UK

**Department of Naval Architecture, Yildiz Technical University, Turkey

ABSTRACT

This paper presents an approach adopted to assess the damage survivability of a ship which derives from an examination of a number of realisable damage scenarios chosen from accident statistics and IMO recommendations, on the basis of maximising the danger of potential capsizing. Damage scenarios analysis refers to the procedure of identifying the "worst damage scenario" by studying the dynamic behaviour of the damaged vessel in a realistic environment using time simulation. The practical applicability of the proposed approach is demonstrated by presenting the results of a case study for a modern car/passenger ferry on the basis of which some revealing conclusions on the damage survivability of passenger ships are drawn and recommendations made.

1. INTRODUCTION

The survivability of ships is, in general, related to both intact and damage stability requirements. For passenger vessels, this is normally assessed by their stability in a damaged condition, i.e. by their residual stability. However, in spite of the long history of Naval Architecture and the plethora of accidents at sea that have darkened the history pages, the first specific quantitative standard of residual stability has been introduced for the first time as recently as the 1960 Safety of Life at Sea (SOLAS) Convention addressing, in spite of better judgement, only the metacentric height (0.05m GM).

Despite a late start, considerable progress has been achieved since then. Indeed, we are living now through the very exciting transitional phase in the history of standard development. The profession is at the brink of abandoning the traditional "one compartment standard" and deterministic procedures, specified by existing codes and conventions, adopting instead a probabilistic approach to address damage that could occur at any location throughout the ship, the extent and location of which are based on statistics of actual ship damage. The probabilistic approach is much less arbitrary and offers a means of calculating the relative safety of ships of all types exposed to collision damage, regardless of the type of compartmentation.

Whilst this development represents a major change and indeed real success, the probabilistic approach does not go anywhere near enough in providing a satisfactory solution to the problem of meaningfully assessing a ship's survivability. The main reason for this is twofold:

Firstly, limiting understanding of the particularly complex dynamics involved and, secondly, lack of availability of suitable tools for evaluating designs. More specifically, in both approaches, the dynamic behaviour of the vessel and the progression of flood water through the damaged ship in a random sea state are altogether ignored. In other words, both are still water approaches.

The tragic accident of the *Herald of Free Enterprise* was the strongest indicator of yet another gap in assessing the damage survivability of ships with large undivided deck spaces. In view of the above, it would appear that the only approach to assessing realistically the damage survivability of ships, perhaps within the logical framework of the probabilistic approach, must of necessity offer the means of taking into consideration meaningfully both the operating environment and the hazards specific to the vessel in question. To this end, the need to develop suitable tools pertaining to the required analysis is becoming progressively more critical.

This paper presents an attempt towards satisfying this need. The work presented is based on research undertaken at the University of Strathclyde over a number of years, two of these in association with the UK's Department of Transport Ro-Ro Research Programme.

2. PROBABILISTIC ASSESSMENT OF DAMAGE STABILITY

At about the same time as the 1974 SOLAS Convention was introduced, the International Maritime Organisation (IMO) published Resolution A265 (VIII), [1]. These regulations used a probabilistic approach to assessing damage location and extent drawing upon statistical data to derive estimates for the likelihood of particular damage cases. The method consists of the calculation of an *Attained Index of Subdivision*, A , for the ship which must be greater than or equal to a *Required Subdivision Index*, R , which is a function of ship length, passenger/crew numbers and lifeboat capacity. A is in turn a function of three different probabilities, "a", "p" and "s".

Factor "a" accounts for the probability of damage as related to the position of the compartment in the ship's length; "p" reflects the effect of variation on the longitudinal extent of damage; "s" represents the probability of survival given the damage under consideration. The total attained index is the sum of the products of "a", "p" and "s" for each of the compartments and compartment groups within the ship.

However, it is only the factor "s" where attention is focused in the present study. It is true to state that the ship damage stability problem has not received much attention in the past mainly because a meaningful treatment of it, particularly one involving progressive flooding in a random seaway, was perceived to be too difficult an undertaking by theoretical/numerical means. For this reason an experimental approach was adopted aiming to establish a simplified relationship between environmental and stability-related parameters for a damaged ship and hence determine capsizal resistance in a given sea. On the basis of limited model tests carried out separately in the United Kingdom, [2], and the USA, [3] such a relationship was established between critical GM's (limit of capsizal resistance) and vessel freeboard in a given sea state, characterised by the significant wave height, (H_s). From the results of these tests it was decided to use flooded metacentric height (GM_f) and effective freeboard (F) rather than the GZ curve and GZ curve characteristics to judge capsizal resistance. Supplementary model tests have shown that for a given freeboard in any given sea state the critical GM is proportional to the beam of the vessel, (B). Consequently, the following relationship was invoked:

$$(H_s)_{\text{critical}} = f(GM_f * F / B) \quad (1)$$

Deriving from the above, the probability "s" that a ship with a given value of ($GM_f * F / B$) will survive damage in a given sea state will be equal to the probability of not exceeding (H_s)_{critical}. Therefore, the probability "s" can be derived from the significant wave height distribution relevant to the area of the particular accident in conjunction with the relationship indicated in (1), i.e.:

$$s = P [H_s (GM_f * F / B)] \quad (2)$$

Hence, provided the damage stability parameter ($GM_f * F / B$) was determinate for each group of compartments in any loading condition, vertical extent of damage and permeability, the calculation of the factor "s" would be very simple. This, however, requires knowledge of the joint probability distribution of all the relevant parameters, taking also into consideration vessel type and area of operation. This, in practice, is virtually impossible to derive on the basis of statistical data alone. The need for a realistic theoretical model of damaged vessel behaviour cannot, therefore, be over-emphasised.

The UK Ro-Ro Research Programme provided the impetus for such a model to be developed at the University of Strathclyde as explained briefly in the following two sections.

3. UK RO-RO RESEARCH PROGRAMME

The need to evaluate the adequacy of the various standards in terms of providing sufficient residual stability to allow enough time for the orderly evacuation of passengers and crew in realistic sea states has prompted the Department of Transport to set up the Ro-Ro Research programme comprising two phases. Phase I addressed the residual stability of existing vessels and the key reasons behind capsizes. To this end theoretical studies were undertaken into the practical benefits and penalties of introducing a number of devices, [4], for improving the residual stability of existing Ro-Ro's. In addition, model experiments were carried out by the British Maritime Technology Ltd, [5] and the Danish Maritime Institute, [6] in order to gain an insight into the dynamic behaviour of a damaged vessel in realistic environmental conditions and of the progression of flood water through the ship. Phase II was set up with the following objectives in mind:

- To confirm the findings of Phase I in respect of the ability of a damaged vessel to resist capsize in a given sea state.
- To carry out damaged model tests, in which the enhancing devices assessed in Phase I would be modelled to determine the improvements in survivability achieved in realistic sea-going conditions.
- To confirm that damage in the region amidships is likely to lead to the most onerous situation in respect of the probability of capsize.
- To undertake theoretical studies into the nature of the capsize phenomenon, with a view to extrapolating the model test results to Ro-Ro passenger ships of different sizes and proportions.

The Department of Ship and Marine Technology at the University of Strathclyde was one of three organisations that received a contract to develop and validate a theoretical capsize model which could predict the minimum stability needed to prevent capsizing in a given sea state. This was subsequently to be used to establish limiting stability parameters that might form the basis for developing realistic survival criteria. Full details are given in [7].

4. STRATHCLYDE APPROACH

4.1 General

Simply stated the Strathclyde approach is an attempt to assess damage stability and survivability requirements on the basis of the '*worst realisable damage scenario*' (as determined from actual accident records) by taking into account the dynamic behaviour of the damaged vessel in a realistic environment. The technique used is time simulation. The mathematical model, described in detail in [7], comprises the following:

- Coupled non-linear sway-heave-roll motions together with instantaneous sinkage and trim
- wind and wave excitation
- regular or random waves
- experimentally derived coupling and large angle roll coefficients
- progressive flooding
- water accumulation and sloshing

On the basis of the above, the dynamic behaviour of a damaged vessel is investigated in selected scenarios - chosen to maximise the danger of potential capsize - during and after flooding, in the presence of realistic environmental conditions. The results are presented in the form of boundary stability curves involving relationships between ship design and environmental parameters (e.g. freeboard, F , and significant wave height, H_S) and stability-related parameters (e.g. GM).

4.2 Effects of Water Accumulation

The dynamic effect deriving from this is due to water sloshing. Treating flood water on the vehicle deck as a free surface tank, water sloshing is likely to be important when the excitation frequency is close to the natural frequency of the water in the tank. This, however, is unlikely to be the case in ferries because of their low natural roll frequency, unless the amount of water is small in which case the ensuing dynamic effect will also be small. In addition, water accumulated on a deck corner would result in a system with a small effective breadth and large water depth, thus having a high natural frequency and hence unlikely to be excited in sloshing. As a result, the more likely effect of water accumulation will be a static one giving rise to static heel when asymmetric flooding takes place.

4.3 Modelling of Progressive Flooding

This is a very difficult phenomenon to model as it involves very complex hydrodynamic flows. Some degree of approximation is, therefore, necessary in order to derive engineering solutions. In the model presently considered, water ingress is modelled as an intermittent probabilistic event based on the calculation of the relative position between wave elevation and damaged location as shown in Figure 1. The emphasis here is placed on hydrostatic effects, including edge effect, wave direction and damage location and extent. Formulations for different damage cases are shown in Figure 2 whereby, using this approximation, the whole problem of progressive flooding reduces to evaluating the flow coefficient K which can be done experimentally.

4.4 Validation of the Theoretical Capsize Model

Following the development of the numerical model, the experimental results from the physical model tests, conducted during the Ro-Ro Research Programme, were reproduced by undertaking a series of "*numerical experiments*" using the same data for the vessel and the environment as in [5]. This involves the following:

a) Selection of Ship

The main particulars of the vessel chosen for the parametric investigation are given in Table I, with general arrangement plans shown in Figure 3. This ship sails mainly between UK and the Continent and is similar to the *Herald of Free Enterprise*.

Table 1: Main Particulars of Vessel A

Length Between Perpendiculars (L_{BP})	126.10 m
Breadth (B_{mld})	22.70 m
Depth (D_{bhd})	7.3 0m
Draught (T_{mld})	5.70 m
Displacement (D)	8,807 tonnes
KG (Design)	10.10 m
GM (Intact)	1.72m

b) Particulars of Damage

The damage compartment is situated amidships such that there is sinkage only, with no significant trim. The length of the compartment used in the investigation is 27.7m and extends from -19.0m to 8.7m, providing a 7.12m draught. Following given specifications, the form of

the opening is trapezoidal. It starts at the double bottom and extends to the top, Figure 4. Its sides slope at 15° to the vertical and its width at the waterline, W_D , is given as follows:

$$W_D = (0.03L_s + 3.0) \text{ metres or } 11 \text{ metres, whichever is less.}$$

c) Sea States

The random sea states used are generated on the basis of the JONSWAP spectrum with repeat period of twenty minutes, defined according to the North Sea wave statistics provided in [5]. The zero crossing periods and significant wave heights presently used, are given in Table 2 below:

Table 2: North Sea Wave Statistics

Significant Wave Height, H_s (metres)	Zero Crossing Period, T_0 (seconds)
0.00 - 0.99	4.50
1.00 - 1.99	5.50
2.00 - 2.99	6.00
3.00 - 3.99	6.25
4.00 - 4.99	6.50

d) Capsize Scenario

Before the start of the simulation the damaged compartment below the bulkhead deck is flooded up to the level of the external waterline, as was the case in the physical model tests, with a damage hole at the side and above the bulkhead deck, Figure 4. As simulation begins and the damaged ship starts to move under the effect of random waves, the instantaneous water ingress is modelled by taking into account the wave height and ship motions which are also estimated at each time step. Simulations are carried out for different loading conditions and freeboards while the sea state used is progressively increased to a limit at which the ship capsizes systematically.

e) Loading Conditions and Freeboards

Three freeboards were used, simply by modifying the depth to the bulkhead deck, in order to investigate the influence of freeboard on the damage survivability of the vessel. These are 0.18m, 0.75m and 1.0 m. The associated loading conditions (KG's) and damaged GM's are given in Table 3 next.

Table 3: KG and GM Values Used in the Validation

KG (metres)	GM (metres)	GM factor
12.15	0.10	0.0058
11.75	0.50	0.0293
10.50	1.75	0.1026
8.90	3.35	0.1960

The GM factor is a non-dimensionalised GM which was used in [5], to present their model experiment results and is calculated by using the following expression:

$$GM\ factor = 10\ GM_f C_b T/B^2$$

f) Comparison Between Theoretical and Experimental Results

Figure 5 shows the results from the numerical experiments for all the freeboards considered with a mean boundary curve drawn through the results, in accordance with the presentation of the experimental results. A comparison between the mean boundary curve derived from the simulation results and the corresponding curve derived from physical model experiments, shows an exceptionally good agreement as illustrated in Figure 6.

On the basis of such boundary curves, survival criteria could now be developed. For example, the probability of ship survival could be derived directly from the weather statistics pertaining to the area of operation.

5. PRACTICAL APPLICATION OF THE NEW APPROACH

5.1 General

To demonstrate the practical applicability of the developed procedure, the influence of damage location and extent of flooding on the damage survivability of a modern car/passenger ferry in the presence of random waves is presently investigated. To this end, the dynamic behaviour of the vessel is assessed in a number of scenarios selected on the basis of maximising the danger of potential capsize (or sinkage) while taking into account actual accident records. The influence of different loading conditions is also examined by changing the vessel's KG.

5.2 Selection of Ship

The main particulars of the vessel chosen for this investigation are given in Table 4, with the general and subdivision arrangements shown in Figure 7. This ship sails in international waters. There are two car decks above the bulkhead deck and another half car-deck below it. It is interesting to note that compartmentation and damage stability calculations were carried out according to the probabilities approach. In this respect, with the vessel having side tanks at B/5 depth and the double bottom at B/10 depth, a large inner compartment is allowed, the length of which is limited by the requirement $A > R$. This particular ship has a 60m long inner compartment.

Table 4: Main Particulars of Vessel B

Length Between Perpendiculars (L_{BP})	169.50m
Breadth (B_{mld})	25.08m
Depth (D_{bhd})	7.85m
Draught (T_{mld})	6.12m
Displacement (D)	18,883 tonnes
KG (Design)	11.84m
GM (Intact)	1.80m

5.3 Description of Damage Scenarios

The UK Ro-Ro Research Programme has identified that damage near amidships is likely to lead to the most onerous situation in respect of the probability of capsizing. The most critical location of damage in this case is shown by the shaded area in Figure 8. Relevant information regarding the particulars of damage and sea states is as described in Section 4. With reference to Figure 8, a brief description of each of the damage scenarios considered is given here. In all the scenarios, simulation starts with the vessel at the intact upright condition in beam seas.

Table 5: Damage Scenarios

Scenario	Description
DS1	Side tank at B/5 depth damaged with cross-flooding in operation. The same damage with cross-flooding disabled is also considered. The capacity of the side tank is approximately 500 tonnes.
DS2	Side tank and vehicle deck damaged with cross-flooding in operation.
DS3	Side tank and inner compartment damaged with cross-flooding disabled.
DS4 (<i>Herald of Free Enterprise</i>)	Damaged vehicle deck above the bulkhead deck.
DS5	DS1 with cross-flooding disabled.
DS6 (<i>European Gateway</i>)	Combination of DS3 and DS4.

6. RESULTS AND DISCUSSION

In accordance with an earlier publication, [6], the vessel is judged to be safe, critical or unsafe depending on the roll angle attained. In this respect, a roll angle $>20^\circ$ is considered safe, between 20° and 40° critical and $>40^\circ$ unsafe. Based on this, the capsial resistance of the vessel was examined in each of the scenarios described above for a range of KG's (given in Table 6) and sea states. In the light of the derived results a number of noteworthy comments are presented next.

Table 6: KG's and GM's Used in the Scenario Analyses

KG (metres)	GM (meters)	GM factor
13.34	0.30	0.021
12.59	1.05	0.072
11.84	1.80	0.124
11.04	2.60	0.179
10.29	3.35	0.231

a) Damage Scenario 1 (Figures 9 and 10)

With the cross-flooding arrangement disabled, the static heel varies from 7° to 17.5° , depending on the KG, with the vessel capsizing at the highest KG. It will be noted from Figure 9b that the maximum roll angles occur at the intermediate stages of flooding. With the cross-flooding arrangement in operation and the vessel KG at 12.59m (GM factor 0.072) a sudden increase in the roll oscillation occurs which is believed to be the result of parametric excitation due to heave, the heave period being half the roll period for this case. This is shown in Figures 10b and 10c and reflected in Figure 9a which also provides a clear illustration of the importance of dynamics in assessing the damage survivability of ships. The damage survivability diagrams of Figures 9a and 10a suggest that the vessel could survive this damage, with or without a cross-flooding arrangement, at even extreme sea states and higher than design KG's.

b) Damage Scenario 2 (Figure 11)

When the vehicle deck is damaged, the capsizal resistance of the vessel reduces substantially with the vessel capsizing very rapidly at extreme sea states irrespective of KG and at moderate sea states with high KG's. The dominant nature of the flood water on the vehicle deck on the vessel behaviour can be seen clearly in Figures 11b and 11c.

c) Damage Scenario 3 (Figure 12)

This scenario aims to address the danger in using large inner compartments beyond the B/5 depth at side. If this compartment is to be flooded, the margin line will immerse below the waterplane by nearly a metre at the design KG. In addition, transient and parametrically excited roll motion in the presence of waves will exacerbate the ensuing problems. It is interesting also to note that the parametrically excited roll motion, which appears to be absent at 1m Hs, becomes evident at the higher sea states as shown in Figures 12b and 12c. The damage survivability diagram of Figure 11a suggests that this damage scenario could cause a great threat to the vessel's survivability.

d) Damage Scenario 4 (Figure 13)

This scenario has been dealt with previously, [8], where it has been clearly demonstrated that flooding of the vehicle deck is very dangerous with vessels capsizing very rapidly when progressive flooding taking place, the rate dictated by the KG. In addition, the flood water on the vehicle deck governs the vessel behaviour which in the majority of cases tends to be quasi-

static, and hence predictable. In this respect, the roll motion and flood water follow identical trends as shown in Figures 13b and 13c.

e) Damage Scenario 5 and 6 (Figures 14 and 15)

These scenarios depict progressive flooding of the vehicle deck with some degree of asymmetry and sinkage both of which reduce the effective freeboard and hence exacerbate flooding of the vehicle deck. As a result the vessel under examination could not survive either of these scenarios even at the lowest of sea states and KG's. Again the dominant influence of the water on deck in both cases is evident.

7. CONCLUDING REMARKS

On the basis of the foregoing investigations the following points are worth noting:

- A realistic theoretical model has been developed capable of assessing the survivability of a damaged ship in a random sea while allowing for water ingress. Applications so far have focused on Ro-Ro's but the approach adopted and the developed numerical simulation model could be applied widely to other hull forms and ship types and sizes. This, in turn, offers a unique "tool" to re-examine the damage stability of ships, perhaps within the logical framework of the probabilistic method.
- In assessing the damage survivability of ships, the analyses of realisable damage scenarios that a vessel may have to survive offers substantial insights on the vulnerability of a vessel type as well as an invaluable aid to the designer to evaluate alternative designs or subdivision arrangements.
- In relation to Ro-Ro vessels, research so far has clearly demonstrated the need for improving their capsizal resistance when flooding of the vehicle deck takes place. In all cases considered this appears to be the determining factor affecting vessel capsize.
- The only meaningful approach to improving the survivability of a damaged ship is by taking full account of her dynamic behaviour in a realistic environment.

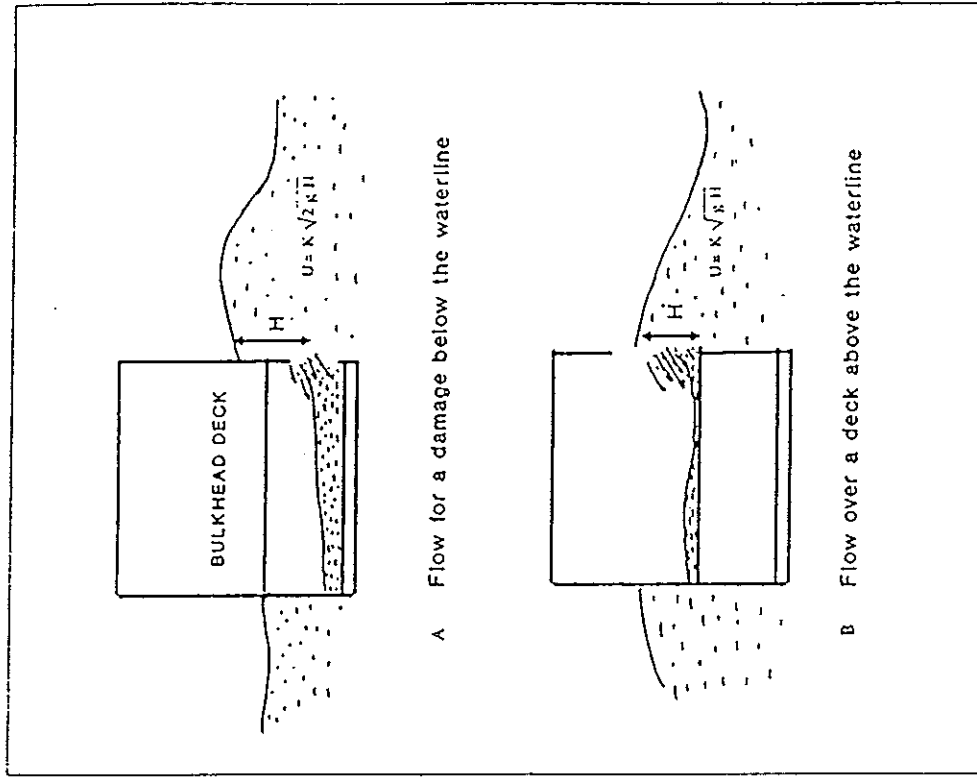
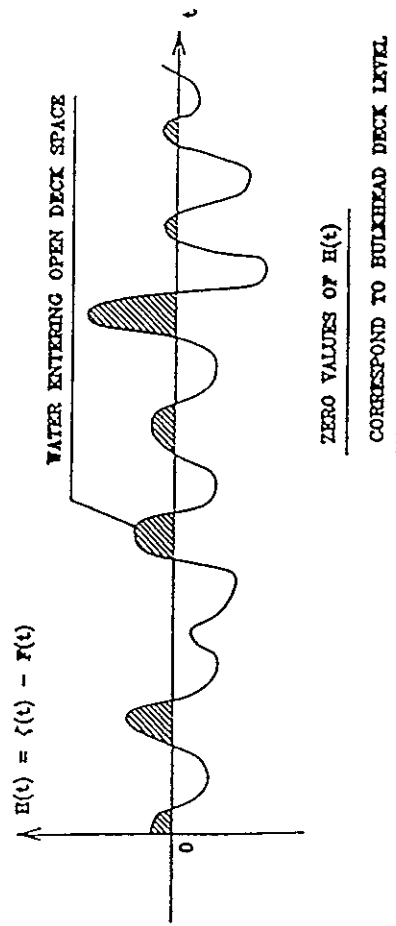
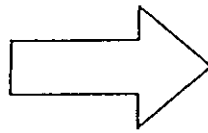
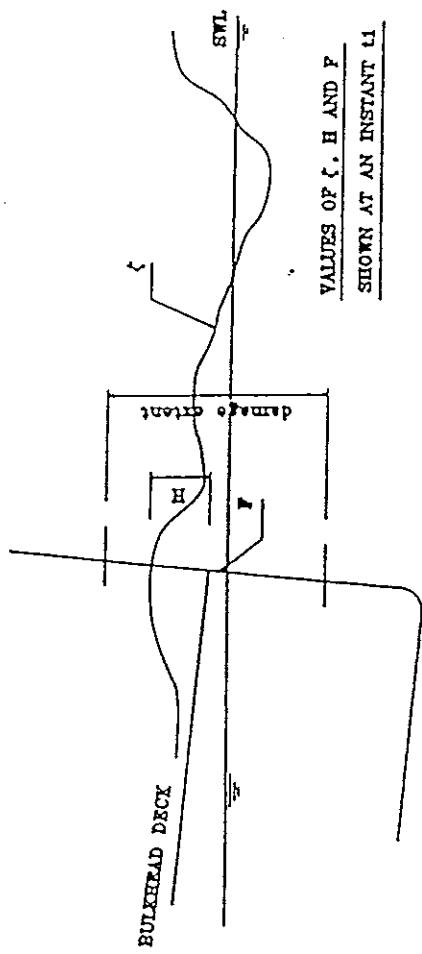


Figure 1: Water Ingress as an Intermittent Probabilistic Event

Figure 2: Models of Water Ingress

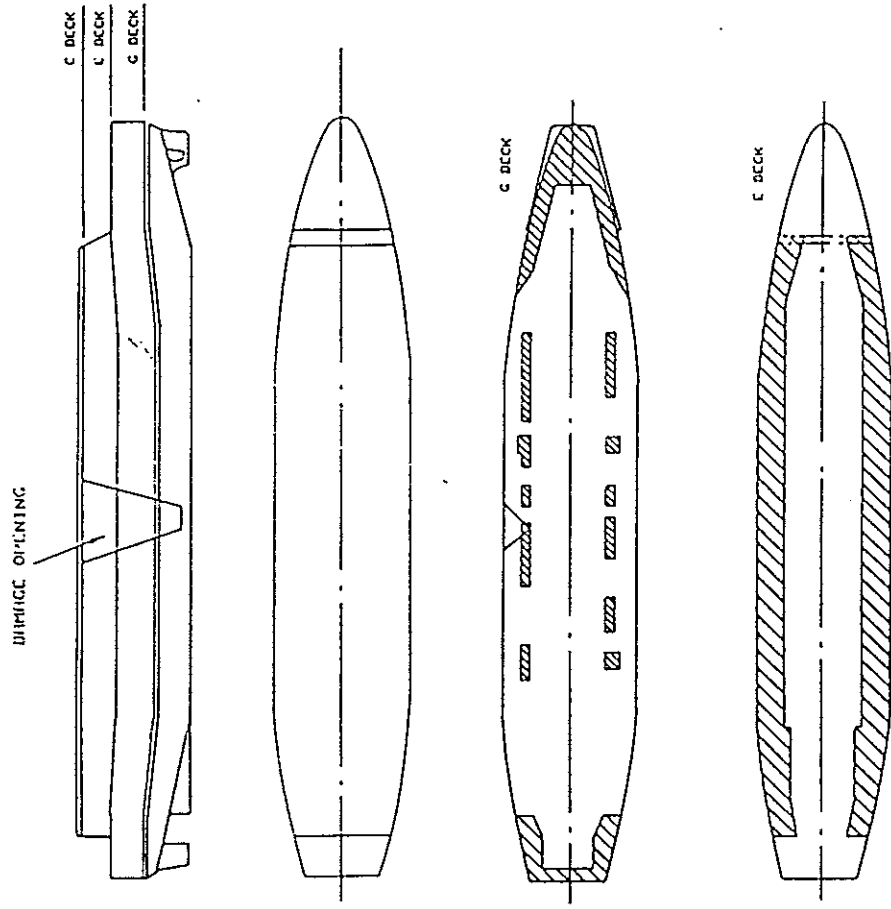


Figure 3: General Arrangement Plans (Vessel A)

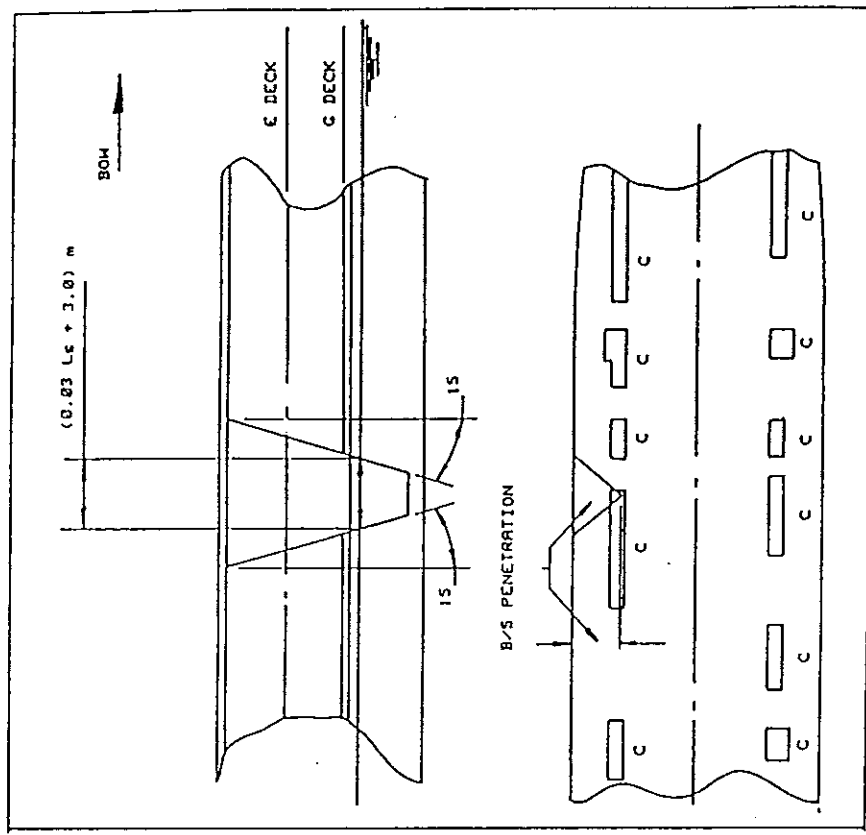


Figure 4: Particulars of the Damage Opening

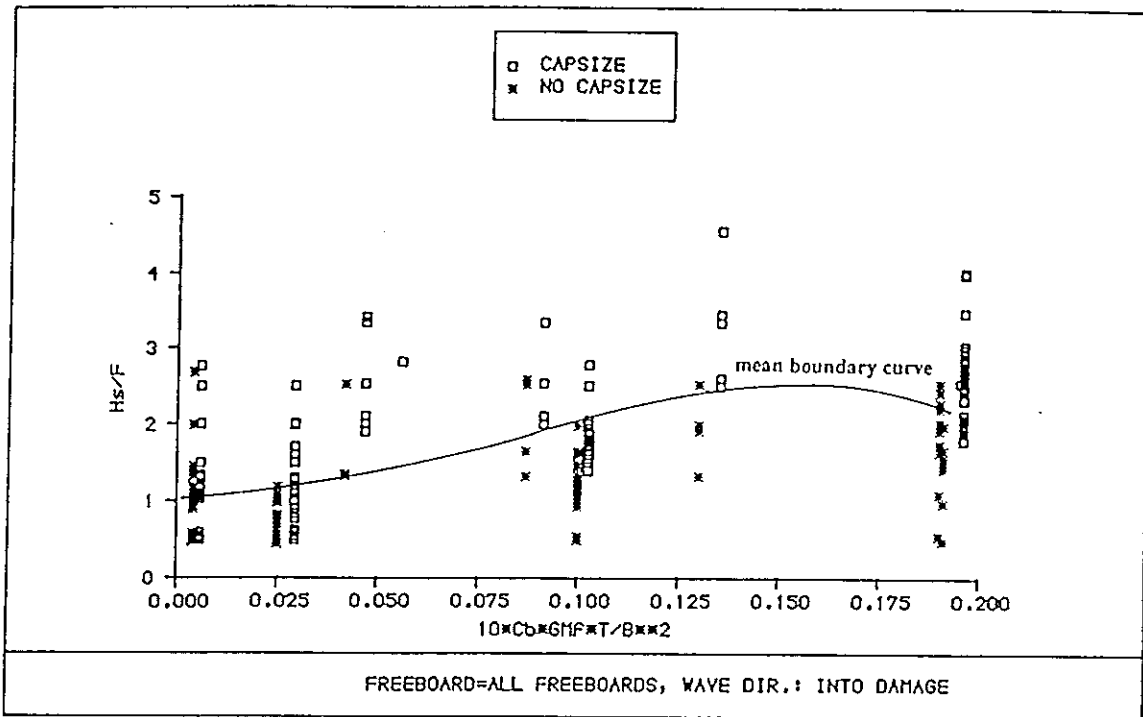


Figure 5: Effect of Ship Design and Environmental Parameters on Damage Survivability

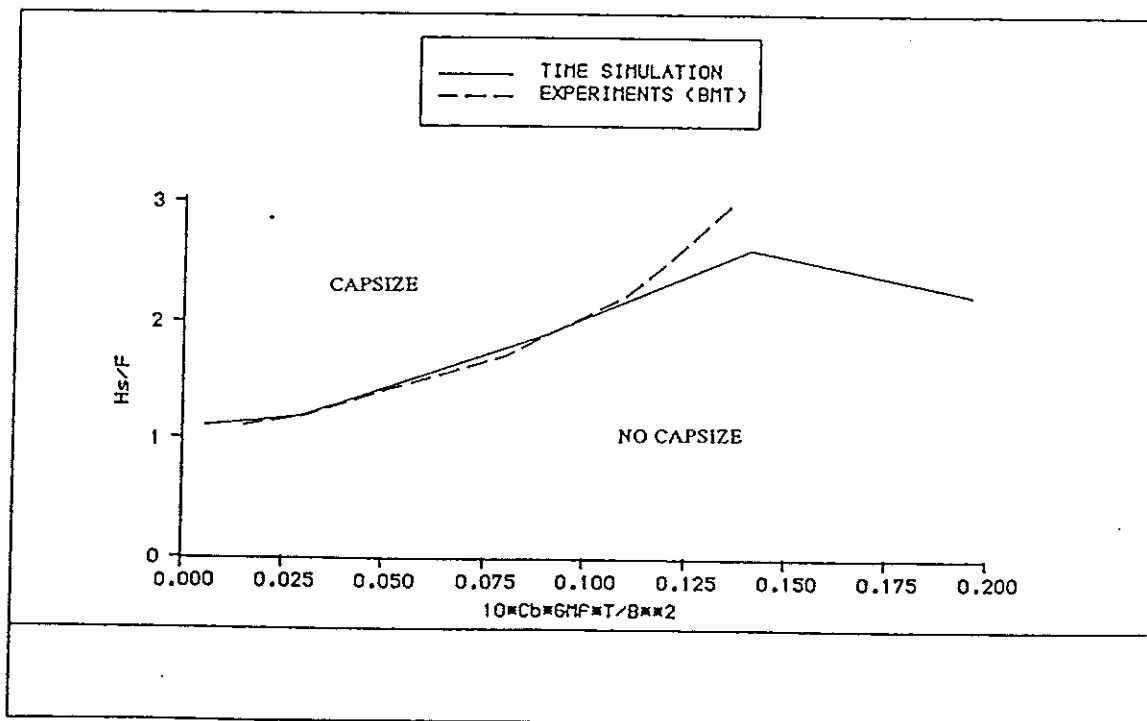


Figure 6: Comparison Between Theoretical and Experimental Results

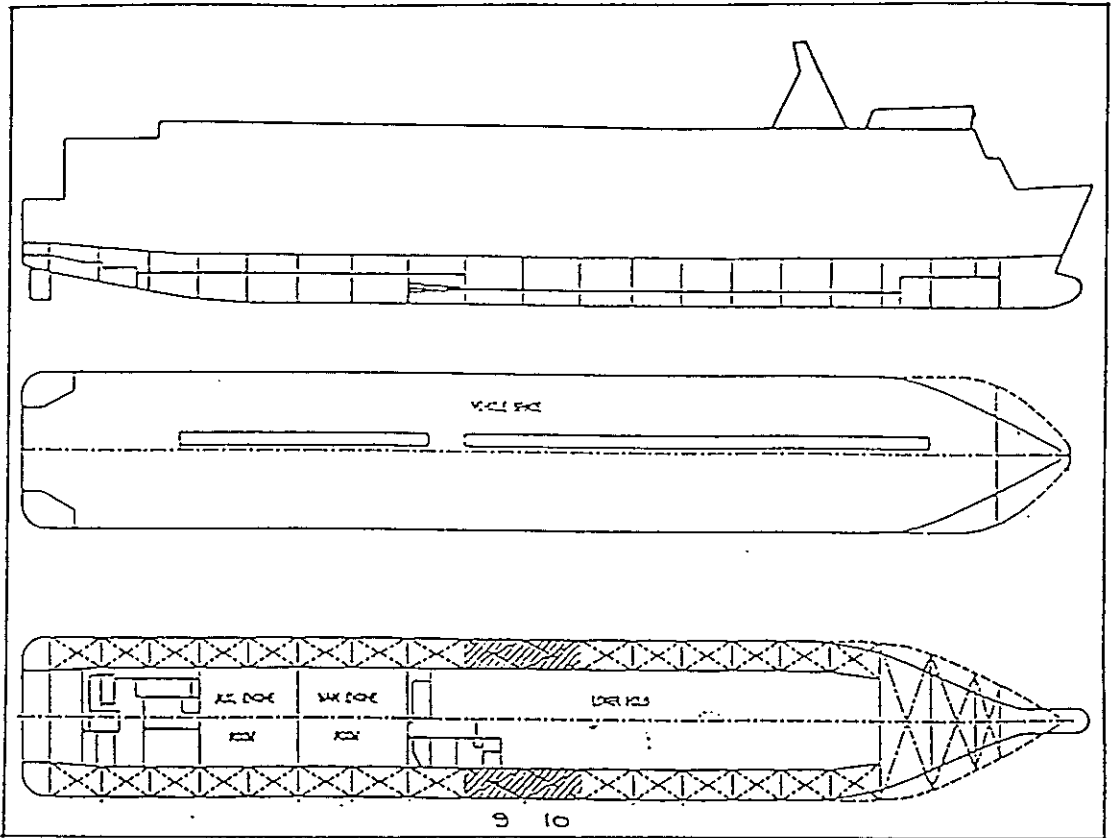


Figure 7: General and Subdivision Arrangement Plans (Vessel B)

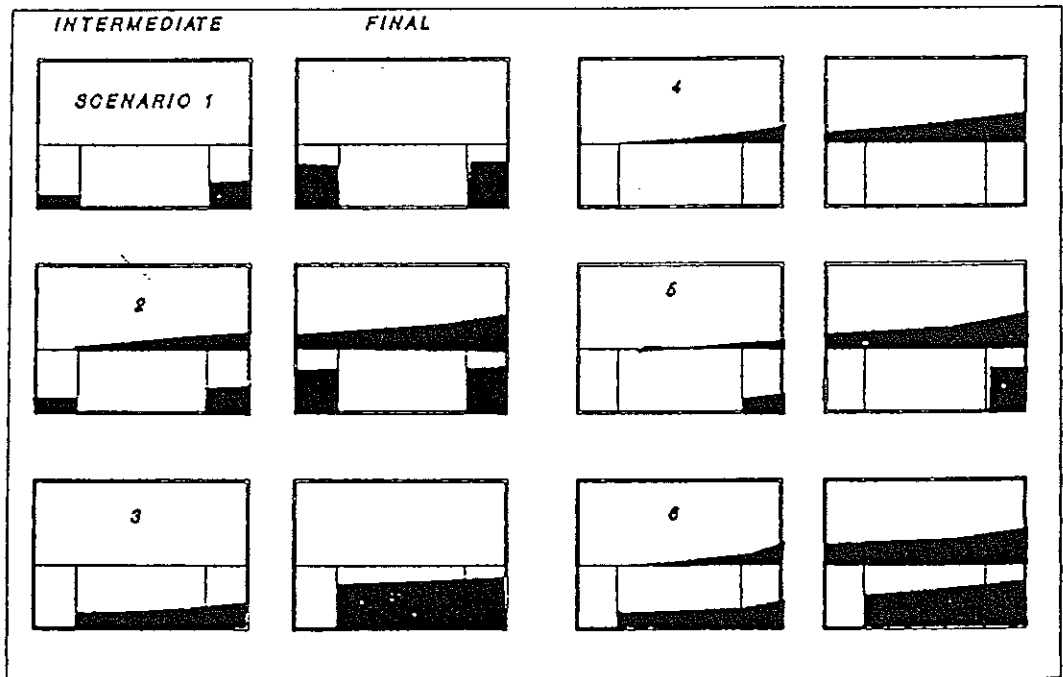
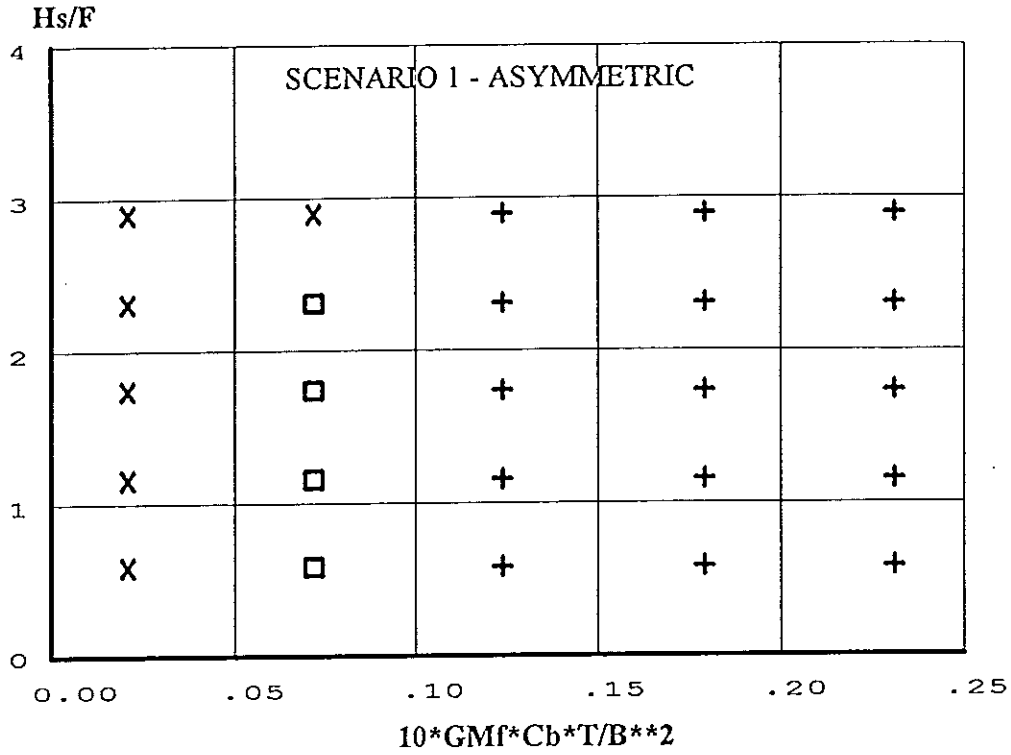
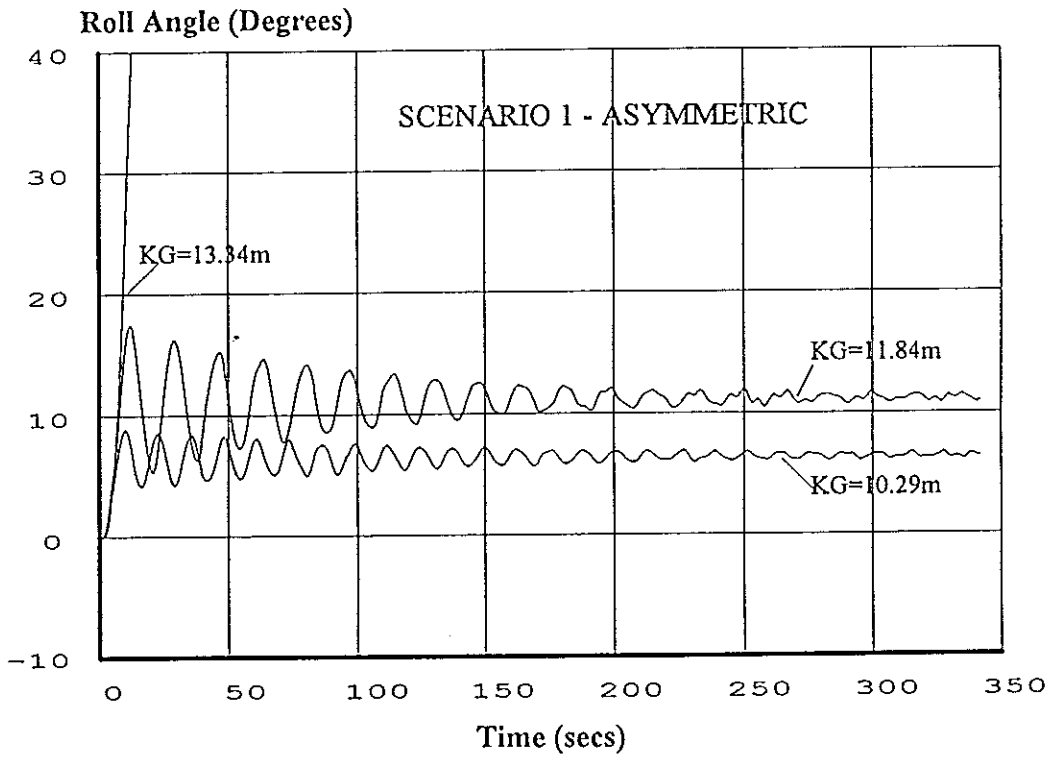


Figure 8: Pictorial Description of Damage Scenarios

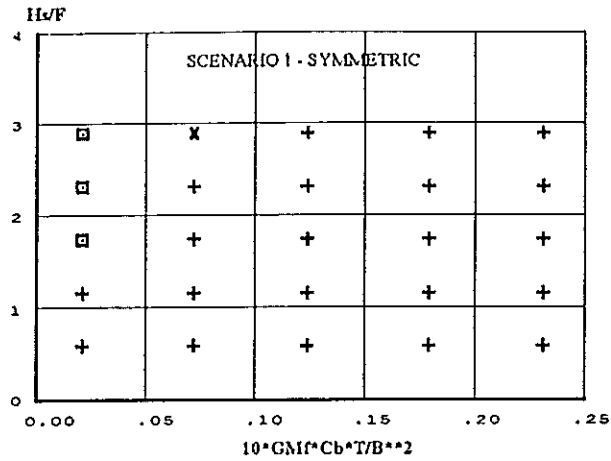


a) Damage Survivability Diagram
 + safe; □ critical; x unsafe

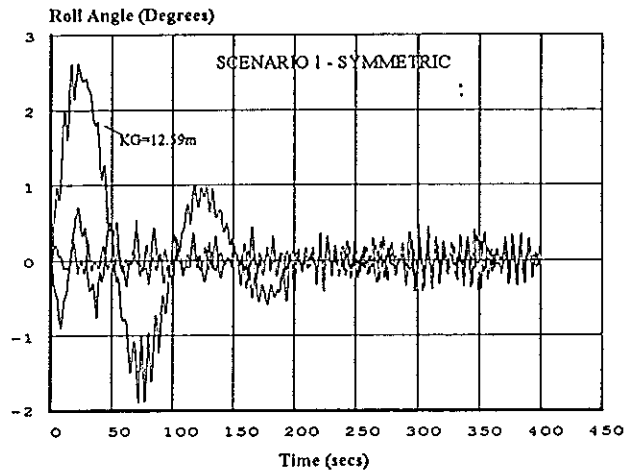


b) Roll Motion Realisations; Hs=1m, To=4.5s

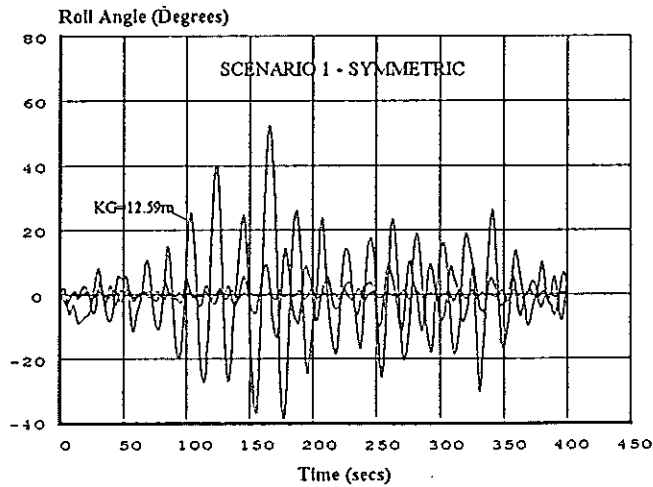
Figure 9: Effect of Damage Location & Extent on Survivability



a) Damage Survivability Diagram
 + safe; □ critical; x unsafe

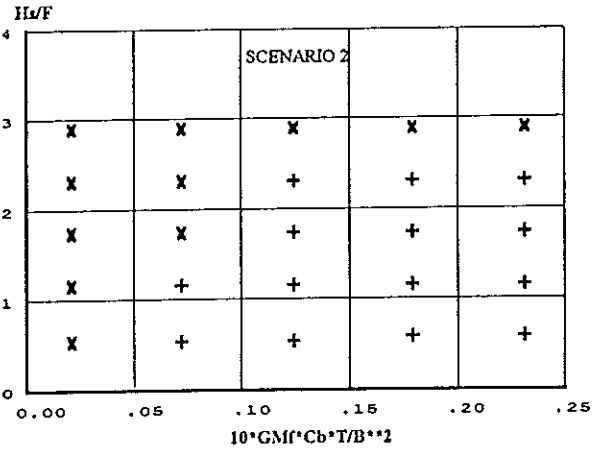


b) Roll Motion Realisations; H_s=1m, T_o=4.5s

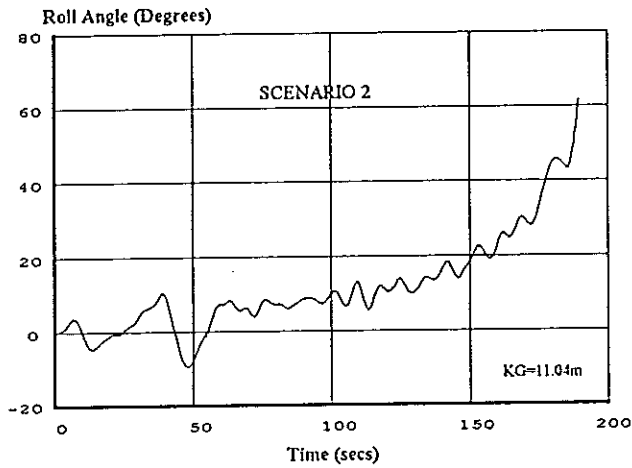


c) Roll Motion Realisations; H_s=5m, T_o=6.5s

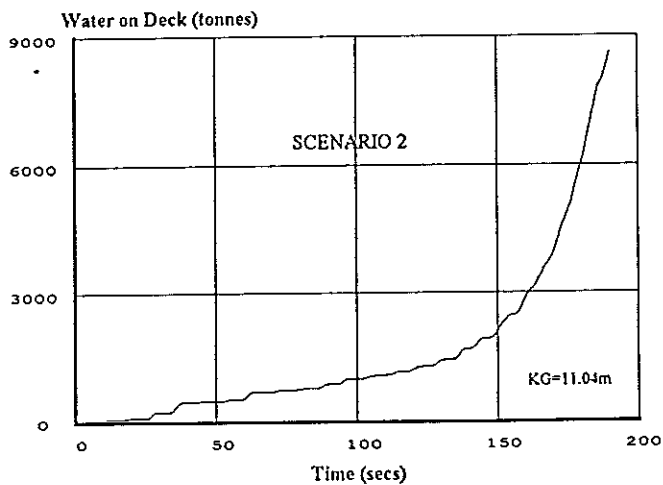
Figure 10: Effect of Damage Location & Extent on Survivability



a) Damage Survivability Diagram
 + safe; □ critical; x unsafe

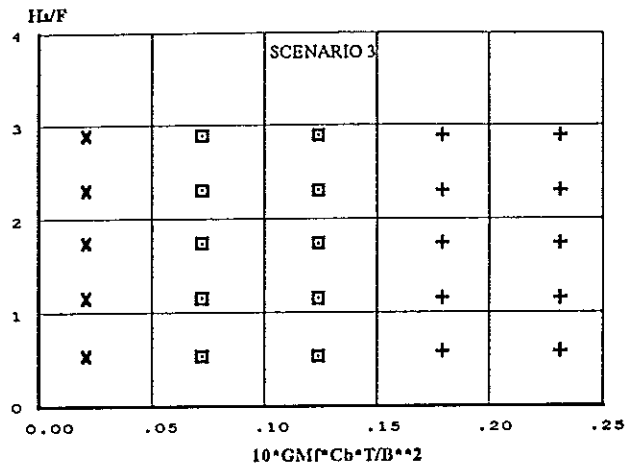


b) Roll Motion Realisation; Hs=5m, To=6.5s

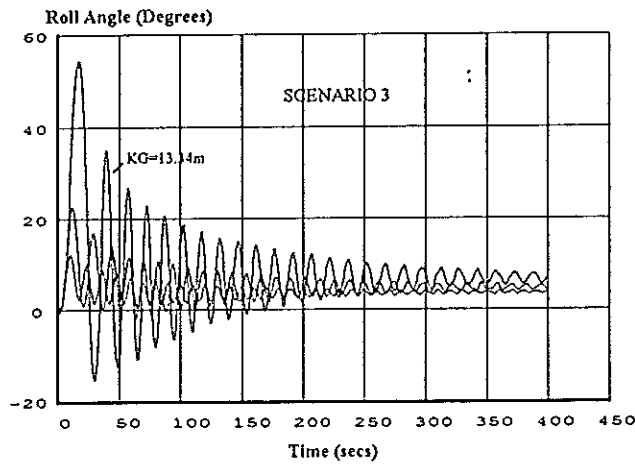


c) Flood Water on the Vehicle Deck; Hs=5m, To=6.5s

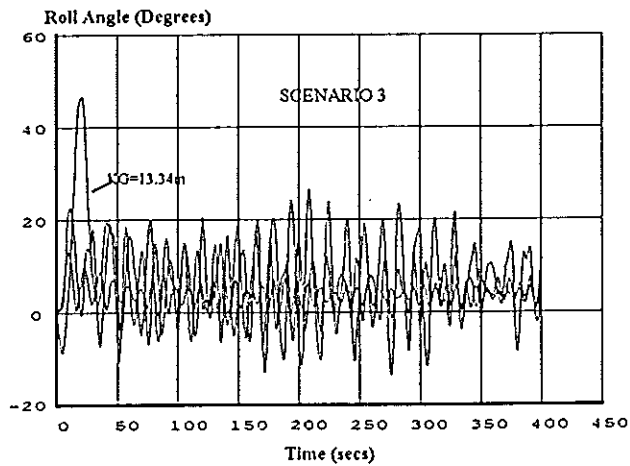
Figure 11: Effect of Damage Location & Extent on Survivability



a) Damage Survivability Diagram
 + safe; □ critical; x unsafe

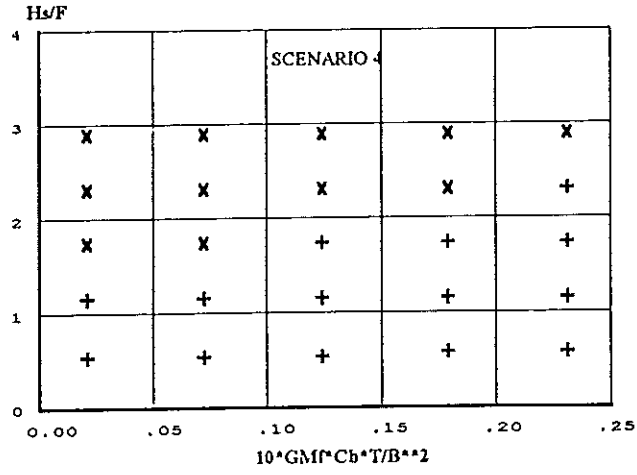


b) Roll Motion Realisations; $H_s=1m$, $T_o=4.5s$

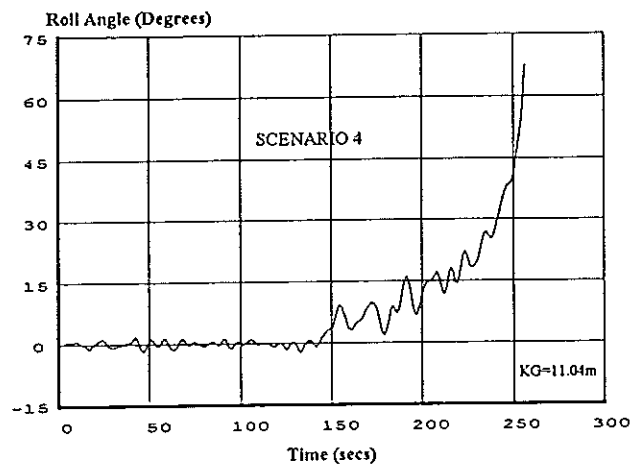


c) Roll Motion Realisations; $H_s=5m$, $T_o=6.5s$

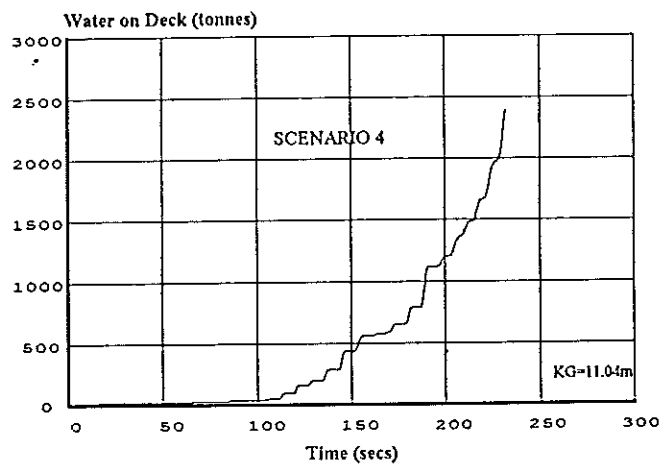
Figure 12: Effect of Damage Location & Extent on Survivability



a) Damage Survivability Diagram
 + safe; □ critical; x unsafe

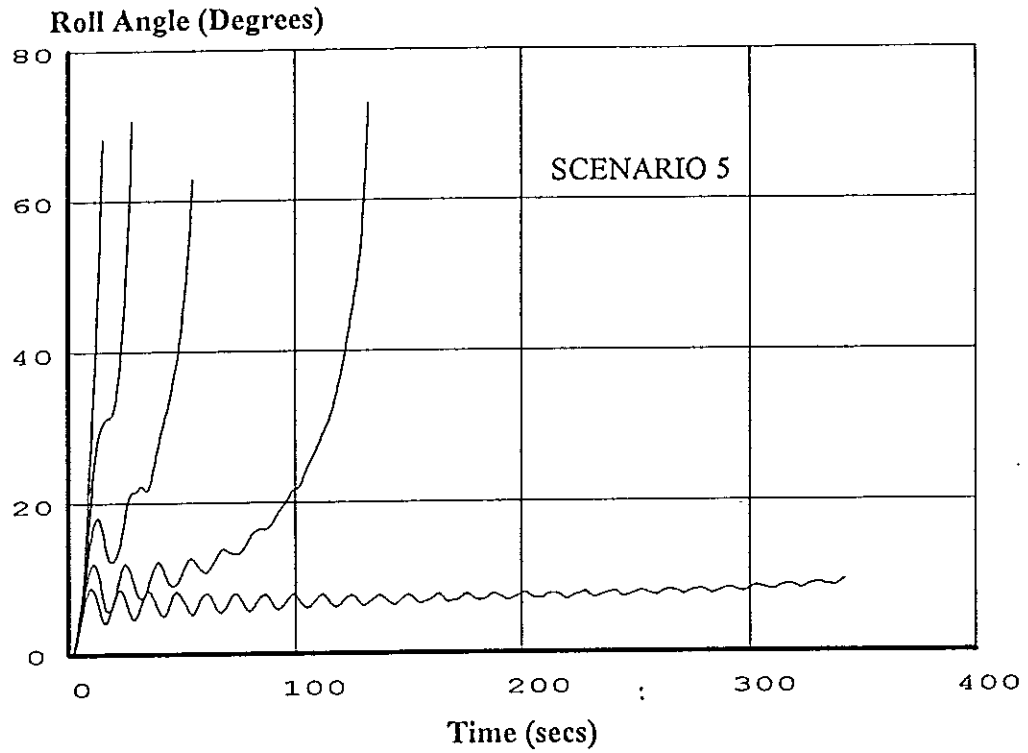


b) Roll Motion Realisation; Hs=5m, To=6.5s

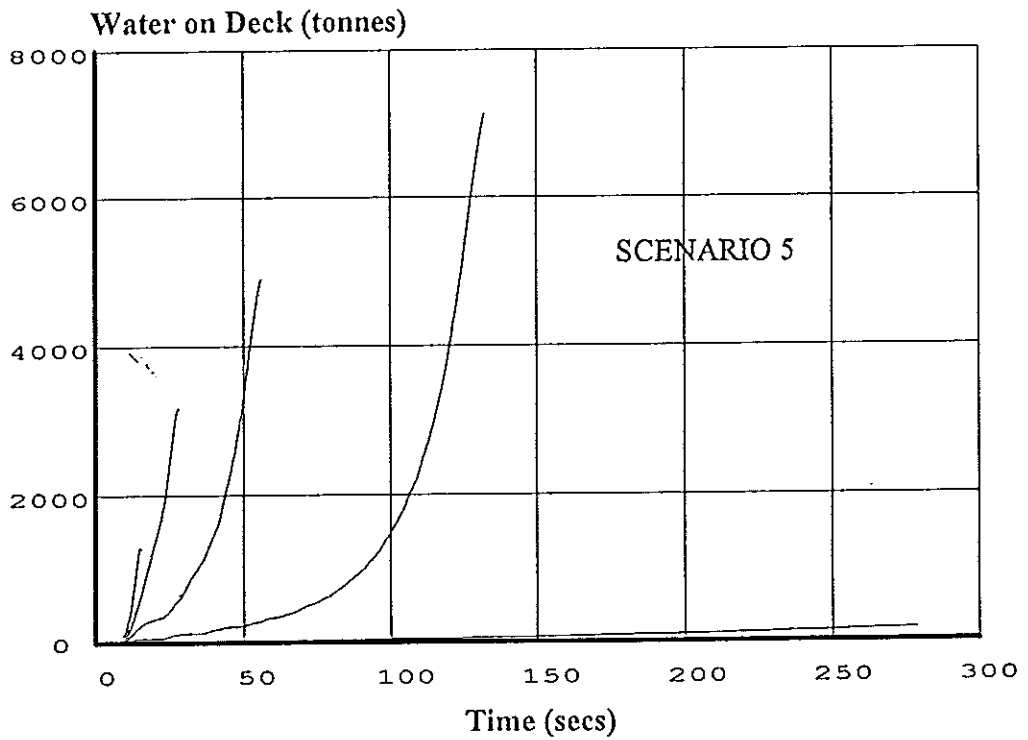


c) Flood Water on the Vehicle Deck; Hs=5m, To=6.5s

Figure 13: Effect of Damage Location & Extent on Survivability

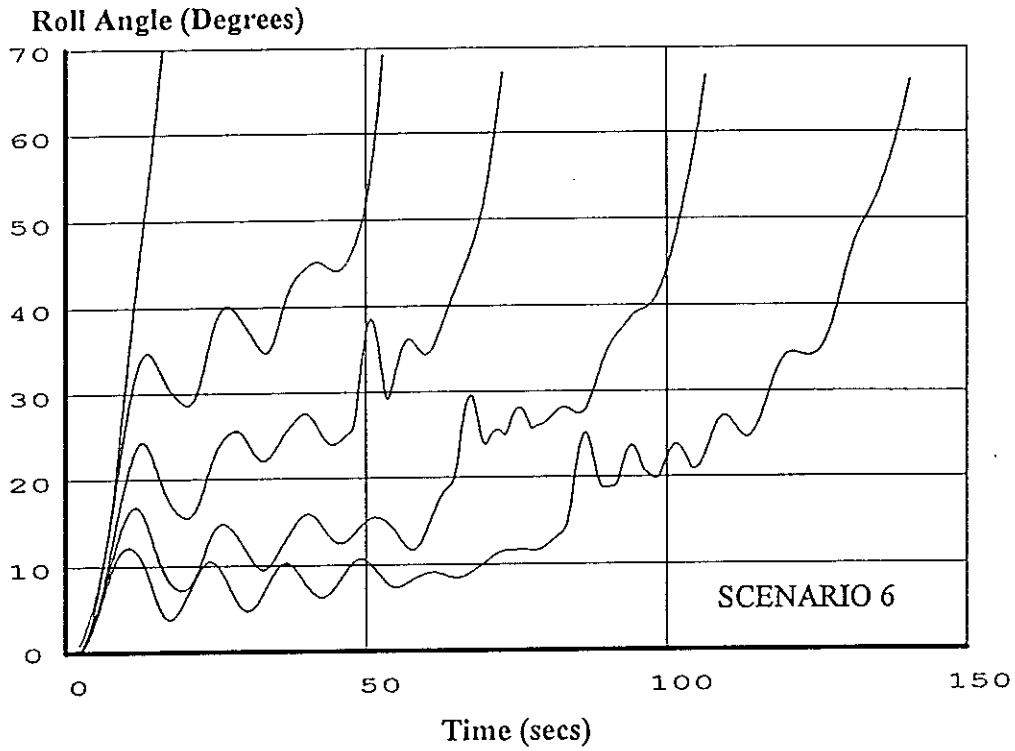


a) Roll Motion Realisations for a Range of KG's; $H_s=1m$, $T_o=4.5s$

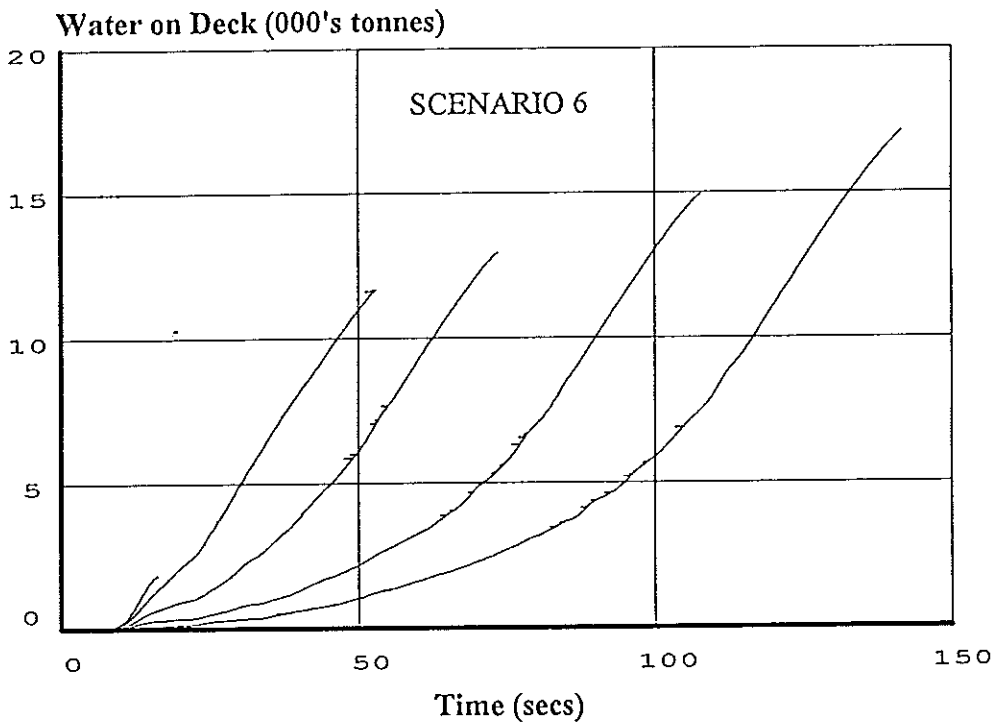


b) Flood Water on the Vehicle Deck for a Range of KG's; $H_s=1m$, $T_o=4.5s$

Figure 14: Effect of Damage Location & Extent on Survivability



a) Roll Motion Realisations for a Range of KG's; $H_s=1m$, $T_o=4.5s$



b) Flood Water on the Vehicle Deck; $H_s=1m$, $T_o=4.5s$

Figure 15: Effect of Damage Location & Extent on Survivability

8. ACKNOWLEDGEMENTS

The support of the Department of Transport in undertaking part of this research is gratefully acknowledged. Thanks are also due to Ms Morag Rutledge for her help in the preparation of this paper.

9. REFERENCES

- [1] **IMO Resolution A.265 (VIII)**, "Regulations in Subdivision and Stability of Passenger Ships as Equivalent to Part B of Chapter II of the International Convention for the Safety of Life at Sea 1960", IMO, London, 1974.
- [2] **Bird, H. and Browne, R.O.**, "Damage Stability Model Experiments", Trans. RINA, Vol. 116, 1974, pp. 69-91.
- [3] **Middleton, E.H. and Numata, E.**, "Tests of a Damage Stability Model in Waves", SNAME Spring Meeting Paper No.7, April 1970, Washington D.C.
- [4] "Research Into Enhancing the Stability and Survivability Standards of Ro-Ro Passenger Ferries: Overview Study", BMT Ltd., Report to the Department of Transport, March 1990.
- [5] **David, I.W.**, "Experiments with a Floodable Model of a Ro-Ro Passenger Ferry", BMT Project Report to the Department of Transport, BMT Fluid Mechanics Ltd., February 1990.
- [6] "Ro-Ro Passenger Ferry Studies, Model Tests for F10", Danish Maritime Institute, Final Report of Phase I to the Department of Transport, DMI 88116, February 1990.
- [7] **Vassalos, D. and Turan, O.**, "Development of Survival Criteria for Ro-Ro Passenger Ships - A Theoretical Approach", Final Report on the Ro-Ro Damage Stability Programme, Phase II, Marine Technology Centre, University of Strathclyde, December 1992.
- [8] **Vassalos, D. and Turan, O.**, "A Realistic Approach to Assessing the Damage Survivability of Passenger Ships", SNAME Annual Meeting, New Orleans, Nov. 1994.

STABILITY CRITERIA: DEVELOPMENT OF A FIRST PRINCIPLES METHODOLOGY

by

William H. Buckley

To Be Presented At The Fifth International Conference On Stability Of Ships and Ocean
Vehicles, 7-11 November 1994

STABILITY CRITERIA: DEVELOPMENT OF A FIRST PRINCIPLES METHODOLOGY

by
William H. Buckley

THE AUTHOR

Recently retired from the David Taylor Research Center. He received bachelor degrees in Aeronautical Engineering ('48) and Business Administration ('49) from the Massachusetts Institute of Technology and a Master of Science Degree in Ocean and Marine Engineering ('82) from the George Washington University. He was employed for 20 years by the Bell Aerospace Company where he was responsible for structural design criteria and loads for the X-22A aircraft, SKMR-1 air cushion vehicle and SES-100B surface effect ship. He joined the U.S. Navy's David Taylor Research Center in 1971 where he conducted hydrofoil structural loads research. In 1978 he initiated a loads research program for displacement ships with emphasis on casualty analysis, statistical analyses of non-linear random processes, extreme wave characteristics and most recently the development of world wide seaway criteria and its use in a first principles design methodology.

ABSTRACT

This paper summarizes recent developments in the establishment of seaway criteria which are suitable for use in a First Principles Methodology (FPM) approach to ship design. The establishment of seaway criteria employing Operability and Survivability envelopes for Northern and Southern hemispheres is described together with three parameter approximations to the measured wave spectra used in defining the envelopes. The nonlinearity of hurricane driven waves associated with the Seaways of Limiting Steepness segment of the Survivability envelope is identified. Initial results of test tank and computer modeling of hurricane seaway are described.

The necessity for identifying critical design conditions in an FPM approach to ship design is discussed together with certain aspects of resolving this problem. Critical design conditions associated with ship stability matters are discussed in the light of previous free-running model capsizing experiments and case testimony relating to the loss of the M/V TUXPAN in a severe winter storm. The role which analytical methods should play in the near and long term are described. Response criteria are discussed considering several cases of practical importance to ship stability in Survivability seaways.

Recommendations are briefly summarized for furthering the development of FPM. An update of findings regarding episodic wave characteristics is presented in an appendix.

INTRODUCTION

What is meant by First Principles Methodology? FPM employs operational and seaway criteria which broadly define required ship performance, safety and durability characteristics. It employs analytical methods by means of which required seakeeping and structural characteristics can be achieved. These methods employ quantitative cause and effect relationships involving basic design variables thereby facilitating design trade-offs and optimizations.

What benefits does it offer? FPM is most useful in the design of ships which (a) have unique characteristics such that existing empirical criteria and analytical methods are not appropriate, or (b) have failed to perform as required when designed using empirical methods. In the long term it is expected that the as-designed safety and utility of all ships will also be improved.

This paper describes the major elements of FPM and the manner in which they interrelate. Recent progress in the establishment of Seaway Criteria is summarized together with a recommended approach

simulating extreme seaways. Critical Design Condition Criteria as they relate to ship stability problems are considered next together with examples of ship losses which have been examined in the light of recent seaway criteria developments. This is followed by a brief discussion of the role of Analytical Methods and Response Criteria. Recommendations are offered for further development of seaway criteria, seaway simulations and methods for identifying critical design conditions as required by an FPM approach to ship stability criteria. Definitions and an update of episodic wave information are appended.

ELEMENTS OF A FIRST PRINCIPLES METHODOLOGY

The elements are:

Operational Requirements which identify ocean areas and routes of operation, speeds in calm and rough water, design displacements and operational life.

Seaway Criteria which define both world-wide climatic (i.e. long-term average) wave conditions and extreme storm wave conditions. The scope of each of these may be significantly reduced if the operating areas are restricted. These criteria will generally involve wave spectrum formulations for linear response analyses and time domain formulations for nonlinear analyses. In the case of the latter both random wave and episodic wave conformations must be considered.

Critical Design Condition Criteria identify those particular wave and operating conditions which a designer should consider in satisfying Response Criteria. When identifying critical wave conditions the entire range of the Seaway Criteria should be considered. Critical Design Conditions are likely to be different for each area of concern in seakeeping and structural design (e.g. severe rolling, broaching, slamming, deck wetness, wave impact loads etc.).

Analytical Methods which permit the establishment of ship design characteristics which satisfy Critical Design Condition and Response Criteria. These methods must lead ultimately to deterministic results for design purposes. Methods must be available for both preliminary and final design, and must be suitable for analyzing linear and nonlinear responses and apply to local or global hull areas as the problem at hand requires.

Response Criteria which define acceptable or unacceptable behavior of a ship under Critical Design Conditions for seakeeping and structural design purposes.

With respect to these elements it is important to note that they are strongly interrelated. Seaway Criteria for example must not only encompass world wide wave conditions, but it must be expressed in a format that permits analytical methods to lead directly to design values of loads and motions. Similarly, Response Criteria should relate in a straight forward manner to the output of Analytical Methods. It will be noted that analytical methods are not suggested here as being design criteria so as to avoid impeding state-of-the-art developments in this area.

SEAWAY CRITERIA

This section is a synopsis of ref.1 which contains details of the developments summarized here. In order to clarify some of the unfamiliar concepts involved, the Definitions section of ref.1 is presented in Appendix A. Because of its importance to FPM development, the viability of simulations of the proposed seaway criteria is considered here.

A BASIS FOR SEAWAY CRITERIA DEVELOPMENT

The primary source for the seaway criteria presented here is a National Oceanic and Atmospheric Administration (NOAA) data base of over 2 million wave spectrum measurements from buoys moored in a wide variety of offshore wave climates. The wave spectra measured at each of the 13 buoy stations considered were obtained over a period of more than 12 years. Climatic Wave Spectra (CWS) have been determined for significant wave height (H_{m0}) class intervals of one meter. In order to characterize the

wave climate at each buoy station, the modal period (T_p) for each CWS was plotted vs H_{m_0} . For those groups of buoy stations which were found to have similar trend lines of H_{m_0} vs T_p , a Generalized Wave Climate trend line was established as discussed below. For each generalized trend line three parameter (closed form) wave spectrum approximations were determined which provided close approximations to the measured CWS. The upper bound of each trend line was terminated at an averaged annual maximum H_{m_0} value corresponding to one occurrence per year. The curve formed by this upper bound and by the more extreme wave climate trend lines serve to define a baseline Operability envelope.

Using individual outlying values of H_{m_0} vs T_p from severe storms an empirical envelope of extreme values was drawn. For wave spectra from very steep seas a parametric boundary was identified and designated Seaways of Limiting Steepness. Using extreme spectra from seaways of lesser steepness, a connecting boundary was drawn and labeled Seaways of Extreme Significant Wave Height. The resulting envelope defined the baseline Survivability envelope. Based upon the associated measured wave spectra, generic three parameter spectrum approximations were defined for both envelopes and associated trend lines.

As a result of comparisons of NOAA buoy wave data and data from other sources for the same ocean areas, it was concluded that the percentage occurrences of high values of significant wave height given in ref. 2 appeared to be reliable for open ocean areas. Using this data source, the NOAA baseline envelopes were expanded to establish Operability and Survivability envelopes for northern and southern hemispheres. Using the measured wave spectra which defined the Baseline envelopes, closed form approximations were defined for the hemispheric envelopes.

Inasmuch as time series wave height data for NOAA buoys have not been available for use in approximating critical wave conformations, this initiative has not been developed with one important exception.

NOAA BASELINE ENVELOPE DEVELOPMENT

The baseline Operability envelope which was derived from NOAA buoy data is defined by the dashed lines in Figure 1. The Climatic Steep Seas modal period trend line was derived from East Coast and Gulf of Mexico buoy data such that the steepness of this empirical trend line was approached but not exceeded by either data set. The Climatic Long Period Seas trend line was based upon data from Pacific buoys located between 40 and 50 deg N. Lat. The modal period of the empirical trend line was also approached but not exceeded. The Climatic Northern High Latitude Seas trend line was determined using data from Pacific buoys above 50 deg N. Lat. In this case the trend line was developed as an approximation to the CWS data where some liberties were taken in matching the data in order to obtain a coherent trend intermediate to the foregoing trend lines. It is noteworthy that when modal period data from other sources (mostly from North Atlantic ocean weather ships) were plotted on Figure 1 they fell relatively close to this trend line. In the case of Ochi's "most probable spectrum for mean North Atlantic", the results fell close to the NOAA buoy data in question except at low values of H_{m_0} .

The upper bound of the Operability envelope was determined using the "average of annual maximums" statistics presented in Table 5 of ref.1. A further average of maximums for the individual buoy stations in each wave climate was taken which led to the "Defining Points" of Figure 1.

Satisfactory closed form approximations to those individual CWS which fell closest to the three trend lines were found using Ochi's three parameter formulation which is defined in Appendix A. This formulation permits matching H_{m_0} , f_p and peak energy density for each CWS. Figure 2, for example, presents the results of approximating CWS from the Gulf of Mexico. λ is the shape parameter for the spectrum approximation while "n" is the number of individual spectra averaged in obtaining the CWS. In the case of data from the East Coast offshore buoys (which share the same Climatic Steep Seas trend line) multiple Ochi 3p spectra were generally required to obtain good approximations. The Gulf of Mexico

CWS approximations were more peaked (i.e. had higher values of λ) than those for East Coast CWS which reflected a more prevalent mix of sea and swell waves in the latter area. Single Ochi spectrum approximations were satisfactory for those CWS from NOAA buoys which established the Climatic Northern High Latitude Seas trend line. This was also true of CWS from the buoys which established the Climatic Long Period Seas trend line except for the two lowest values of H_{m_0} . Figure 24 of ref.1 provides a comparison of the peakedness of the CWS approximations for the four data sets. It shows that the Gulf of Mexico CWS are the most peaked while CWS for Pacific buoys from 40 to 50 deg N.Lat. are the least peaked. Ochi shape parameters (λ) for all single spectrum approximations for the Operability envelope are summarized in Figures 26 and 27 of ref.1 while parameters for all multiple Ochi 3p approximations for the Operability envelope are given in Table 15 of ref.1.

Statistics defining the percentage occurrence of H_{m_0} values are more difficult to generalize. For reference purpose these statistics are given in Tables 16 thru 20 of ref.1 for the thirteen NOAA buoy stations considered in defining Generalized Wave Climates.

The baseline Survivability envelope which was derived from NOAA buoy data is shown by the solid lines in Figure 1. It consists of two segments which are designated Seaways of Limiting Steepness and Seaways of Extreme Significant Wave Height. The former resulted from an earlier search for wave spectra from steep, storm driven seaways in the NOAA data base. These spectra led to an empirical boundary corresponding to $H_{m_0}/T_p^2 = 0.00776 g$. Confirmation of this boundary was subsequently obtained from an independent (Canadian) data base of measured spectra as shown in Appendix A to ref.1. The upper end of the boundary was terminated at values of H_{m_0} and T_p using data obtained at an offshore platform during hurricane Camille. As shown in Figure 3, with the exception of this point the connecting Seaways of Extreme Significant Wave Height boundary was drawn with a small margin on measured values of H_{m_0} vs T_p , i.e. roughly one-half meter for the points corresponding to maximum H_{m_0} and approximately one second for points corresponding to maximum T_p . This was done to forestall the need for revising this empirical boundary for small increases in H_{m_0} or T_p measured in subsequent storms. The establishment of closed form approximations to extreme spectra was accomplished using the three parameter Modified JONSWAP spectrum formulation defined in Appendix A. As in the case of the formulation used to approximate CWS, this selection was based entirely on the quality of data fit which was achieved. The identification of individual spectra which fell close to the Seaways of Limiting Steepness boundary encountered several problems which lead to the scarcity of spectra evident in Figure 3. For values of H_{m_0} above about 8 meters, the rapidly developing winter storms which produce steep seas tended to shift to significantly longer modal periods for increasing values of H_{m_0} as the seaway matured. At low values of H_{m_0} it is common to find swell wave energy mixed in with the steep wind driven seas. This resulted in few acceptable spectra given that the selection criteria sought steep, wind driven seaways in which the majority of the wave energy was wind driven. (The swell wave component of open-ocean seaway development also produced occasional violations of the empirical Seaways of Limiting Steepness boundary at low values of H_{m_0} because a swell wave constituent generally increases H_{m_0} but not T_p with the result that such a seaway can plot somewhat above it). Modified JONSWAP approximations to the selected spectra are shown in Figure 4 with the associated values of the shape parameter γ . Approximations to the selected spectra from Seaways of Maximum H_{m_0} are shown in Figure 5. In a marked contrast to the spectra of Figure 4, the values of the shape parameter are nearly constant. Figure 6 presents the range of values of γ recommended for spectra associated with the entire Survivability envelope.

EXTRAPOLATION OF NOAA BASELINES

Inasmuch as the NOAA buoy locations involve only a fraction of the earth's ocean areas, extending the baseline seaway criteria to provide world-wide, open-ocean area coverage presented a significant problem. Only three atlases were known to provide the wide area coverage necessary:

- a) U.S. Navy SOWM Hindcast Wave Climatology Data for North Atlantic and North Pacific oceans. This data base had previously been compared to NOAA buoy data for similar ocean areas and found to have important differences in regard to probability distributions for significant wave height. (See Appendix A of ref.1.)
- b) Long Term Visual Observation Data for both hemispheres. This milestone work of Hogben and Lu which is contained in ref. 3 had previously been compared to NOAA buoy data in unpublished studies and found to have important differences regarding probability distributions of significant wave height. Wave period information based upon visual observations was also known to be unreliable.
- c) British Maritime Technology Global Wave Statistics (BMT-GWS) for both hemispheres. This recent work of Hogben, Dacunha and Olliver employed long-term shipboard wind speed observation data together with empirical correlations between wind speed and wave height and period for selected ocean areas. Comparisons with NOAA buoy data in this case were encouraging.

Figures 4 thru 9 of ref.1 provide comparisons of NOAA buoy and BMT-GWS wave height probability distributions, long-term wind direction statistics and approximate modal periods which were favorable with the exception of the Gulf of Mexico. For open ocean areas the H_{m_0} distributions were surprisingly good especially for high values of H_{m_0} . The wave period information did not compare well but the basis for comparison was tenuous at best, i.e. modal periods of long term CWS were compared to rough estimate BMT-GWS modal period using an empirical factor of 1.4 times \bar{T}_z (averaged zero upcrossing period). Figure 10 of ref.1, however, revealed that good agreement existed with respect to the question of which ocean areas were climatically steep and which were climatically long period. Given this finding, the establishment of increments on H_{m_0} to provide for hemispheric extremes along each of these boundaries could proceed. For example BMT-GWS Area 23 (see Figure 2 of ref.1), which was taken as a reference area, included the NOAA buoys that defined the Climatic Steep Seas boundary. A search of all Northern hemisphere BMT-GWS areas which had a comparably steep wave climate and also high values of H_{m_0} , led to BMT-GWS Area 11 (North Sea). No comparably steep wave climate experiencing high values of H_{m_0} was found in the Southern hemisphere. For the Climatic Long Period wave climate the analogous BMT-GWS Areas were Area 13 (ref.) and combined Areas 8 and 9 in the Northern hemisphere. Area 10 in the Southern hemisphere (Furious 50's west of Australia) contained more extreme values of H_{m_0} than Areas 8 and 9. Before determining the applicable increments on maximum H_{m_0} for the two wave climates, a study was conducted to compare the high end (H_{m_0} greater than 5 meters) probability distributions for NOAA buoy and BMT-GWS data. The results which are presented in Figure 13 of ref.1 showed generally good agreement out to an occurrence level of 0.1% (about 9 hrs./year). Beyond this, the data sets tended to diverge with the buoy data suggesting less likelihood of occurrence of higher values of H_{m_0} than the BMT-GWS data. The one storm per year occurrence level of the upper bound of the Operability envelope and 9 hours of exceedance per year of the BMT-GWS data are considered to be comparable. The appropriate increments on H_{m_0} beyond the baseline envelope were determined as shown in Figures 14 a and b of ref.1, namely, 1 meter for the Northern hemisphere along the Steep Wave Climate boundary and 1.5 meters along the Long Period Wave Climate boundary. In the Southern hemisphere an increment of 2.5 meters was added along the Long Period Wave Climate boundary. The resulting extrapolations are incorporated in Figure 7 where it will be noted that the upper limit of the Steep Wave Climate boundary for the Southern hemisphere has been made the same as that for the Northern hemisphere to account for typhoon activity.

Extrapolation of the NOAA baseline Survivability envelope to cover hemispheric extremes presents several problems beyond those discussed above. First of all, the Survivability envelope lies well beyond the Operability envelope such that statistical extrapolations into this region would necessarily produce criteria which could neither be proved or disproved. Moreover, long term measurements of extreme seaways at a fixed buoy location tend to be applicable to design of a fixed offshore platform but not for a ship which spends part of its total life (of say 20 years) in port and in transiting ocean areas where extreme seas do not occur. Considering these matters the following steps were taken:

- a) Since the upper end of the Seaways of Limiting Steepness boundary was determined by data from hurricane Camille which produced an extreme combination of H_{m0} and T_p , extrapolation was considered unnecessary to provide for hemispheric extremes. In this storm the steepness of the seaway and wind strength were unusually severe.
- b) Along the extension of the Climatic Long Period Seas boundary the NOAA baseline Survivability envelope was increased by the same increments used to extend the Operability envelope for Northern and Southern hemispheres. These increments were also applied to the baseline Survivability envelope at $T_p = 25$ seconds. The resulting hemispheric envelopes are shown in Figure 7.

During the later stages of preparation of ref.1, an exceptional winter storm near NOAA buoy Station 46003 (south of Kodiak, Alaska) produced a substantially higher value of H_{m0} (16.92 meters) than any previously measured value (i.e. 15 meters). This measurement is plotted in Figure 8 where it will be seen to lie just within the Northern Hemisphere Survivability envelope. Given that the measured spectrum was available, two checks of the generic spectrum recommendations of Figure 6 were possible. Figure 9 illustrates that the Modified JONSWAP formulation and the recommended generic shape parameter ($\gamma = 1.3$) result in a satisfactory approximation to the measured spectrum.

SEAWAY SIMULATIONS

The subject of simulations refers here to an ability to transition from a seaway characterized by a wave spectrum or by a particular wave height time series to a simulated seaway of the same character. The purpose of the simulation in this discussion is the establishment of a rational basis for determining load and motion responses of a ship under specified seaway conditions. Two main avenues of approach are available, i.e. analytical and experimental. Where seaway and ship responses are substantially linear in character, an analytical approach employing input wave spectra, response amplitude operators and statistical analyses of the resulting responses is believed appropriate. Where ship stability is at issue and both the seaway and the ship responses to it tend to be substantially nonlinear, the experimental (model scale) approach is believed to be the more reliable at the present time. The characterization "more reliable", however, raises the question of whether it is in fact realistic, i.e. whether potentially critical wave conformations of the full scale seaway will be generated and whether a model can be made to encounter these waves if a spectrum defined seaway is modeled. The latter requires repeatability in time and location.

Reference 4 in a preliminary fashion attempted to answer these questions. The investigation was facilitated by the existence of the time series wave height data gathered during hurricane Camille which produced the wave spectrum defining the upper end of the Seaways of Limiting Steepness boundary. A prior assessment of nonlinearity of this wave height data had been made by the HACYM (half-cycle matrix) method of analysis which had limited validation at this time. A study was conducted (Task 1) using the existing results of a nonlinear analytical simulation using a third degree functional polynomial model previously generated by Dalzell, ref.5. The linear constituent employed constants so as to make it similar to a relatively heavily damped ship roll response to wave slope.

The results of HACYM analysis of the individual and combined constituent outputs showed that a previously undefined statistic (the mean value distribution of amplitude events, MVDAE) provided a clear indication of the influence of each of the polynomial constituents on the output, i.e. the linear constituent

resulted in a linear MVDAE distribution, the quadratic led to a curved (symmetrical about the null diagonal) MVDAE distribution, while the cubic produced an orthogonal nonlinear elongation along the Reference Level Diagonal (see definitions of Appendix B of ref. 1).

An MVDAE analysis of consecutive half hour segments of hurricane Camille wave height data revealed that a significant degree of nonlinearity followed a final rapid increase in average wind velocity with a lag of about 30 minutes. Those time series wave height events which exhibited the most pronounced nonlinearity corresponded to large waves having considerable elevation above mean water level and very steep forward faces. An additional feature of these waves was that their period was substantially less than the modal period of the spectrum derived from the same half-hour of time series data. Values of T_p vs H_{m_0} for the Seaways of Limiting Steepness boundary imply an approximate wave height to length ratio of 1/20 for the largest waves in the time series, whereas the most nonlinear waves in the Camille time series actually had a height to length ratio of about 1/7.

Having determined from HACYM analysis that substantial nonlinearity existed in the Camille wave height data for the 1500 to 1530 hours interval the associated wave spectrum was chosen for replication two different towing tank facilities (Task 2). The purpose of the experiments was to determine if their replication of this spectrum produced a model-scale time series of wave height which exhibited the same nonlinearity as the full-scale data. One facility had a single flap and the other a dual flap wave maker. In each case only long crested waves were produced. The scale of wave making was not stipulated except to request that it be maximized, consistent with the capabilities of the wave maker to replicate the wave spectrum. Results of the experiment as summarized in ref. 4 were as follows. The MVDAE curve for the primary wave staff measurements was very similar to that from the Camille data out to a point where the highest wave heights occurred. At that point the data suggest that the Camille waves were more nonlinear (i.e. more elevated and steeper). With respect to the parametric characteristics of the largest waves, Table of the reference suggested that there may be less variability associated with the largest of the Camille waves. In the case of the measured time series events shown in Figure 10 there was an apparent trend toward steepness in the upper half of the forward face of the waves as the elevation/amplitude ratio increased.

Because of the availability of time series wave height measurements from the breaking-wave model capsizing experiments of Duncan, Wallendorf and Johnson (ref. 6), further characterization of the wave in Figure 10c is possible. In these experiments breaking waves of a plunging character were generated by deterministic means as described in the reference. One such wave is shown in Figure 11. Using a scale factor derived from the trough to crest height of this wave and the corresponding height of the Camille wave, the former was scaled-up and plotted over the latter as shown in the figure. In this comparison, the time scale of the tank wave was increased by the square root of the scale factor and the mean water level were made coincident. It is apparent that there is considerable similarity in the two time series wave events so that one may infer that the Camille wave was breaking and that it was replicated in this particular experiment. This is in contrast to the tank waves recorded on video tape in the wave spectrum simulation where only spilling breakers were observed. While the limited data base at hand precludes drawing firm conclusions, this finding is at least consistent with the trend toward greater nonlinearity in the largest of Camille's waves as compared to those from either of the simulation experiments. This should not be construed as an inherent limitation of tank wave making, however, since no consideration was given to improving the state-of-the-art in this study.

Based on this study, ref. 4 concluded that the nonlinearity of waves generated in two different towing tanks approached those of the original hurricane seaway when the wave spectrum was replicated by a mechanical wave maker. Differences in nonlinearity appeared to be related to difficulties involved in

attaining the same high frequency energy levels as the full-scale spectrum. High frequency energy was also noted to decrease with distance down the tank from the primary wave probe.

The reference included an additional study (Task 3), conducted by Dalzell which resulted in a numerical model of the Camille seaway for the same 1500-1530 hrs. spectrum employed in the tank wave simulations. The conclusion drawn was that while the numerically modeled hurricane waves showed somewhat less nonlinearity than the original data, the flattening of the wave troughs and elevation of crests due to nonlinear wave-wave interaction was realistic. At the same time, however, the forward-face wave steepness was greater than that of the largest hurricane waves apparently due to failure of the numerical waves to become unstable and break. (The interested reader is encouraged to read Appendix 3 of ref.4 for the details of Mr. Dalzell's simulation and its results.)

Although based upon constrained results (i.e. no state-of-the-art development) the conclusion drawn here from Tasks 2 and 3 of ref.4 is that test tank wave simulations are more appropriate for advancing FPM development at this time. It should be noted that Figure 27 of ref.4 illustrated the necessary repeatability of an extreme wave as to time and location in the test tank.

CRITICAL DESIGN CONDITION CRITERIA

The need for identifying conditions critical for ship responses to the various wave conditions of the seaway criteria discussed here is almost entirely pragmatic. That is, considering the wide range of seaway conditions of this criteria and the additional range of design variables associated with hull configuration, speed, heading and displacement an enormous matrix exists for possibly critical conditions. When one also considers the inherently random character of the seaway, it is obvious why an empirical rather than an FPM approach to ship stability has been the norm for so long.

AN APPROACH

Several obstacles to the establishment of critical design condition criteria must be overcome. The first is the heuristic nature of critical condition criteria. Given the nonlinear character of Seaways of Limiting Steepness and the likelihood of highly nonlinear motion responses of ships to both segments of the Survivability envelope, there seems little hope of an immediate formal approach to the identification of critical stability design conditions. Instead we must in the near term proceed on an ad hoc basis until such time as general principles become clear from experimental and/or analytical developments.

There are, nevertheless, some encouraging developments in the search for critical design conditions. The wave making assessments discussed under Seaway Simulations are promising given the fact that closed form approximations to all elements of the Survivability and Operability envelopes are available for wave modeling purposes. Moreover, HACYM analysis is at least one means of identifying critical nonlinear wave, motion and loading events. Nonlinearity, while seriously complicating analytical developments, often helps to simplify the identification of critical seaway and operating conditions. Appendix B to ref.1 under "Critical Loads and Motions" provides some examples of this tendency.

CRITICAL DESIGN CONDITIONS FOR SHIP STABILITY INVESTIGATIONS

With respect to ship stability, the free running model experiments of Oakley, et al (ref.7) are of interest because of the three modes of capsizing which were identified and related qualitatively to the visual character of the waves which produced them. It is useful to first characterize the wave spectra measured during the peak of the afternoon thermal wind in San Francisco Bay. The representative spectra of Figures 5 {Seq.4} and 15 {Seq.3} of the reference are shown here in Figures 12 and 13. It is apparent that the modified JONSWAP formulation used to model full scale Survivability boundary spectra also provides a reasonable approximation to these spectra (for tank wave modeling purposes). The parametric steepness of these spectra is characterized in Figure 8 at 1:1 and 35:1 scales. The spectrum of Figure 12 at a 35:1 scale corresponds approximately to that of a severe North Sea storm while that of Figure 13 at this scale

corresponds approximately to an extreme northern high latitude (North Atlantic) storm. The results of testing the 30:1 scale AMERICAN CHALLENGER model in these Bay seaways are clearly more representative of measured full-scale seaways than the 55:1 scale model of the SL-7 container ship for which equivalent full scale significant wave heights are 19.5 and 25 meters which are outside of the bounds of the Survivability envelope.

Despite such scaling problems, the results of the model tests are valuable from the point of view of identifying critical wave conformations associated with three capsizing modes in following seas, namely

Mode 1: - - - a group of especially steep and regular waves.

Mode 2: - - - one or more very steep and higher waves - -

Mode 3: - - - three or four steep breaking seas in succession.

The fact that the above wave characterizations apply in the encounter domain complicates the identification of critical wave conformations but not severely since under extreme conditions normal ship speeds are significantly reduced. HACYM analysis (then unavailable) of wave height and model motion data would have helped to identify those seaway spectra corresponding to the onset of significant nonlinear behavior as well as those wave conformations which led to severe nonlinear motions. In any case it is believed that continuous time series wave height measurements are essential for characterizing model test seaways and associated critical wave conformations. With follow-up testing under controlled test tank survivability wave conditions, free running model tests can be an asset to critical condition identification.

Information relating to ship casualties which have occurred under severe seaway conditions is often of interest where testimony has been recorded. Such is the case with regard to the court testimony of ref. 8 regarding the loss of the M/V TUXPAN. Those aspects of the testimony which are of primary interest here relate to (a) meteorological characterization of the storm, (b) the seaway which it produced and its relationship to the Survivability envelope of Figure 8, (c) the actions taken by the masters of vessels in the vicinity of the M/V TUXPAN, and (d) a photograph of a large breaking wave taken by the second officer of the M/V SELKIRK SETTLER (see Appendix B).

Item a. The testimony of ref. 8 classified this storm as a "meteorological bomb", i.e. a severe winter storm in which the central pressure dropped 24 millibars or more in 24 hours. Hurricane wind speeds were in fact measured in the vicinity of the casualty. (A description of the meteorological features of this type of maritime storm is presented in ref.9 while Section 5.2 of ref.10 describes several major ship casualties which have occurred in such storms.)

Item b. A variety of seaway height estimates during the worst of the storm are contained in the testimony of ref. 8. These include:

(1.) U.S. Navy (Fleet Numerical): $H_{m0} = 51$ ft. (15.5m)

(2.) M/V ALFRED NEDDLER: $H_{m0} = 40$ to 50 ft. (12.2 to 15.2m)

(3.) M/V EXPORT PATRIOT (from a radioed weather report to NOAA): Seas of 24.5 ft. plus southwest waves of 44 ft. H_{m0} can be taken as approximately equal to the square root of the sum of the squares, i.e. 50.4 ft. (15.3m).

Estimates of individual maximum wave heights contained in the testimony of ref. 8 can be used to obtain rough estimates of H_{m0} by dividing them by an empirical factor of 1.65.

(1) Captain Perslow of the EXPORT PATRIOT: $H_{max} = 80$ ft., hence H_{m0} roughly = 14.8m.

(2) Captain Matthew of the SELKIRK SETTLER: $H_{max} = 75$ ft., hence H_{m0} roughly = 13.9 m.

Given that all but one of the above estimates are visual in nature and thus are approximate at best, there is a surprising degree of consistency among them. Significant wave heights were apparently in/or near the range 13.5 to 15.5 meters.

The court testimony provides no quantitative estimates of the steepness of the seaway but the slamming of the bridge structural damage, and steering problems in following seas taken together with the measurement

hurricane strength winds suggest exceptionally steep seas. This assessment is reinforced by Captain Purslow's comment that "*- - this definitely was the most violent and severe storm that I have been in in my 38 years at sea, is that the distance between the crests of the waves was very short but very high, which I have never seen before.*"

Based upon these characterizations it is concluded here that the seaway at its peak probably corresponded to conditions on or near the Survivability envelope in the range of significant wave heights from about 13.5 to 15.5m as shown in Figure 8. The fact that the M/V TUXPAN was lost with no survivors and that the M/V BALSA 24 was lost due to capsize with one survivor, suggest that seaway conditions associated with this segment of the envelope be investigated to determine the adequacy of current ship stability criteria.

Item c. The actions taken by the several masters to survive the storm are of interest from the point of view of identifying critical operating conditions. It is implicit from Captain Purslow's testimony that the M/V EXPORT PATRIOT had no major difficulty in maintaining its heading into the seaway at least until the bridge was flooded due to collapse of the bridge windows. Moreover, in view of his reluctance to turn and run from the storm, the ships characteristics in beam and/or following seas must have been of some concern to him. Captain Matthew of the M/V SELKIRK SETTLER was sufficiently "*concerned with the short distance between the waves*" that he ran before the storm. At this heading he called for the ship's speed to be held down otherwise "*She would start to surf. Fall off the wind. Broach. Capsize.*" At the same time he was concerned with loss of steerageway due to too slow a speed. His strategy was such that "*- - when the wheelman usually says 'I am losing steerage way' you kick her up using your combinator from 8.5 or what you have and you kick her a burst to give her the extra momentum to get her out.*" Captain Jens of the M/V WESTERHAM testified by deposition that he felt compelled to turn and run before the storm "*- - And the reason to turn the ship around was also from the engine, that they told me that they cannot keep any more revolution or the speed, and because we had not enough speed, the ship couldn't keep her course.*"

It is believed apparent from these comments that the subject of ship stability under survivability conditions in an FPM approach cannot be divorced from consideration of a ship's ability to maintain its heading in both head and following seas.

With regard to the matter of critical wave conformations, the current lack of time series wave height data from winter storm wave conditions is unfortunate and especially so since there are a number of offshore platforms in the stormy North Sea from which accurate measurements can be made and analyzed to identify nonlinear and other wave characteristics. Somewhat the same can be said of model test results in random seas and of the resulting loads and motions where nonlinear events could have been identified and correlated with concurrent wave height data.

ANALYTICAL METHODS

This subject is addressed in the context of the anticipated role of analytical methods in facilitating FPM development. Because of the concern for implementing and demonstrating the feasibility of FPM in the near term, emphasis is placed on model testing in regard to three objectives, namely:

- Realistic seaway simulations
- Critical design condition identification
- Analytical method validation

In all three regards it is presumed that because of the nonlinearities involved it is essential that carefully controlled wave conditions be employed and that wave heights and all important response parameters be measured and correlated with respect to time. As noted under the discussion of Seaway Simulations, while tank wave making requires additional development, it is nevertheless believed to be the most viable

alternative for demonstrating the validity of FPM at the present time. The emphasis here on model testing however, should not be construed as suggesting that it continue indefinitely to play a major role in FPM applications. Computer based methods in the long term are less expensive and time consuming. Moreover use of multi-level analysis codes has recently been found useful in critical condition identification. (ref. 1)

It is important to note that in the early stages of FPM development analytical methods have a dual role to play. The first is obvious, i.e. the prediction of full scale ship responses to given input wave conditions. The second is less obvious. Analytical methods are needed to provide a rational explanation for experimentally determined critical wave and ship response conditions. Insights gained from such findings need to be generalized to other hull forms and ship sizes so as to influence the development or revision of the Conditions of Assignment contained in International Load Line regulations which have a significant impact on commercial ship design.

RESPONSE CRITERIA

An FPM approach to ship stability requires criteria defining acceptable or unacceptable ship responses to critical design conditions. In general, it is recommended that within the bounds of the Operability envelope a ship should remain free of damage which would require repair or replacement and that all ship systems should function normally. Because of the rarity of seaway conditions associated with the Survivability envelope damage which does not lead to significant loss of water tight integrity is acceptable. Where stability is concerned one must obviously stipulate that the ship should not capsize. This might appear to say it all; however, service experience suggests otherwise. For example in the case of bulk carriers, substantial shifting of the cargo can lead to subsequent capsize so that rolling in extreme seas may be related to the tendency of a given cargo to shift considering the effectiveness of any restraints involved. Obviously it would be logical to require that restraints to be effective up to roll angles at which capsizing would occur anyway. Given the lack of cargo restraint in ore carriers, for example, it would appear necessary to require that such ships not roll beyond an angle which would cause the cargo to shift. But is this practical? Are restraints essential? The answer lies in the realm of an FPM approach to ship design in the writer's opinion.

For ship types less subject to cargo shifting, inherent stability is the major consideration. Maintenance of steerageway, however, is a matter which bears heavily on the avoidance of capsize. In the case of ships which have steering problems in following seas, should the ability to maintain a headseas heading under survivability conditions be required? In such a case freedom from heavy slamming and bridge window damage would also appear to be essential. If this cannot be assured, the ability to maintain heading in following seas so as to avoid broaching would appear to be vital.

In these and other potentially critical design conditions an FPM approach is believed to be appropriate for resolving such questions. Clearly, Response Criteria must be regarded as an element of FPM as important as any other.

RECOMMENDATIONS

In order to further the development of an FPM approach to ship stability problems the following actions are recommended:

1. The seaway criteria contained in ref.1 should be critiqued, modified as necessary and then adopted for use in the development of ship stability criteria.
2. Our limited knowledge of the linear and nonlinear time series characteristics of storm driven waves should be improved. Deep water platforms in the North Sea are ideal facilities for this purpose.

3. The ability of seakeeping tank facilities to replicate the generic wave spectra associated with the Operability and Survivability envelopes should be investigated.
4. Conduct model tests to begin identifying critical design conditions for subsequent use in ship model stability tests.
5. Integrate the model test results of 4. into ship load and motion computer code development so as to (a) help obtain code validation and (b) direct such developments toward seaway and operating conditions which are critical from a ship stability point of view.
6. Facilitate the use of the HAYCM or equivalent methods of random time series data analysis so as to determine the onset of nonlinear behavior and the time series character those of waves and ship motions associated with the extreme nonlinear behavior.
7. Enlarge upon and summarize the seaway and storm development information now available. Using this information, conduct interviews of ship masters to obtain first hand information on ship handling and response characteristics in severe storm driven seaways.
8. Consider cooperative development of the above initiatives by interested parties.

References:

1. Buckley, W.H., "Design Wave Climates for the World Wide Operation of Ships, Part I: Establishment of Design Wave Climates", Oct. 1993. (In publication by U.S. Coast Guard).
2. Hogben, N., N.M.C. Dacunha and G.F. Olliver, Global Wave Statistics, compiled and edited by British Maritime Technology, Limited, England, Unwin Brothers Limited, 1986.
3. Hogben, N. and F.L. Lumb, Ocean Wave Statistics, Her Majesty's Stationary Office, London, 1967.
4. Buckley, W.H., "An Analysis of Wave Characteristics in Extreme Seas", Ship Structure Committee Report SSC-353, 1991.
5. Dalzell, J.F., "An Investigation of the Applicability of the Third Degree Functional Polynomial Model to Non-Linear Ship Motion Problems", Davidson Laboratory Report SIT-DL-82-9-2275, December 1982.
6. Duncan, J.H., L.A. Wallendorf, B.H. Johnson, "An Experimental Investigation of the Kinematics of Breaking Waves", Proceedings of IAWR Seminar on Wave Analysis in Laboratory Basins, 1-4 Sept. 1987, pp. 411-422.
7. Oakley, Jr., O.H., J.R. Pauling and P.D. Wood, "Ship Motions and Capsizing in Astern Seas", Tenth Symposium Naval Hydrodynamics, June 24-28, 1974.
8. Pierson, Jr., W.J., "Ship Stability in Heavy Weather: The Real Situation and Models Thereof", 1993. Unpublished.
9. Sanders, F. and J.R. Gyakum, "Synoptic-Dynamic Climatology of the 'Bomb' ", American Meteorological Society, Monthly Weather Review, Vol.108, pp. 1589-1606, Oct. 1980.
10. Buckley, W.H., "A Study of Extreme Waves and Their Effects on Ship Structure", Ship Structure Committee Report SSC-320, 1983.
11. Salvesen, N. and Woei-Min Lin, "SAFE SEAS - Vessel Safety Assessment for Extreme Seas, A New National Capability", U.S. Coast Guard Academy Vessel Stability Symposium, 15-17 March 1993.
12. Su, M-Y, M. Bergin, P. Marler and R. Myrick, "Experiment on Nonlinear Instabilities and Evolution of Steep Gravity-Wave Trains", Journal of Fluid Mechanics, Vol. 124, 1982, pp. 45-72.

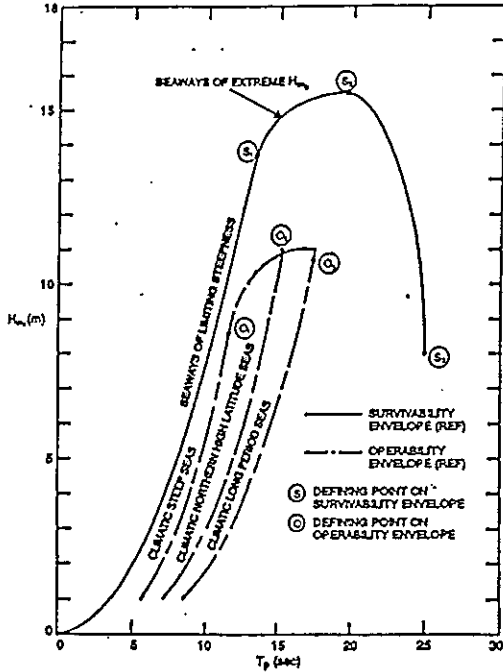


FIGURE 1 BASELINE SURVIVABILITY AND OPERABILITY ENVELOPES DERIVED FROM LONG-TERM NOAA BUOY DATA

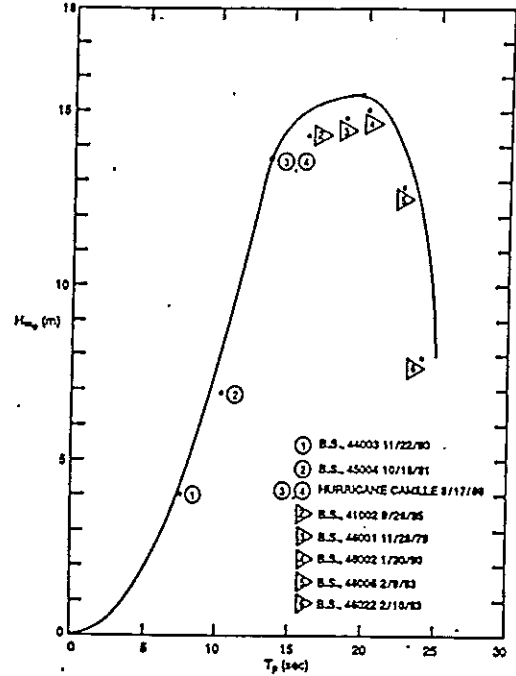
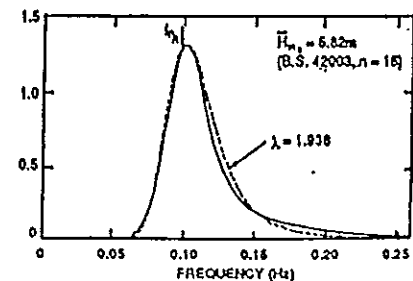
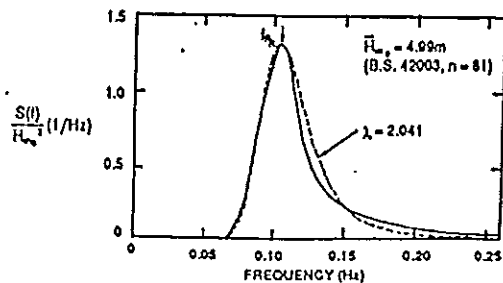
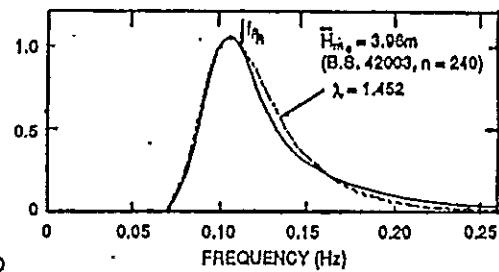
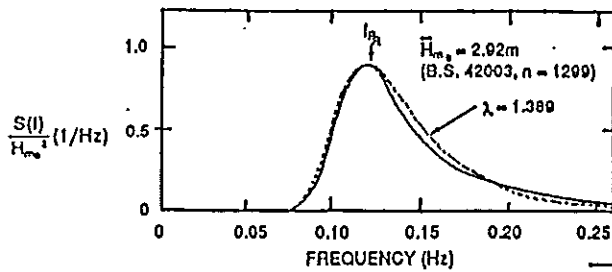
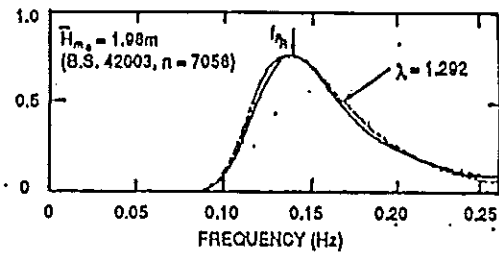
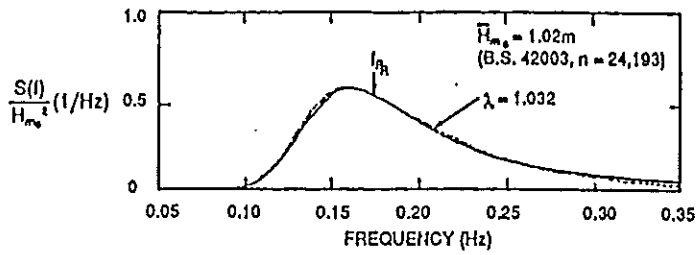


FIGURE 3 PROXIMITY OF EXTREME WAVE SPECTRA TO NOAA SURVIVABILITY BASELINE



— MEASURED
 - - - APPROXIMATION

FIGURE 2 SELECTED CLIMATIC WAVE SPECTRA FROM STEEP SEAS WAVE CLIMATE: GULF OF MEXICO

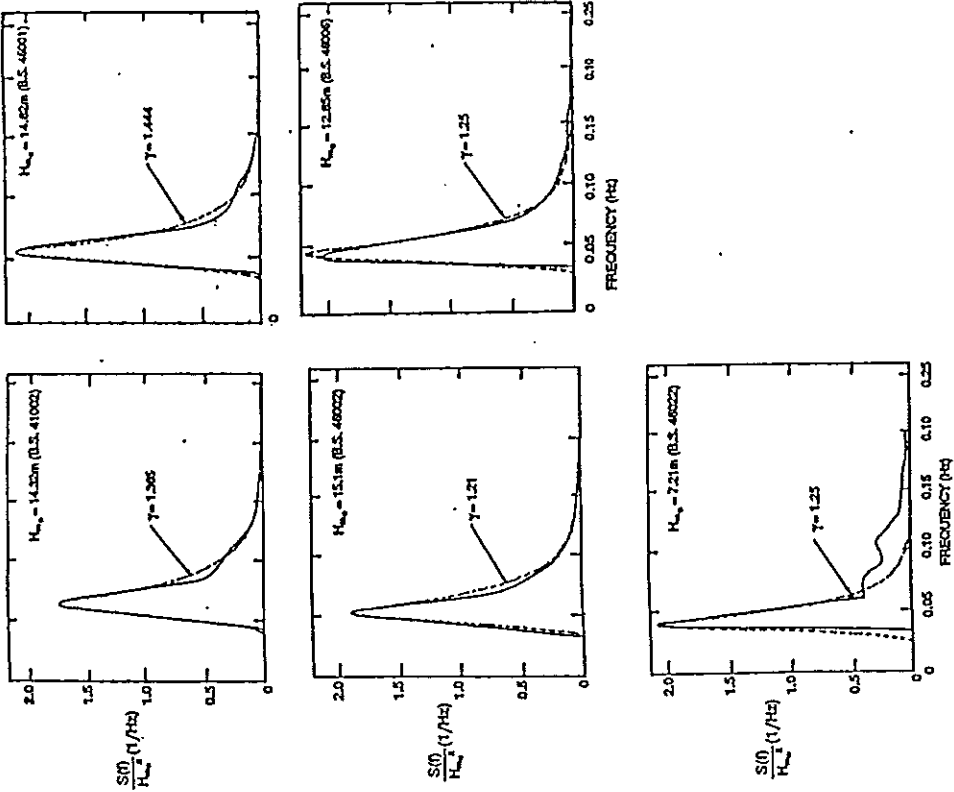


FIGURE 5 SELECTED SPECTRA FROM SEAWAYS OF MAXIMUM SIGNIFICANT WAVE HEIGHT

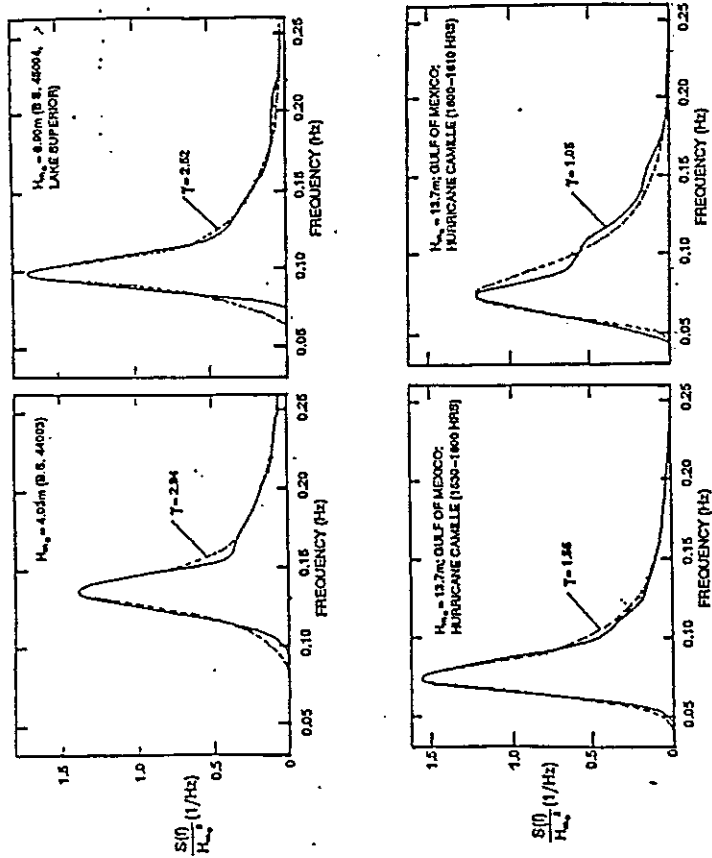


FIGURE 4 SELECTED WAVE SPECTRA FROM SEAWAYS OF LIMITING STEEPNESS

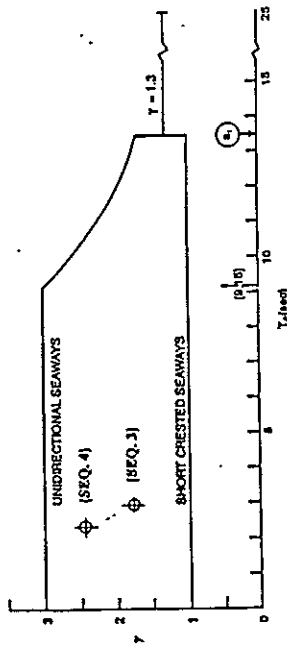


FIGURE 6 JONSWAP SHAPE PARAMETER FOR SURVIVABILITY BOUNDARY WAVE SPECTRA

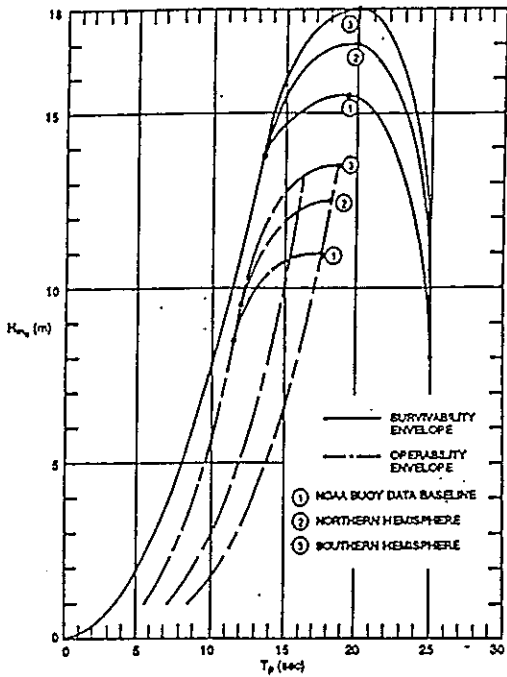


FIGURE 7 SURVIVABILITY AND OPERABILITY ENVELOPES FOR NORTHERN AND SOUTHERN HEMISPHERES

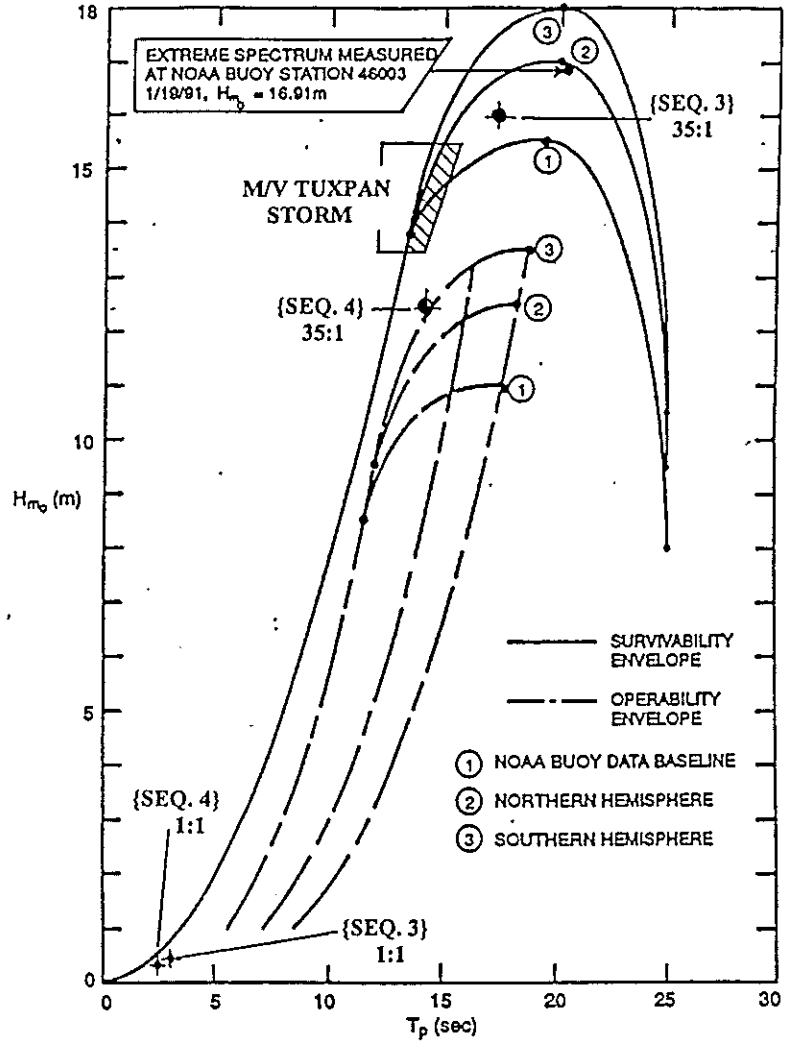


FIGURE 8 PROXIMITY OF EXTREME WAVE SPECTRUM TO SURVIVABILITY ENVELOPE FOR THE NORTHERN HEMISPHERE

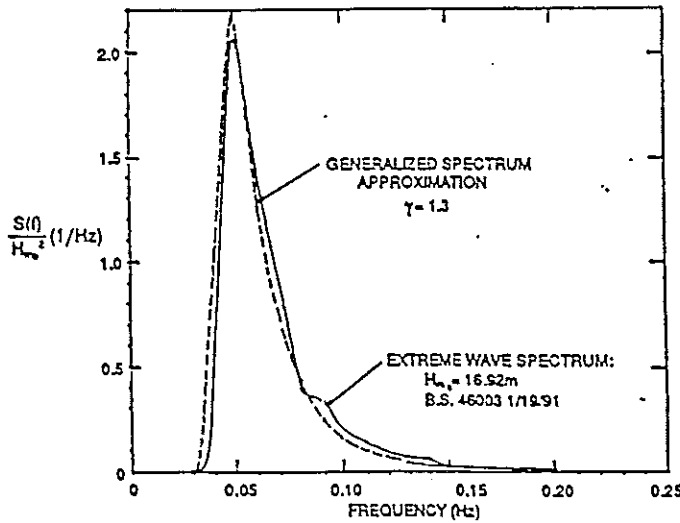


FIGURE 9 GENERALIZED WAVE SPECTRUM COMPARED TO EXTREME WAVE SPECTRUM

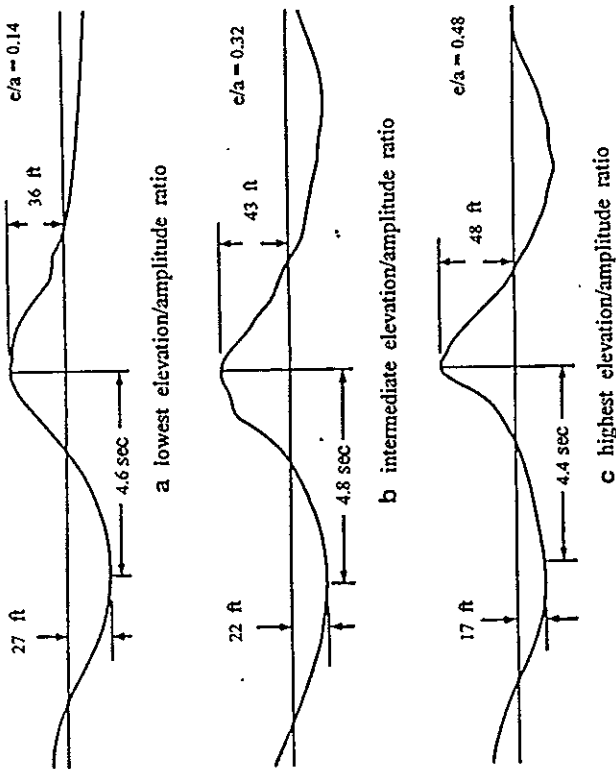


Fig. 10 Time Series Characteristics of Highest Waves — Hurricane Camille 1500-1530 Hours.

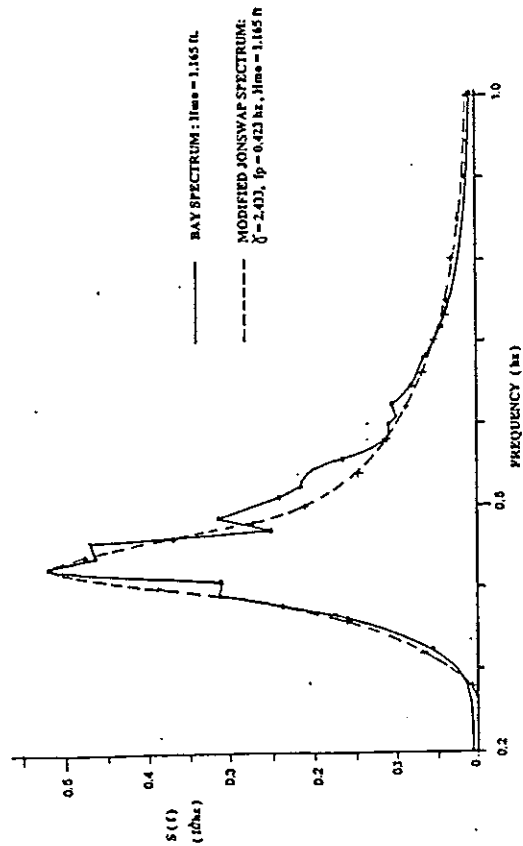


FIGURE 12 COMPARISON OF PARAMETRIC AND MEASURED WAVE SPECTRUM FROM SAN FRANCISCO BAY: SEPT. 17 1973 (SEQ. 4)

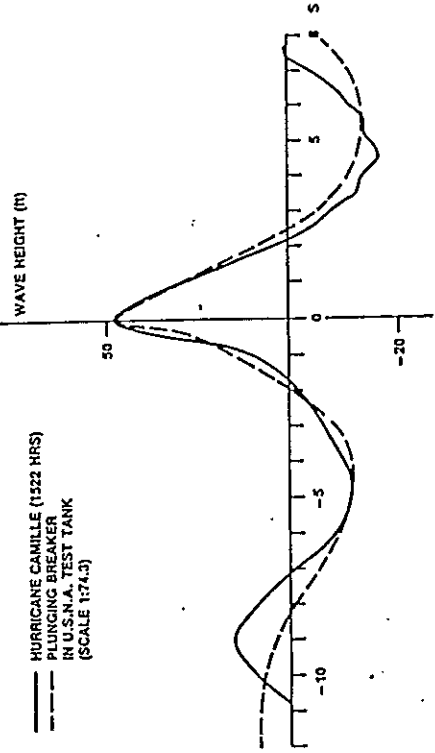


Fig. 11 Time Series Comparison of Model Scale Plunging Breaker and Wave From Hurricane Camille (1522 hours).

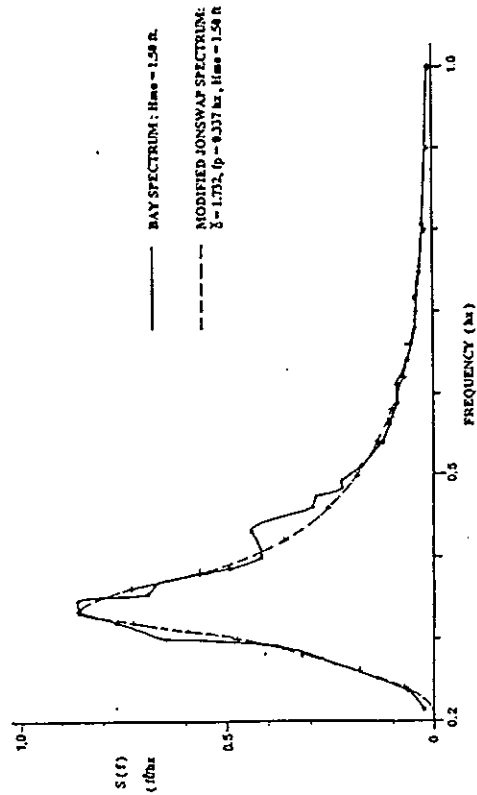


FIGURE 13 COMPARISON OF PARAMETRIC AND MEASURED WAVE SPECTRUM FROM SAN FRANCISCO BAY: AUG. 14 1973 (SEQ. 3)

APPENDIX A: DEFINITIONS

Wave Spectrum: $S(f)$ = a scalar plot of wave energy density versus wave frequency. The energy density is expressed in terms of M^2/hz unless otherwise indicated.

Significant Wave Height: $H_{m_0} = 4 [\text{area under wave spectrum} = m_0]^{1/2}$. It is expressed in meters unless otherwise indicated.

Modal Period: $T_p = 1/f_p$. f_p is the frequency corresponding to the peak energy density of a wave spectrum.

Normalized Wave Spectrum: A wave spectrum in which the energy density ordinates have been divided by the $H_{m_0}^2$ of the wave spectrum. Its peak energy density is given by $S(f_p)/H_{m_0}^2$ (1/hz).

Climatic Wave Spectrum: A wave spectrum which results from averaging the energy density ordinates of a number of measured wave spectra. It is determined for specified significant wave height class intervals, typically 1 meter.

Extreme Wave Spectrum: A spectrum corresponding to the highest value of significant wave height from a long term (approximately 10 year) collection of multi-site measured wave spectra. Extreme wave spectra are identified over a range of modal frequencies so as to define an empirical envelope of values of H_{m_0} versus T_p . They are also characterized by the peak energy density parameter ($S(f_p)/H_{m_0}^2$) for spectrum modeling purposes.

Wave Climate: A seaway characterization determined primarily from climatic wave spectra obtained at a particular geographic location. It is characterized by parametric and other properties of the local climatic wave spectra and by the associated probability density distribution of H_{m_0} .

Constituent Wave Spectra: Two or more wave spectra in a weighted combination which approximates a particular individual or climatic wave spectrum.

Generalized Wave Climate: An estimate of the wave climate of a designated ocean, sea, lake or bay area based upon characterizations of one or more families of climatic wave spectra. Generalized wave climates are also inferred from wave statistics presented in reference 11.

Modal Period Trend Line: A plot of H_{m_0} versus T_p supplemented by a separate plot of climatic wave spectrum shape parameters versus T_p which are considered to best characterize a particular generalized wave climate. The upper limit of the trend line corresponds to an average of the highest annually measured values of significant wave height in the generalized wave climate.

Design Wave Climate: An envelope of H_{m_0} versus T_p which includes all applicable generalized wave climates and associated modal period trend lines together with criteria defining acceptable

or unacceptable ship or vessel behavior in the design wave climate. In this study world wide wave climates are applicable. With respect to ship or vessel behavior, two levels of design wave climates are defined which are expressed as an Operability Envelope and a Survivability Envelope.

Operability Envelope: An assembly of design wave climates in which a ship or vessel is required to operate without experiencing structural damage requiring repair or replacement. A baseline envelope is established using NOAA buoy modal period trend line data and then extrapolated to cover Northern and Southern Hemisphere wave climate extremes.

Survivability Envelope: An envelope of extreme wave spectrum parameters within which a ship is required to operate without experiencing loss of water tight integrity, hull girder failure, capsizing, or loss of communication or survivability equipment. Structural or other local damage which does not impair survivability is acceptable. A baseline envelope is established using NOAA buoy extreme wave spectrum measurements and then extrapolated to cover Northern and Southern Hemisphere wave climate extremes. The baseline envelope consists of two connected segments: one corresponding to seaways of limiting steepness and one corresponding to seaways of extreme significant wave height.

Seaways of Limiting Steepness: An empirical boundary defined in terms of H_{m_0} versus T_p which is derived from a large number of wave spectrum measurements which converge to an apparent limiting parametric relationship, i.e. $H_{m_0}/T_p^2 = 0.00776g$ (m/sec^2). The highest value of H_{m_0} associated with this boundary was measured during hurricane Camille ($H_{m_0} = 13.7$ meters). A range of spectrum shape parameters is determined from measured spectra which fall on or near this boundary.

Seaways of Extreme Significant Wave Height: An empirical boundary defined in terms of H_{m_0} versus T_p which is based upon extreme wave spectra measured at a variety of NOAA buoy stations during a period of approximately 12 years. A small margin is maintained between the NOAA buoy spectrum measurements and the empirical boundary to absorb future small increases in H_{m_0} and/or T_p . A constant value of spectrum shape parameter versus T_p is found to adequately model the extreme wave spectra associated with this segment of the Survivability Envelope.

<u>Formulation</u>	<u>Parent Form</u>	<u>Comment</u>
Ochi (3P)	$S(f) = \frac{1}{4} \frac{(\lambda + 1/4)^\lambda}{\Gamma(\lambda)} H_{m_0}^2 \left(\frac{f_p}{f}\right)^{4\lambda} \frac{1}{f} e^{-(\lambda + 1/4)(f_p/f)^4}$ $\lambda = f \left(\frac{S(f_p)}{H_{m_0}^2}\right) \cdot f_p$	Reduces to Bretschneider for $\lambda = 1$
Modified JONSWAP	$S(f) = [\text{Bretschneider}] (\gamma^{-1/3}) (\gamma^a); 1 \leq \gamma \leq 4$ $\gamma = f \left(\frac{S(f_p)}{H_{m_0}^2}\right) \cdot f_p$ $a = e^{-(f/f_p - 1)^2/2\sigma}$	Reduces to Bretschneider for $\gamma = 1$

$$\sigma = \begin{cases} 0.07 & \text{for } f < f_p \\ 0.09 & \text{for } f > f_p \end{cases}$$

APPENDIX B: UPDATE OF EPISODIC WAVE INFORMATION

While conducting the study of ref. 10, the writer encountered circumstantial evidence of certain unusual and dangerous types of storm waves. Because of their distinctive appearance they were termed "episodic" waves, i.e. waves which clearly stood apart from the majority of other storm waves. Table B-1 which is taken from ref. 10 is an initial categorization of these waves. The U.S. Coast Guard officers who had called attention to the Steep Long-Crested Waves of Item IIa, when shown the wave photo of Figure B-1a immediately identified it as the wave type they had previously described. Figure B-1b is an additional photo of this same type of wave.

Visual evidence of the remaining wave types had been lacking until a photo, taken by the second officer of the M/V SELKIRK SETTLER, appeared in Prof. Pierson's paper, ref. 8. This wave, shown here in Figure B-2, appears to correspond to the "Rogue" wave classification of Table B-1 for the following reasons:

- (a) the severely breaking character and size of the wave
- (b) the wave impacting at a substantial angle to the other waves in the seaway
- (c) the associated storm being classified as a meteorological "bomb".(ref.8)

The storm characterization given in Table B-1 for this type of wave is based upon the ref. 9 description of the origin of a meteorological bomb. Knowledge of the ability of such a storm to produce rogue waves stems from the storm damage and meteorology correlations of ref. 10.

A review of the tank wave making experiments of Su, et al (ref. 12), suggests that "Rogue" waves may result from an instability associated with very steep two-dimensional (i.e. long crested) waves; see their Figure 5. The localized nature of the instability results in a Vee shaped breaking crest in their experiment. This geometry may be the origin of the apparent misalignment of the breaking crest with other waves in the seaway, see their Figure 5 and Figure B-2 (above the aircraft). Reference 12 may also have identified the origin of the "Three Sisters". They found oblique wave groups radiating at 30 deg. from the decay of the steep, long crested waves which they initially generated.

Those episodic wave types of Table B-1 which are of particular interest from a ship stability point of view are:

- (a) Steep long-crested waves when encountered in following seas. These can result in steering/broaching problems because of their size and steepness.
- (b) The "Three Sisters" when encountered in head seas. Because of their oblique approach they lead to heavy rolling and serious concern for cargo shifting. (ref. 10, pg. 26)
- (c) "Rogue" waves are of indirect importance. Here loss of water tight integrity due to structural damage and subsequent flooding can result in capsize and foundering.

TABLE B-1 AN INITIAL CHARACTERIZATION OF LARGE NON-GAUSSIAN AND EPISODIC WAVES (REV. A)

Type	Characterization	Basis for Characterization
I. Nonlinear: short crested, breaking waves	<ul style="list-style-type: none"> • Steep and elevated above mean water level. Short crested. • Elevation/amplitude ratio ≈ 0.5 • Produced by strong, rapidly increasing winds 	<ul style="list-style-type: none"> • Time-series wave data from Hurricane Camille and associated wind velocity increase. • Casualty cases associated with strong rapidly increasing winds: <ul style="list-style-type: none"> — SEA-LAND MARKET — LPD-12 — CHESTER A. POLING — FV FAIR WIND
II. Episodic Waves:		
a. Steep Long-crested Waves	<ul style="list-style-type: none"> • Recurring as every 7th or 9th large wave in a storm driven seaway containing waves at least 20 ft high 	<ul style="list-style-type: none"> • Observations by officers from ocean weather ships. • See Figures B-1a and B-1b
b. Large Grouped Waves	<ul style="list-style-type: none"> • Group of three large waves in seaway. Second wave frequently largest in group. • Occur in storm winds which are no longer increasing, or which have begun to decrease. 	<ul style="list-style-type: none"> • Waves encountered by CV-62, SEA-LAND McLEAN, LST-1193 • Observations by officers from ocean weather ships.
c. Episodic Wave Packets	<ul style="list-style-type: none"> • "Three Sisters": group of three long-period waves intruding into existing seaway at angles of about 30° from principal wave direction. Generally occur in vicinity of storm with central winds of 60 kn or more. • "Rogue" Wave: large breaking wave intruding into existing seaway at angles up to 50° from principal wave direction. Likely to occur in vicinity of upper altitude "TROF" as it overtakes an existing or developing low. High altitude comma shaped cloud usually associated with TROF. 	<ul style="list-style-type: none"> • Observations by officers from ocean weather ships as well as ship masters of considerable at-sea experience • Rogue Wave encounters by U.S. NAVY FRIGATE, CHU FLUING, and MUNCHEN, and associated synoptic weather patterns. • See Figure B-2

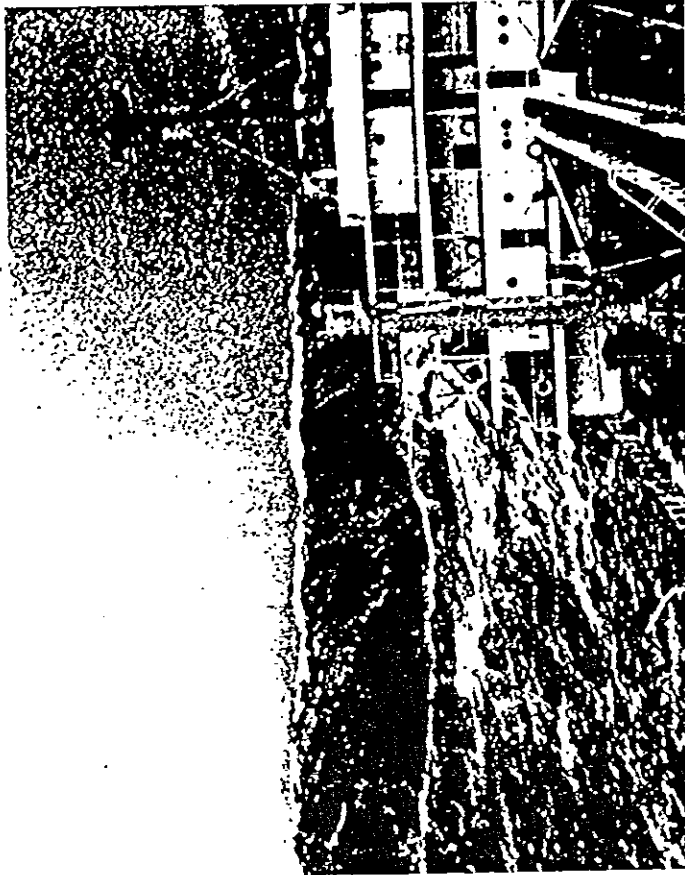


Figure B-1a Steep Long-Crested Wave

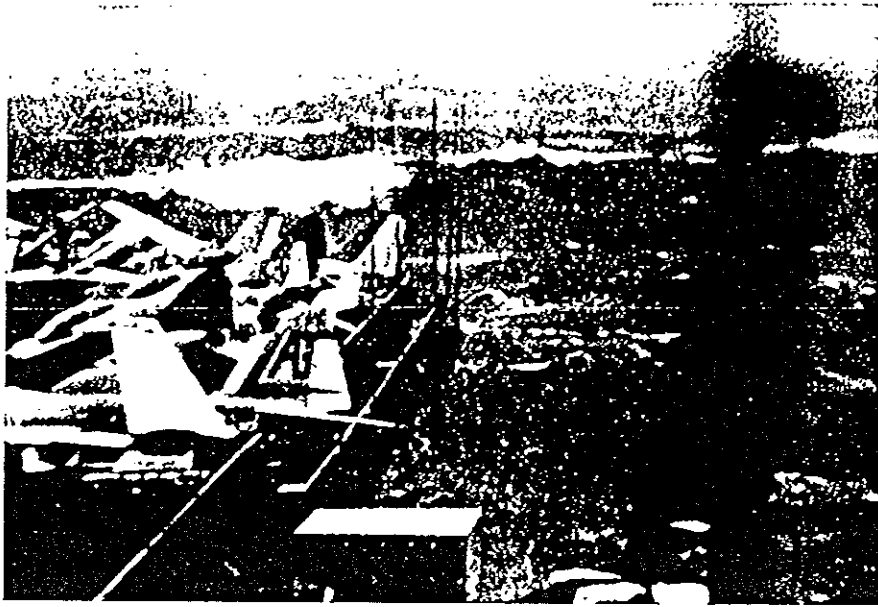


Figure B-1b Steep Long-Crested Wave Breaking Locally



Figure B-2 "Rogue" Wave

Lech Kobyliński

**METHODOLOGY OF THE DEVELOPMENT OF STABILITY CRITERIA
ON THE BASIS OF RISK EVALUATION**

Abstract

Present international stability criteria are considered as not being entirely satisfactory. Therefore since 1974 IMO initiated the programme aimed at development of rational criteria. Several approaches to the development of such criteria were tried, however not much has been achieved. Author proposes to apply risk analysis and estimation of probability of capsizing as the basis for development of criteria. Definite methodology has been proposed which allows to differentiate criteria depending on ship's type, route and size, number of passengers and other factors.

Introduction

In 1968 IMO adopted resolutions A.167 and A.168 containing the set of stability criteria. Those criteria were developed by a semi-statistical method where stability parameters of two group of ships - those which capsized and those which were considered as operated safely - were compared.

The main drawback of the semi-statistical method used in the developing of IMO criteria in the form of a set of critical values of stability parameters consist of the fact that the population of ships investigated, and particularly ships which were capsized was rather small. In addition those ships were of different types and sizes, of different age, the

circumstances of casualty were widely different and in many cases additional effects, such as shifting of cargo, icing etc. were of importance. The stability characteristics in many cases were also uncertain. Moreover, when establishing critical values, it appeared that quite large proportion of ships having stability parameters in excess of critical values capsized, whereas many ships with stability parameters below critical were considered safe. The critical remarks are well known and were pointed out at many occasions. Similar critics is applicable to any existing criteria consisting of a set of critical values of stability parameters.

Because of these deficiencies IMO decided to develop stability criteria based on the equalisation of restoring moments with the heeling moments acting on the ship. This was eventually fulfilled in the form of the so called "weather criterion" included in the resolution A.562 [1]. A.562 was based on earlier requirements included in the national regulations of some countries.

Generally the physical model in this approach is highly simplified, moreover, wind pressure and angle of rolling were chosen so that the criterion is satisfied for ships considered safe. In IMO resolutions and in some national requirements there are also included some other criteria based on calculation of heeling moments due to external forces, however all of them include arbitrary assumptions and far reaching simplifications. Realizing, that criteria contained in the above mentioned resolution have some deficiencies, IMO Subcommittee decided that at some future date so called "rational" criteria should be developed. The meaning of "rational" criteria was understood initially as criteria based on the analysis of physics of capsizing and calculation of probability of non capsizing of the ship in a seaway. At the later stage the differences in understanding of the essence of rational criteria, however, caused lack of determination regarding future programme of work of the Working Group on Intact Stability created at 17th Session of the STAB Sub-Committee in 1975 on development of rational stability criteria.

The programme agreed in 1974 by the STAB Sub-Committee was subsequently many times modified and the main task consisting of developing rational stability criteria was showed away to the distant future whether long term programme of the group was supplemented with current tasks. The programme agreed upon initially [2] included studies of the physics of capsizing and formulating suitable mathematical models of capsizing in order to develop practical criteria on this basis.

The programme adopted could in fact eventually lead to development of rational

stability criteria understood as criteria for safe operation in stormy sea. It was, however, unrealistic in view of lack of results of research work, execution of which would require years of work of many scientific institutions. Due to this fact, consideration of various points of the programme was delayed to the time when more research results are available. In the context of work of the Working Group on Intact Stability attention should be drawn to the document submitted in 1978 by Poland [3]. Poland stated in this document that in spite of the lengthy discussion on the IMO forum there is still no concept how to develop "rational" stability criteria. The need for application of probabilistic methods in development of criteria was underlined, but it was stated that there are serious difficulties in application of such methods. In spite of the great effort of the Working Group as well as of the establishing of several comprehensive research programmes in some countries (e.g. "Safeship" project in UK, SiS project in Norway, HSVA project in Germany and others) and organisation of four large International Conferences on Stability of Ships and Ocean Vehicles (STAB-Conferences) the results achieved towards development of "rational" criteria were rather meagre. Nevertheless much better understanding of dynamical behaviour of ships in a seaway leading to capsizing was achieved.

Possibilities of establishing rational stability criteria

In the meaning which was adopted by the IMO Working Group, rational criteria mean criteria taking into account all external forces acting on ship in a seaway and physics of capsizing. However, broader understanding, as according to Oxford Dictionary where "rational" means "sensible, that can be tested by reasoning" does not exclude e.g. criteria obtained by means of statistic or on the basis of model tests, or by any other sensible method. Therefore, considering possibilities of developing rational criteria we should not exclude all possible methods.

The philosophy behind methods of development of rational stability criteria was discussed by many authors. It appears that this is the most difficult problem and apparently no single methodology could be established and rather various approaches have to be pursued which eventually may lead to satisfactory result. Works and ideas advanced by Krappinger, Hormann, Morrall, Kuo, Caldwell, Sevastyanov, and others should be mentioned in this context. Full review of those ideas was presented by the author. [4]

Several possibilities of development of rational criteria were discussed in the above mentioned papers. As the phenomena occurring in reality are basically of a random character and data on accidents enable a posteriori risk assessment, therefore it seems logical to adopt risk level as a basis for safety assessment, safety criteria and operational procedures. This is particularly applicable to the risk of capsizing, because majority of factors affecting stability, such as wind and wave forces, sea currents, and centre of mass related to loading condition are obviously of random character.

The probabilistic approach to safety against capsizing was advocated by several authors [5,6,7,8] although all of them drew attention to the basic difficulties involved in this approach. The basic philosophy of the probabilistic approach consists of calculation of the probability of capsizing of the ship either during its whole life time or in certain selected situations considered dangerous.

In many fields of technology methods based on comparison of demand and capability of the system are used in order to develop safety criteria with a great success. In this concept failure of the system is estimated by the probability that the demand -D- of the system exceeds its capability -C-. Safe condition would be then:

$$P_s = 1 - P[D > C] = P[D \leq C]$$

Demand and capability, being random quantities are defined by density functions. Comparison of demand and capability of a system could be done also in deterministic way. In deterministic method mean or characteristic values of demand and capability are compared and safe condition is determined as:

$$P_s = C^* > D^*$$

where C^* and D^* are characteristic values, arbitrarily chosen.

It is virtually impossible to apply the above described method to safety against capsizing, because probability density functions for demand and capability are strongly coupled. The comparison of the characteristic values of demand and capability (deterministic method) constituted a basis for majority stability criteria in several requirements and recommendations, national and international.

The most important external forces acting on ship are forces exerted by wind and waves. Both are of random character. The majority of studies of the behaviour of a ship in a seaway are limited to study ship motions under action of wind and waves. This is

understandable because those are the most important factors which may cause capsizing. Those are also most difficult factors to be dealt with because of their random character. Other external forces could be more easily dealt with by deterministic approach.

In the above approach the problem of stability criteria is reduced to the problem of evaluation of extreme values of rolling angles. This is the problem of dynamics of a ship rolling in a seaway. The concept of establishing of stability criteria on the basis of predicting extreme rolling angles was discussed by several authors e.g. [6,9,10] and it is a direct consequence of the concept of comparing demand and capability probability density distributions (f_D and f_C) of the system. Morral [11] presented definite proposal of the methodology of developing stability criteria on this basis.

Another concept originating from the demand-capability idea is method developed at Strathclyde University and reported in several papers (e.g. [12]). It developed in a way of balancing of energy between exciting and restoring moments for a ship in following sea including wind effect in quasi-dynamic mode.

There is also possibility to develop stability criteria on the basis of statistics. Criteria based on the statistics were included in IMO resolutions A.167 and A.168, but more rigorous discrimination analysis was used in more recent analysis by Krappinger and Sharma [13] but due to the fact that the population of capsized ships available is rather small, especially if ships are divided in groups according to type, and size, not much more could be expected from the application of this method unless much more data are available.

Further possibility of developing stability criteria are model tests of capsizing. Model tests of capsizing which require long runs on realistic irregular sea were conducted in open water. Work done in United States, Germany, Poland and Japan may be mentioned, the results of those investigations being published in many articles. Review of those test is included in [14] Basically, in this method an attempt was made to calculate probability of capsizing for a model in certain wind and sea condition and in relation to ship parameters (GM_0 , freeboard etc.). Theoretically this method may provide reliable results but it requires tremendous effort and is extremely expensive.

Development of the suitable mathematical models of ship rolling in a seaway which ultimately should lead to the probability of exceeding certain limiting angles of heel attracted many scientists and literature of the subject is immense.

The majority of studies concentrates on investigation in the time domain of the

peculiarities of the one-degree of freedom non-linear equation of rolling which may be written in the form:

$$J(\ddot{\varphi}, t) + D(\dot{\varphi}, t) + R(\varphi, t) = K(\varphi, t)$$

where: φ is roll angle, $\dot{\varphi}$ is roll velocity, $\ddot{\varphi}$ is roll acceleration, **J** is inertia term, **D** damping term, **R** restoring term and **K** excitation term due to waves.

These studies did not, however, lead to the development of practical stability criteria. Only in the most recent study a method of development of rational stability criteria based on probabilistic approach has been proposed which includes also probability of capsizing calculated with non-linear model of rolling.

Are rational criteria really needed?

After the international stability criteria including weather criterion had been developed the question arose whether further work on stability criteria is really needed. It is, however obvious, that actually the existing criteria do not ensure hundred per cent safety. In the opposite, analysis of the effectiveness of the criteria revealed that there were several ships satisfying criteria which capsized and on the other hand several ships not satisfying criteria were operated safely for the long time.

Result of such analysis performed by Sevastyanov [15] using criteria of Resolution A.168 against vessels taken from casualty statistics collected by IMO is shown in Fig.1, where the distribution of the deviation of the parameter ϵ is plotted, where

$$\epsilon = \frac{\overline{KG}_{act} - \overline{KG}_{crit}}{\overline{KG}_{act}} \cdot 100$$

and \overline{KG}_{act} - KG for the vessel at the time of casualty

\overline{KG}_{crit} - KG for the same vessel required to meet A.168 criteria

The distribution of ϵ is almost Gaussian displaced towards the positive direction of about $\epsilon = 6.6\%$. Mean square deviation is equal $\sigma_{\epsilon} = \pm 5.4\%$ what means that the system of criteria of Res.A.168 requires decrease of KG with respect to the really dangerous value of about 7% but is not perfectly safe because probability of capsizing when satisfying this system of criteria is approximately at given ϵ and σ_{ϵ} .

$$P_{caps} = \int_{-\infty}^0 f(\epsilon) d\epsilon = 11,5 \%$$

In fact 3 of the 37 vessels considered in this exercise capsized in spite of the fact that they fully satisfied criteria. Obviously this is too much and it may be concluded that improvement of criteria is necessary.

The obvious measure of safety is probability of capsizing. There are several methods of calculation of the probability of capsizing proposed. Calculations using method proposed by Belenky [16] for 17 vessels in 3 loading conditions which in each case just satisfied IMO criteria of res.A.167 and A.562 revealed wide differences between computed probabilities (see table 1).

Notwithstanding the fact, the method of calculation may be not perfect, the relative values of computed probabilities reveal that degree of safety for different ships when satisfying existing criteria is widely different, the fact which should not be acceptable. This is further proof that there is a need to improve criteria.

The existing criteria except weather criterion consist of the set of critical values of stability parameters. Weather criterion, although taking into account environmental conditions i.e. wind and waves in fact also ultimately resolves into estimating critical value of stability characteristics. This method of ensuring safety from capsizing is based on design approach and consists of the notion that if the ship possesses inherent stability characteristics which satisfy certain criteria it is considered safe.

Most stability casualties are, however, the result of the chain of events where different factors play their parts and rarely casualty could be attributed solely to the deficient stability characteristics. Constructional deficiencies or operational errors are also important factors. Human factor may contribute in 70 to 80 per cent of casualties. Takaishi [17] published data on main causes of capsizing of Japanese vessels. From the data it may be seen that in majority of cases the main cause of accident could be attributed to operational factors.

The importance of operational aspects for safety against capsizing is obvious, although work towards establishing stability requirements is concentrated on hardware development, i.e. criteria of physical characteristics of ships. The view prevailed that safety against capsizing is exclusive responsibility of ship's master. This view, which caused that, in principle, operational requirements were banned from safety requirements (e.g.SOLAS

Convention), has to be revised. It is well known that in complex technical installations operational procedures constitute main framework of safety requirements. Only quite recently several authors pointed out of the necessity of including operational aspects in stability requirements [18,19,20,21,22,23].

The obvious fact that the ship's built - in stability characteristics satisfying design criteria can not prevent loss of stability accident was indirectly confirmed by including at least some operational and constructional provisions in stability requirements, for example IMO recommendations concerning stability include provisions concerning closures of openings on deck and in superstructures, operational procedures during ice formation and require information on stability to be available on board.

Consideration of safety against capsizing as a system which includes four basic subsystems-environment, ship inherent characteristics, operation and information service was proposed for the first time by the author in [24,25]. This idea was supported by Dahle and Nedrelid [22] and Kastner [23,26], who presented it in the form of Venn's diagram (Fig.2).

System safety approach to complex engineering problems was applied in many cases including ship design [27]. This approach consists of looking at the problem as including several subproblems mutually interrelated. It is an approach where the process of achieving main aspects (aims) of the problem are exactly defined and connected with the subprocesses in accordance with adopted scheme.

The above considerations reveal that there is the need for development of "rational" stability criteria and the reasons for this could be summarized as follows:

1. present criteria do not refer to probability of capsizing. Rational criteria should be based on probabilistic approach;
2. present criteria refer to built-in stability characteristics. Rational criteria should be based on system approach taking into consideration environment, operation incl. human factor and information service;
3. present criteria do not safeguard sufficient safety level;
4. safety level achieved with present criteria could be widely different for different ships.

Application of safety assessment methods.

System of safety against capsizing is a complex one because of multiple interrelations between elements of its subsystems. Therefore its analysis is difficult. Nevertheless this constitutes starting point to the modern approach to safety problems - safety assessment. (SA) Application of SA methods may be useful in studying safety against capsizing as it appeared to be in some other areas.

Suppose there are k-situations consisting of loading conditions, sea states and wind forces, headings and speeds in which a ship may find itself during a year. The total probability of capsizing could be expressed as:

$$T P F = \sum_{k=1}^k C_k P F_k$$

where: $P F_k$ = probability of capsizing accident in k-th situation, and
 C_k = probability of occurrence of this situation.

Factors in each situation may be events such as shifting of cargo, crowding passengers on one side, rudder action, excessive rolling, openings not closed, water trapped on deck, human factor, considered separate or in groups.

In practical application of the above formula it would be necessary to identify situations which could include geographical area, weather force, ship's heading relative to wind direction and loading condition. Therefore

$$C_k = \sum_{i=1}^m \sum_{j=1}^h \sum_{k=1}^p \sum_{l=1}^r p_i \cdot p_{ij} \cdot p_{ik} \cdot p_{il}$$

where: $p_i = \frac{T_i}{T}$ = probability that the ship is in the i-th geographical area

T_i = part of the voyage time (or ship's lifetime) spent in the i-th area;

T = total voyage time (or ship's lifetime);

p_{ij} = probability of meeting j-th weather force in the i-th area;

p_{ik} = probability of meeting m-th encounter angle relative to wind in the i-th area;

p_{i1} = probability of occurring 1-th loading condition in the i-th area.

The above circumstances could be estimated on the yearly basis of the analysis of ship's route, statistics of weather conditions and loading conditions. Discrete values for all of the above five circumstances have to be chosen and then number of situations identified. Probabilities of each situation occurring should be then estimated with the condition that the sum of the probabilities has to be equal unity.

Considering the above mentioned factors such as crowding of passengers; rudder action, etc., each of them may cause failure of the whole system, i.e. capsizing. The formula for PF_k taking into account these factors with n factors considered, takes the form:

$$PF_k = 1 - \prod_{i=1}^n (1 - PF_{ki})$$

where symbol \prod has the meaning as follows:

$$\prod_{i=1}^n p = p_1 \cdot p_2 \cdot p_3 \cdot \dots \cdot p_n$$

The above formulae have virtually the same meaning as formula developed by Sevastyanov [28,29], but they provide possibility to include influence of various factors, including operational and human factor.

Then factors for each situation have to be identified and probabilities attached to them estimated. From them TPF could be calculated. TPF is interpreted as risk function Λ , and knowing it, total probability of capsizing during ship's lifetime is calculated as

$$LPF = 1 - \exp(-\Lambda T)$$

where: T = ship's lifetime.

Proposed method of development of stability standards

Probability of capsizing in a seaway during the time t_i during which stationary conditions K_i exist is

$$PF/K_i = 1 - \exp(-\lambda_o t_i)$$

λ_o in this equation is so called risk function, i.e. probability of capsizing within a unit time divided by the probability of safe operation up to that time. The application of this formula

requires estimation of function λ_0 .

This, in principle, could be done by three different methods [31,32].

- a. Formulation of the satisfactory mathematical model of ship's behaviour in a seaway,
- b. Conducting model experiments in various sea states, observing frequency of capsizings,
- c. Collecting statistical data on loss stability accidents.

As pointed out in [32] all three possibilities pose tremendous difficulties. But it seems that mathematical models recently developed may provide acceptable tool for evaluation of risk function in relative sense if not in absolute sense. One method of calculation of short term prediction of capsizing or risk function was already mentioned [18], and results of calculations for seventeen ships are shown in table 1.

The sample calculations of probability of capsizing revealed that the most important parameter is damping coefficient in rolling motion. In the calculations rough estimate of this coefficient was adopted, as accurate methods of its estimation do not exist. It is essential, however, that such method has to be developed and there exist the possibility that an approximate method based on regression analysis with damping coefficient as one of the main parameters could be developed.

Calculation of probabilities C_k for each situation k although posing some difficulties, could be performed if the particular route of ship operation is known. Using discretization of this route and available data on weather conditions on a yearly basis allows establishment of operating envelope of the ship. Loading conditions should be included in this envelope and for this purpose vector method as proposed by Sevastyanov may be used.

The difficulty may arise if the possibility to avoid heavy weather areas is introduced. This depends on the availability of weather information and on the decision of the master, i.e. on the human factor. However, possibly in this case it might be assumed that the master will obey in all cases the directives given in the stability operational diagram which is under consideration by SLF Subcommittee of IMO [33] and which will be recommended in near future. Human factor could be taken into account separately.

Human factor is an important element in the scheme and in taking account of it difficulties could be met. Human performance, first of all performance of the master who is responsible for all decisions onboard ship depends on training and experience consciousness,

physical conditions, performance under stress, ability to use information, etc. In no way stability criteria could be related to all these characteristics, but on the basis of statistics training and experience could be taken into account.

This kind of analysis will certainly provide a very good sense of the relative importance of each circumstance in an assumed situation. However the application of above method has not been tried yet and its efficacy is not known. For certain, several difficulties must be overcome in order to achieve practical results.

The most important and most difficult to evaluate from the point of view of safety against capsizing is probability of capsizing due to action of a seaway. Most other factors could be handled in the deterministic way.

In order to check the practical applicability of the method some test calculations were performed. Details of the test calculation were presented in an Appendix to the paper [34] and therefore are not repeated here. In the test calculation the following results were obtained:

$$T P F = \Lambda = 0,07 \cdot 10^{-2}$$

It is known from statistics, that rate of loss of ships due to capsizing is of the order of 0,06 to $0,1 \cdot 10^{-2}$, which shows that the result obtained is reasonable.

The values of TPF calculated in the described above way are rather small, of the order of $1 \cdot 10^{-2}$ and bearing in mind assumptions made in the calculation model, must be considered as stipulated values. The main point is, how to derive stability criteria on the basis of calculation of TPF.

It is proposed that TPF be considered as attained safety index which is calculated for each ship considered. Then the condition of safety should be

$$T P F < R$$

where: R = required safety index

Formally this proposal is in line with the method adopted in the probabilistic subdivision requirements included in IMO recommendations [35,36]. The physical background of the method of calculation of the attained safety index is, however, totally different.

The evaluation of the required safety index is an important element in this scheme. R could be chosen depending on ship's type (whether passenger, cargo or other), on ship size (possibly smaller R should be chosen for small ships), on number of passengers, on type of cargo and on ship's route.

$R = \text{required } f(\text{type, } L, N, \text{ cargo})$

Obviously in this scheme the smaller R the greater safety level.

Critical values of R have to be evaluated on the basis of systematic calculations of TPF for a population of existing ships considered safe in operation as well as for ships which suffered casualties. For this purpose, at least partially, data bank on casualties collated by IMO could be utilized especially that it was recently computerized [37]. It is extremely important that before work on calculations of TPF is started, the method of calculations has to be agreed internationally because different methods obviously would lead to different results, and in any case the calculated values of TPF have to be considered as relative values only. It is suggested a simple method of calculation of the required safety index R

$$R = k_1 \cdot k_2 \cdot f(L)$$

where: $k_1 = f(L, N)$ - coefficient depending on the number of passengers and length of the ship;

$k_2 =$ - coefficient depending on the type of the ship and its cargo.

Both coefficients and also $f(L)$ should be chosen in such a way that for increasing number of passengers and decreasing L , R should be smaller. R should be smaller also for ships' types for which increased safety level is required, e.g. ships carrying dangerous cargo. It is possible also to introduce additional coefficients which may take into account operation in high risk zones (e.g. arctic zone) and human factor. The inclusion of the coefficient related to human factor by e.g. decreasing R when the master does not possess required qualifications pose some legal problems, but this approach is widely used by insurance companies which increase fees for certain age groups of drivers for example. Why not to apply this approach to ships?

Obviously coefficients k_1 , k_2 and function $f(L)$ would depend on the adopted method of calculation of TPF, therefore at present it is impossible to suggest any definite values.

Conclusions.

The proposed methodology of developing stability criteria is a realistic one. It is based on the estimation operating envelope of the ship and on the calculation of the short and long term prediction of the probability of capsizing. There are no basic difficulties in both, although it is essential that standard method of calculation of short term prediction of probability of capsizing has to be agreed internationally. As one of the most important

parameters in this prediction is damping coefficient of rolling motion reliable method of calculation of this coefficient for various ship types has to be elaborated.

For estimation of required safety index R sample calculations for a number of ships of various types and sizes which are considered safe in operation and preferably also for those which capsized have to be performed.

Table 1

SHIP Name type	Dimensions L * B * T	Loading Condition	Probability of capsizing Damping	
			normal	initial
B 448	136.1 * 20.5 * 6.80	0	4.07.E-7	
		1	1.37.E-7	
		2	7.35.E-5	
HEL	150.6 * 23.3 * 8.42	0		7.81.E-8
		1		2.25.E-6
		2		1.48.E-6
B-MAL	159.8 * 24.0 * 10.19	0		0
		1		3.74.E-6
		2		1.25.E-5
930	145.4 * 23.6 * 8.00	0		4.6 E-5
		1		9.1 E-5
		2		1.75.E-5
B-68	143.0 * 20.6 * 7.40	0		2.43.E-5
		1		7.70.E-5
		2		4.40.E-5
CORST	189.07 * 24.4 * 10.69	0		2.32.E-6
		1		1.2 E-3
		2	8.82.E-4	0.019
B-431	79.59 * 13.6 * 5.29	0	1.27.E-3	
		1	8.2 E-4	
		2	2.2 E-3	
B-446	125.34 * 17.69 * 6.78	0	0	3.71.E-5
		1	0	1.40.E-4
		2	7.74.E-9	2.45.E-3
B-342	161.6 * 23.17 * 9.75	0		7.85.E-9
		1		7.61.E-6
		2		7.85.E-5
B-340	171.2 * 26.6 * 9.60	0	0	1.57.E-6
		1	0	2.62.E-7
		2	1.23.E-5	1.23.E-5
B-361	85.1 * 13.4 * 5.35	0	2.43.E-4	
		1	7.89.E-4	
		2	8.8 E-5	
B-472	98.7 * 16.0 * 5.74	0	2.17.E-9	
		1	3.17.E-10	
		2	9.36.E-5	
B-445	137.3 * 18.8 * 7.30	0	5.34.E-7	3.43.E-5
		1	0	1.53.E-4
		2		
B-348	151.55 * 24.0 * 9.30	0		8.83.E-6
		1		2.39.E-5
		2		1.44.E-4
B-436	143.80 * 21.0 * 8.69	0		4.09.E-6
		1		5.55.E-5
		2		1.78.E-4
B-467	183.06 * 25.34 * 9.56	0	9.11.E-6	
		1	0	2.75.E-6
		2	0	1.36.E-4
B-442	146.1 * 20.6 * 7.79	0		3.84.E-6
		1		8.10.E-5
		2		1.05.E-4

* - For the loading condition "0".

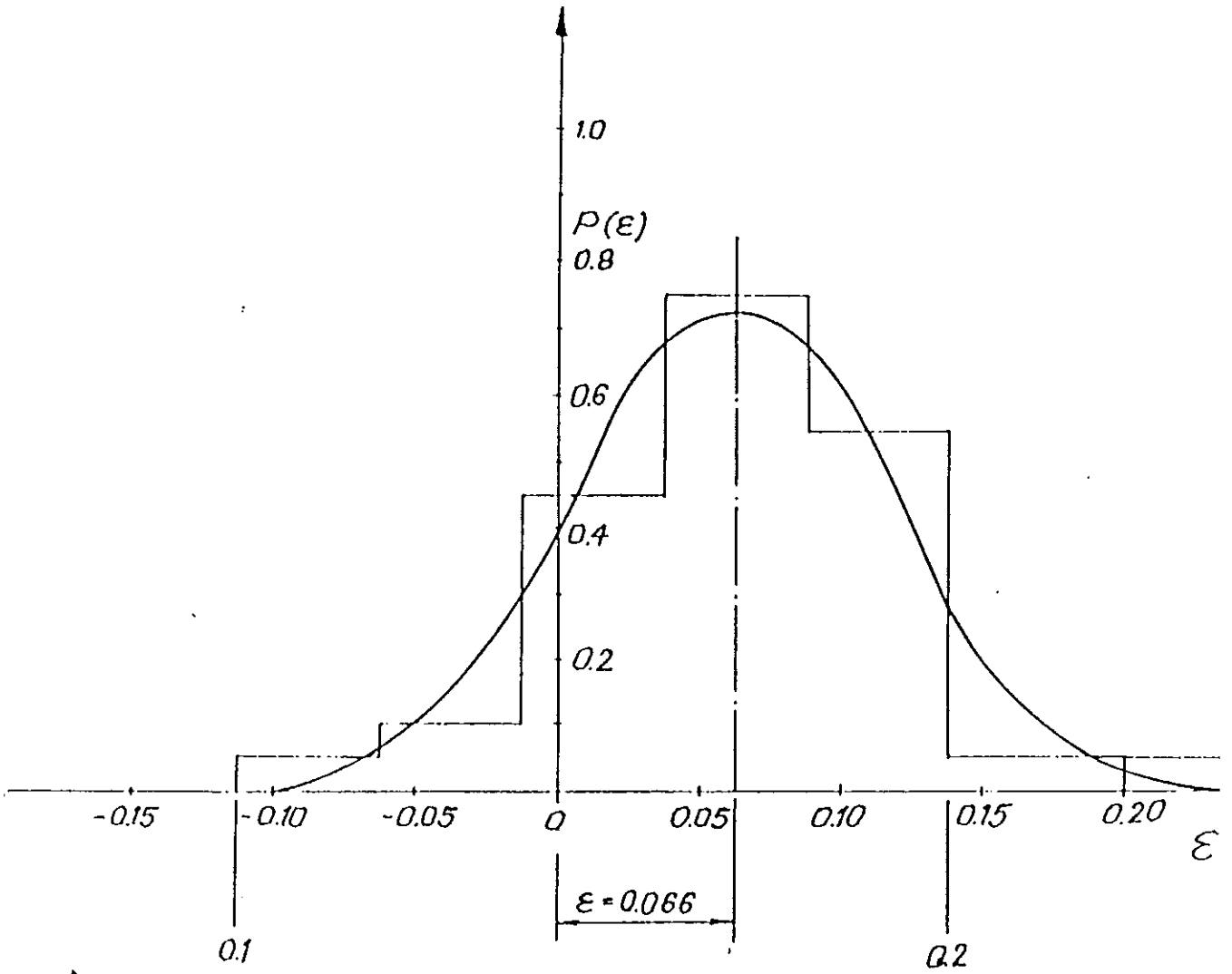


Fig. 1.

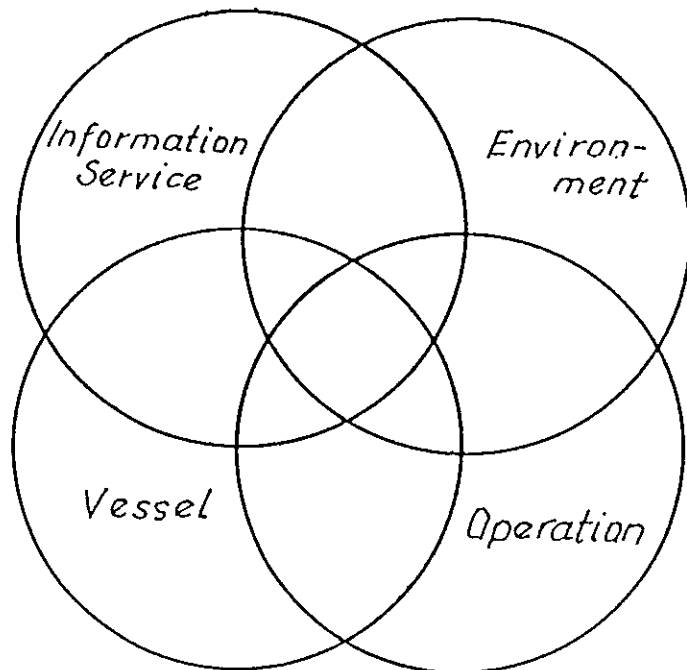


Fig. 2 - Four-Fold Interaction of Cargo, Vessel, Environment, and

References

- [1] "Recommendation on a Severe Wind and Rolling Criterion (Weather Criterion) for the Intact Stability of Passenger and Cargo Ships of 24 metres in Length and Over", IMO, Resolution A.562(14), 1985.
- [2] "Draft Terms of Reference for an Ad Hoc Group", IMO, doc.STAB XVI/WP.2, 1974.
- [3] "Intact Stability. General Philosophy for Ships of All Types", Submitted by Poland. IMO, doc. STAB XXII/6, 1978.
- [4] Kobyliński, L.: "On the Possibility of Establishing Rational Stability Criteria", IV-th STAB Conference, Naples 1990, Vol.II, p.501.
- [5] Sevastyanov, N.B.: "On probability Methods of Finding Stability Standards", IMO, doc.STAB/INF.48, 1969.
- [6] Caldwell, J.B., Yang, Y.S.: "Risk and Reliability Analysis Applied to Ship Capsize: a Preliminary Study", The Safeship Project: Ship Stability and Safety, International Conference, RINA, 1986.
- [7] Krappinger, O.: "Uber Kenterkriterien", Schiffstechnik 1962, p.145.
- [8] Kobyliński, L.: "Rational Stability Criteria and Probability of Capsizing", I-st STAB Conference, Glasgow 1975, paper 1.
- [9] Morrall, A.: "Philosophical Aspects of Assessing Ship Stability", II-nd STAB Conference, Tokyo 1982, p.647.
- [10] Kobyliński, L.: "Safety of Ships Against Capsizing", Third International Congress on Marine Technology, Athens'84, Vol.I, p.387.

- [11] Morrall, A.: "Panel Discussion I: Philosophy and Research". II-nd STAB Conference, Tokyo 1982.
- [12] Kuo, C., Welaya, Y.: "A Review of Intact Ship Stability Research and Criteria", Ocean Engineering, 1981, p.65.
- [13] Krappinger, O., Sharma, S.D.: "Sicherheit in der Schiffstechnik", Jahrbuch der STG, Bd.68, 1974.
- [14] Kobyliński, L.: "Safety against capsizing Pt.IV ", Prace Badawcze Nr 9/94, T.U.Gdańsk.
- [15] Sevastyanov, N.B.: "Contemporary State of Work on Standardisation of Stability of Fishing Vessels". III-rd Scientific Conference for the Development of Fishing Industry, Leningrad 1968. (in russian)
- [16] Belenky, V.L.: "A Capsizing Probability Computation Method", Journal of Ship Research, Vol.37, No 3 Sept.1993.
- [17] Takaishi, Y.: "Consideration of the Dangerous Situations Leading to Capsizing of Ships in Waves", II-nd STAB Conference, Tokyo 1982, p.243.
- [18] Caldwell, J.B.: "Prospects of a Rational Approach to Marine Safety", The 4-th International Shipbuilding and Ocean Engineering Conference, Helsinki 1986.
- [19] Hormann, H.: "Judgement of Stability - Questions to be Solved - a Contribution from the Point of View of Approving Authority". II-nd STAB Conference, Tokyo 1982, p.641.
- [20] Stasiak, J.: "Safety of Seagoing Ships". Zagadnienia Eksploatacji Maszyn. Z.2-4, (82-84) 1990 (in polish).

- [21] Horman, H., Wagner, D.: "Stability Criteria for Present Day Ships Designs", III-rd STAB Conference, Gdańsk 1986, Vol.I.p.125.
- [22] Dahle, E.A., Nedrelid, T.: "Operational Manuals for Improved Safety in a Seaway". III-rd STAB Conference, Gdańsk 1986, Vol.I.p.217.
- [23] Kastner, S.: "Operational Stability of Ships and Safe Transport of Cargo". III-rd STAB Conference, Gdańsk 1986, Vol.I.p.207.
- [24] Kobyliński, L.: "Safety of Ships Against Capsizing". Third International Congress on Marine Technology, Athens'84, Vol.I.p.387.
- [25] Kobyliński, L.: "Philosophische und Hydrodynamische Probleme der International Kenterkriterien von Schiffen". Internationales Schiffstechnisches Symposium, Rostock 1984.
- [26] Kastner, S.: "Inclusion of Theoretical Achievements on Ship Stability in Ship Design Process and in Ship Operation". IV-th STAB Conference, Naples 1990, Vol. II, p.677.
- [27] Gillmer, T.C.: "Modern Ship Design". Tri - Service Press.
- [28] Sevastyanov, N.B.: "Stability of Fishing Vessels". Morskoi Transport, Leningrad 1970. (in russian)
- [29] Sevastyanov, N.B.: "On Probability Methods of Finding Stability Standards". Sudostrojenie, No 1, 1978 (in russian).
- [30] Kobyliński, L.: "Safety of the Vessel in a Seaway". Institut for Skipsprosjektering, Universitet Trondheim, Norges Tekniske Hogskole, Rep.PP 5, 1974.
- [31] Kobyliński, L.: "Rational Stability Criteria and Probability of Capsizing". I-st STAB Conference, Glasgow 1975, paper 1.

- [32] **Bielański, J.:** "Ship Rolling under the Action of the Random Beam Wind and Sea as a Background of Comparison IMO Stability Criteria", "Otradnoye'93" International Workshop, Kaliningrad 1993.
- [33] "Draft Safety Operational Manual in Following and quartering Seas. Draft Report to the Maritime Safety Committee". IMO,doc.SLF 37/WP.7, 14 January 1993.
- [34] **Kobyliński, L.:** "Possibility of Application of Safety Assessment to the Development of Stability Criteria". Otradnoye'93" International Workshop, Kaliningrad 1993.
- [35] "Regulations on Subdivision and Stability of Passenger Ships as an Equivalent to Part B of Chapter II of the SOLAS Convention". IMO, Resolution A.265 (VIII).
- [36] "Amendments to the 1974 SOLAS Convention". IMO, Resolution MSC 16(58),1990.
- [37] **Kubiczek, R.:** "Data Base of Stability Casualties for Cargo Ships and Fishing Vessels". Prace Badawcze T.U.Gdańsk Nr 76/93 (in polish).

OPERATIONAL STABILITY AND ON-BOARD COMPUTER

V.Lipis³ , S.Palekhov¹ , V.Peresyphkin²
Russia

Summary

General approach to the shipboard facilities providing safeguards against capsizing are discussed along next lines :

- ship stability monitoring using shipboard PC within Loadcalculators ;
- expert systems used for prediction and diagnostic of seakeeping performance and selection of safe sailing conditions ;
- means for monitoring of actual stability of a ship as a part of an integrated ship control systems ;
- requirements to ship stability in operating conditions (criteria and operational software for ship-masters).

1. What is " operational stability " ?

In practical attitude " stability " means ability of a vessel not be lost because of capsized. Obtaining with stability has two aspects: design and operational. Design stability - is such which can be reached during creation of vessel with " good " by seaworthy qualities. It is a design quality of vessel - to be safe against capsized on level of guarantees of design methods and classification rules. Operational stability - is such which a vessel actually has in various real situations during her life. It is significantly defined by ability of captain to load and to control vessel in a right way, to observe conditions of design warranties and to know how to act during more dangerous circumstances outside design criteria of prudence . Decisive role of the " human factor " is evident and technical proof of captain's actions in a great degree depends on level of technology of used on-board facilities.

2. How the operational stability can be provided?

In order to help captain to be in a full measure responsible for stability of the vessel two types of technology are used :

- facilities for informational support and calculated forecast;
 - equipment for monitoring, diagnostics and management based on measurement of actual parameters.
- Classical example of facility of first type, of course is "Stability booklet" which according to convention SOLAS each captain should dispose in order to reach stability data of the vessel in operation in various conditions by "fast and easily modes"[1]. It is not so easy to satisfy these clear requirements . Practically captain can use the conventional "Stability booklet" only in standard load cases . For any particular condition the task was resolved through automation of calculations and representation of information with aid of on-board PC. It is much harder to receive accurate results. As far as actual initial data do not correspond to present information, calculated parameters of stability and seaworthiness differ from actual. First of all it relates to initial information about loading as well as about components of deadweight, external conditions and emergency circumstances. Calculation error on practice can be prohibitively high [2], [3] . Automation of calculations does not save situation because methods and facilities of monitoring of actual characteristic are needed.

On modern level of informational and measuring marine technology vessel can be equipped with specialized on-board system with a computer as central chain with special software capable to operate both in " off line " and " on line " modes.

The system has three main functions executed by three subsystems:

- loading of cargo and ballast according to conditions of trim, stability and strength;

1. S.Palekhov - Capt. Deputy Director Department of Marine Transport. Russian Federation Ministry of Transport, Moscow
2. V.Peresyphkin - Prof., Ph. Dr., Director of Central Marine Research and Design Institute, St.Petersburg
3. V.Lipis - Prof., Ph. Dr., Head of Dept. of Naval Arch., Central Marine Research and Design Institute, St.Petersburg

- choosing safe modes of ship operation in rough seas;
- obtaining survivability of damaged vessel;

First two of functions are connected with stability and seaworthiness of a vessel in intact condition and constantly are executed in process of her regular normal operation. The third - with damage stability and seaworthiness in emergency. All functions can be used for training the ship's crew.

This way, functionally, the computer system for operational stability relates to on-bridge equipment aimed for safety of navigation.

3. Loading and ballast management.

This is the most advanced kind of technology providing a transport ship with operational stability especially in calculation and informational parts. Function chart is presented on Fig. 1.

3.1. Algorithms of calculation and programs have been developed and used on ships of many countries. Complete information from the "Stability booklet" for any loading case have been used there. However, opportunities are considerably broader: not only check of IMO criteria and national Rules, but also, for example draught and stability optimization in variational conditions and/or to limitations, such as:

- condition of rotation of cargo in ports during the voyage;
- optimal up to fuel consumption trim;
- condition of minimum of ballast;
- needed draughts on shallow water;
- limitations caused by seaworthiness (top limit of stability, loss of stability on following seas etc.)

From the point of view of organization of algorithms and data base two kinds of programs exist. For each case of load calculation is executed basing on

- a) the initial data of the ship's hull form, or
- b) already designed documentation from "Stability booklet".

Main time expenditure of operator and his possible errors are caused by hand-operated enter of initial data of loading especially in cases of large number of cargo units on large container carriers and "roll-on" ships. Efficiency and reliability of calculation are considerably increased if the program contains a module for automatic enter of initial data of cargoes in EDIFACT standard from diskettes or modem on terminal.

3.2. The next step in this direction is automation of monitoring of tanks filling levels and draughts with aid of gauges of actual condition. In fact it is already an element of measuring technology. Today it is used in diagnostics and management systems which do not provide direct control of actual stability and include only special interface. From the other side there is a practice of recommendations and application of non-automatic facilities for approximate check of actual stability based either on method of roll or on method of inclining (calibrated cargo or inclining tanks and static heel sensor on bridge) [4], [5]. And, of course there is long enough (more than 50 years) history of attempts of creation automated facilities which today receives powerful pulse based on new technology [2], [6], [7], [8], [9]. Principles are the same: operational inclining experiment and parameters of roll. The cargoplan functionally is supported by systems of the first type, which include three main functional parts:

- automated inclining system;
- measuring unit i.e. gauges with analog - code transformation;
- computer with a special software and interface.

Main measured parameters are: draughts fore and aft, filling levels of tanks (including inclining tanks) and static angle of heel. Software executes:

- communication with gauges;
- processing and measurements quality surveillance with definition of actual trim of vessel and metacentric high;
- correction of calculated characteristics of stability and draught.

Specifications for design and automation of inclining system, to parameters of gauges, their installation and interrogation, factory tests - all are caused by the central task - providing the accuracy of result.

Is it possible to trust the measuring system more than to calculation? Today sure positive answer is absent. And philosophy of system use depends on it: use only as a facility of diagnostics

or also for regulation of loading? It is clear that reasonable norms for definition of errors of parameters and technique of valuation of operational inclining test's quality with consideration of time expenditure limitation are needed. For example, in order to get the standard error of measurement of small (0.2 - 0.4 m) metacentric height on level 3 - 5%, it is necessary to measure the heel with accuracy 0.01 - 0.02, then to have an opportunity to conduct three-four inclinings within one hour and, at last to execute the condition of getting the probable error of experiment (with discard exception) inside the standard confidence interval (Fig. 2). Proposals for such requirements were developed for Register and offered to IMO Subcommittee SLF for development of Code of stability for all types of ships in intact condition [10].

The technology of stability measurement of a ship at sea provides consideration of dynamic factors such as influence of speed etc. and probability treatment of continuous random process of ships roll. This task meets the analysis of seaworthiness of a vessel.

4. Safe modes of ship operation in rough seas.

4.1 Function chart is presented on Fig. 3. Computational program is designed on algorithms of complex hydrodynamic analysis of quantitative criteria of seaworthiness of a vessel based on probability dynamic models [11]. Research in this field has history beginning from 1930-th and large literature. For determination of safe sailing modes on boards of vessels mainly two types of diagrams: universal diagram of resonant roll and diagram of admitted speed and course in conditions of negative effect of wind and waves of various rate and direction have been offered [12], [13]. This approach lives up today - it is enough to mention the last proposals for the Guidance for captain for choosing safe modes of navigation in following seas considered by IMO Subcommittee SLF [14]. At the same time the already reached level of hydrodynamical analysis which combines results of theory, natural and serial model tests and experience of fine seamanship gives an opportunity to design an enough efficient common algorithm. Main thesis:

- quantitative criteria of dangerous influence;
- safe level (norms)
- service: "invisible" to the navigator complexity of software design and very simple user interface.

Result should follow the directions of IMO Code [5] of order of operation in dependence from weather conditions (p.2.5), particularly p.2.5.11: "In avoidance of dangerous situations in severe weather conditions it is recommended to use... on-board computer based systems. The method should be simple to use".

Example of result is presented on Fig.4 (a,b).The operator receives these simple pole diagrams on on-board computer with consideration of effects of individual characteristics of the vessel, particular loading and actual conditions of navigation in heavy seas while disposing minimum of initial information.

Of course choose of safe modes of heavy seas navigation based on such information is in greater degree "in hands of captain" than valuation the "pure" stability. Therefore requirements to accuracy of calculation of the diagram are not so high. Nevertheless shortage of initial data about ship motions and conventionality of standards of dangerous effects results in necessity of use measuring facilities.

4.2. First and enough effective level of measuring support - is monitoring of accelerations during ship motions in waves (Fig.3).

Decision following tasks should be achieved:

- direct registration of rolling parameters (with output to stability control);
- determination of intensity rate of external indignation with updating of calculated values of all dependent of ship motion in waves.

In combination with use of standard ship measuring facilities (speed, course, rudder angle, number of revolutions and pitch of screw) the monitoring permits to extract actual information if it have been skillfully processed. Transition to direct control of draughts, static and dynamic movements of vessel is the second level of the system.

Experience of use of experimental monitoring equipment have been received in different countries. Requirements to the software are substantially broader than specified in p.3.2. for stability monitoring systems. Main addition: economic methods of processing measured random processes for definitions

short- and long-term characteristics of seaworthiness. Of course the central question remains supplying of reliability of measurements and valuation of their quality.

5. Survivability of damaged vessel.

Function scheme is presented on Fig.5. Algorithms of calculation are based on standard methods of forecast of trim, damage stability and buoyancy reserve of a vessel in particular loading case and real wreck circumstances. Sufficient condition are defined by known IMO requirements and national rules for subdivision and damage stability used in any intermediate stage of singe.

Features of calculation program are:

- Non-calculation visual informational unit with directions of prime actions with account of requirements of the SOLAS Convention to scheme of control in case of wreck [1].
- monitoring and forecast of change of parameters of a vessel in emergency in time;
- expert logical analysis (heuristic methods) of actual situation, degree of danger and plan of actions;
- sufficient speed for operational application in extreme situation.

Errors of calculation of parameters of vessel in emergency are caused first of all by discrepancy of information about permeability of cargo holds and about conditions of wreck (place and area of breach of the hull, speed of receipt of water, filtration etc.). Actual condition can be determined only with aid of in-time monitoring of water level in rooms and draughts of vessel. Measuring control provides as well a connection with automation of equipment (signaling about condition of systems and equipment, means of closure, pumps inclusion). Calculations and monitoring of actual condition become considerable complicated in case of influence of wind, waves and roll; practical methods are in initial stage of elaboration. This subsystem is used in everyday life for training the ships crew on struggle for survivability of the vessel.

Acknowledgment

The authors of this paper has been sponsored by the Department of Maritime Transport of the Russian Federation Ministry of Transport.

References

1. Consolidated text of the 1974 SOLAS convention. IMO.1993.
2. Lipis V.B.,Salov V.E. Problem of the Stability Control on Transport Ships in Operation. STAB'90, Naples, Italy,1990.
3. H.Kaps, S.Kastner. On The Determination of Ship Stability During Service. STAB'90, Naples,Italy, 1993.
4. Rules for the Classification and Construction of Sea-Going Ships. Register of Shipping, "Transport", 1990.
5. Code of intact stability for all types of ships covered by IMO instruments. SLF 37/25, 1993.
6. S.Kastner. On Ship-Borne measurements to Control Stability and Safety. International Workshop OTRADNOYE'93,Russia,1993.
7. Chen H., D.Sucharski. The Role of Shipboard Decision Support Systems and Instrumentation in Enhancing Maritime Safety. US Coast Guard Vessel Stability Simposium, 1993.
8. F.W. De Bord,Jr., B.Hennessy. Development of a Generalised Onboard Response Monitoring System. Phase I. US Coast Guard.Ship Structure Committee,1990.
9. Cojeen H.P., Chazal E.A.,Jr.,Help for Human Beings - it's Instrumental,Proseeding of the Maritime Safety Council, v.39,1982.
10. Documents SLF 35/3,1990; SLF 37/3/7,1992.
11. P.Alman, W.A.Cleary,M.G.Dyer,J.R.Paulling,N.Salvesen. The International Load Line Convention: Crossroad to the Future Marine Technology, 1992.
12. S.N.Blagoveschensky. Theory of Ship Motions in Waves. 1954 (In Russian).
13. V.B.Lipis, Y.V.Remez, The Safety Modes of the Ship Operation in Rough Seas."Transport",1982 (In Russian).

14. Report to the Maritime Safety Committee SLF 38/WP.5.,1994.
15. H.Kaps, S.Kastner. Beurteilung der Stabilität von Schiffen in der Praxis. Hochschule Bremen, 1989. Absch.FE.

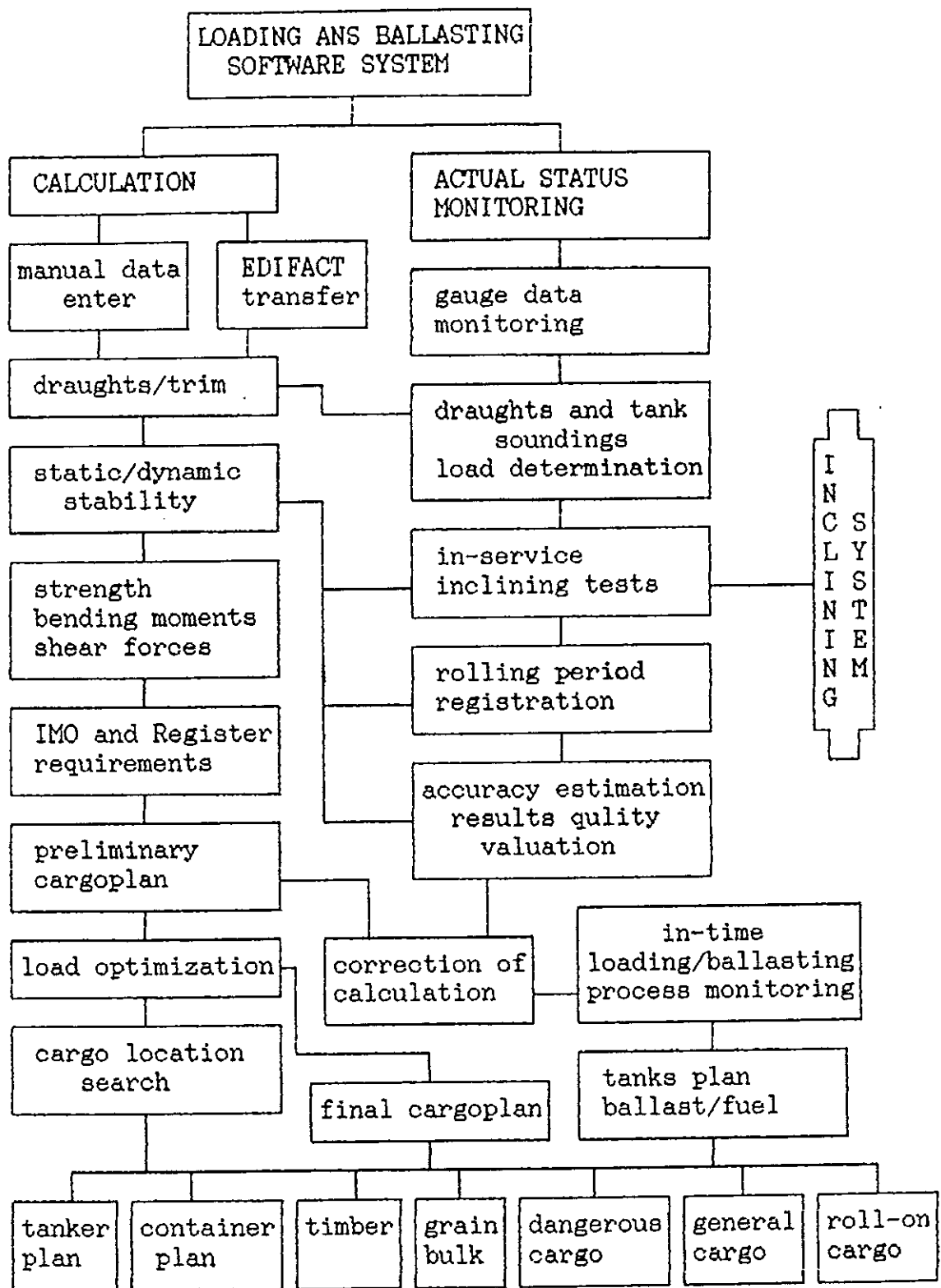
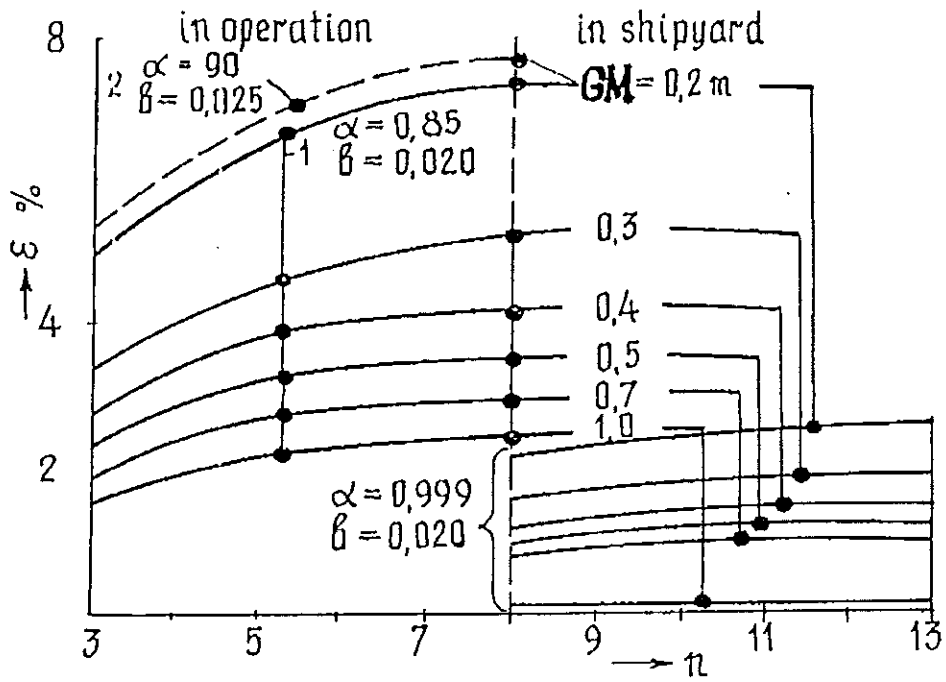


Fig.1



ε - standard error of GM

n - number of measurements

GM- average value of initial stability results from ship inclining tests

α - standard confidence probability (reliability)

β - standard coefficient of a confidence interval.

Fig. 2

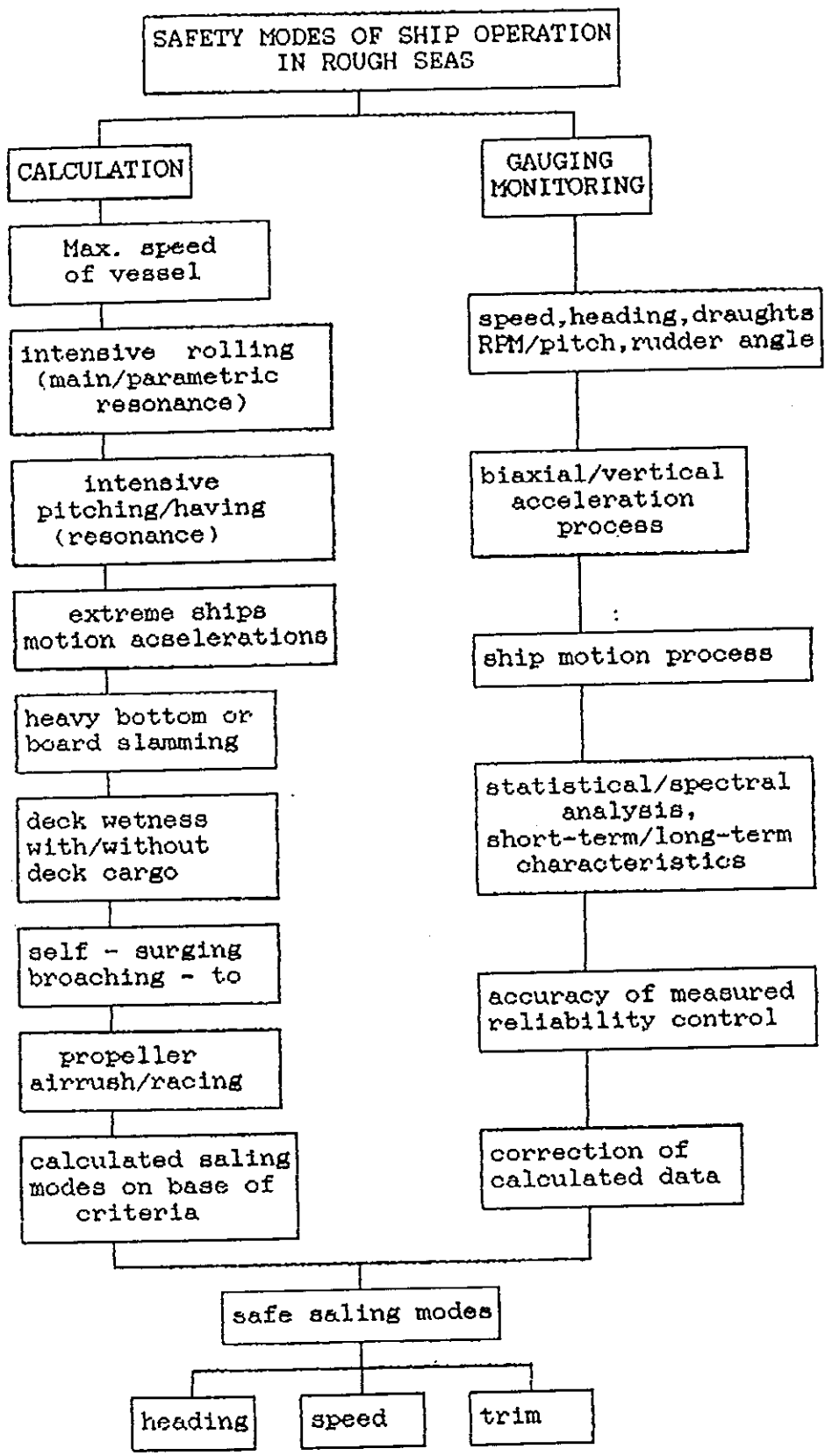


Fig.3

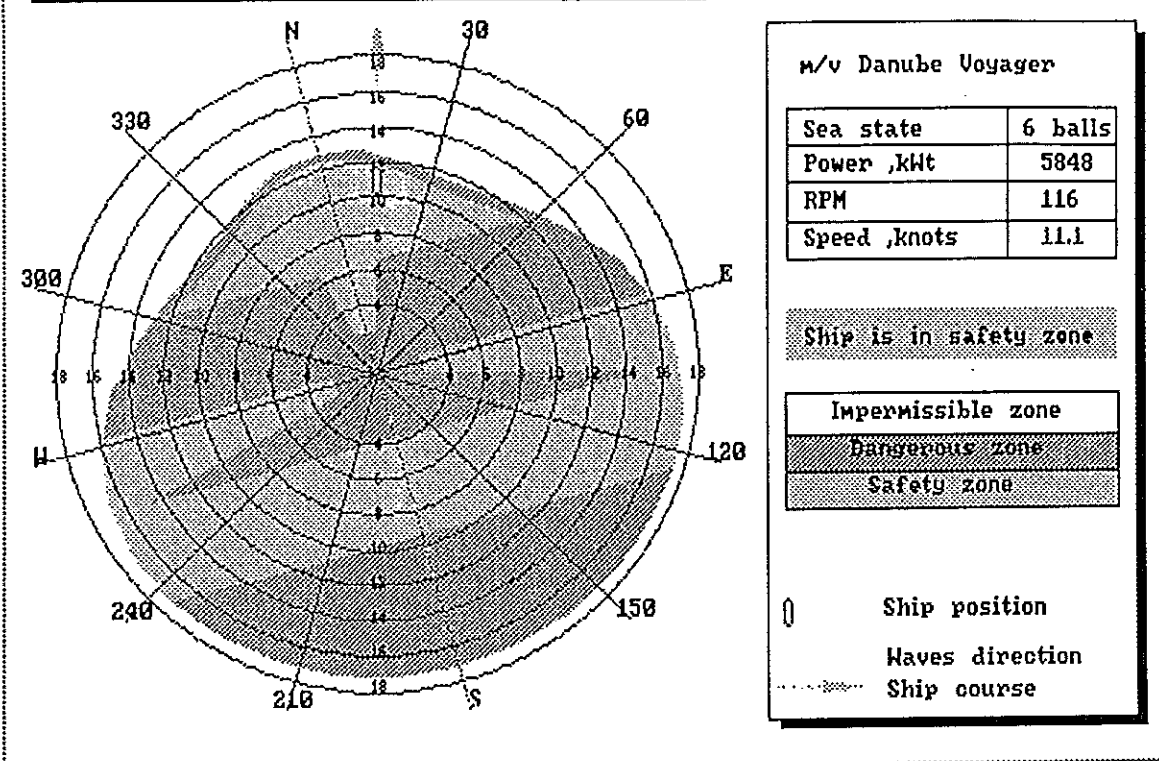


Fig. 4a

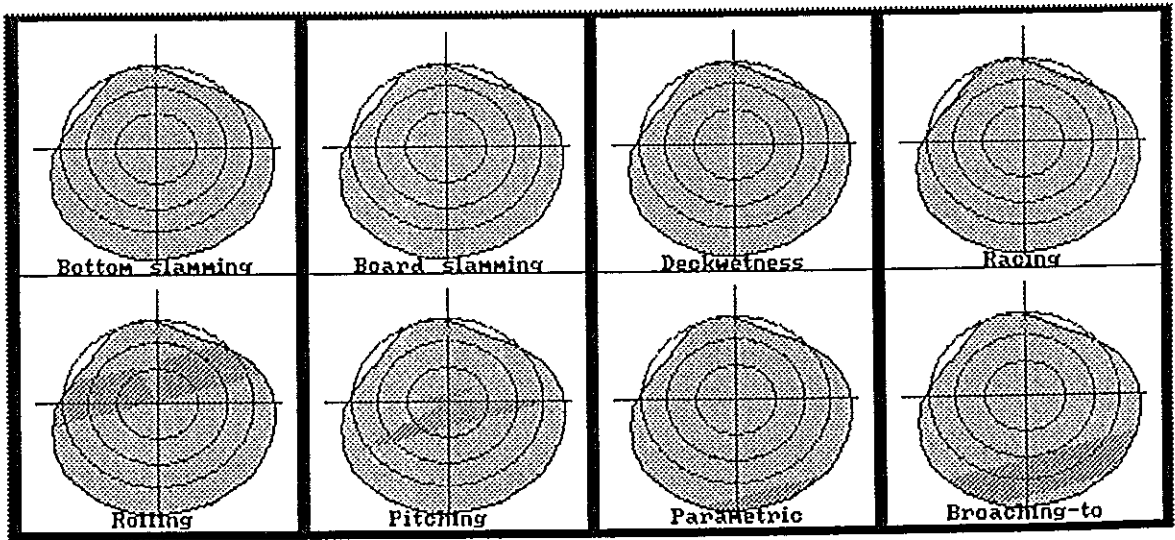


Fig. 4b

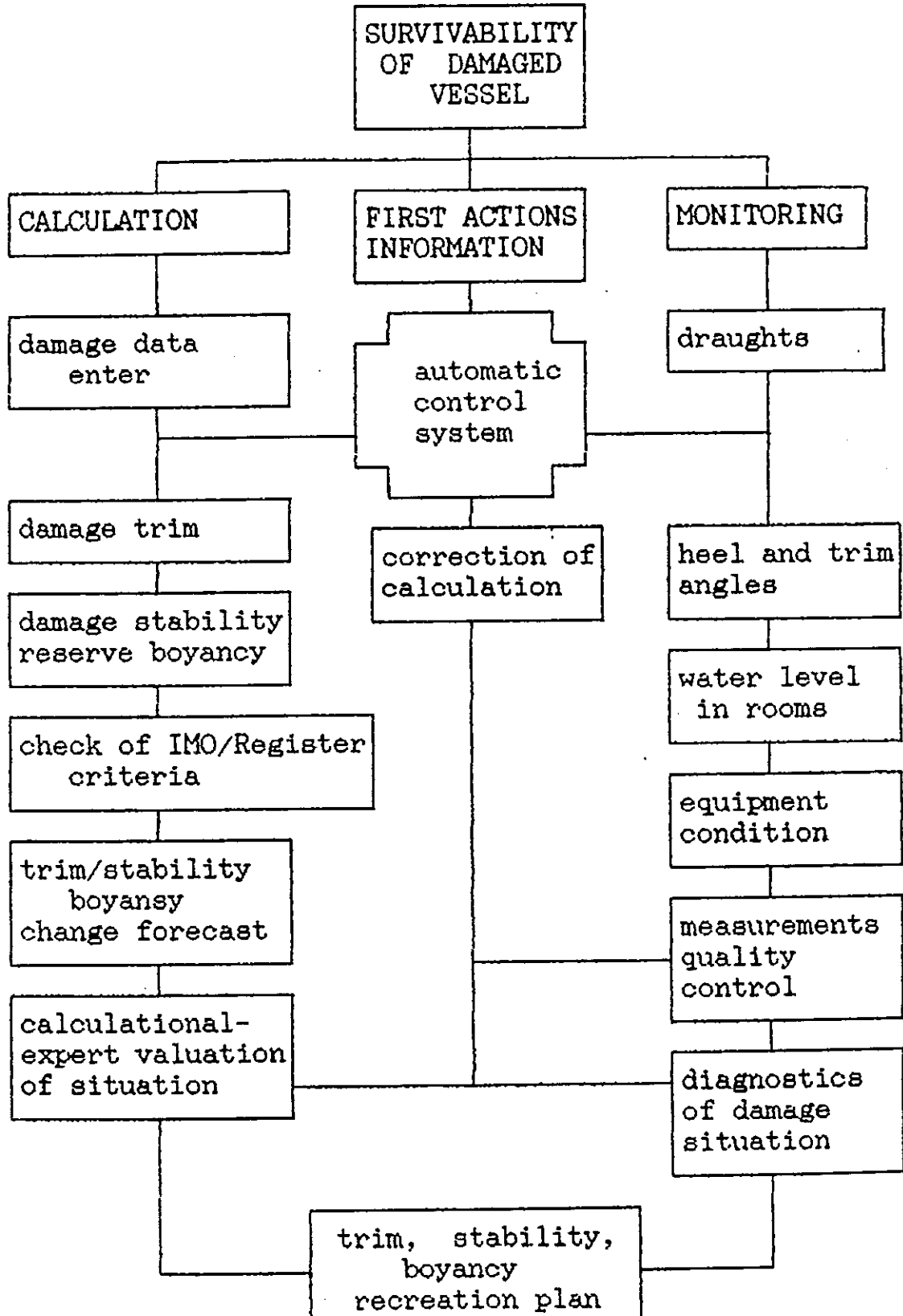


Fig.5

Broaching of a Fishing Vessel in Following and Quartering Seas -Nonlinear Dynamical System Approach -

by

N. Umeda

National Research Institute of Fisheries Engineering, Japan
and

M.R. Renilson

Australian Maritime Engineering CRC Ltd.

ABSTRACT

The nonlinear dynamical system theory has been applied to the broaching phenomenon, which is an unstable and non-periodic yaw behaviour of a ship running with a wave. First, a mathematical model for surge-sway-yaw-rudder motion with low encounter frequency is presented and a prediction method for wave forces in the model is validated with experimental results of a displacement-type fishing vessel in a seakeeping basin. Then, nonlinear analysis associated with equilibria is used to identify a necessary condition for broaching. Further, a methodology for nonlinear analysis associated with periodic orbits is presented. Some numerical examples for fishing vessels are also shown.

NOMENCLATURE

AE	=	aft end of ship
B	=	ship breadth
B(x)	=	breadth of the section
c	=	wave celerity
d(x)	=	draught of the section
FE	=	fore end of the ship
F_n	=	nominal Froude number ($= U / \sqrt{Lg}$)
g	=	gravitational acceleration
H	=	wave height
I_{zz}	=	moment of inertia in yaw
J_{zz}	=	added moment of inertia in yaw
K_p	=	rudder gain
L	=	ship length between perpendiculars
m	=	mass of ship
m_x	=	added mass of ship in surge
m_y	=	added mass of ship in sway
N_w	=	wave induced yaw moment
R	=	resistance of ship
r	=	yaw rate
S(x)	=	area of the section
$S_y(x)$	=	added mass of the section
T	=	propeller thrust

T_D'	=	nondimensional time constant for differential control
T_E'	=	nondimensional time constant for steering gear
U	=	ship velocity ($=\sqrt{u^2+v^2}$)
U_0	=	designed ship velocity
u	=	component of ship speed in x-axis direction
v	=	component of ship speed in y-axis direction
X_w	=	wave induced surge force
Y_w	=	wave induced sway force
δ	=	rudder angle
ξ_w	=	wave amplitude
λ	=	wave length
ρ	=	water density
χ	=	heading angle
χ_0	=	desired course
ω	=	wave circular frequency

INTRODUCTION:

In a seaway, a ship usually travels with periodic motions. When a wave height increases, the ship can be captured by a wave and then may suddenly and violently yaw from her desired course despite application of maximum opposite rudder angle. This is known as broaching and has been identified as one of the major reasons for capsizes of small high speed vessels, such as fishing vessels. Thus, it is important to predict critical conditions of broaching for preventing sea disaster.

A pioneering attempt to investigate broaching was carried out by Davidson (1948) using linear analysis. He showed that even a ship that is directionally stable in calm water may be directionally unstable in following seas. However, he could not explain a direct relationship between directional instability and broaching, because broaching is not a linear phenomenon but fully nonlinear one.

Latest developments in computer technology realized time domain simulations of nonlinear motions with a set of initial conditions. With this technique, Motora et al. (1982) and Renilson (1982) clarified that the wave induced yaw moment of a ship and the rudder force due to maximum opposite rudder angle have dominant factors for broaching.

These time domain simulations are, however, limited in their ability to identify the critical conditions for broaching, because, like any other nonlinear phenomena, broaching is very sensitive to initial conditions. To overcome this difficulty, a nonlinear dynamical approach was applied to broaching by the authors (1992A). For a nonlinear dynamical system described with a mathematical model of the surge-sway-yaw motion, they found equilibria of the system with the maximum opposite rudder angle and examined local stability near the equilibria. The equilibria correspond to surf-riding of a ship. Then, they discussed broaching itself with unstable invariant manifolds from the unstable equilibria to identify critical conditions for broaching. Their prediction method for wave

force in their mathematical model was validated with existing experiments for a semi-displacement-type fishing craft. However, other than the equilibria, the dynamic system for ship motions in quartering seas has important attractors, namely, periodic orbits. And the experimental validation of the prediction method is not enough because a semi-displacement-type craft is not a typical example of conventional vessels.

Therefore, in this paper, the authors extend their mathematical model to the surge-sway-yaw-rudder motion and validate their prediction method for wave forces with new model experiments for a displacement-type fishing vessel. Further, as well as the analysis on equilibria, a methodology to analyze periodic orbits for broaching is presented.

MATHEMATICAL MODEL

The mathematical model for the surge-sway-yaw-rudder motion in this paper is an extension of that for the surge-sway-yaw motion, which was briefly described by the authors (1992A).

As can be seen in Fig.1, two coordinate systems are used: wave fixed with origin at a wave trough, ξ axis in the direction of wave travel; and body fixed with origin at the centre of gravity, the x axis pointing towards the bow, the y axis to starboard and the z axis downwards. The symbols follow the usual notation and are defined in the nomenclature.

For a given wave condition and propeller revolutions, the state vector of this system is defined as follows:

$$\mathbf{x} = \{\xi_G / \lambda, u, v, \chi, r, \delta\}^T \quad (1)$$

The dynamical system can be represented by the following state equation:

$$\dot{\mathbf{x}} = \mathbf{F}(\mathbf{x}) = \{f_1(\mathbf{x}), f_2(\mathbf{x}), \dots, f_6(\mathbf{x})\}^T \quad (2)$$

where

$$\begin{aligned} f_1(\mathbf{x}) &= \{u \cos \chi - v \sin \chi - c\} / \lambda \\ f_2(\mathbf{x}) &= \{T(u) - R(u) + X(\xi_G / \lambda, \chi)\} / (m + m_v) \\ f_3(\mathbf{x}) &= \{-(m + m_v)ur + Y_v(u)v + Y_r(u)r + Y_\delta(\xi_G / \lambda, u, \chi)\delta + Y_w(\xi_G / \lambda, u, \chi)\} / (m + m_v) \\ f_4(\mathbf{x}) &= r \\ f_5(\mathbf{x}) &= \{N_v(u)v + N_r(u)r + N_\delta(\xi_G / \lambda, u, \chi)\delta + N_w(\xi_G / \lambda, u, \chi)\} / (I_{zz} + J_{zz}) \\ f_6(\mathbf{x}) &= \left[(U_0 / L) \{-\delta - K_p(\chi - \chi_c)\} - K_p T_D' r \right] / T_E' \end{aligned} \quad (3)$$

Since external forces are functions of surge displacements but not time, this equation is nonlinear and autonomous.

The wave induced surge force, X_w , are calculated using the Froude-Krylov component of the force. The wave induced

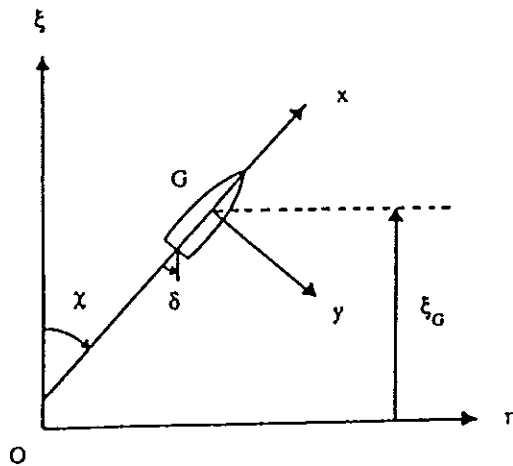


Fig.1 Coordinate systems

Table 1 Principal particulars of a displacement-type fishing vessel (small trawler)

Length	L	[m]	14.40
Breadth	B	[m]	3.05
Draft fore	d_f	[m]	0.35
Draft midship	d	[m]	0.873
Draft aft	d_a	[m]	1.396
L.C.B. (aft)	l_{cb}/L		0.0889
Block Coefficient	C_b		0.719
Gyro radius in pitch	k_{yy}/L		0.274
Rudder area ratio	A_R/Ld		1/14.8

Table 2 Principal particulars of a semi-displacement-type fishing craft

Length	L	[m]	7.14
Breadth	B	[m]	1.87
Draft fore	d_f	[m]	0.26
Draft midship	d	[m]	0.3835
Draft aft	d_a	[m]	0.507
L.C.B. (aft)	l_{cb}/L		0.0842
Block Coefficient	C_b		0.471
Gyro radius in yaw	k_{zz}/L		0.2976
Propeller diameter	D_p		0.440
Rudder area ratio	A_R/Ld		1/27.18

sway force, Y_w , and yaw moment, N_w , are calculated using both the Froude-Krylov and diffraction components. The following formulae for these wave forces are based on a slender body theory (Ohkusu, 1986) with some simplifications (Umeda & Renilson, 1992B).

$$X_w(\xi_G / \lambda, \chi) = -\rho g \zeta_w k \cos \chi \int_{AE}^{FE} C_1(x) S(x) e^{-k d(x)/2} \sin k(\xi_G + x \cos \chi) dx \quad (4)$$

$$Y_w(\xi_G / \lambda, u, \chi) = \rho g \zeta_w k \sin \chi \int_{AE}^{FE} C_1(x) S(x) e^{-k d(x)/2} \sin k(\xi_G + x \cos \chi) dx + \zeta_w \omega_e \sin \chi \int_{AE}^{FE} \rho S_y(x) e^{-k d(x)/2} \sin k(\xi_G + x \cos \chi) dx - \zeta_w \omega u \sin \chi \left[\rho S_y(x) e^{-k d(x)/2} \cos k(\xi_G + x \cos \chi) \right]_{AE}^{FE} \quad (5)$$

$$N_w(\xi_G / \lambda, u, \chi) = \rho g \zeta_w k \sin \chi \int_{AE}^{FE} C_1(x) S(x) e^{-k d(x)/2} x \sin k(\xi_G + x \cos \chi) dx + \zeta_w \omega \omega_e \sin \chi \int_{AE}^{FE} \rho S_y(x) e^{-k d(x)/2} x \sin k(\xi_G + x \cos \chi) dx + \zeta_w \omega u \sin \chi \int_{AE}^{FE} \rho S_y(x) e^{-k d(x)/2} \cos k(\xi_G + x \cos \chi) dx - \zeta_w \omega u \sin \chi \left[\rho S_y(x) e^{-k d(x)/2} x \cos k(\xi_G + x \cos \chi) \right]_{AE}^{FE} \quad (6)$$

where

$$k = 2\pi / \lambda \quad (7)$$

$$\omega_e = \omega - k u \cos \chi \quad (8)$$

$$c_1(x) = \frac{\sin(kB(x) \sin \chi / 2)}{kB(x) \sin \chi / 2} \quad (9)$$

To validate these formulae, captive model experiment was carried out in the seakeeping and manoeuvring basin of the National Research Institute of Fisheries Engineering with a model of displacement-type fishing vessel, whose principal particulars can be seen in Table 1. Experimental results are shown in Figs. 2-4 with calculated results by the above formulae. In the numerical calculation, two dimensional added mass $S_y(x)$ was obtained by a boundary element method. The forces are non-dimensionalized as follows:

$$X' = X / (\rho g \zeta_w BL) \quad (10)$$

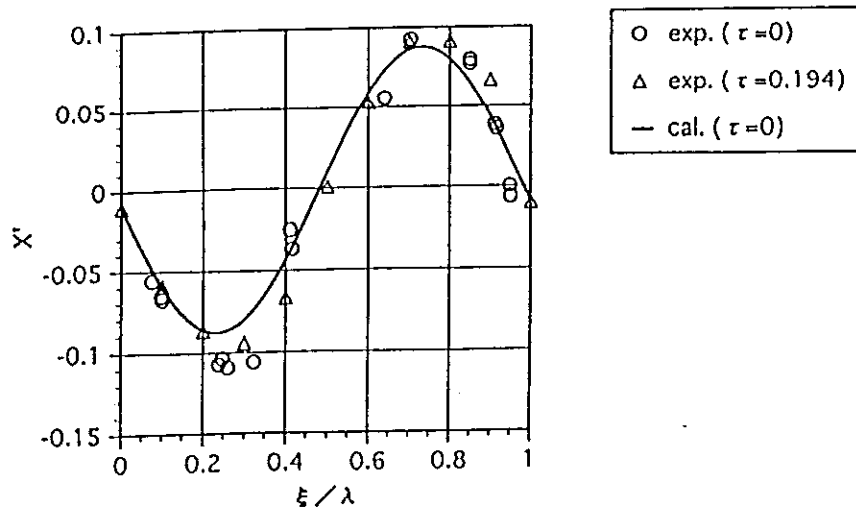


Fig.2 Wave induced surge force of the small trawler ($H/\lambda=1/20$, $\lambda/L=1.6$, $\chi=30$ degrees)

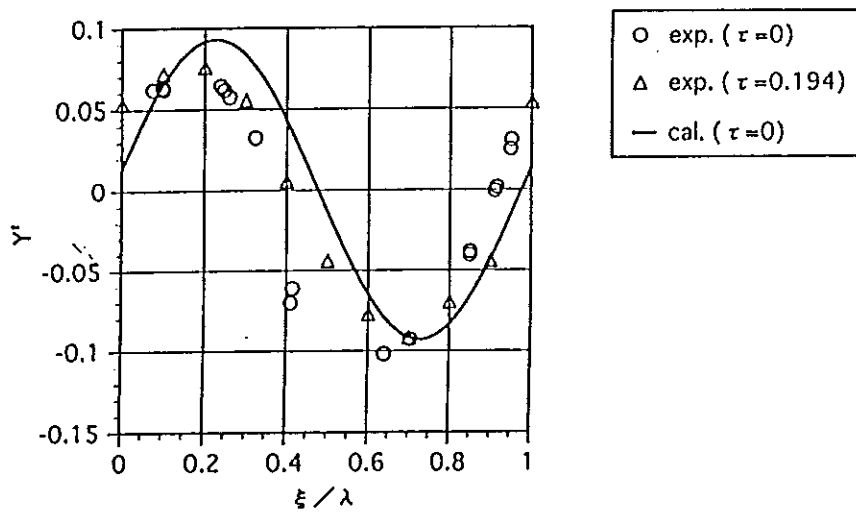


Fig.3 Wave induced sway force of the small trawler ($H/\lambda=1/20$, $\lambda/L=1.6$, $\chi=30$ degrees)

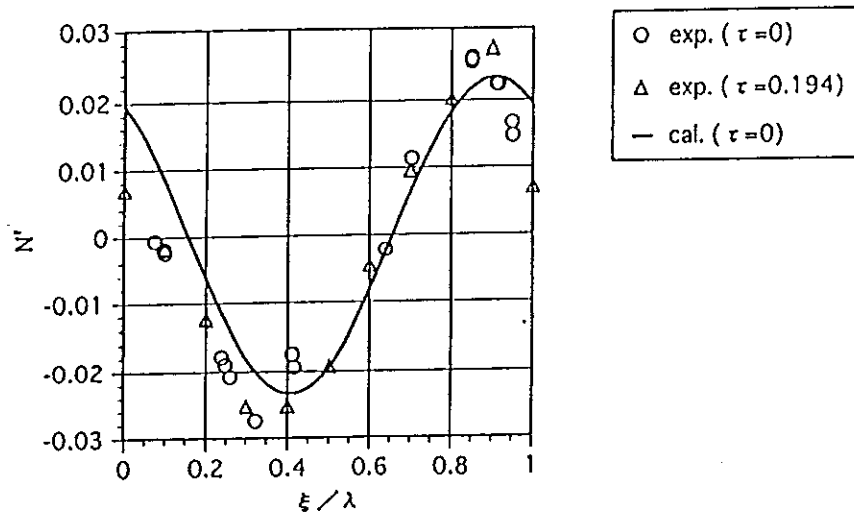


Fig.4 Wave induced yaw moment of the small trawler ($H/\lambda=1/20$, $\lambda/L=1.6$, $\chi=30$ degrees)

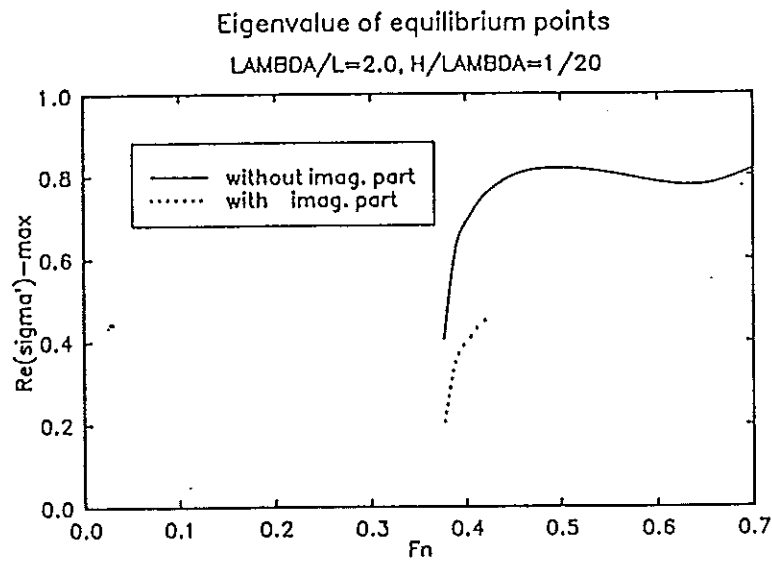


Fig.5 Eigenvalues of equilibria for the fishing craft with $\delta=-35$ degrees

$$Y' = Y / (\rho g \zeta_w BL) \quad (11)$$

$$N' = N / (\rho g \zeta_w BL^2) \quad (12).$$

In this experiment, the model was towed by a X-Y carriage both with zero encounter frequency, $\tau = U\omega_e/g = 0$, and with small encounter frequency, $\tau = 0.194$. Since the comparison between the experiment and calculation shows fairly good agreement, the calculation method for wave forces was validated for a displacement-type vessel as well as a semi-displacement craft. Details of this experiment will be published in a separate paper.

The rudder derivatives in the mathematical model are calculated using the inflow velocity modified to take into account the orbital velocity due to the wave, together with the change in the propeller race due to the longitudinal force from the wave (Umeda & Renilson, 1993). Thomas (1991) well validated this method with his model experiment in following seas. Other coefficients are assumed to be independent of waves, since their effects are not significant for broaching (Renilson, 1982). These coefficients can be obtained from conventional model experiments or empirically.

STABILITY OF EQUILIBRIA

A nonlinear dynamical system, such as the system described by Eq.(2), may have several attractors. Among the attractors equilibria should be firstly focused to clarify a broaching phenomenon. Because, equilibria play a dominant role for a nonlinear dynamic analysis on surf-riding (Umeda, 1990).

First, the equilibria, $\bar{\mathbf{x}} = (\bar{\xi}_G / \lambda, \bar{u}, \bar{v}, \bar{\chi}, \bar{r}, \bar{\delta})$, are obtained by solving the following equation:

$$\mathbf{F}(\bar{\mathbf{x}}) = \mathbf{0} \quad (13).$$

If the solution exists, the vessel will be in an equilibrium position surf-riding on the wave with a drift angle, heading angle, rudder angle and no relative velocity to the wave. $\mathbf{F}(\mathbf{x})$ is linearized at $\bar{\mathbf{x}}$, putting $\mathbf{x} = \bar{\mathbf{x}} + \mathbf{y}$ to obtain the following equation:

$$\dot{\mathbf{y}} = \mathbf{DF}(\bar{\mathbf{x}})\mathbf{y} \quad (14)$$

where

$$\mathbf{DF}(\mathbf{x}) = \frac{\partial}{\partial x_i} (f_j(\mathbf{x})) \quad 1 \leq i, j \leq 6 \quad (15).$$

If an eigenvalue of $\mathbf{DF}(\bar{\mathbf{x}})$ have a positive real part, local asymptotic behaviour at $\bar{\mathbf{x}}$ is unstable. Based on the above procedure, the following nature was found. If we consider only longitudinal motion in heavy following seas, two

equilibria can exist within one wave length. An unstable equilibrium is near wave crest; stable one is near wave trough. The latter equilibrium corresponds to surf-riding. If we consider also lateral motions, the wave induced yaw moment can make the equilibrium near wave trough unstable. If the rudder gain of auto pilot is large enough, this instability can be prevented. However, when the heading angle increases and the rudder angle in a equilibrium exceeds the maximum angle, such as 35 degrees, the auto pilot loses their ability. On the other hand, when the heading angle increases, static balance of force in the wave direction may disappear. That is, the vessel escapes from surf-riding and is overtaken by waves. Therefore, it is crucial for broaching which of the two situation occurred first, the maximum rudder angle or disappearance of equilibrium.

Fig.5 shows calculated example of eigenvalues for equilibria at $\delta = -35$ degrees. The ship used here a semi-displacement-type fishing craft, whose principal particulars can be seen in Table 2. When the nominal Froude number is slow enough, there is no equilibrium. Here the vessel experiences periodic motions only. When the nominal Froude number increases, equilibria exist. The largest real part of eigenvalues of equilibria is positive and other eigenvalues have negative real parts. Thus, equilibria are unstable and become saddle points. As a result, the vessel approaching the equilibrium point cannot maintain the static balance for a long period and then suffers dynamic behaviour. Therefore, the existence of a saddle point with $\delta = -35$ degrees is a necessary condition for broaching.

To discuss not only asymptotic instability but also broaching itself, we should examine trajectories associated with saddle points in a phase space spanned by the state vector. A theorem in dynamical system theory (Guckenheimer & Holmes, 1983) indicates that the invariant manifolds represent all trajectories associated with equilibria and can be obtained by tracing trajectories backwards and forwards in time from eigenspace spanned by eigenvector at a hyperbolic equilibrium.

With the maximum rudder angle, Figs.6 -7 show an example of five-dimensional invariant manifolds projected onto three-dimensional spaces. In this case there is one equilibrium within one wave length. A trajectories from the saddle point shows an increasing yaw behaviour from the nearly surf-riding condition regardless of the maximum opposite rudder angle. This unstable invariant manifold represents a typical example of broaching. And a ship near this invariant manifolds can suffer similar behaviour. This can be also regarded as broaching. While it is difficult to exactly determine a zone for broaching, a practical index will be desirable. The authors (1992A) used the heading angle where yaw rate becomes a maximum on the manifold, χ_B , as a practical index for broaching. Because, a violent increase in yaw exists at $\bar{\chi} < \chi < \chi_B$ at least on the unstable invariant manifold.

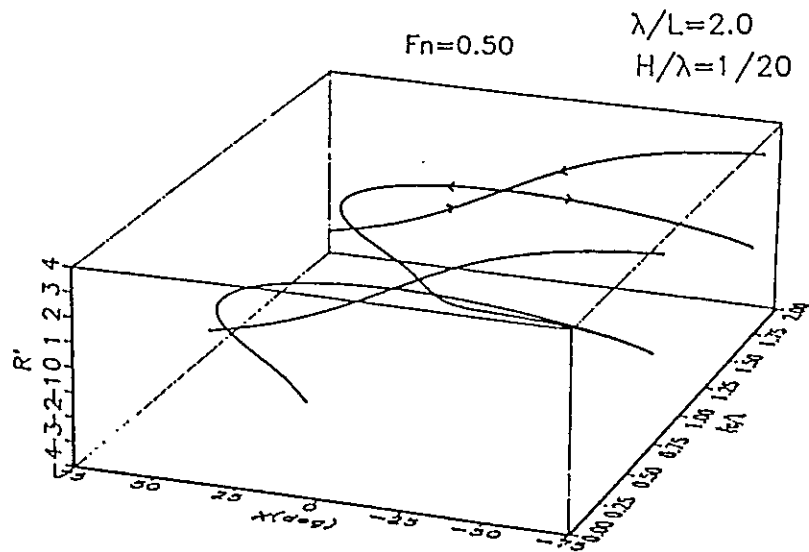


Fig.6 Invariant manifolds for the fishing craft projected onto a surge-yaw-yaw rate space

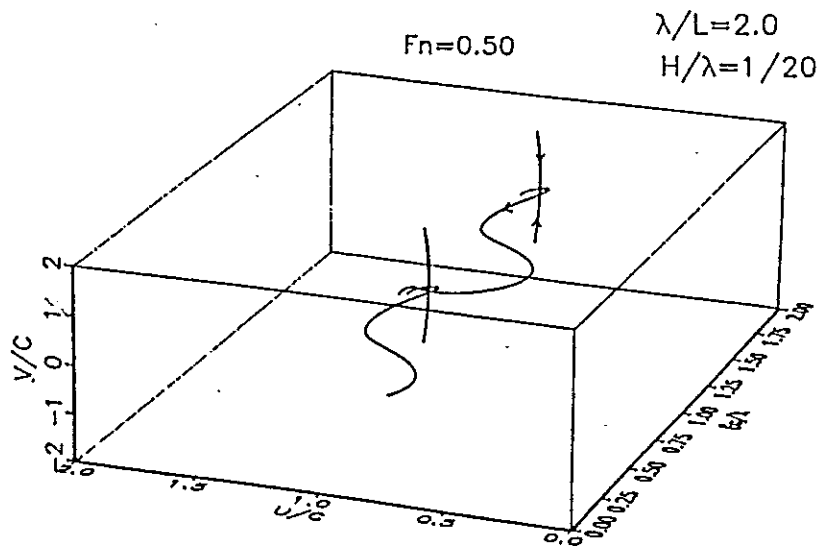


Fig.7 Invariant manifolds for the fishing craft projected onto a surge-surge velocity-sway velocity space

Some numerical results for critical conditions of broaching are shown in Figs. 8 - 10 with results for a free running model of the semi-displacement fishing craft by Fuwa (1982). These numerical results indicate that, if the ship in following seas suffers surf-riding, the ship with good steering may keep stable surf-riding between $\chi=0$ and $\bar{\chi}$. However, the auto pilot or helmsman is not good enough, the ship can have a further increase in yaw. When the heading angle reaches $\bar{\chi}$, the ship can suffer broaching. The increase in yaw rate may continue between $\bar{\chi}$ and χ_B . Overall, the prediction compares reasonably well with measured results. Nevertheless, we should note that critical condition from the analysis of equilibria is only a necessary condition for broaching.

STABILITY OF PERIODIC ORBITS

Another important attractor is periodic orbits in this dynamical system. Because, if a periodic orbit loses its stability, presumably broaching can occur. Nevertheless, nonlinear analysis associated with periodic orbits has not been known so far.

Since the Eq. (2) are described by displacements and velocities in the body-fixed coordinate system, it is not convenient to analyze nonlinear periodic motions. Thus, we define an inertial coordinate system translating with constant forward velocity \bar{U} and constant heading angle $\bar{\chi}$. Around centre of this coordinate, a ship is assumed to have periodic motions, namely, surge \tilde{X}_G , sway \tilde{Y}_G , yaw $\tilde{\chi}$ and rudder $\tilde{\delta}$.

While most of these periodic motions have much smaller amplitude than wave length, surge amplitude is not so small. Thus, we assume small parameters as follows:

$$\tilde{Y}_G/\lambda, L\tilde{\chi}/\lambda, B\tilde{\chi}/\lambda, \dot{\tilde{X}}_G/\bar{U} = O(\varepsilon), \varepsilon \ll 1 \quad (16).$$

And we redefine ω_e with averaging nature by

$$\omega_e = \omega - k\bar{U} \cos \bar{\chi} \quad (17).$$

Transforming Eq. (2) to the inertial coordinate system and ignoring higher order term of ε , nonlinear equations of periodic motions are obtained as follows:

$$A_{11}\ddot{\tilde{X}}_G + B_{11}\dot{\tilde{X}}_G = F_1 \sin(\omega_e t - \varepsilon_r - k\tilde{X}_G \cos \chi) \quad (18)$$

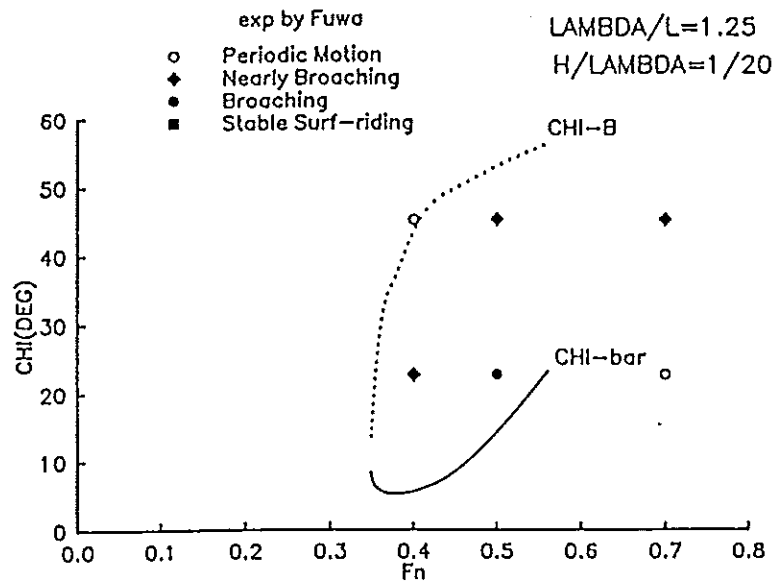


Fig.8 Critical condition for broaching of the fishing craft ($\lambda/L=1.25$)

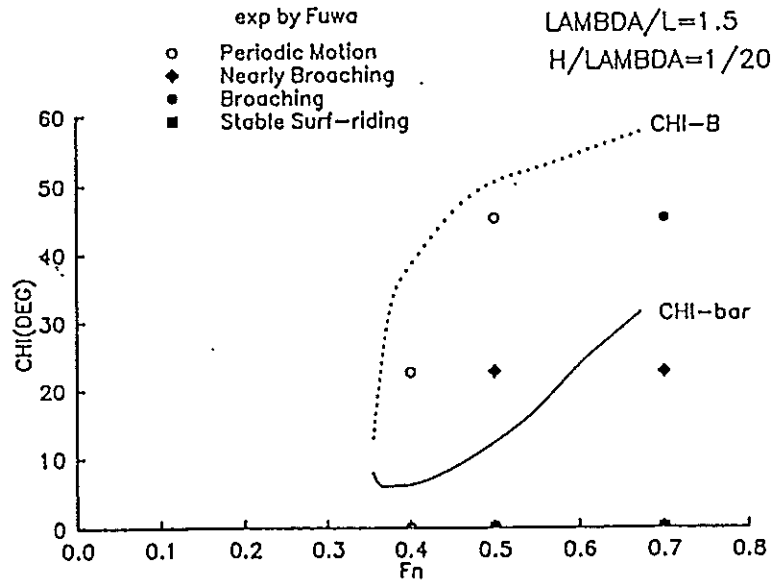


Fig.9 Critical condition for broaching of the fishing craft ($\lambda/L=1.5$)

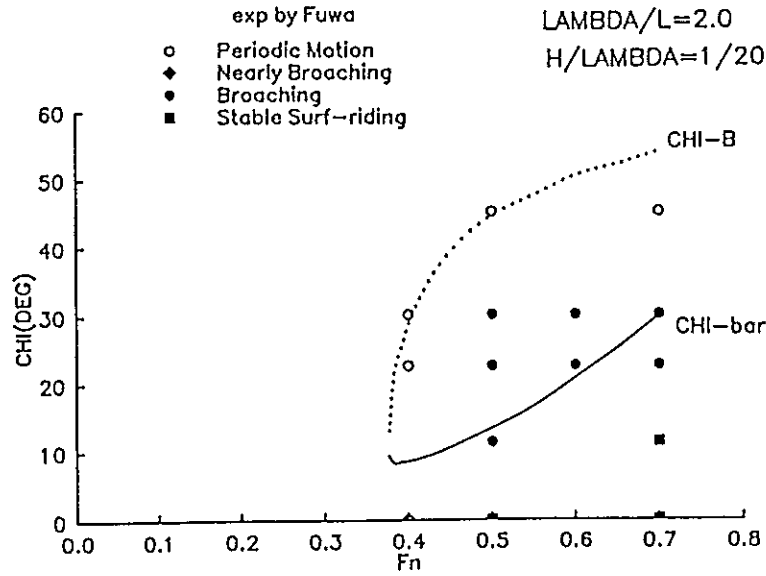


Fig.10 Critical condition for broaching of the fishing craft ($\lambda/L=2.0$)

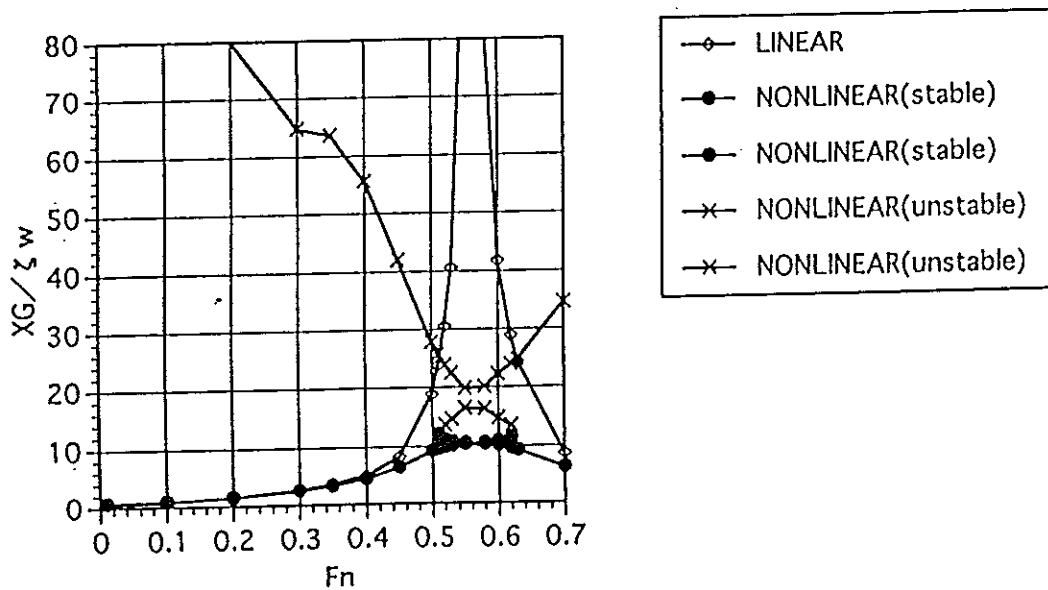


Fig.11 Amplitude and stability of periodic surge motion of the stern trawler ($H/L=1/20$, $\lambda/L=2$, $\chi=0$)

$$\begin{aligned}
& A_{22}\ddot{\tilde{Y}}_G + B_{22}\dot{\tilde{Y}}_G + B_{26}\dot{\tilde{\chi}} + C_{26}\tilde{\chi} + D_{21}\dot{\tilde{\chi}}\dot{\tilde{X}}_G + D_{22}\tilde{\chi}\dot{\tilde{X}}_G \\
& + D_{23}\tilde{\chi}\ddot{\tilde{X}}_G + C_{27}\ddot{\tilde{\delta}} + D_{24}\dot{\tilde{\delta}}\dot{\tilde{X}}_G \\
& = F_{21}\sin(\omega_c t - \varepsilon_F - k\tilde{X}_G \cos \bar{\chi}) \\
& + F_{22}\left(\omega_c - k\dot{\tilde{X}}_G \cos \bar{\chi}\right)\sin(k\tilde{X}_G \cos \bar{\chi} - \omega_c t) \\
& + F_{23}\left(\omega_c - k\dot{\tilde{X}}_G \cos \bar{\chi}\right)\cos(k\tilde{X}_G \cos \bar{\chi} - \omega_c t) \\
& + F_{24}\left(\bar{U} + \dot{\tilde{X}}_G\right)\cos(k\tilde{X}_G \cos \bar{\chi} - \omega_c t) \\
& + F_{25}\left(\bar{U} + \dot{\tilde{X}}_G\right)\sin(k\tilde{X}_G \cos \bar{\chi} - \omega_c t)
\end{aligned} \tag{19}$$

$$\begin{aligned}
& A_{66}\ddot{\tilde{\chi}} + B_{66}\dot{\tilde{\chi}} + C_{66}\tilde{\chi} + B_{62}\dot{\tilde{Y}}_G + D_{61}\tilde{\chi}\dot{\tilde{X}}_G + D_{62}\dot{\tilde{\chi}}\dot{\tilde{X}}_G \\
& + C_{67}\ddot{\tilde{\delta}} + D_{63}\dot{\tilde{\delta}}\dot{\tilde{X}}_G \\
& = F_{61}\cos(k\tilde{X}_G \cos \bar{\chi} - \omega_c t + \varepsilon_M) \\
& + F_{62}\left(\omega_c - k\dot{\tilde{X}}_G \cos \bar{\chi}\right)\sin(k\tilde{X}_G \cos \bar{\chi} - \omega_c t) \\
& + F_{63}\left(\omega_c - k\dot{\tilde{X}}_G \cos \bar{\chi}\right)\cos(k\tilde{X}_G \cos \bar{\chi} - \omega_c t) \\
& + F_{64}\left(\bar{U} + \dot{\tilde{X}}_G\right)\cos(k\tilde{X}_G \cos \bar{\chi} - \omega_c t) \\
& + F_{65}\left(\bar{U} + \dot{\tilde{X}}_G\right)\sin(k\tilde{X}_G \cos \bar{\chi} - \omega_c t)
\end{aligned} \tag{20}$$

$$B_{77}\ddot{\tilde{\delta}} + \ddot{\tilde{\delta}} + B_{76}\dot{\tilde{\chi}} + C_{76}\tilde{\chi} = 0 \tag{21}.$$

Here the coefficients, A_{ij} , B_{ij} , C_{ij} , D_{ij} , F_{ij} , ε_F , ε_M are obtained by the coefficients in the right hand side of Eq. (2). As you can see, the obtained equations are still nonlinear but not autonomous.

Further, we assume that

$$\tilde{X}_G / \lambda = O(\nu), \quad \nu = O(\varepsilon^{2/3}) \tag{22}.$$

This additional assumption means that non linearity due to surge is not so large. As a result, we can expect the following form of solutions:

$$\tilde{X}_G = r_1 \cos(\omega_c t - \phi_1) \tag{23}$$

$$\tilde{Y}_G = r_2 \cos(\omega_c t - \phi_2) \tag{24}$$

$$\tilde{\chi} = r_6 \cos(\omega_c t - \phi_6) \tag{25}$$

$$\tilde{\delta} = r_7 \cos(\omega_c t - \phi_7) \tag{26}.$$

Then we put the van der Pol transformation as follows:

$$\begin{pmatrix} u_1 \\ v_1 \end{pmatrix} = \begin{bmatrix} \cos \omega_c t & -\frac{1}{\omega_c} \sin \omega_c t \\ -\sin \omega_c t & -\frac{1}{\omega_c} \cos \omega_c t \end{bmatrix} \begin{pmatrix} \tilde{X}_G \\ \dot{\tilde{X}}_G \end{pmatrix} \quad (27)$$

$$\begin{pmatrix} u_2 \\ v_2 \end{pmatrix} = \begin{bmatrix} \cos \omega_c t & -\frac{1}{\omega_c} \sin \omega_c t \\ -\sin \omega_c t & -\frac{1}{\omega_c} \cos \omega_c t \end{bmatrix} \begin{pmatrix} \tilde{Y}_G \\ \dot{\tilde{Y}}_G \end{pmatrix} \quad (28)$$

$$\begin{pmatrix} u_6 \\ v_6 \end{pmatrix} = \begin{bmatrix} \cos \omega_c t & -\frac{1}{\omega_c} \sin \omega_c t \\ -\sin \omega_c t & -\frac{1}{\omega_c} \cos \omega_c t \end{bmatrix} \begin{pmatrix} \tilde{\chi} \\ \dot{\tilde{\chi}} \end{pmatrix} \quad (29)$$

$$\begin{pmatrix} u_7 \\ v_7 \end{pmatrix} = \begin{bmatrix} \cos \omega_c t & -\frac{1}{\omega_c} \sin \omega_c t \\ -\sin \omega_c t & -\frac{1}{\omega_c} \cos \omega_c t \end{bmatrix} \begin{pmatrix} \tilde{\delta} \\ \dot{\tilde{\delta}} \end{pmatrix} \quad (30).$$

Substituting Eqs.(27)-(30) to Eqs.(18)-(21) and averaging them over one period, that is,

$$0 < t < 2\pi / \omega_c \quad (31).$$

we obtain the following averaged equation.

$$\dot{\mathbf{v}} = \mathbf{G}(\mathbf{v}) = \{g_1(\mathbf{v}) \ g_2(\mathbf{v}) \ g_3(\mathbf{v}) \ g_4(\mathbf{v}) \ g_5(\mathbf{v}) \ g_6(\mathbf{v}) \ g_7(\mathbf{v}) \ g_8(\mathbf{v})\}^T \quad (32)$$

where

$$\mathbf{v} = (u_1 \ v_1 \ u_2 \ v_2 \ u_6 \ v_6 \ u_7 \ v_7)^T \quad (33).$$

As you see, the obtained equation is nonlinear and autonomous.

The averaging theorem (Guckenheimer & Holmes, 1983) indicates that, if an averaged equation has a hyperbolic fixed point, \mathbf{v}_0 , the original equation possesses a unique hyperbolic periodic orbit of the same stability type as \mathbf{v}_0 . Therefore, the periodic orbits, \mathbf{v}_0 , of the dynamical system described by Eq.(2) are obtained by the following equation:

$$\mathbf{G}(\mathbf{v}_0) = 0 \quad (34).$$

$\mathbf{G}(\mathbf{v})$ is linearized at \mathbf{v}_0 , putting $\mathbf{v} = \mathbf{v}_0 + \mathbf{q}$ to obtain the following equation:

$$\dot{q} = DG(v_0)q \quad (35)$$

where

$$DG(v) = \frac{d}{dv_j}(g_i(v)) \quad 1 \leq i, j \leq 8 \quad (36).$$

If an eigenvalue of $DG(v_0)$ has a positive real part, the periodic orbit, v_0 , is unstable. Moreover, if the eigenvalues of $DG(v_0)$ have nonzero real parts, the global behaviour associated with periodic orbits on the Poincaré map can be investigated by calculating invariant manifolds.

To examine the effectiveness of the above method, a numerical calculation by this method was carried out for uncoupled surging motion of a ship in following sea. The used ship is a stern trawler, whose principal particulars are given in Table 3. Fig.11 shows results of this numerical calculation. The surging amplitude by a linear calculation tends to infinity when encounter frequency tends to zero. The linear periodic orbit is always unique for each the nominal Froude number and always stable. On the other hand, two nonlinear periodic orbits exist when the nominal Froude number is smaller than 0.51 and larger than 0.62. One of them is stable and the other is unstable. Since the stable orbit is very close to the linear orbit, stable orbit is usually expected to be observed in this region. When the nominal Froude number is larger than 0.51 and smaller than 0.62, four nonlinear orbits coexist and unstable orbits are near stable orbits. In this region unstable behaviour in surge can be expected. In free running model experiments (Kan et al., 1988) normal periodic surging motion was observed when the nominal Froude number is smaller than 0.42; surf-riding was observed when the nominal Froude number is larger than 0.42. And no experimental value is available for the nominal Froude number larger than 0.62. Thus, the potentially unstable region identified by the present nonlinear calculation is involved within the surf-riding region by the model experiments. This is reasonable because surf-riding can be regarded as a result of unstable periodic motion with the inertial coordinate system translating with the nominal Froude number. Of course, it is enough for accurately predicting surf-riding region to analyze equilibria with the wave fixed coordinate system (Umeda, 1990). However, for broaching, the analysis of periodic orbits is complementary to the analysis of equilibria. Because, the analysis of equilibria can provide only a necessary condition for broaching.

CONCLUSION

On the basis of this study the following conclusions can be drawn:

- (1) The mathematical model was extended to the surge-sway-yaw-rudder motion.
- (2) The prediction method for wave forces was validated by model experiments with a displacement-type fishing vessel.

- (3) The analysis on equilibria provided a necessary condition for broaching and validated by free running model experiments with a semi-displacement-type fishing craft.
- (4) The methodology for the analysis on periodic orbits is presented with some numerical results.

We would like to express our sincere thanks for the support of Australian Maritime College as well as the Shipbuilding Research Association of Japan. We are grateful to Mr. S. Suzuki and Mr. Y. Yamakoshi of National Research Institute of Fisheries Engineering for their help with the model experiments. We also wish to thank Dr.K.Spyrou from the same institute for his comments.

REFERENCE

- Davidson, K.S.M. (1948). "A Note on the Steering of Ships in Following Seas" *Proceedings of the 7th International Congress of Applied Mechanics*, London, pp.554-568.
- Fuwa, T., Sugai, K., Yoshino, T. and Yamamoto, T. (1982). "An Experimental Study on Broaching of a Small High Speed Craft" *Papers of Ship Research Institute*, 66, pp.1-40.
- Guckenheimer, J. and Holmes, P. (1983). *Nonlinear Oscillations, Dynamical Systems, and Bifurcations of Vector Field* Springer-Verlag, New York.
- Kan, M., Saruta, T., Yasuno, M., Yamakoshi, Y. and Suzuki, S. (1988). "Model Experiments on Surf-Riding of a Fishing Boat in Following Waves" *Papers of Ship Research Institute*, 25, 3, pp.25-54, in Japanese.
- Motora, S., Fujino, M. and Fuwa, T. (1982). "On the Mechanism of Broaching-to Phenomena" *Proceedings of the 2nd International Conference on Stability of Ships and Offshore Vehicles*, Tokyo, pp.535-550.
- Ohkusu, M. (1986). "Prediction of Wave Forces on a Ship Running in Following Waves with Very Low Encounter Frequency" *Journal of the Society of Naval Architects of Japan*, 159, pp.129-138.
- Renilson, M.R. (1982). "An Investigation into the Factors Affecting the Likelihood of Broaching-to in Following Seas" *Proceedings of the 2nd International Conference on Stability of Ships and Offshore Vehicles*, Tokyo, pp.551-564.
- Thomas, G.A. (1991). "Surf-Riding and Loss of Control of Fishing Vessels in Severe Following Seas" Master thesis, University of Newcastle upon Tyne, pp.67-83.
- Umeda, N. (1990). "Probabilistic Study on Surf-Riding of a Ship in Irregular Following Seas" *Proceedings of the 4th International Conference on Stability of Ships and Offshore Vehicles*, Naples, pp.336-343.
- Umeda, N. and Renilson, M.R. (1992A). "Broaching - A Dynamic Behaviour of a Vessel in Following Seas -" from *Manoeuvring and Control of Marine Craft* (edited by Wilson, P.A.), Computational Mechanics Publications, Southampton, pp.533-543.
- Umeda, N. and Renilson, M.R. (1992B). "Wave Forces on a Ship Running in Quartering Seas - A Simplified Calculation Method -" *Proceedings of the 11th*

Australian Fluid Mechanics Conference, Hobart, pp.363-366.

Umeda, N. and Renilson, M.R. (1993). "Broaching in Following Seas - A Comparison of Australian and Japanese Trawlers -" *Bulletin of National Research Institute of Fisheries Engineering*, 14, pp.175-186.

Table 3 Principal particulars of a displacement-type fishing vessel (stern trawler)

Length	L	[m]	30.58
Breadth	B	[m]	7.38
Draft fore	d_f	[m]	1.62
Draft midship	d	[m]	2.62
Draft aft	d_a	[m]	3.62
L.C.B. (aft)	l_{cb}/L		0.0886
Block Coefficient	C_b		0.779
Gyro radius in pitch	k_{yy}/L		0.297
Propeller diameter	D_p		2.3
Rudder area ratio	A_R/Ld		1/27.3

PARAMETRIC STABILITY OF FISHING VESSELS

by

Neves, M.A.S.* and Valerio, L.*

1. ABSTRACT

The paper highlights the influence of stern shape on the parametric stability of fishing vessels. Vessels TS and RS have very similar main characteristics, but their sterns are different. Although their linear responses are comparable, both analytical and experimental investigations indicate substantial differences in their dynamical stability in longitudinal regular waves. An uncoupled Mathieu equation is employed to model the behaviour of the vessels in waves. Limits of stability are used to stress the connections between hull form and parametric excitation.

2. NOMENCLATURE

I_x -transversal mass moment of inertia with respect to axes

A_{44} -added inertia in roll due to roll angular acceleration

$D(\dot{\phi})$ -damping moment

M_r -restoring moment

M_{w_0} -amplitude of external wave action

W -wave frequency

γ -phase between excitation and wave

W_n -roll natural frequency

ϕ -roll angle

Z -heave motion

θ -pitch motion

ζ -wave amplitude

C_{44} -linear roll restoring coefficient

C_{444} -third order roll restoring coefficient.

C_{44z} -second order roll restoring coefficient due to heave motion

$C_{44\theta}$ -second order roll restoring coefficient due to pitch motion

$C_{44\zeta}$ -second order roll restoring coefficient due to wave passage

$F_{1,2\zeta}$ -components of the second order roll restoring coefficient due to wave passage

B_{44} -linear roll damping coefficient

B_{444} -second order roll damping coefficient

e_0 -amplitude of parametric excitation

φ -phase of the parametric excitation

λ -wave length

Z_g -vertical position of center of mass

g -gravity

ρ -density

A_w -water plane area

x_f -longitudinal centroid of water line

$b_0(x)$ -breadth at the water line

h_w -wave height

*COPPE/UFRJ, Federal University of Rio de Janeiro, Brazil.

3. INTRODUCTION

The motions of a rigid ship in regular waves are in general a result of complex non-linear couplings in six degrees of freedom. Stability analysis of these motions, even for the particular case when the ship takes waves by the stern, still attracts wide attention [1,2,3,4,5]. Parametric instabilities, as defined by the uncoupled Mathieu equation are supposed to be responsible for some ship capsizes, and quite a lot of attention has been devoted to the understanding of the connection between hull characteristics and parametric resonance [4,6,7].

The present paper aims at contributing (although at a small scale) to an increased understanding of the mechanisms of parametrically excited roll motions and their relevance to the risk of capsizing of fishing vessels.

Two hulls are analysed here. The two hulls have been tested previously by Morral [8]. They have quite similar main characteristics but their sterns are different. The first hull, here denominated *TS*, is a typical transom stern fishing vessels. The other one, denominated *RS*, is a more conventional rounded stern fishing vessel. The lines plans of the two hulls are shown in Fig. 1.

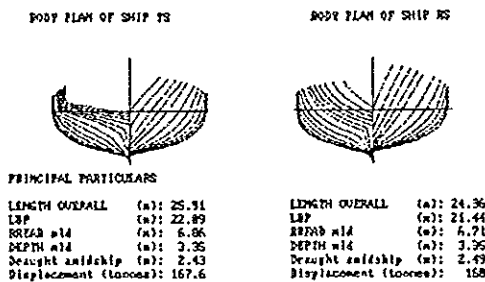


Fig. 1 Body plans of the two vessels

Both experimental and numerical investigations have been conducted. Experimental studies involved damping assessment by means of roll decrement tests for the two hulls with and without bilge keels, and parametrically excited heave-roll-pitch motions in regular longitudinal waves. Numerical studies are based on an uncoupled roll motion equation with nonlinearities in the damping and restoring moment. The present investigation is restricted to longitudinal regular waves of small amplitudes with ships with zero speed of advance.

The results indicate that the transom stern hull is much more sensitive to parametric instabilities, and confirm that, at least in test conditions, this type of hull may reach a capsizing in few cycles, when excited by small longitudinal waves. Simulations are made for two regions of parametric resonance, $W = 2W_n$ and $W = W_n$. The differences in the responses for the two resonant regions are pointed out.

4. EQUATION OF MOTION

Let *Cxyz* be a right handed coordinate system, Fig. 2, with axis *Cz* passing through the center of mass *G*, *Cx* pointing forward and coinciding with the calm water surface.

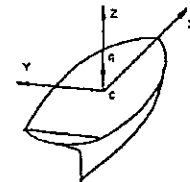


Fig. 2 Coordinate system

The mathematical model employed in this study is of the form:

$$(I_x + A_{44})\ddot{\phi} + D(\dot{\phi}) + M_r(\phi, z, \theta, \zeta) = M_{wo} \cos(\Omega t - \gamma) \quad (1)$$

The damping moment is assumed to be given by:

$$D(\dot{\phi}) = B_{44} \dot{\phi} + B_{444} |\dot{\phi}| \dot{\phi} \quad (2)$$

The restoring moment is derived under the assumption that vertical motions due to small amplitude waves are small, such that relative vertical displacement at a point of the length of the ship may be taken as the sum of three effects, heave motion $z(t)$, pitch motion $\theta(t)$ and wave profile $\zeta(x,t)$. The roll restoring moment is then assumed to be given by:

$$M_r(\phi, z, \theta, \zeta) = C_{44} \phi + C_{444} \phi^3 + C_{44z} z \phi + C_{44\theta} \theta \phi + C_{44\zeta} F_\zeta \phi \quad (3)$$

where $F_\zeta(t)$ represents time-dependent variations of hull characteristics due to wave passage. For the coordinate system defined above [4,9]:

$$C_{44} = \Delta \overline{GM} \quad (4)$$

$$C_{44z} = -\rho g \left[\frac{1}{2} \int_L b_0^2(x) \frac{dy}{dz} \Big|_{b,x} dx - z_g A_v \right] \quad (5)$$

$$C_{44\theta} = -\rho g \left[\frac{1}{2} \int_L b_0^2(x) \frac{dy}{dz} \Big|_{b,x} x dx - z_g A_v x_f \right] \quad (6)$$

$$C_{44\zeta} F_\zeta = -\rho g \zeta \left[F_{1\zeta} \cos Wt + F_{2\zeta} \cos Wt \right] \quad (7)$$

with $F_{1\zeta}$ and $F_{2\zeta}$ given by

$$F_{1\zeta} = -\frac{1}{2} \left[\int_L b_0^2(x) \frac{dy}{dz} \Big|_{b,x} \cos kx dx - z_g \int_L b_0(x) \cos kx dx \right] \quad (8)$$

$$F_{2\zeta} = -\frac{1}{2} \left[\int_L b_0^2(x) \frac{dy}{dz} \Big|_{b,x} \sin kx dx - z_g \int_L b_0(x) \sin kx dx \right] \quad (9)$$

The reader should refer to section 2 of this paper for the definitions of symbols given above.

As the present study is limited to longitudinal waves, $M_{w0} = 0$, that is, there is no external excitation.

Dividing all terms in equation (1) by $(I_x + A_{44})$ the equation of roll motion assumes the form:

$$\ddot{\phi} + (b_1 + b_2 |\dot{\phi}|) \dot{\phi} + (C_1 + C_2 \phi^2 + e_0 \cos(Wt + \varphi)) \phi = 0 \quad (10)$$

where, of course, e_0 contains contributions from heave, pitch and wave passage.

5. DETERMINATION OF THE COEFFICIENTS

Great care was exercised in the evaluation of added masses and damping coefficients in the heave, roll and pitch modes, and exciting forces and moments in the heave and pitch modes in longitudinal waves. A 3-D panel method has been used in the potential calculations. The coefficients for the two hulls have been presented in ref. [10]. In order to incorporate viscous effects in the roll damping moment, use was made of the procedure proposed by Ikeda, described by Himeno [11], which takes into consideration bilge keels effects.

Damping for the two hulls with and without bilge keels are given in Fig. 3 for a roll amplitude of 15 degrees. The results indicate that the TS hull is substantially more damped than the RS in both conditions, with and without bilge keels.

As the damping moment in roll is considered to be the most complicated term to be evaluated theoretically, roll decrement tests were performed with the two models with and without bilge keels.

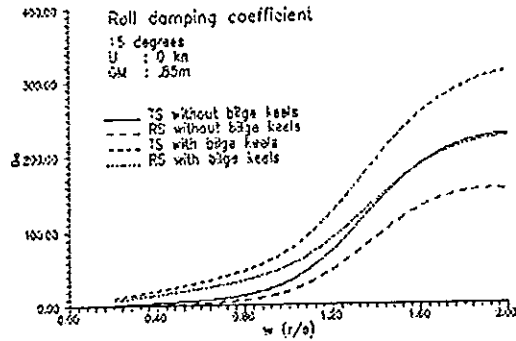


Fig. 3 Damping coefficients for 15 Degrees

The coefficients C_1 and C_3 were obtained by fitting the restoring curves with polynomials using the least-squares method.

6. LIMITS OF STABILITY

Stability of motion may be investigated in an approximated way by means of the so called Mathieu diagram.

By suitable transformations [12], the linear variational of equation (10) may be expressed in the form of a damped Mathieu equation:

$$x'' + 2u x' + (a + u^2 + 16q \cos 2t)x = 0 \quad (11)$$

Limits of stability corresponding to equation (11) may be determined and the effect of damping on the various regions of parametric resonance may be assessed. Fig. 4 shows the effect of three different levels of damping coefficient, $u=0$, $u=0.035$, and $u=0.070$, on the limit curves corresponding to the first three regions of parametric resonance. It is seen that by raising the damping level, the first region ($W=2W_n$) is practically unaffected, while the subsequent regions are more and more affected by damping. As a consequence, the third region of parametric resonance practically

disappears for small levels of damping.

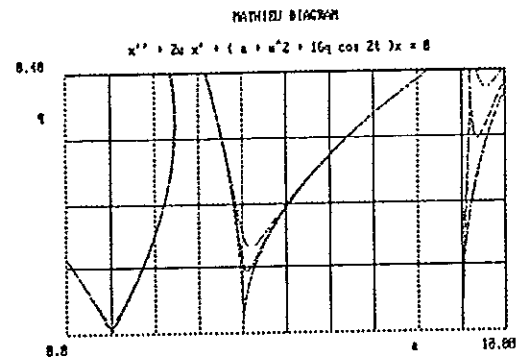


Fig. 4 Mathieu diagram for three damping values.
 $u: 0, .035$ and $.07$

Stability limits for a damped Mathieu equation are also affected by the natural frequency. Fig. 5 shows the limits of stability near the $W=2W_n$ and $W=W_n$ regions of resonance for two values of metacentric height, $\overline{GM}=0.35m$ and $\overline{GM}=0.85m$ for TS hull. It may be noticed that the higher the metacentric height is, the higher the limits are. That results from the frequency dependence of the roll damping coefficient, given in Fig. 3. At the first region of resonance, the damping level is much higher than at the second one.

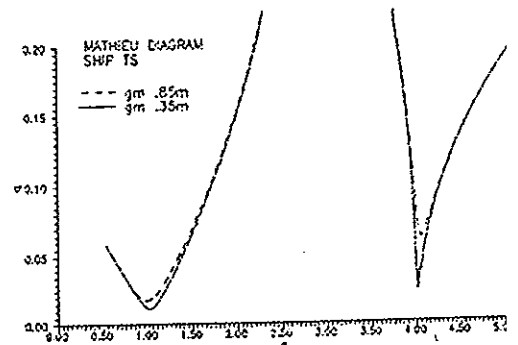


Fig. 5 Limits of stability for TS hull for two values of metacentric height.

7. DESCRIPTION OF THE EXPERIMENTS

The tests were conducted at the ship model basin of the Austral University of Chile, where regular waves can be generated by means of a flap-type wave generator.

The two models were constructed to scale 1:30. The experiments performed up to now are all for the case of zero speed of advance. In the experiments, weight distribution, wave amplitude and frequency were varied in order to:

- a) perform roll decrement tests at different natural frequencies.
- b) investigate sensitiveness of the two similar hulls to parametric instabilization in the first two regions of resonance of the Mathieu diagram.

Roll decrement tests were performed for initial angles near 15 degrees.

The procedure in the parametric tests was to position the ballasted model longitudinally in the tank, loosely prevented from drifting by a thread, and, by generating waves in one extreme of the tank, roll angular displacements were recorded with the model free to oscillate.

In order to investigate the influence of the increased damping in the stabilization process, each model was tested in turn with and without bilge keels.

The bilge keels were identical for the two models, fitted along two-thirds of model length, with a constant breadth of 15 cm (to ship scale).

8. RESULTS

8.1 ROLL DECREMENT

The results from roll decrement tests for the two hulls are presented in Fig. 6. Froude method [13] was used to calculate the results.

As with semi-empirical results given in Fig. 3, test results also give higher damping effect for the TS hull as compared with RS hull when the two models are not fitted with bilge keels. With bilge keels, TS hull is more damped than RS for frequencies above $W = 1.25r/s$.

The results given in Fig. 6 can not strictly be compared to those given in Fig.3. Yet, simulations of decaying motion at different initial angles using the two sets of results for the values of metacentric height used in the experiments indicated, in general, that:

- i) damping for RS hull without bilge keels is well described by Ikeda method.
- ii) for TS hull without bilge keels, Ikeda method produces slightly lower damping than that obtained through the experimental procedure.
- iii) Ikeda method underestimates the damping effect introduced by the bilge keels in both models.

8.2 PARAMETRIC EXCITATION

As a consequence of the similitude of the two hulls, linear responses in heave and pitch are almost the same. Transfer functions in waves by the stern ($\chi = 0$) for zero speed of advance are shown in Figs. 7 and 8 for the heave and pitch motions, respectively.

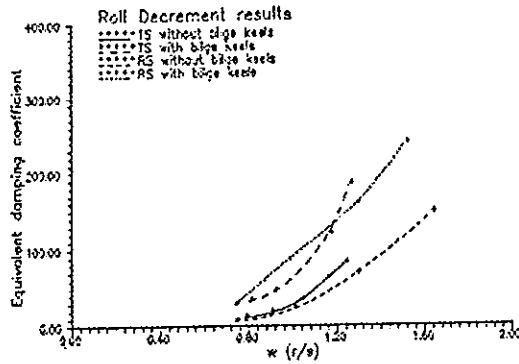


Fig. 6 Equivalent damping coefficient for two hulls derived from roll decrement tests.

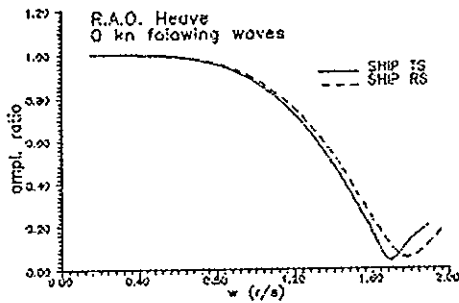


Fig. 7 Transfer function in the Heave mode

As the tests indicated quite different roll behaviour for the two hulls, it was found interesting to investigate numerically the different terms in the parametric excitation and to see how these would suggest different influences from the different stern shapes.

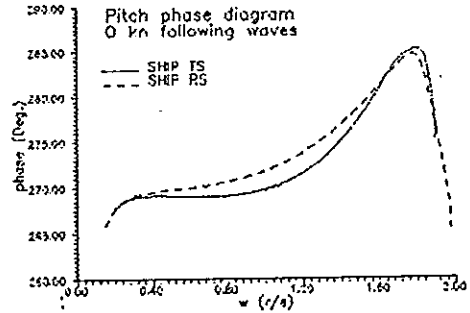
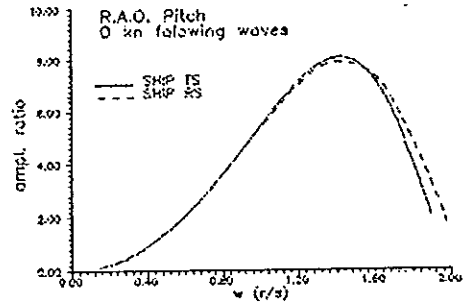


Fig. 8. Transfer function in the Pitch mode

Fig. 9 shows the curves of parametric excitation amplitude θ_p for the two hulls, for different frequencies and wave amplitude $\zeta = 1.0m$ (real scale). Parametric excitation is much higher for the TS hull, when compared with the other hull, for the whole frequency range considered. Fig. 10 shows the influence of the heave motion, wave passage and pitch motion for TS hull. For small frequencies, up to $\omega = 1.0$ rad/seg, the heave motion effect is cancelled out by the wave passage effect and parametric excitation is dominated by the influence of pitch motion.

It should be noticed that for this low frequency range the linear responses in pitch for the two hulls are, in practice, the same. It can be deduced from this comparative analysis that the distinct levels of parametric excitation found for the two hulls are due to the different stern arrangements. In fact, as can be seen in Fig. 11, the lines plan fo

a vessel with transom stern leads to a non-symmetrical longitudinal distribution of sectional breadth and flare at water line, resulting in a large C_{440} coefficient, as given in equation (6). This second order form coefficient is three-times larger for the TS hull than for the RS ship when metacentric is $\overline{GM} = 0.85m$.

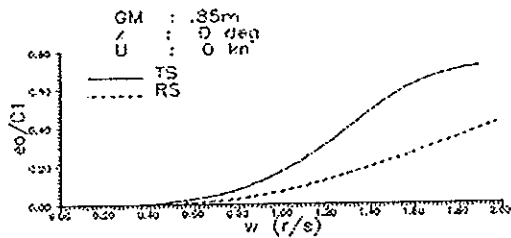


Fig. 9 Amplitude of parametric excitation

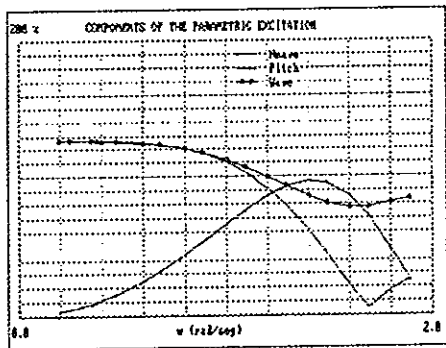


Fig. 10 Components of the parametric excitation for TS hull ($\overline{GM} = 0.85m$)

The round-stern hull, having a more "smooth" longitudinal distribution of flare, is less exposed to internal excitation in roll. For higher frequencies the vertical motions are just slightly different for the two vessels, and so the large resulting differences in parametric excitation is essentially geometrical.

Another aspect disclosed by the analysis is that maximum amplitude of parametric excitation does not

coincide with pitch natural frequency.

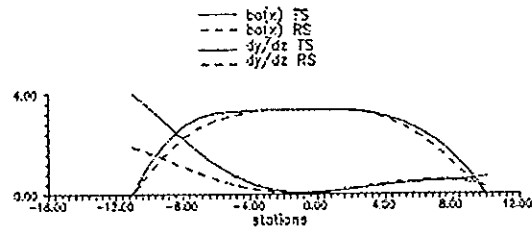


Fig. 11 Sectional distribution of breadth and flare at water line for the two hulls.

8.3 ROLL MOTION

A fourth-order Runge-Kutta algorithm was implemented for the numerical integration of equation (10). Numerical investigations are compared with experimental results in Figs. 12, 13 and 14, for different waves and hulls configurations. The tuning in all the three figures is near $W = 2W_n$. In these figures, the motions are all unstable.

It has been found that good agreement is reached between numerical and experimental results in all the frequencies considered, and even for quite high waves inducing high roll angles, as in Fig. 12. This is a quite good surprise, considering that the mathematical model employed in this study is very simple. Use of experimental damping contributes to improve the agreement between numerical simulation and experiment.

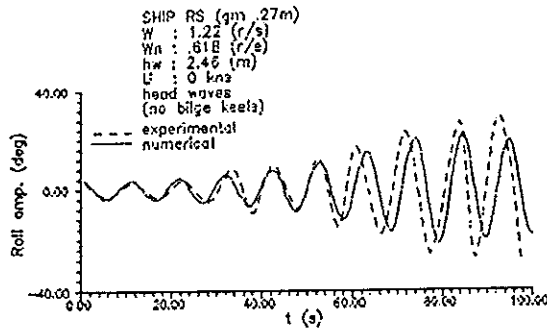


Fig. 12 Comparison of numerical integration with experiment for RS hull, $\overline{GM} = 0.27m$

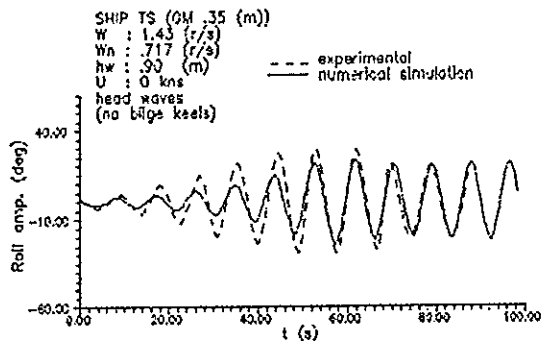


Fig. 13 Comparison of numerical integration with experiment for TS hull, $\overline{GM} = 0.35m$

Considering that the mathematical model represents very nicely the dynamics involved in the experiments, Figs. 15 through 19 have been prepared with the purpose of helping in the interpretation of the experimental results. In each of these figures, graphics (a) and (b) show the time series of each particular test condition, and graphics (c) show the corresponding points in the Mathieu diagram.

Fig. 15(a) shows a case of strong instability for the TS hull, with bilge keels, in the range $W = 2W_n$, with $\overline{GM} = 0.32m$. In less than six cycles roll angle reaches approximately 40 degrees. A very

dangerous condition, meaning a real risk of capsizes. For the RS hull to undergo such intense instabilization, it was necessary to reduce the metacentric height to $\overline{GM} = 0.27m$ and to remove the bilge keels. Yet, the resulting instability requires more than 8 cycles to reach roll angles of the order of 28 degrees. This result is given in Fig. 16(a), and demonstrates that the TS hull is much more unstable in longitudinal waves than the RS hull.

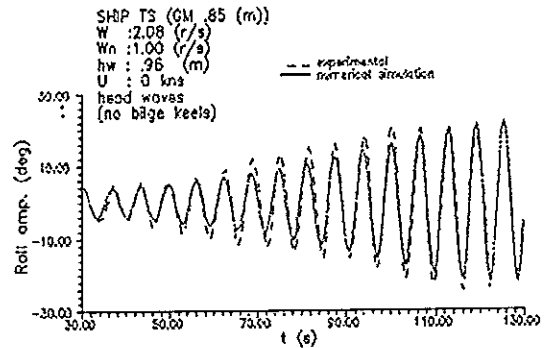


Fig.14 Comparison of numerical integration with experiment for TS hull, $\overline{GM} = 0.85m$

Comparing Fig. 16(b) with Fig. 17(b), it is seen that both ships reach approximately 30 degrees, but with TS hull doing so in 6 cycles, while for RS it takes 10 cycles. It should be noticed that in this comparison both ships are without bilge keels and that TS hull is more damped than RS hull. Metacentric height for RS is smaller and wave height is much higher. This is clearly another demonstration that TS hull is much more sensitive to parametric instabilization than RS hull. Comparing point 2 in Fig. 16 (c) with point 2 in Fig. 17(c), it can be observed that the former is nearer to the limit curve than the latter. Point 1 in Fig 16(c) is

located in the stable region. The wave height is high ($h_w = 2.0m$), but as shown in Fig. 16(1), no amplification of roll motion occurs.

The influence of increased damping may be observed by comparing Fig. 15(b) with Fig. 17(b). In Fig. 15(b) TS hull is fitted with bilge keels, $\overline{GM} = 0.32m$ and $h_w = 2.4m$. Roll angle reaches approximately 32 degrees in 9 cycles. In Fig. 17(b) the same ship, without bilge keels, but with a larger \overline{GM} and lower wave height ($h_w = 0.9m$) reaches 30 degrees in only 6 cycles. Introduction of the bilge keels contributes to reduce the distance in the Mathieu diagram from the plotted point to the limit curve, thus decreasing the intensity of the amplification of the motion. But, as the hull is strongly subjected to parametric excitation in frequencies around the tuning $W = 2W_n$, the effect of fitting bilge keels is quite limited in this range of frequencies.

Another interesting comparison is between Fig 17(b) and Fig.19(b). Both cases correspond to TS hull without bilge keels, excited by waves of equivalent height. But the metacentric height in the two cases is very different. The wave frequency in Fig. 19(b) is high ($W = 2.08$ rad/seg), corresponding to a large parametric excitation e_0 (see Fig. 3), but large metacentric height ($\overline{GM} = 0.85m$). The resulting unstable motion is less strong than the motion given in Fig. 17(b), and another view of that can be seen in the location of point 2 in the Fig. 19(c), which lies very close to the curve of the stability limit, as compared with point 2 in Fig. 17(c), located well inside the unstable region. As a consequence of the large metacentric height considered in Fig.19 ($\overline{GM} = 0.85m$)

the limits of stability are relatively high, specially for the $W = W_n$ zone, as shown in Fig. 19(c). The wave tested in the condition shown in Fig. 19(c) is a very steep one, ($h_w = \lambda/14.8$). This is comparable to the steepest wave generated in this study, that corresponding to point 1 in Fig. 15(c). In that case, $h_w = \lambda/14.1$.

Clearly, the key to understand the mechanics of the parametric instability of a damped system with internal excitation is the distance of the plotted point to the curve of stability limit in the damped Mathieu diagram; this distance defines the amplification of motion. This result was persistent in all the tests performed, with the plottings defined by the mathematical model employed here.

This is also applicable to points 1 and 2 plotted in Fig. 20(c), representative of the motions shown in Fig. 6 (a) and 20(b), respectively. These two conditions have large values of the parameter q ($q = 0.55$ and $q = 0.72$, respectively), much higher than those presented in Figs. 16(c), 18(c) and 19(c). Nevertheless, the time series in Figs. 20(a) and 20(b) have both a very slow amplification, due to the fact that the unstable region is narrow near the $W = W_n$ tuning, and the points are necessarily near the limit of stability. The wave in Fig. 20(b) is reasonably smooth ($h_w = \lambda/26.2$).

Yet, even for very steep waves, no significative resonance occurs in the $W = W_n$ zone of stability.

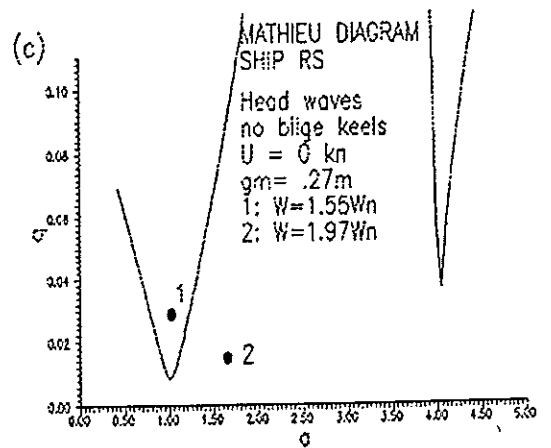
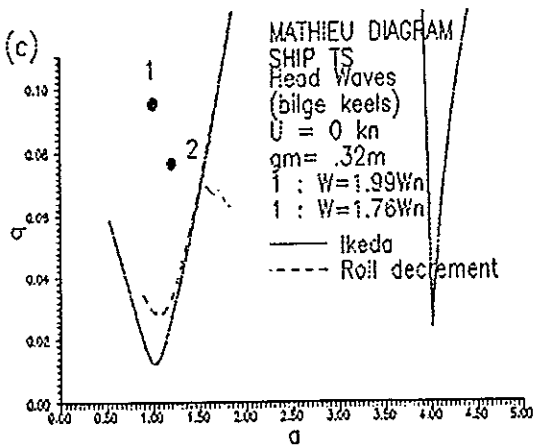
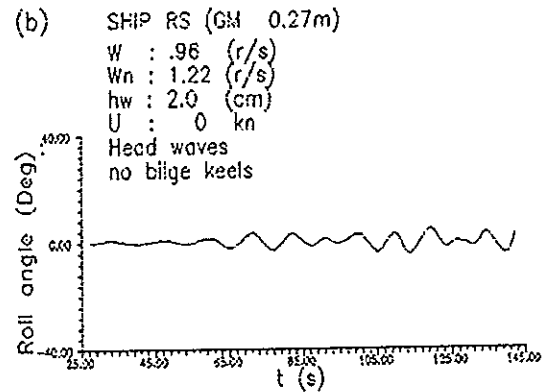
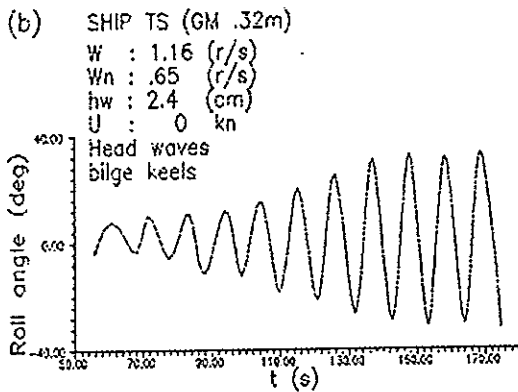
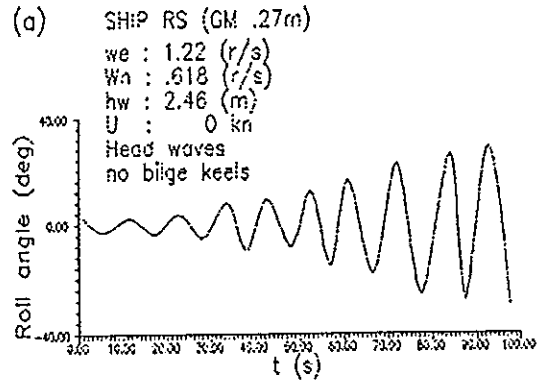
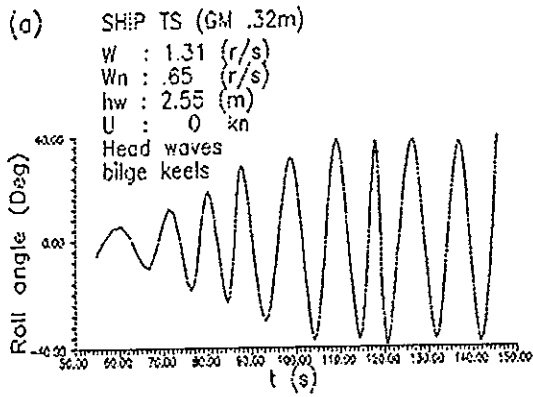


Fig. 15 Transom Stern hull with bilge keels, $GM = 0.32m$

Fig. 16 Round Stern hull without bilge keels, $GM = 0.27m$

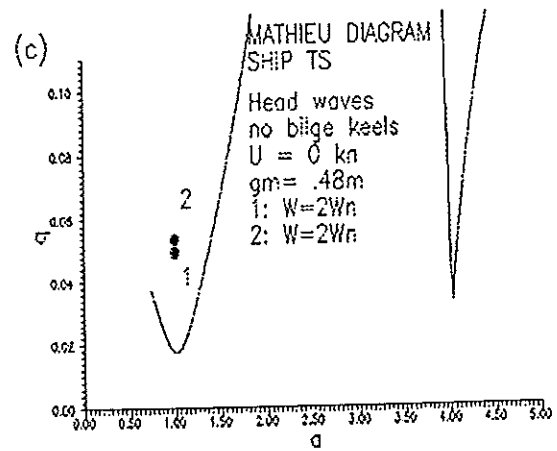
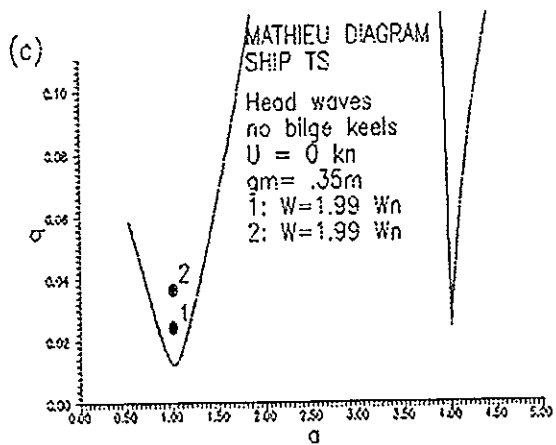
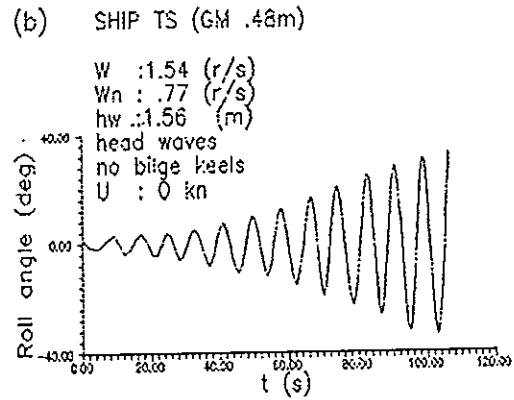
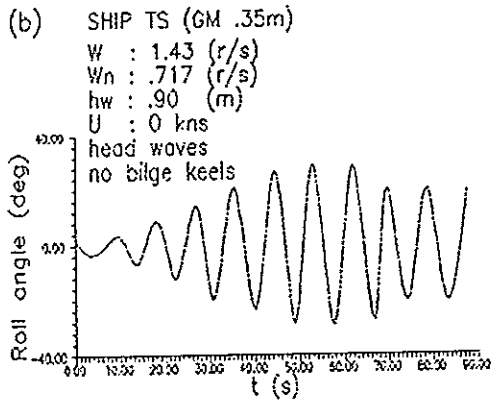
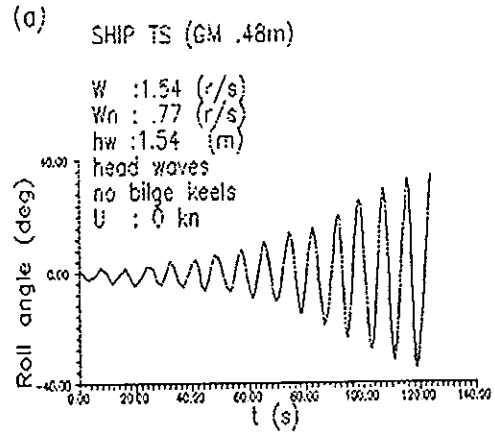
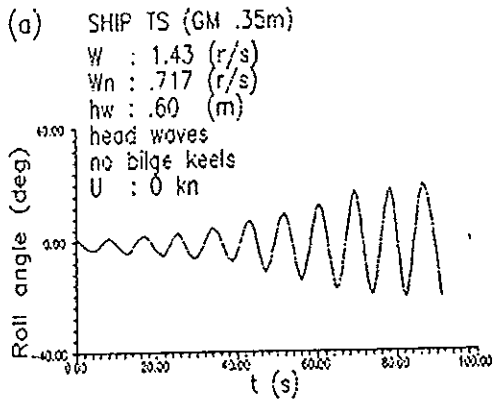


Fig. 17 Transom Stern hull without bilge keels, $\overline{GM} = 0.35m$

Fig. 18 Transom Stern hull, without bilge keels, $\overline{GM} = 0.48m$

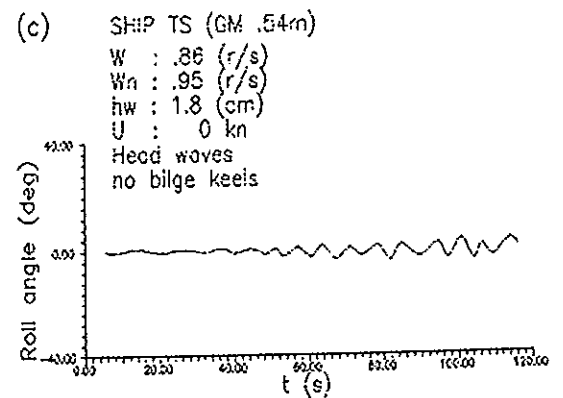
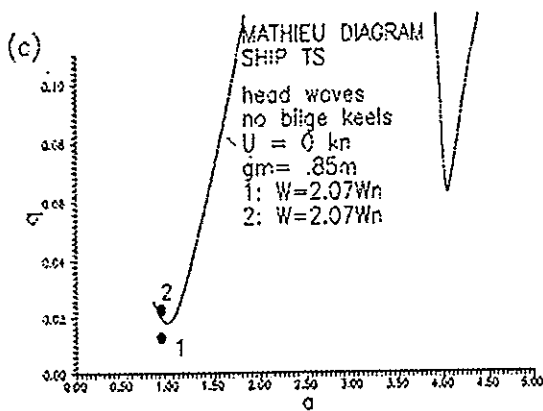
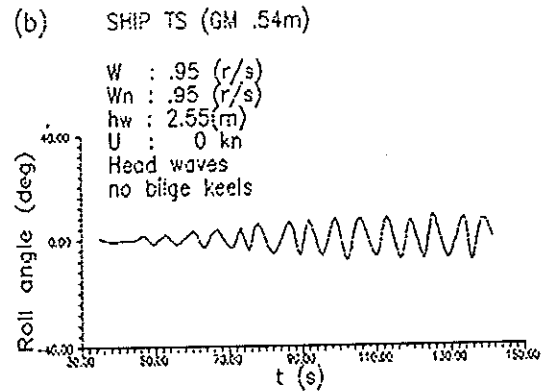
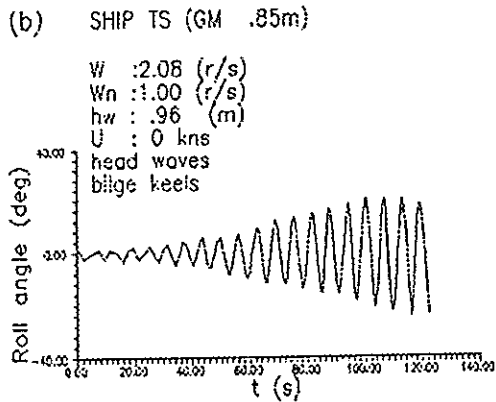
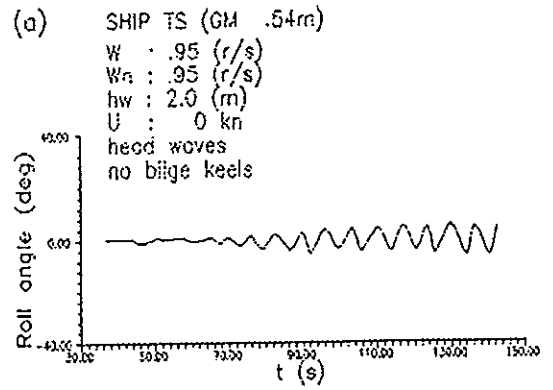
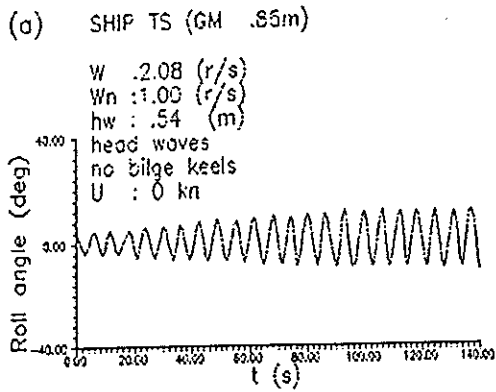


Fig. 19 Transom Stern hull
 without bilge keels, $\overline{GM} = 0.85m$

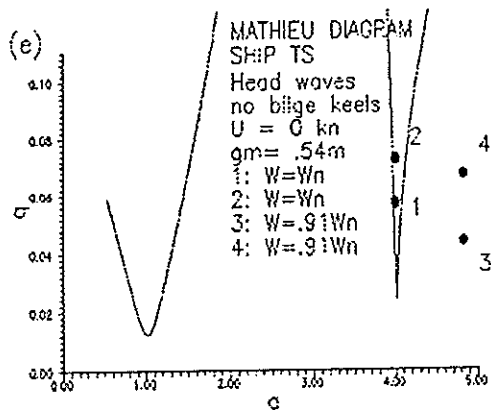
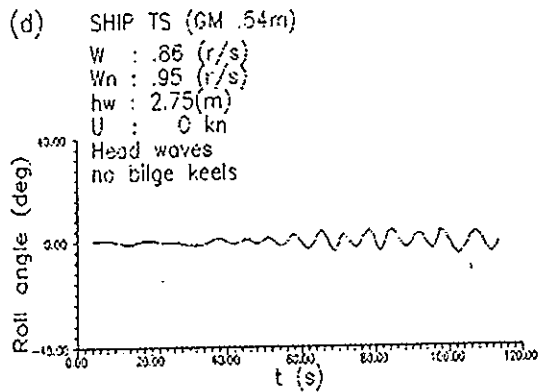


Fig. 20 Transom Stern hull without bilge keels, $\overline{GM} = 0.54m$

9. CONCLUSIONS

Although a very simple mathematical model was used, good agreement has been found between numerical investigation and experiment. The results indicate that form variation due to relative vertical motions provide relevant information to the analysis of fishing vessels under parametric excitation. Two ships of similar linear responses tended to behave in a very different way when these terms are considered. Transom sterns tend to play an important role in allowing high levels of parametric excitation. Model experiments produced very strong instabilities leading to large roll angles in few cycles for the transom stern hull with low metacentric height, in the $W = 2W_n$

zone of resonance. No significant resonance occurred in the $W = W_n$ zone of the Mathieu diagram.

Only zero speed of advance was considered in this study. Hopefully tests with ship speed in following waves will become available in the near future.

10. ACKNOWLEDGEMENT

The author's wish to express their thanks to Prof. Nelson Pérez from Universidad Austral de Chile who kindly gave permission for the reproduction of test results presented in this paper in figs 17(a) and (b), Figs. 18(a) and (b), Figs. 19(a) and (b).

This work was partially supported by CNP_q of Brazil.

11. REFERENCES

1. KERWIN, J. E. - "Notes on Rolling in Longitudinal Waves". Inter. Shipbuild. Progress., No 16, 1955.
2. PAULLING, J. R. - "The Transverse Stability of a Ship in a Longitudinal Seaway". Journal of Ship Research, No 4, 1961.
3. BLOKI, W. - "Ship Safety in Connection with Parametric Resonance of the Roll". Inter. Shipbuild. Progress., No 306, 1980.
4. SKOMEDAL, N. G. - "Parametric Excitation of Roll Motion and its Influence on Stability". Proceeding Second International Conference on Stability of Ships and Ocean Vehicles, Tokyo, Oct./1982.
5. MING-CHUNG FANG and CHWANG-KWO LEE - "On the Dynamic Stability of a Ship Advancing in Longitudinal Waves". Inter. Shipbuild. Progress. No. 422, 1993.

6. CAMPANILE, A. and CASELLA, P. - "Form Stability Reduction Among Waves for Series 60 Hulls". Ocean Engineering, Vol. 16, No 5/6, 1989
7. ZBOROWSKI, A. and CHU, HUI-SHEN - "Hard Chine Versus Round Bottom-Comparison of Stability in Waves and Seakeeping Performance of Small Displacement Ships". T. SNAME, Vol. 100, 1, 1992.
8. MORRAL, A. - "Capsizing of Small Trawlers". The Royal Institution of Naval Architects, Joint Evening Meeting, Glasgow and Rina Spring Meetings, London, 1979.
9. PAULLING, J. R. and ROSENBERG, R. M. - "On Unstable Ship Motions Resulting from Nonlinear Coupling". Journal of Ship Research, 1959.
10. NEVES, M.A.S.; PEREZ, N. A. and SANGUINETTI, C.O.F. - "Estudio Analitico-Experimental de la Estabilidad Dinámica de Buques Pesqueros en Olas Regulares". Ingeniería Naval No. 638-639, Spain, 1988.
11. HIMENO, Y. - "Prediction of Ship Roll Damping - State of Art". Department of Naval Architecture and Marine Engineering, The University of Michigan. Report No 239, September 1981.
12. NAYFEH, A. H. - "Perturbation Methods". John Wiley & Sons inc., 1973.
13. SPOUGE, J. R. - "Non Linear Analysis of Large-Amplitude Rolling Experiments". Inter. Shipbuild. Progress., No 403, 1988.
14. SANCHEZ, N.E. and NAYFEH, A. H. - "Non Linear Rolling Motions of Ships in Longitudinal Waves". Inter. Shipbuild. Progress., Vol. 37, No.441, 1990.

The Capsizing of the F.V. 'Straits Pride II' ; A Study of the Dynamics of Paravanes.

D. W. Bass and Chi Weng,
(Faculty of Engineering, Memorial University, St. John's,
Newfoundland, Canada).

1. Introduction.

In recent years it has become increasingly common to see, off the coasts of Canada, small fishing vessels with paravane stabilisers deployed. Their evident popularity is indicative of the practical usefulness of these devices in reducing roll motion. Just how effective they are has not been fully investigated. Some studies have been done [1,2], but they could not be considered exhaustive. There are a number of questions that remain to be answered. For example what is the most effective design (or efficient design -some designs significantly increase resistance)? Are they equally effective at all speeds and at all amplitudes of roll? These questions have only been partially addressed in the present study. The main impetus for the current investigation relates to the problems of asymmetric roll motion, such as might pertain to a vessel subject to a constant heeling moment, or 'bias' (as it is referred to in this study). In particular the effect on the motion of a vessel of losing a paravane is the underlying theme. It was prompted by the release of a report [3] by the Transportation Safety Board of Canada on the capsizing of the small fishing vessel, the 'Straits Pride II', which partially implicated the loss of the weather side paravane in the capsizing. In that report, it is remarked that at least one other capsizing of a Canadian fishing boat had occurred in which the loss of a paravane was considered to be a contributing factor. The precise manner in which the loss of a paravane can lead to capsizing is not entirely clear. Speculation on the mechanics of the effect of the single lee-side paravane on the roll motion in [3], is based on quasi-

static considerations and has no basis in experiment or dynamics. It is frankly admitted that little is known of the dynamics of ship motions with paravanes deployed. From the evidence gathered in a number of experiments performed at Memorial, it would appear that some of the speculations in that report may be wrong. For example, the report assumes (probably correctly) that the near-steady bias was partly caused by the quasi-static effect of the asymmetric 'lift' generated by the single paravane while under way, but further conjectures that with the lee-side paravane deployed (only), the bias to lee would increase (eventually leading to the ingress of water and the further increase in bias and final capsize). In fact this is not substantiated by the experiments, and surprisingly the reverse may be true, that is the bias to lee may decrease. This is part of a more general phenomenon associated with direction of bias relative to wave direction and is discussed later. It would also appear from the experiments that the moment generated by the single paravane to lee is unlikely to have been sufficient for a significant bias to lee to result. It is possible that the list was due primarily to the ingress of water into the fish hold, and the subsequent shift of the fish cargo. We shall return to these topics later.

It has not been possible to come to any definitive conclusion regarding the mechanics of this capsize. This study suggests that the cause for capsize was due to a complex interaction of a number of factors associated with asymmetric roll. Asymmetric roll motion is caused primarily by a transverse shift in the centre of gravity of a vessel due to cargo movement, icing, or asymmetric flooding. Wind heel may also cause or exacerbate asymmetric roll. These may be regarded as quasi - static effects. We refer to them as bias conditions.

There are factors affecting asymmetric roll that act 'asymmetrically'. One such major factor is wave direction relative to bias direction. That is the roll response for a vessel biased towards the waves (i.e. to the weather-side) may be quite different from that for a vessel biased away from the waves (i.e.

to the lee-side). It would appear from a number of studies conducted by the first author [4 ,5] that these differences are associated with or are dependent on a number of factors including wave length (and/or wave frequency), wave amplitude, 'dynamic swell-up', hull geometry, heave motion, and asymmetric roll damping. 'Dynamic swell-up' refers to the disturbance of the oncoming wave train by both radiation and diffraction effects due to the presence and motion of the vessel, thereby modifying the wave exciting forces and moments acting on it. These various factors may act together to give substantial increases or decreases in roll motion for various conditions of bias. Alternately there may be a 'cancellation' of effects leading to no significant variations in roll response with bias. It is this latter observation that makes the analysis of capsizing, based on experimental evidence, difficult. Figures 1 and 2 illustrate the point. The first shows roll response for a small fishing boat restrained in sway and heave in beam waves of small amplitude. There are substantial differences in response for the three bias conditions, unlike the situation in figure 2 in which the experiments were repeated for a somewhat higher GM. Similar results are shown in figures 3 and 4 for a vessel with a broadly similar but different hull geometry. It is clear that the experimental conditions here were artificial. That in fact is part of the methodology adopted for extreme motion analysis. Restrained conditions have been used to exaggerate the influence of various parameters on the roll motion; this is particularly apparent when the vessels have a bias. Rather than try and isolate these effects in extreme wave conditions, small amplitude waves with various conditions of restraint can be used instead. For example the coupling of heave into roll is simpler to analyze when the vessel is restrained in heave, since it is 'relative' heave that is significant rather than the absolute heave motion.

As has already been remarked the sensitivity of roll to bias is quite pronounced in restrained motion testing [5]. It was conjectured that a strong beam wind might act as a partial

restraint to natural sway, leading to similar sensitivities of roll to bias as for the restrained condition. Sellars [6] found that in a series of roll response tests on a drifting model in beam waves, significant increases in roll occurred for increases in drift speeds. The drifts were simulated by lateral tows using a specially designed towing hawser, that allowed a certain degree of freedom in sway. Certainly some restraint was required to achieve significant drift speeds. It is likely that there was some disturbance of the incident wave train due to the diffraction and radiation effects associated with the restraint and the lateral drift of the model (that is there were dynamic swell-up effects). This may have been the cause of the increases in roll observed by Sellars. It is not clear from these experiments if the simulation of drift by towing, would give results similar to those that would obtain for a vessel subject to wind drift. From the experiments conducted at Memorial, using both wind generated drift, and towing, it is likely that roll responses for both situations are quite similar. The experiments are described below. Unfortunately the results so far are inconclusive. That is, dynamic swell-up effects are not readily apparent, and the effect of drift on the small fishing boat models is to reduce roll. Roll decay tests on a towed ('drifting') model indicates that roll damping for these vessels, increases significantly with drift speed. For the vessel tested by Sellars, the increase in roll with drift makes it seem unlikely that there would have been a significant increase in damping with drift speed. It is possible that the results from the tests at MUN, exhibited the 'cancellation' effects referred to above, associated with the particular choice of GM (and therefore natural frequency), displacement, wave amplitude or drift speed.

The variation of roll response with respect to bias direction, is symptomatic of the presence of parametric excitation. This primarily comes from the fluctuation of the restoring moment with local draft changes. These in turn are dependent on such factors as wave length, wave amplitude, dynamic swell-up, and relative heave motion. The particular amplitude of the fluctuations of the

restoring moment is a function of hull geometry and can be seen quite clearly in the experiments with different fishing boats conducted at Memorial [5]. Surprisingly another source of parametric excitation come from the variation of damping with roll direction. This is apparent in the roll motion tests described below in which a single paravane is deployed. In fact the dependence of the damping on direction signifies a modification of the amplitude and phase of the righting moment fluctuations relative to the wave excitation. As such the effect is dependent on factors such as hull geometry, wave length, etc. This asymmetry in damping has been noted before by other authors, for example , Watanabe, [7], Grochowalski, [8], Bass [9]. In these studies, the asymmetry was associated with deck-edge immersion. For a model fitted with bulwarks there are in addition inertial effects. In a series of capsize tests carried out at AMTE (Haslar) in cooperation with the University of Southampton [10] , a low freeboard model (with no bulwarks) in large amplitude waves capsized only when it was biased towards the weather side. Moreover the responses for the different bias conditions differed significantly. Parametric excitation was implicated as the most likely cause of this phenomenon. This was thought to be due to the relative heave motion coupling with roll, giving rise to righting moment fluctuations. Bass [9] demonstrated the differences in response for different bias directions in numerical simulations. The differences only became significant for quite large relative heave. It is possible that there were dynamic swell-up effects. It is also likely that the asymmetry in damping due to deck edge immersion (which probably occurred more frequently for the model biased towards the waves) was a significant factor in producing the different responses and capsize behaviour.

To summarize, it is believed that the capsize was due to an accumulation of asymmetries or parametric excitations in the roll, associated with wind, drift, the single paravane deployment, and the movement of water and fish in the fish hold. This latter effect has not as yet been investigated. The effects that are

described below do not seem to be sufficient to result in enough parametric excitation to lead to capsizing. However testing has only been carried out in moderate conditions and extrapolations to more extreme conditions should be treated with caution.

TABLE 1

Vessel	M365, full scale	Straits Pride II
LWL (m.)	17.8	19.8
Beam (m.)	6.75	6.64
Draft (m.)	2.70	-
Mass (tonnes)	104	93
GM (m.)	0.45	-
Roll freq. (r/s)	1.05	-

2. Experiments with Paravanes.

Experiments have been carried out for a number of small fishing boat models. The work reported in this paper relates particularly to the fishing vessel, referred to in various papers as model 365. Its lines are shown in figure 5 and its particulars are shown in table 1. The overall geometry of the vessel is broadly similar to that of the Straits Pride II. Details of this vessel are also given in table 1. No lines or stability booklet for the Straits Pride II are available.

Steady Heel with Forward Speed. Experiments were carried out in the wave tank at Memorial University, which is 57 m. long, 3 m. wide and 2 m. deep. The first set of tests carried out were to determine the likely angles of heel associated with the loss of a single paravane at various Froude numbers. Two types of paravanes were employed. The first was based on the design that was used on the Straits Pride II, as shown in figure 6 (a) (taken from [3]). In fact the design used in the experiments had to be modified to

obtain a reasonable balance point position (the weighted nose had to be extended). The second was a rather more typical modern version with smaller dimensions. It is shown in figure 6 (b).

The model 365 was fitted with a paravane deployed from a light metal boom mounted athwartships, from which was suspended a paravane at the end of a one metre length of nylon line (see figure 7). The line was at a distance of 80 cm. from the centre line of the model. The model was towed in calm water at Froude numbers 0.1, 0.2, 0.3, and 0.4 down the length of the tank. Stable angles of heel were observed after a short transient. The results for the two types of paravane are shown in figure 8. The 'large' paravane (its horizontal 'wing' area was 22.4 sq. cm.) was that of the Straits Pride II. It is surprising to note that this was the paravane that was least effective at the higher Froude numbers, with maximum angle of heel of 1.5° produced at Froude number 0.2. For the smaller paravane (with 'wing' area 14.0 sq. cm.) an angle of 2° resulted at Froude number 0.4. It was thought that the position of the point of attachment of the line to the larger paravane might give different, larger angles of heel. Four different points were used in a subsequent series of tests. The results are shown in figure 9. The positions 1 to 4 start from the nose and move back to the tail. The point of attachment used in subsequent tests was number 2. At steaming speed the Straits Pride II would have listed only slightly, if the GM had been of the order 0.45m. It is possible that with free surface effects, GM could have been quite low. However even for a GM of 0.2 m., the list at steaming speed would only be of the order of 3° due to the lift force on the port-side paravane. That of course assumes that the model experiments scale to full size as expected. It is reasonable to assume that they do, since the forces associated with paravane motion are primarily lift forces which scale according to Froude scaling laws. There is also the quite different conditions under which the vessel was operating. It is possible that with large surge motions, and roll in large amplitude waves, the effect of the paravane on the mean roll angle would be different. In fact tests at zero speed

(with no surge) in beam waves show little effect on mean roll angle due to paravane deployment. To simulate the possible added heel due to forward speed, tests were carried out with the model biased and there was still no appreciable effect on mean roll angle. We return to this later.

Roll Damping. A number of roll decay tests were carried out at various Froude numbers to determine the effect of paravanes on roll damping. Tests were carried out using two, one and no paravanes of both designs. Since the roll damping is typically non-linear for these small fishing vessels, the non-dimensional equivalent linear damping ratio, ζ , was determined for various amplitudes of roll, using decay tests at different initial angles. Figures 10 to 13 show roll damping for different roll amplitudes at Froude numbers from 0.0 to 0.3 with no paravanes (figure 10), with one 'large' paravane (figure 11), two 'large' paravanes (figure 12) and two 'small' paravanes (figure 13). The damping at higher Froude numbers with paravanes is fairly high and the results from decay tests are not very reliable. This is particularly a problem for the tests with the 'large' paravanes at certain Froude numbers. However it is apparent that there is a definite loss of effectiveness at the higher amplitudes of roll at Froude numbers above 0.2 for these paravanes. For the smaller paravanes the results are quite different. Figure 13 shows damping for the same ranges of amplitude and Froude number with a substantial increase in non-linearity at Froude number 0.3. At Froude number 0.2, the damping is almost linear over this range of roll amplitudes.

It is possible that the non-linearity of the Straits Pride II's paravane at the higher speed may have contributed to increasing the asymmetry of the response. Unfortunately it is not feasible to carry out suitable tests in waves at forward speed in a small towing tank to determine whether or not this was the case. In fact soon after the initial heel developed with the loss of a paravane the ship's master reduced speed to a few knots. At these speeds the difference in damping relative to that at zero speed is not great, both in terms of magnitude and non-linearity.

Paravanes contribute quite significantly to the roll damping even at zero speed. For this vessel, the damping is more than doubled when using 2 paravanes, and increases by over 50% when just one is used. For the more efficient small paravanes, it is clear that at low speeds, there is little non-linearity introduced into the roll damping by the use of a paravane. This is particularly clear in figures 10 and 13, comparing the damping at Froude numbers less than 0.2, with and without the small paravanes. The slopes of the damping curves are quite similar for the three lower speeds. This indicates that even at zero speed, the damping comes from 'lift' forces rather than 'drag'. The lift forces on the paravane are generated as it moves in a circular path induced by the upward pull of the line at the point of attachment.

Roll Response in Beam Waves. Experiments in waves were carried out with the model lightly tethered across the tank. Various wave heights were employed, with values generally low to moderate. As was previously discussed, the intention of the experiments with a single paravane deployed, was to ascertain the possible mechanism that might have contributed to the capsize of the Straits Pride II. There are two possibilities. One of them is that the paravane led to an increase in the already biased (to lee) condition. The second is that the paravane dynamics were a contributing factor in the parametric excitation of the vessel. That together with additional parametric excitation, associated with wind, drift, dynamic swell-up etc. (as discussed in section 1) may have led to larger than expected roll amplitudes, leading to the shipping of green water and the further degradation of stability. The tests carried out at Memorial were at zero speed, and it is possible that these results cannot be applied to the motions of the full scale vessel which was underway. However after the initial loss of the paravane the vessel slowed and it is apparent from the experiments discussed above that the effects of the paravanes at low speed do not differ appreciably from those at zero speed. In the experiments in waves the model was given a 7 degree bias by a transverse movement of a small weight. As has

already been noted, an asymmetric response to an apparently symmetric excitation is indicative of parametric excitation effects. As is shown in figure 14, the responses of the model vary according to bias direction. These differences are not significant. However with a single paravane deployed, the differences increase; moreover the differences depend on the side on which the paravane is deployed relative to both bias direction and wave direction. The response of the model biased towards the waves with the paravane deployed to the lee, is some 30% greater (for frequencies above the natural frequency) than that for the model with the paravane on the weather side (see figures 15,16 and 17). In contrast, there is little difference in mean angle associated with either bias condition or side of paravane deployment (see figure 18). It would seem therefore that the dynamics of the Straits Pride II could have been significantly affected by both its bias condition and the deployment of the paravane on the lee-side. It is worth pointing out again that in some instances these two asymmetries effectively cancelled one another, while at other times they acted in concert. It seems unlikely that it was these two alone that led to the loss of the vessel. The next source of asymmetry (or parametric excitation) to be considered is that due to wind drift.

Experiments with Wind Drift in Waves. The experimental set-up for the experiments with wind drift is shown in figure 19. The centre of wind pressure was at midships, equidistant from the top of the bulwarks and the waterplane. Since the model had no superstructure, it was not possible to induce wind heel. Instead the model was given a bias, as above. The wind induced drift velocities in the range of 10 to 15 cm/s. The drift of the model significantly reduced the roll motion by effectively increasing damping. In 8 cm. waves, with the wind at full strength, it was difficult to restrain the model from excessive yaw. The roll responses for the model at some frequencies are therefore subject to some uncertainty or error. The results for the three bias conditions (using 8 cm waves) are shown in figure 20. It is noticeable that the results for the away bias condition are

significantly lower than for the other two conditions. That is a little misleading since the reason for that is due in part to the higher drift speed attained in the bias to lee condition (probably due to the reduced drag at this orientation). In order to determine if it was possible to simulate the effect of wind drift, by towing the model laterally, experiments were carried out in which the model was towed. Towing affords much greater control over such things as drift speed, and yaw. The results of the experiments (with 8 cm. waves) performed with tow induced drift are shown in figure 21. The results are broadly in agreement with those for wind drift, if account is taken of the fact that for the bias to lee condition, drift speeds were quite different (they were nearly 40% higher). Certainly for the bias to weather condition, the results are nearly identical. Experiments at higher drift speeds confirm the similarity for the bias to lee response. It was therefore decided to conduct the remainder of the tests with drift simulated by towing.

Tests were carried out at a drift speed of 10 cm./s. in 10 cm. waves, with a paravane deployed to lee and to weather for various bias conditions. The results are shown in figures 22 to 26. For the experiments with the paravane on the weather side, in 10 cm. waves, there is little difference between the responses for the three bias conditions. Larger waves were used here to ensure responses were of a similar magnitude to those with no paravanes. There is a noticeable reduction in response for the model with drift induced, but mainly for frequencies less than the natural frequency. This can be seen in figures 22 and 23. In fact the reduction in roll is less than might be expected considering that the evidence from decay tests points to an increase in damping of approximately 50% due to drift. For the model with the paravane on the lee side there is a greater difference between responses for the three bias conditions. The differences between the responses relative to paravane position also appears to change (comparing figures 24 - 26 with figures 15 - 17). This is most noticeable for the bias to weather condition. The difference is too small for an

unequivocal conclusion, but suggests that drift may play some role in generating parametric excitation effects.

More obviously drift changes the bias angle in the lee direction. Thus for the vessel biased to lee the effect of drift is to increase the lee bias angle (negative to lee), but for a bias to weather the bias angle is reduced. The results are shown in figure 27. This effect increases with drift speed.

3. Discussion.

It is clearly not possible to reproduce the conditions experienced by the Straits Pride II at the time of its capsize. Even if it was possible to demonstrate a capsize in a series of model experiments, there would remain the question as to the applicability and interpretation of the results, based, as they would have to be, on a number of (questionable) assumptions. Historically the analysis of a capsize has been in terms of a static (or quasi-static) analysis of the presumed stability of the vessel at the time of the event. The inadequacy of that approach has long been recognised by many of those concerned with Safety at sea. However it has as yet not been possible to arrive at a consensus for a methodology for an analogous dynamic analysis. Dynamic effects are, by their very nature difficult to assess, quantify and analyse. The approach used here demonstrates dynamic effects by exploiting possible asymmetries in the motion. This is done in a sufficiently controlled manner to make assessments of dynamic effects possible. For example it has been shown that deployment of a single paravane may significantly modify the roll motion of a vessel under certain conditions. The next step is to gain insight into those particular conditions leading to the most significant dynamic effects. This may be done using numerical simulation tools and/or further experimental work. It is not a simple task, since the effects are subtle and multifaceted. Preliminary investigations indicate that even sophisticated time domain simulation codes [11] are not able to predict some of the dynamic effects encountered in the studies conducted at Memorial [5], including those reported here with single paravanes. That in

itself may lead to insights into these effects. With the insights gained through further investigation it may be possible to establish scenarios in which these dynamic effects are both significant and dangerous. For example, it was hypothesised that the restraint associated with wind drift might exacerbate the asymmetry due to the single paravane. That was not adequately demonstrated in this series of tests, although there were indications of some additional asymmetries.

Returning to the loss of the Straits Pride II, it is not clear whether or how the loss of the starboard-side paravane may have led to capsize. It is clear that there are two significant factors to be considered. One is the additional roll damping afforded to the vessel by the paravane, and the second is the significant modification of the roll of the vessel under certain conditions due to the paravane. The former is an obvious aid to stability, while the second is likely to be otherwise. Would the jettisoning of the remaining paravane have saved the vessel? This is an important question that clearly needs to be answered. Further investigation is necessary. The tests were conducted in regular, 'symmetric' beam waves in a steady beam wind. The conditions experienced by the Straits Pride II would have been much less 'symmetric', with irregular, non-symmetric quartering waves in an unsteady wind and strong surge motions coupled into the roll causing a greater likelihood of the asymmetry of the paravane dynamics to be a contributing factor in its capsize. However this is conjectural, and needs to be substantiated. Surprisingly there is little evidence to suggest that asymmetry in the dynamics leads to significant increases in mean angle of roll. Even the effects of drift or paravane 'lift' may be regarded as quasi-static (as for wind induced heel) . The increasing list experienced by the Straits Pride II, would appear to be of quasi-static or static origin. In fact the quasi-static effects are likely to be steady while the purely static may in fact change with time, with progressively greater transverse shifts of the centre of gravity due to the movement of the fish cargo and the accumulating volume of green

water taken and retained on the lee-side. Preliminary experiments with water on deck suggest that the dynamics of its motion do not lead to increases in mean roll angle, although again the roll of the vessel is significantly modified by its action. Further experiments on the combined effects of bias, single paravane, and water on deck are planned.

4. Conclusion.

It has been shown that paravanes add considerably to the roll damping and thus the dynamic stability of small fishing vessels. Some paravanes clearly do the job better than others. More work needs to be done to find the most effective design over a range of roll amplitudes and Froude numbers. To what extent the loss of a paravane endangers the safety of a vessel is not entirely clear. It is apparent that for a vessel subject to asymmetric roll motions, there are conditions for which the loss of a paravane may significantly affect the subsequent motion. Wind induced drift may further modify roll, if only in so far as to increase the mean angle of roll. From simulations carried out thus far, it would seem that all these effects are dependent on, amongst other things, hull geometry. It will therefore be necessary to conduct a further series of experiments to evaluate the role of hull geometry in this regard.

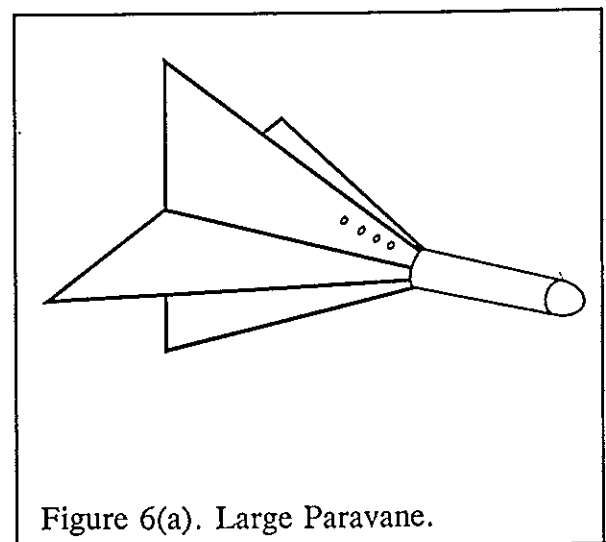
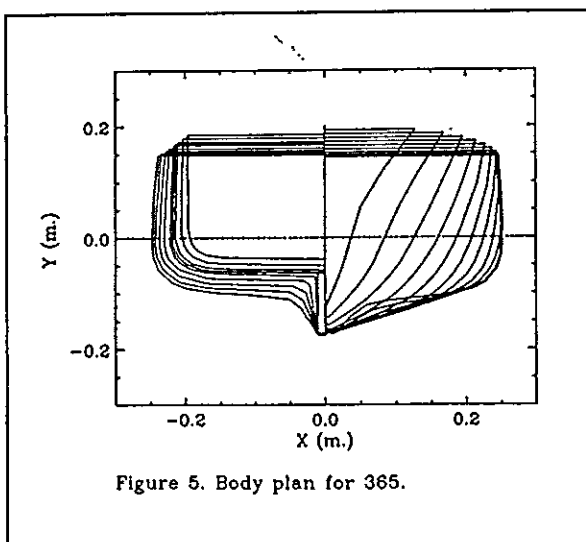
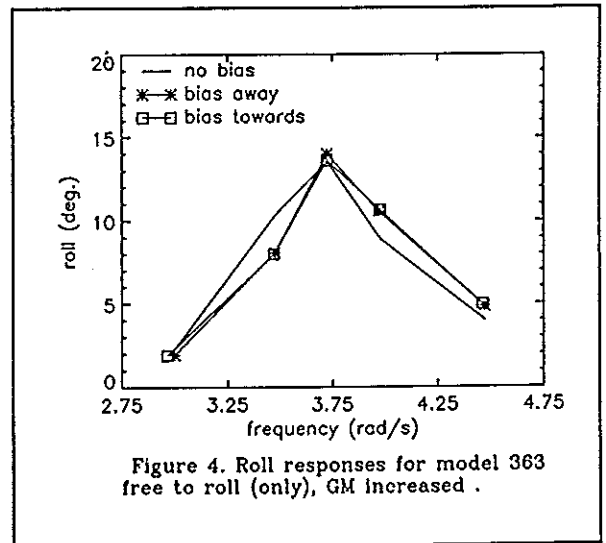
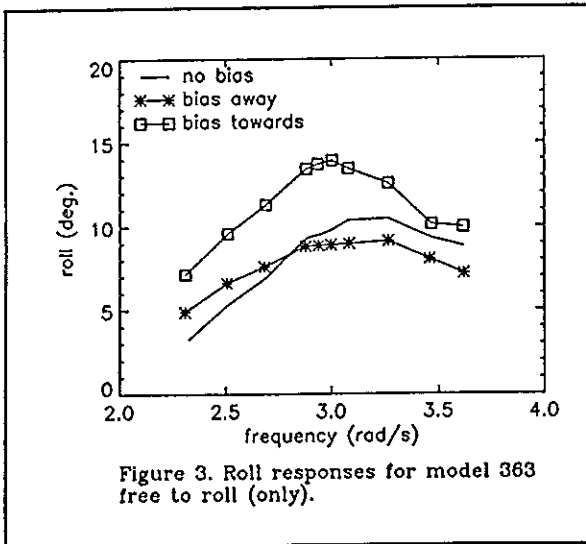
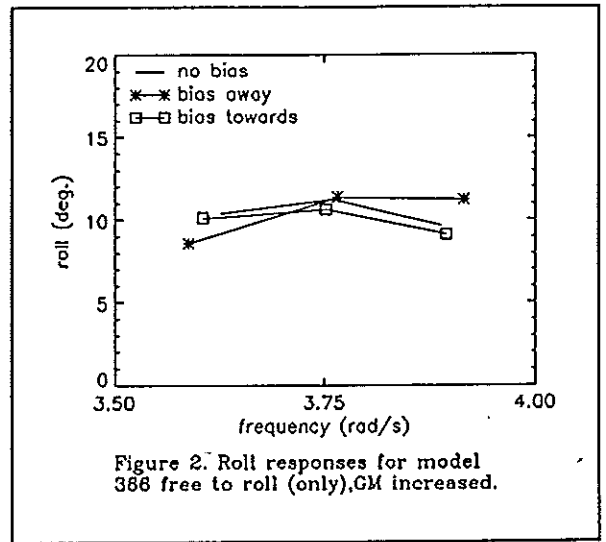
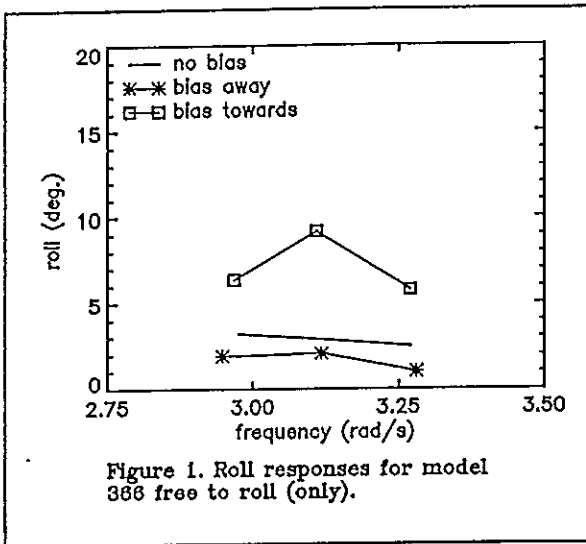
Acknowledgements.

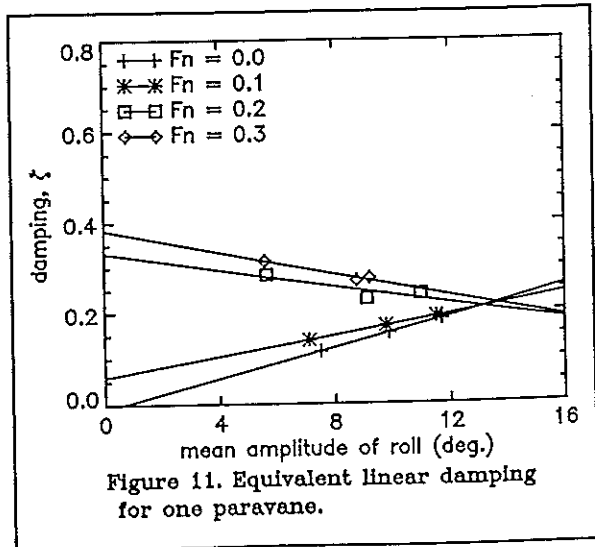
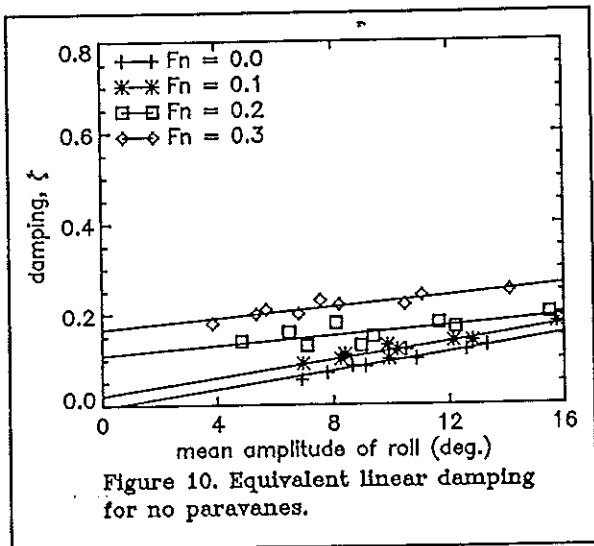
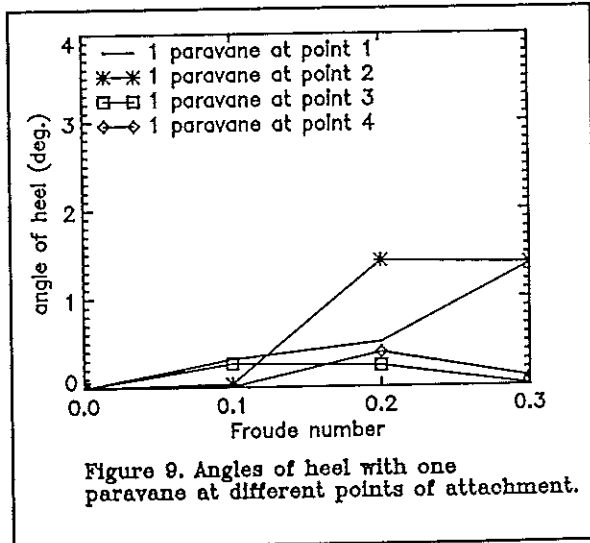
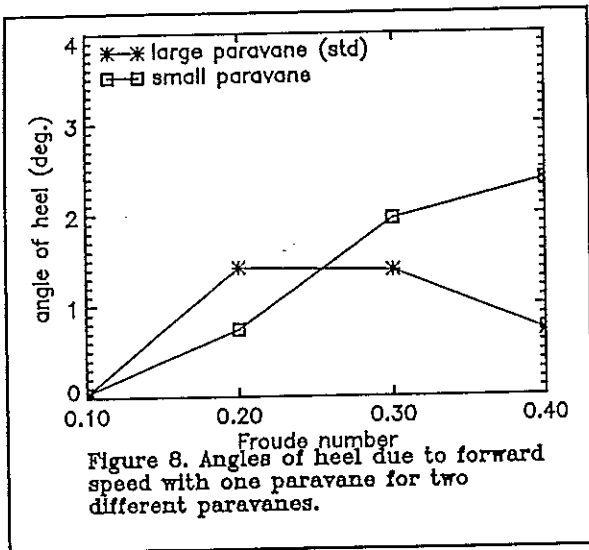
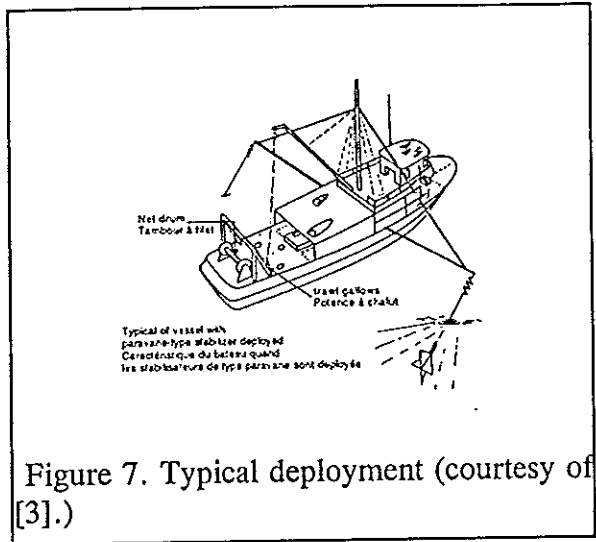
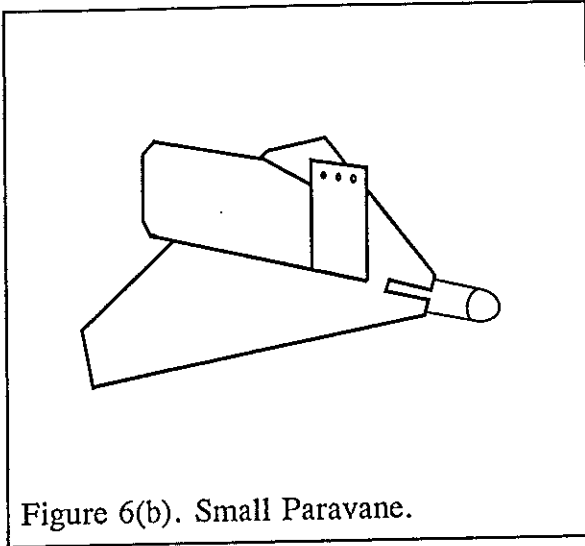
The authors would like to acknowledge the financial assistance of NSERC for this work. Also they would like to thank Kaaren May, Andrew Macneill, and Torfi Thorarinson for their help in conducting a number of the many experiments on asymmetric roll at Memorial.

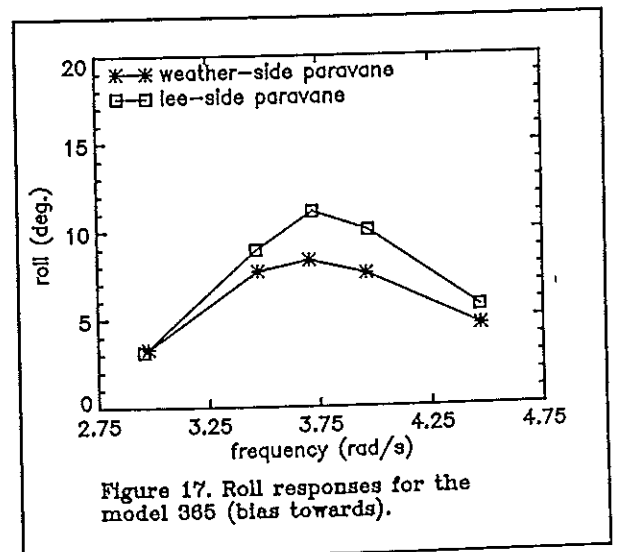
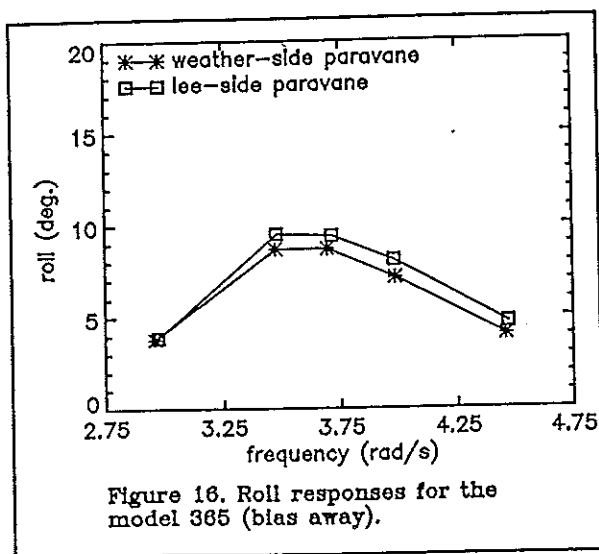
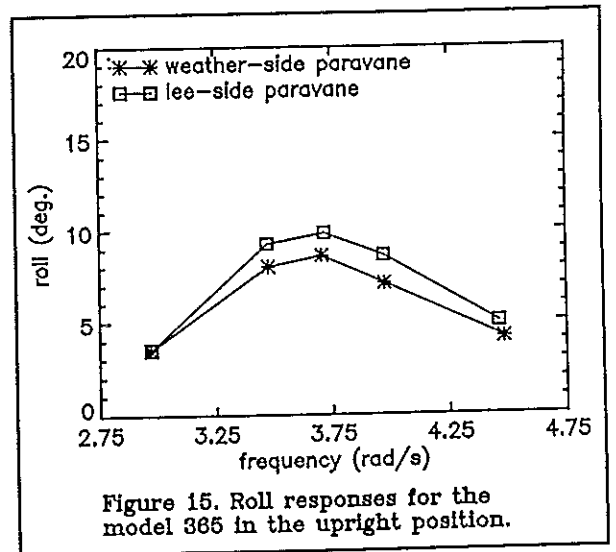
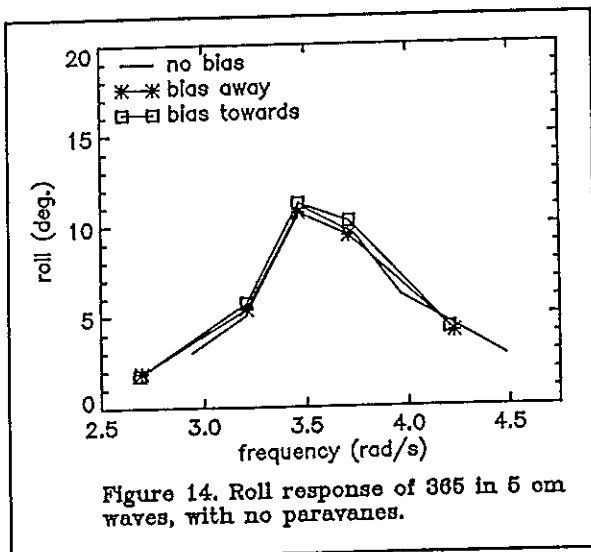
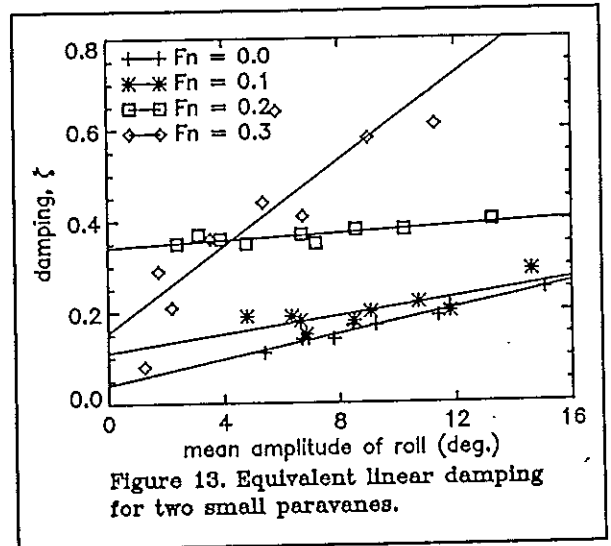
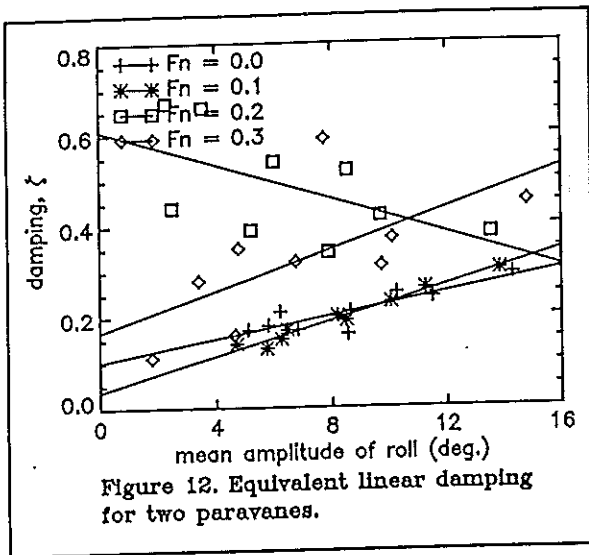
References.

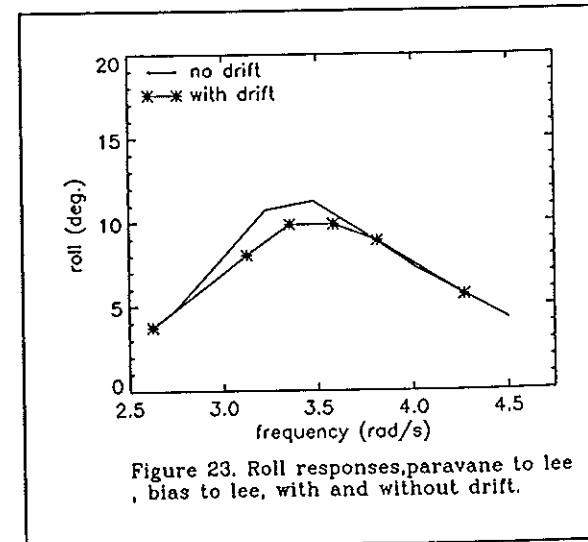
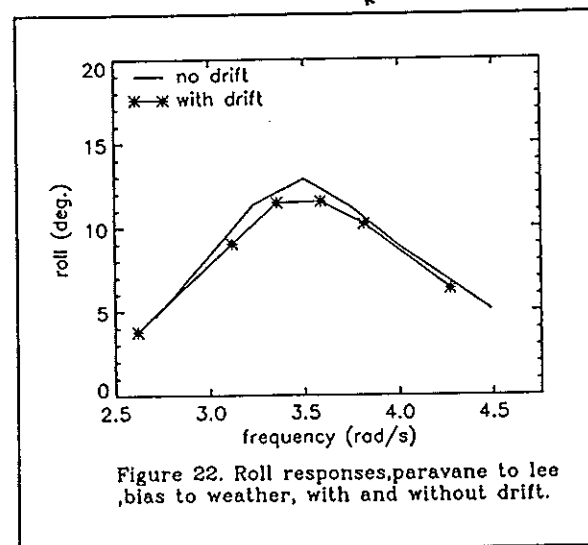
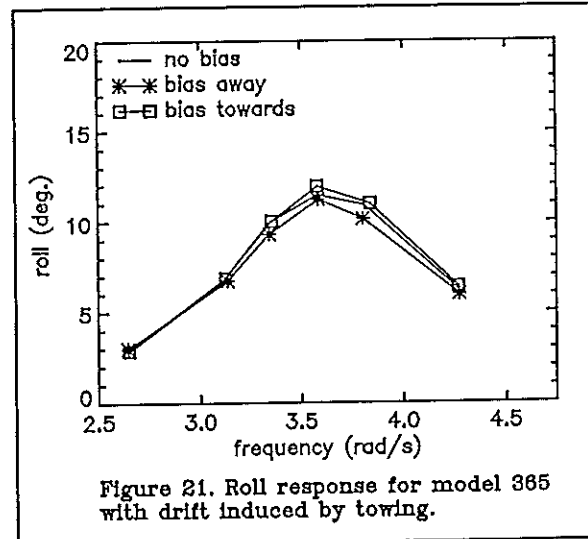
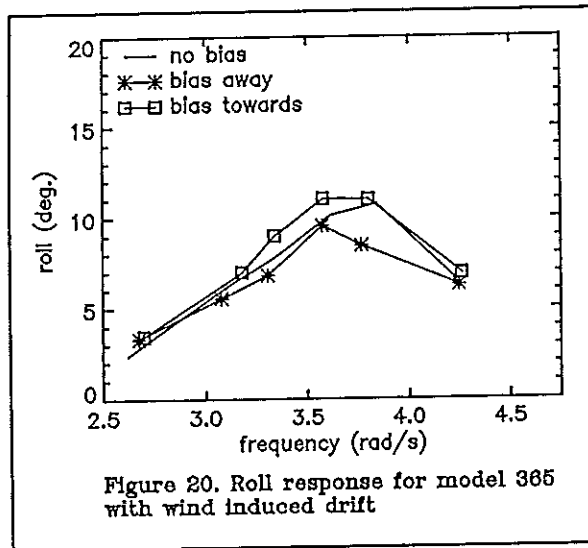
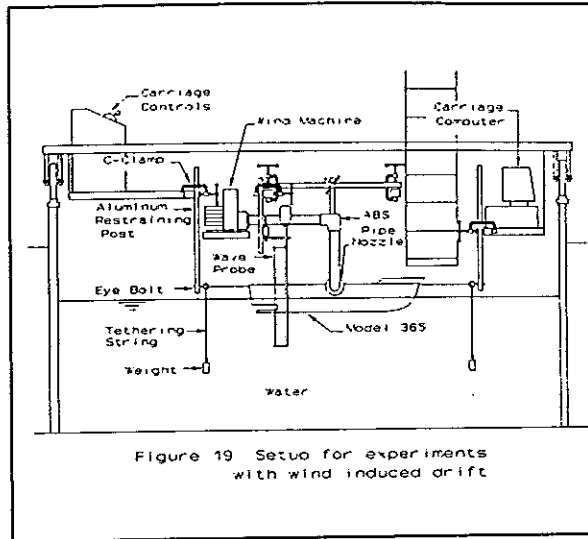
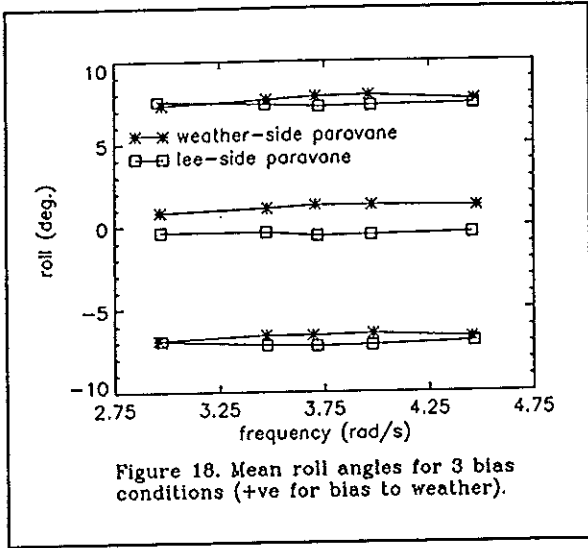
1. Goudey, C.A., Venugopal, M., 'Roll Damping on Two New England Trawlers: An Experimental Study', Marine Technology, Vol. 26, No.2, April 1989, pp. 160-167.
2. Koelbel, J.G., Jr., Fuller, N.R., Jr., Hankley, D.W., 'Paravane

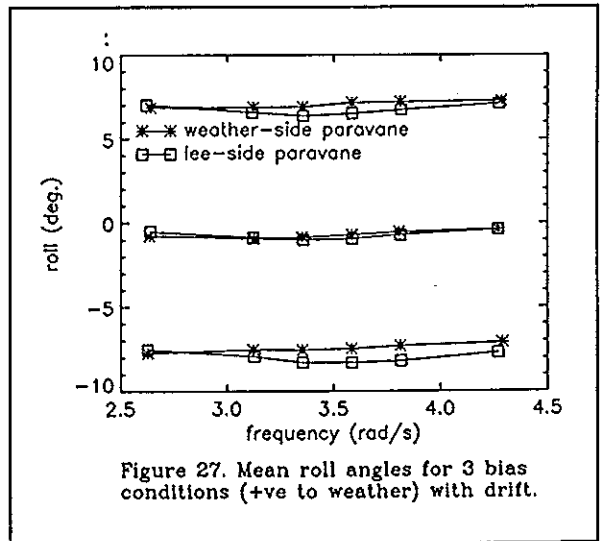
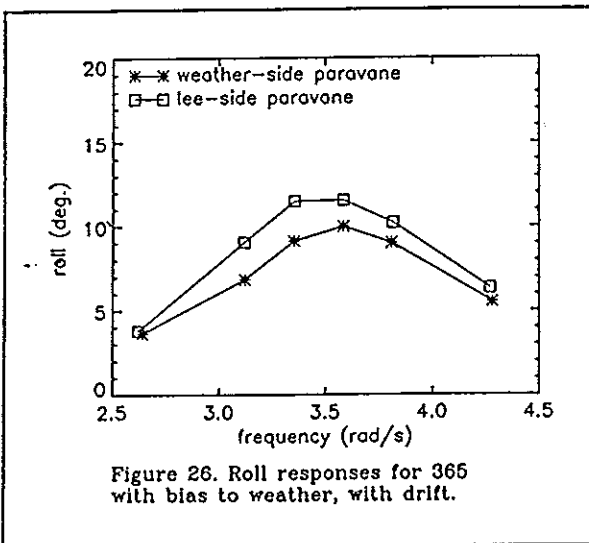
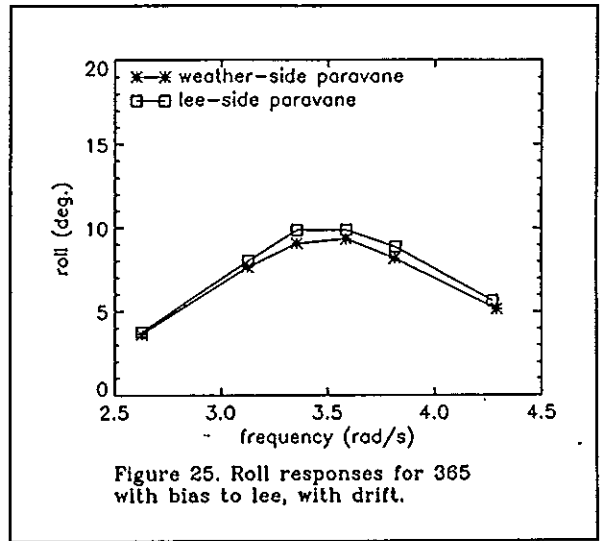
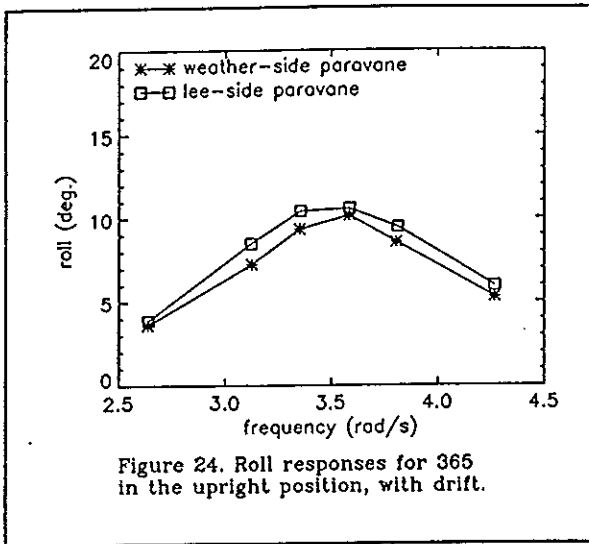
- Roll Stabilisation', STAR Symposium, Spring Meeting, Houston, Texas, April 1979, pp. 313-336.
3. 'Capsize and Sinking of the F.V. "Straits Pride II"', Transportation Safety Board of Canada, Report no. M90N5017, 1992.
 4. Bass, D.W., Haddara, M.R., Wang, Z., 'Asymmetric Motions of a Small Fishing Vessel with a List', CADMO, Oct. 1992, Madrid, Spain.
 5. Bass, D.W., 'On the Motions of Small Fishing Vessels with a List', 2nd Marine Dynamics Conference, Vancouver, 1993, pp. 264-273.
 6. Sellars, F., 'Seakeeping Characteristics of a Drifting Vessel', Journ. of Ship Research, March 1986, pp 26-33.
 7. Watanabe, Y., 'A Consideration on the Instability of an Asymmetric Rolling', Jour. Nav. Arch. West Japan, No. 34, 1967.
 8. Grochowalski, S., 'Investigation into the Physics of Ship Capsizing by Combined Captive and Free-Running Model Tests', Trans. SNAME, vol. 97, 1989, pp. 169-212.
 9. Bass, D.W., 'On the Response of Biased Ships in Large Amplitude Waves', Int. Shipbuilding Progress, vol. 30, (1983), no. 341, pp. 2-9.
 10. Wright, J.H.G., and Marshfield, W.B., 'Ship Roll Response and Capsize Behaviour in Beam Waves', Trans. RINA, Vol. 122, pp. 128-149.
 11. Pawlowski, J.S., and Bass, D.W., 'Theoretical and Numerical Modelling of Ship Motions in Heavy Seas.', Trans. SNAME, (New York), 1991.











Safety for Fishing Vessels in the Hauling Course

T.C.Feng Y.S.Tao

Abstract

A fishing vessel in operating conditions is not only subjected to the waves and winds but also to additional heeling moments, for example, the time dependent hauling moments. The paper discusses the rolling motions with strong nonlinearities in hauling courses. Assuming that the rolling response spectrum is of narrow band, the rolling equation can approximately be solved in time domain by the impulse method. Computing results show that the rolling responses and safety of fishing vessels are significantly influenced by hauling moments.

1 Introduction

Ship stability in waves is one of the most important performances to ensure safety of fishing vessels. It is the inherent ability to resist capsizing of a ship in seas as reacts to the dynamic combinations of forces acting upon the ship. These forces include those generated by waves and winds. Besides they must also include effects which are not directly induced by waves and winds, for example, hauling forces of a fishing vessel in operating conditions.

Vessel safety is related to large amplitude rolling motions requiring the consideration of nonlinear dynamics, therefore nonlinear hydrodynamic forces and exciting forces which are perhaps associated with time dependent coefficients must be taken into account in the motion equation. If the amplitude of the rolling motions are small, the forces corresponding to nonlinear terms may be ignored and the problem reduces to a linear one. The theory for predicting linear motions, as is well known to all, is well developed, and in most practical applications the predictions obtained from linear analysis are sufficient. However, if the amplitude of the rolling motions are large, the effects of nonlinearities appear to be significant. The nonlinearity may not only modify the magnitude that would be predicted by a purely linear analysis, but also change the general characteristics of a response.

The paper discusses the rolling motions of fishing vessels in operating conditions with strong nonlinearities including time dependent hauling moments. The rolling equation can approximately be solved in time domain by the impulse method under the condition of assuming the rolling response spectrum is of narrow band.

2 Hauling Moments in Course of Hauling

In order to determine the stability of vessels under the action of fishing gear pull, an essential problem is to evaluate the fishing gear pull. For this purpose, the pull has been measured on two sister combination fishing vessels in the East China Sea ^[1]. Its principal particulars are as follows:

displacement (t)	350.00
length (m)	34.00
beam (m)	7.00
draught (m)	2.90
machine power (h.p.)	600.00

The course of hauling is divided into four stages:

- (1) at the beginning of hoisting catch;
- (2) hoisting catch clear of the water level;
- (3) hoisting catch in close contact with the bulwark;
- (4) hoisting catch above the bulwark.

The pull of pursuing davit varies with the time. It were measured ten times in all.

As the pursuing davit is intended to sling towards ship's side from commencement to the end in the course of hauling, heeling moment can be obtained provided that heeling arm l is given while the pull has already been determined. The product of the pull and heeling arm l is the heeling moment. Thus a group of curves can be obtained representing the variation of the heeling moment with the time. The average curve of the group curves is shown in Figure 1. As shown in the figure, the duration of the moment acting on the vessel is about thirty seconds. A fishing vessel in a short time being subjected to a specified moment obviously will produce large effects on rolling motion. The average curve given by Figure 1 is taken as the heeling moment curve in our calculations.

3 The Governing Rolling Equation

A fishing vessel in operating conditions is not only subjected to the waves and winds but also to additional heeling moments, for example hauling moment. Nonlinearities of restoring and damping moments of rolling motions must also be considered. Then the pure ship rolling motion about the longitudinal axis passing through its center of weight is discussed in what follows. The governing rolling differential equation can be represented as follows:

$$I_x \ddot{\theta} + NR(\dot{\theta}) + DR(\theta) = M_w(t) + M_b(t) + M_c \quad (1)$$

where

- θ -- relative rolling angle
- I_x -- real and added moment of inertia
- $N(\theta) = k_1 I_x \dot{\theta}$ -- damping moment
- k_1 -- constant
- D -- displacement
- $R(\theta) = D \sum r_{2i+1} \theta^{2i+1}$ -- restoring moment
- r -- coefficients related to the GM curve fit
- $M_w(t) = k_1 I_x \alpha_e \omega^2 \cos(\omega t)$ -- wave moment
- k_1 -- coefficient modified to irregular sea
- α_e -- effective wave slope amplitude
- ω -- wave circular frequency
- $M_b(t)$ -- hauling moments given by Figure 1

M_c -- steady wind moment

We may rewrite the equation (1) as the follow form:

$$I_x \ddot{\theta} + k_1 I_x \dot{\theta} + Dr_1 \theta = M(t, \theta) \quad (2)$$

where

$$M(t, \theta) = M_w(t) + M_b(t) + M_c - D \sum_{i=1}^n r_{2i+1} \theta^{2i+1} \quad (3)$$

The governing roll differential equation is complicated and highly nonlinear, The left side of this equation includes only linear items, while its right side includes all nonlinear items. Providing that $M(t, \theta)$ in the equation (2) is regarded as a exciting moment, the equation may be solved by the impulse response methods which was presented in references [2].

Since rolling motion is a narrow band process, one can assume that hydrodynamic coefficients of rolling motion do not connect with rolling frequencies. $M(t, \theta)$ can be regarded as a series of impulse moments. The rolling history generated by $M(t, \theta)$ can be obtained by a convolution integral, i.e.

$$\theta(t) = \int_0^t M(t, \theta) h(t-\xi) d\xi \quad (4)$$

where

$h(t)$ -- the impulse response function of rolling motion_[2], it can be represented mathematically as the following form:

$$h(t) = \frac{1}{I_x \omega_0} e^{-\frac{k_1}{2} t} \sin(\omega_0 t) \quad (5)$$

where

$\omega_0 = \sqrt{Dr_1/I_x}$ -- the natural period of the rolling motion

Because $M(t, \theta)$ includes value θ which is a value to be solved, we use the previous value instead of the current value during computing process. Of course, the iteration can also be used.

3 Application Example

Based on above described procedure, a numerical example of vessel rolling in the course of hauling was given and the effects of hauling to safety of the fishing vessel were analyzed. The vessel considered here is a chinese VSY812 type fishing vessel and its principal particulars are

displacement (t) 356.760

length (m)	35.00
beam (m)	7.00
draught (m)	2.80
windage area (m ²)	143.90
machine power (h.p.)	600.00

Figure 2 shows a rolling history due to hauling in calm sea. It can be seen from that figure that the maximum roll angle appearing at about 18 s from the hauling beginning is about 9 deg. during hauling in calm water.

Figure 3 and Figure 4 show rolling histories under the wind speed of 15 m/s during hauling in seas. The wave height is 2.0 m for Figure 3 and 3.0 m for Figure 4. Each figure includes three cases of hauling, i.e., hauling in the direction of the windward side, hauling in the direction of the lee side and without hauling. It is clear from these figures that the maximum roll angle increase evidently due to hauling moments.

The variation of the maximum roll angle with the wave length and wave height are shown in Figure 5 and Figure 6. The roll histories in Figure 5 represents hauling in the direction of the windward side and ones in Figure 6 represents hauling in the direction of the lee side. These figures show again that the maximum roll angle is very sensitive to hauling moments and the direction of hauling. It may be dangerous if hauling operates in higher sea states.

4 Conclusion

Roll motions of a fishing vessel which is concurrently subjected to waves, winds and hauling moments have been discusses in which the strong nonlinearities were taken into consideration. Calculated results show that the roll response and safety of fishing vessels are significantly influenced by moments and the direction of hauling. It is reasonable that hauling moments are taken into account in investigation of the safety and stability for fishing vessels in operating conditions.

Acknowledgements

The research work presented in the paper has been supported by State Key Laboratory of Ocean Engineering, Shanghai Jiao Tong University in China. Their support and assistance is gratefully acknowledged.

REFERENCES

1. Full Scale Measurement of Fishing Gear Pull while Hauling Purse Seine of Fishing Vessels (IMO SLF/30), Submitted by China, 13 January 1984.
2. Feng T. C., Rolling Motion under Impulse Moments, The Ocean Engineering (Chinese), No.4, 1983.
3. Bradley K. King, A Fast Numerical Solver for Large Amplitude Ship Motions Simulations, Proceedings of STAB'90, 1990.

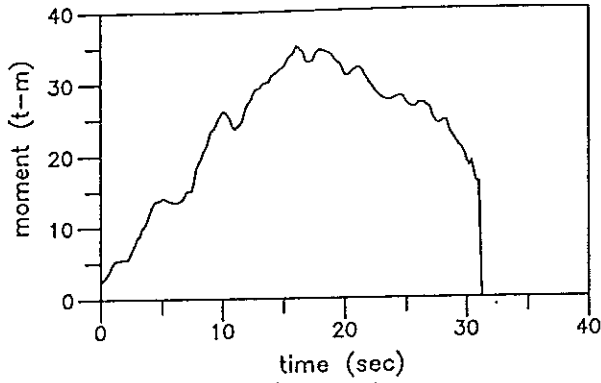


Figure 1
Hauling Moments

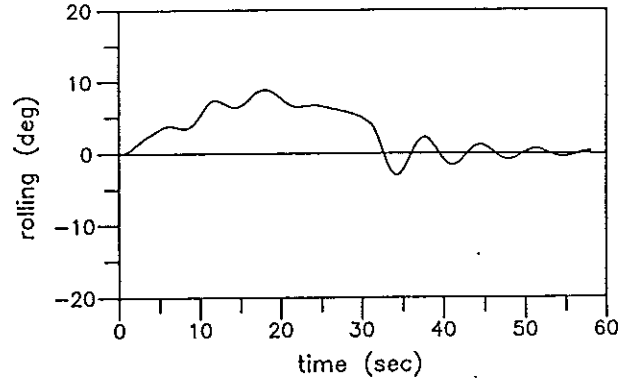


Figure 2
Rolling due to hauling

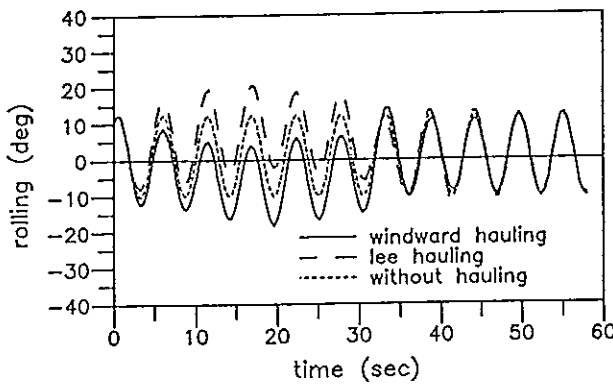


Figure 3
Rolling ($H=2.0$ m)

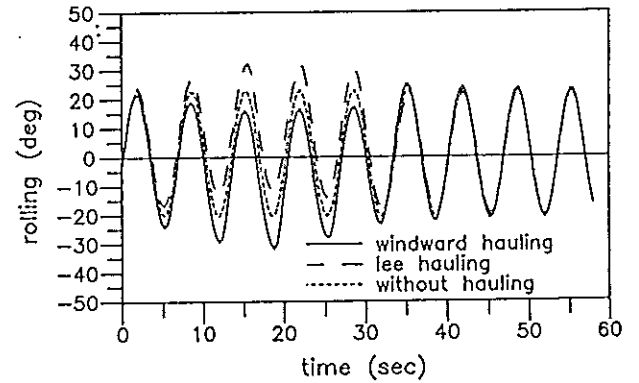


Figure 4
Rolling ($H=3.0$ m)

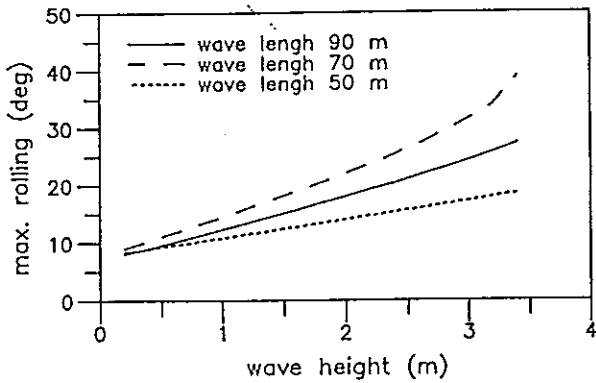


Figure 5
Rolling of Windward Hauling

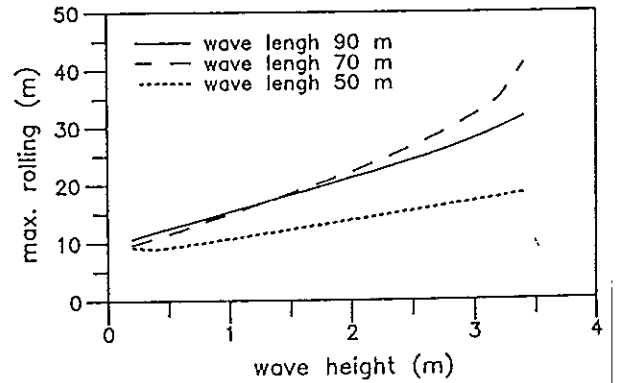


Figure 6
Rolling of Lee Hauling

Nonlinear Dynamics and Capsizing of Small Fishing Vessels

Changben Jiang * Armin W. Troesch † Steve W. Shaw ‡

June 14, 1994

Abstract

Designing ships which resist capsizing is the goal of ship stability analysis. Ship stability has long been analyzed using a highly approximate static approach. The static analysis solely considers the ship righting arm curve as compared to other "successful" vessels. Such an approach totally neglects the influence of external random wave excitation and vessel damping characteristics. For the work presented here, modern methods of dynamical systems analysis are used to evaluate the increased risk of capsize for small Native American fishing boats operating trap-nets in Native American Treaty-ceded waters on the Great Lakes. These trap-nets are being evaluated as replacements for the traditional gill-net.

In the analysis, geometric methods and Melnikov functions are extended to random excitation and applied to the study of large amplitude rolling motion leading to capsizing in real beam seas. With no restriction on the restoring force, the rolling motion is studied as a highly nonlinear dynamic problem. The probability of capsizing and the effect of trap-net induced mean heel angles are estimated by calculating the rate of phase flux. The theoretical results are supported by simulations using random excitation.

*Graduate Student, Dept. Naval Architecture and Marine Eng., Univ. of Michigan

†Assoc. Prof., Dept. of Naval Architecture and Marine Eng., Univ. of Michigan

‡Prof., Dept. of Mechanical Eng., Michigan State Univ.

1 Introduction

Native American Treaty-fishing on the Great Lakes has been a controversial subject in recent history. In order to resolve longstanding disputes, Tribal, State, and Federal governments, along with various sport fishing organizations, established the 1985 Consent Agreement. This agreement defined a mechanism for resolving disputes for a 15 year period while conserving and enhancing valuable fish stocks. One result of the agreement is the proposal to evaluate trap-net fishing as an alternative to the traditional Native American gill-net fishing method. The gill-net is allegedly indiscriminate in the fish it catches, and because of the basic design of the gill-net, fish are alleged to almost always be dead when extracted from the nets. The groups opposing gill-net fishing claim that the inadvertent harvest of Lake Trout is depleting a large sport fishery, a fishery specifically exempt from commercial fishing by the 1985 Consent Agreement. The trap-net, a more complex and expensive fishing system, is designed to hold fish alive until returned to the water, thus potentially preserving trout stocks.

There are significant operational differences between trap-netting and gill-netting. The trap-nets are taken in over the side, producing a steady heeling moment. Gill-nets are generally draped transversely across the deck, producing little change in the vessel's upright position. Nearly three-fourths of the Tribal boats engaged in net fishing are small, trailered boats of 16ft (5m) to 25ft (7.6m) in length. In these small vessels, the overturning moment of the trap-net line effects a large heel bias, and the trap-netting operation may present an additional safety hazard in rough weather.

In the following sections, the increased risk of a steady heeling bias, such as that experienced during trap-net operations in small fishing boats, will be examined. The effects of random waves, characteristic of those spectra found on the Great Lakes, will be included.

2 Background on Various Dynamic Stability Analyses

Existing stability criterion based solely on ship statics is not applicable to small boats which are the most likely to be lost in storms [1]. Large amplitude rolling motion which leads to capsizing is highly nonlinear and rich of complex dynamics. Understanding this nonlinear dynamic phenomenon on a fundamental level is the only way to improve stability standards. In the past fifteen years, many scholars have advanced methods dealing with nonlinear rolling. Most of the methods are perturbation related, based upon the assumption that the restoring force is weakly nonlinear [2,3,4,5]. This may be true when the ship rolls in the range far from capsizing but is certainly untrue when ship motion becomes dangerous. Simulation, which is not restricted to certain forms of the restoring force, has been used and combined with the concepts of safe basin and basin erosion for deterministic and stochastic forcing [6,7]. However, simulations, which are time consuming, are generally inconclusive unless exhaustive studies of the parameter space are performed and thus not suitable for establishing stability standards. If the excitation is random, the method proposed by Roberts [8,9] can handle highly nonlinear restoring forces, but still fails to give an realistic prediction for extreme motion.

Recently, in a series of papers *the global geometric method* employing Melnikov analysis has been used to study ship stability. Falzarano, Shaw and Troesch [10] applied the method to studying capsizing in regular sinusoidal waves. Global analysis techniques have also been applied to periodic and parametric forcing, with and without bias [11]. Hsieh, Troesch and Shaw [12] have successfully applied the Melnikov function method to an unbiased vessel in random beam waves. In a recent paper by Jiang, Troesch and Shaw [13], this method was extended to a biased vessel with arbitrary restoring force. The present paper will apply the same ideas and methods in investigating the stability of a small Great Lakes fishing boat, with and without bias, rolling in random seas.

3 Formulation of Single Degree of Freedom Roll Motion

We start with the linear two-degree of freedom equations involving roll and sway motion:

$$\begin{bmatrix} M_{22} + A_{22} & M_{24} + A_{24} \\ M_{42} + A_{42} & M_{44} + A_{44} \end{bmatrix} \begin{bmatrix} \ddot{y} \\ \ddot{\phi} \end{bmatrix} + \begin{bmatrix} B_{22} & B_{24} \\ B_{42} & B_{44} \end{bmatrix} \begin{bmatrix} \dot{y} \\ \dot{\phi} \end{bmatrix} + \begin{bmatrix} 0 & 0 \\ 0 & C_{44} \end{bmatrix} \begin{bmatrix} y \\ \phi \end{bmatrix} = \begin{bmatrix} F_2 \\ F_4 \end{bmatrix} \quad (1)$$

where y is the sway displacement and ϕ is the roll displacement; the A 's and B 's are added mass and damping coefficients which are calculated by a linear hydrodynamic program SHIPMO [14]. These two modes of motion can not be decoupled because of the damping. For undamped systems or proportionally damped systems, it is easily shown that the ship rolls about a roll center like a pendulum and roll motion can be decoupled from sway. If a pseudo roll center is assumed to exist when general damping is present, we then get a similar single degree of freedom roll equation including quadratic roll damping:

$$I_{44}\ddot{\phi} + B_{44}\dot{\phi} + B_{44q}\dot{\phi}|\dot{\phi}| + \Delta\overline{GZ} = F(t) \quad (2)$$

where

$$I_{44} = A_{44} + M_{44} + A_{42} R_c \quad (3)$$

$$R_c = -\frac{A_{42} + M_{42}}{A_{22} + M_{22}} \quad (4)$$

$$F(t) = F_4(t) + R_c F_2(t) \quad (5)$$

$$\overline{GZ} = C_0 + C_1\phi + C_3\phi^3 + C_5\phi^5 + \dots \quad (6)$$

R_c is the distance of the pseudo roll center above the center of gravity; \overline{GZ} is the restoring arm and Δ is the displacement of the vessel; ΔC_0 is a bias moment which could be caused by wind, shift of cargo, ice on deck or, for the application studied here, the pull of a fishing net; B_{44q} is quadratic damping coefficient and is estimated from empirical formulae [14]. Note that A_{44} , A_{42} , B_{44} and B_{44q} are all frequency dependent and a range of frequencies exists in random excitation. A reasonable frequency for these coefficients could be either the linear natural frequency or the frequency on which the

excitation energy is concentrated. Here we pick the later, since these small boats are generally quite stiff with a roll natural frequency higher than typical sea states.

The ship we are studying is a generic small Great Lakes boat, 16.5ft (5.03m) on the waterline, or 19.25ft (5.87m) in overall length. Figure 1 shows the body plans. Figure 2 shows the \overline{GZ} curves for two different conditions - with and without bias. The estimated line tension due to the trap-net is approximately 700lbs (3,114N) which will cause a 8.95° static heel angle. From the viewpoint of a static analysis, the vessel has sufficient reserve stability with a 4.67ft (1.42m) \overline{GM} . However, a risk assessment of the hull's dynamic performance, with and without the bias induced by the trap-net, is not possible by simply considering the \overline{GM} .

The sea state is considered as a stationary ergodic Gaussian process with an ISSC power spectrum density(psd) function:

$$S_{\zeta}^+(\omega) = 0.11 H_s^2 \frac{\omega_z^4}{\omega^5} \exp(-0.44(\frac{\omega_z}{\omega})^4) \quad (7)$$

where H_s and ω_z are the significant wave height and the characteristic wave frequency respectively. The power spectrum of the rolling moment $F(t)$ is related to $S_{\zeta}^+(\omega)$ in a linear hydrodynamic way:

$$S_f^+(\omega) = |F_{roll}(\omega)|^2 S_{\zeta}^+(\omega) \quad (8)$$

where $F_{roll}(\omega)$ is the moment amplitude per unit wave height at frequency ω and is determined by Equation (5) and the hydrodynamic program SHIPMO. The quadratic damping is due mainly to the hard chine. In order to compare with previously published results, we choose a cubic \overline{GZ} curve.

4 Melnikov Function and Phase Flux

The Melnikov function is a powerful method in nonlinear dynamics used to predict the onset of complex phenomenon like chaos and other qualitative changes in the dynamics. It is especially effective in ship stability analysis where the change from safe basin into capsizing is of paramount interest [10].

The rate of phase flux which is calculated from the Melnikov function can quantify how much of the safe basin is being transported out per unit time, both for deterministic excitation and for random excitation [12,13,15]. Ship capsizing probability, closely linked to the statistics of phase flux, will eventually be predictable by calculating the rate of phase flux. In this work, a rigorous relationship is not derived, but rather empirically determined by comparing theoretical phase flux results with simulation.

In order to apply the Melnikov function and calculate phase flux, Equation (2) is nondimensionalized as follows:

$$\ddot{x}(t) + \epsilon\delta_1\dot{x}(t) + \epsilon\delta_2\dot{x}(t)|\dot{x}(t)| + \delta_0 + x(t) - \alpha x^3(t) = \epsilon f(t) \quad (9)$$

where

$$\begin{aligned} x &\rightarrow \phi, & t &\rightarrow \omega_n t, \\ \omega_n &= \sqrt{\frac{C_1\Delta}{I_{44} + A_{44}}}, & \Omega &= \frac{\omega}{\omega_n}, \\ \delta_0 &= \frac{C_0}{C_1}, & \epsilon\delta_1 &= \frac{B_{44}\omega_n}{C_1\Delta}, & \epsilon\delta_2 &= \frac{B_{44q}}{I_{44} + A_{44}}, \\ \alpha &= \frac{-C_3}{C_1}, & \epsilon f(t) &= \frac{F(t)}{C_1\Delta} \end{aligned}$$

Note that time is scaled by ω_n for convenience; ω_n is the linear natural frequency; the terms indicated by ϵ are small terms and treated as perturbations in the derivation of Melnikov function. After nondimensionalizing, damping and excitation terms become small but the nonlinear restoring terms and the bias term do not [13]. Equation (9) is rewritten in Cauchy standard form:

$$\dot{x}(t) = y(t) \quad (10)$$

$$\dot{y}(t) = -\delta_0 - x(t) + \alpha x^3(t) + \epsilon(-\delta_1 y(t) - \delta_2 y(t)|y(t)| + f(t)) \quad (11)$$

The Melnikov function for the above system is defined as follows [16,17]:

$$M(t_0) = \int_{-\infty}^{\infty} y_h(t)[-\delta_1 y_h(t) - \delta_2 y_h(t)|y_h(t)| + f(t + t_0)]dt \quad (12)$$

where $y_h(t)$ is the ordinate of the homoclinic orbit parameterized by time t in the phase plane of the unperturbed system

$$\dot{x}(t) = y(t) \quad (13)$$

$$\dot{y}(t) = -\delta_0 - x(t) + \alpha x^3(t) \quad (14)$$

Except for $\delta_0 = 0$, it is difficult to find an analytic solution for the above equation but determining a numerical one is straightforward. We denote the homoclinic orbit as $(x_h(t), y_h(t))$. The region enclosed by the homoclinic orbit is called the safe basin because for systems with no forcing and no damping, any point inside this region will stay inside (i.e. remain upright) and any point outside will lead to capsizing. The area of safe basin can be readily integrated:

$$A_h = \int_{-\infty}^{\infty} y_h(t) dx_h(t) \quad (15)$$

It is clear from Equation (12) that the Melnikov function $M(t_0)$ consists of two parts, a constant part and an oscillatory part:

$$M(t_0) = \tilde{M}(t_0) - \bar{M} \quad (16)$$

where

$$\bar{M} = \delta_1 \int_{-\infty}^{\infty} y_h(t)^2 dt + \delta_2 \int_{-\infty}^{\infty} y_h(t)^2 |y_h(t)| dt \quad (17)$$

$$\tilde{M}(t_0) = \int_{-\infty}^{\infty} y_h(t) f(t + t_0) dt \quad (18)$$

As pointed out in [12,13,15], $\tilde{M}(t_0)$ is a linear transformation of the excitation with a time domain input-output relation shown in Equation (18). In the frequency domain, $\tilde{M}(t_0)$ and $f(t)$ are related through the power spectrum:

$$S_{\tilde{M}}^+(\Omega) = (2\pi)^2 |Y_h(\Omega)|^2 S_f^+(\Omega) \quad (19)$$

where $Y_h(\Omega)$ is the Fourier transform of $y_h(t)$ defined as:

$$Y_h(\Omega) = \frac{1}{2\pi} \int_{-\infty}^{\infty} y_h(t) e^{-i\Omega t} dt \quad (20)$$

Combining Equations (19) and (8), we get:

$$S_{\tilde{M}}^+(\Omega) = (2\pi)^2 |Y_h(\Omega)|^2 |F_{roll}(\Omega)|^2 S_{\zeta}^+(\Omega) \quad (21)$$

The wave elevation spectrum is defined as Equation (7) which, after rescaling, becomes:

$$S_{\zeta}^+(\Omega) = 0.11 H_s^2 \frac{\omega_z^4}{\Omega^5 \omega_n^5} \exp(-0.44 (\frac{\omega_z}{\Omega \omega_n})^4) \quad (22)$$

From the power spectrum, the Root Mean Square (RMS) of $\tilde{M}(t_0)$ is easily determined (see the Appendix)

$$\sigma_{\tilde{M}}^2 = \int_0^\infty (2\pi)^2 |Y_h(\Omega)|^2 |F_{roll}(\Omega)|^2 S_\zeta^+(\Omega) d\Omega \quad (23)$$

and the rate of phase flux can be derived (also see the Appendix)

$$\frac{\Phi}{A_h} = \frac{\epsilon}{A_h} [H_s \sigma_0 p_n\left(\frac{\tilde{M}}{H_s \sigma_0}\right) + \bar{M} P_n\left(\frac{\tilde{M}}{H_s \sigma_0}\right) - \bar{M}] \quad (24)$$

In the above, σ_0 is the RMS of $\tilde{M}(t_0)$ for unit significant wave height and is determined by Equation (23). $p_n(\cdot)$ and $P_n(\cdot)$ are the standard Gaussian probability density function and probability distribution function. ϵ is an indicator to show that $\frac{\Phi}{A_h}$ is small. It does not effect $\frac{\Phi}{A_h}$ since it is defined in the rescaling of σ_0 and \tilde{M} in the calculations.

5 Results and Discussions

The phase flux expressed by Equation (24) is evaluated numerically [13]. Figure 3 shows the change of $\frac{\Phi}{A_h}$ with excitation in both the unbiased condition and the biased condition (heel angle=8.95°). The exact quantitative relation between the rate of phase flux and the probability of capsizing is involved [13] and is the subject of future research. However, the Melnikov function tells us that phase flux implies capsizing, sooner or later. The larger the rate, the more probable capsizing becomes [12,13]. The wave height at which the rate of phase flux starts to increase rapidly is very dangerous for the vessel. From Figure 3, we observe that for the fishing boat in its normal condition this critical wave height is between 4ft (1.22m) and 5ft (1.52m). For the biased condition, representing the boat hauling in the trap-net, the critical wave height reduces to 2ft (0.61m) to 2.5ft (0.76m). Simulations with random excitation [12,13,20] were carried out to verify this estimation. The characteristic wave period T_z was chosen as 4.0 sec. Every simulation ran for 34.1 minutes or until the boat capsized. For each wave height, 499 realizations were generated and the probability of capsizing was determined. The result is plotted in Figure 4. For the normal operating condition (i.e. fishing

with a gill-net), the probability of capsizing at $H_s=4.0\text{ft}$ (1.22m) is 0.6% (3 out of 499) and reduces to zero (0 out of 499) at $H_s=2.0\text{ft}$ (0.61m). The rate of the normalized phase flux at 4.0ft (1.22m) is 0.0000111. Conversely, there is nearly 100% probability of capsizing when conducting trap-net operations in $H_s=4.0\text{ft}$ (1.22m) seas.

Applying the results of Equation (24) for varying wave height and period, Figure 5 shows how, by inferring capsizing from the rate of phase flux, the characteristic wave period influences vessel's stability. All of the wave heights in Figure 5 have the same rate of phase flux $\frac{\Phi}{A_h} = 0.000037$. Based upon simulation results, at $T_z = 4.0$, this rate of phase flux induces a probability of 7.8% and 6.4% for capsizing in normal and biased conditions, respectively. However, the wave height at which this occurs in the normal condition (i.e. gill-netting) is between 4ft (1.22m) and 5ft (1.52m) while in the biased condition (i.e. trap-netting) the wave height has been reduced to just over 2ft (0.61m).

The prediction by phase flux agrees well with simulation. Figure 6 shows the effect of bias on relative dynamic stability. The y -axis is the ratio of wave heights (H_{critic}) with the same rate of phase flux ($\frac{\Phi}{A_h} = 0.000037$) in biased conditions and unbiased conditions. The dotted line in Figure 6 is the ratio of asymptotic wave heights (H_s^*) for biased and unbiased condition. The asymptotic wave height is defined in [12] as

$$H_s^* = \frac{\sqrt{2\pi}\bar{M}}{2\sigma_0} \quad (25)$$

It is easy to see from Equation (24) that the rate of phase flux at H_s^* does not depend on characteristic wave period. Calculations also show that the rates of phase flux at H_s^* are roughly the same for biased and unbiased cases. The potential of phase flux in predicting capsizing is verified again by the fact that H_{critic} and H_s^* give the same qualitative information about the effect of bias (see Figure 6).

6 Conclusions

The ship roll equation is suitable for the application of Melnikov function and phase flux analysis without any restrictions placed on the \overline{GZ} curve or the magnitude of the rolling angles. The method can incorporate the irregularity or stochastic nature of the seaway. A ship's ability to resist capsizing can be investigated both in the unperturbed system (in terms of the safe basin) and in the perturbed system (in terms of phase flux). Phase flux is a measure of the area of safe basin being transported out. The rate of phase flux is an important statistical property of a ship. It has been shown to be closely related to capsizing and is a good candidate for assessing the risk of capsizing in given sea states.

Acknowledgment

This paper has been sponsored by the Michigan Sea Grant College Program, Project R/T-32, under grant number NA89AA-D-SG083 Amd#5 from the Office of Sea Grant, National Oceanic and Atmospheric Administration (NOAA), US Department of Commerce, and funds from the State of Michigan. The government is authorized to produce and distribute reprints for government purpose notwithstanding any copyright notation appearing herein. We would also like to acknowledge partial support from National Science Foundation.

References

- [1] Hutchison, Bruce L., 'Seakeeping Studies: A Status Report', *SNAME transactions*, Vol.98, 1990, pp.263-317
- [2] Cardo, A., Francescutto, A. and Nabergoj, R., 'Ultraharmonics and Subharmonics in the Rolling motion of a Ship: Steady-State Solution', *International Shipbuilding Progress*, Vol.28, No.326, 1981
- [3] Cardo, A., Francescutto, A. and Nabergoj, R., 'Subharmonics Oscillation in Nonlinear Rolling', *Ocean Engineering*, Vol.11,663, 1984

- [4] Nayfeh, A.H. and Khdeir, A.A., 'Nonlinear Rolling of Ships in Regular Beams Seas', *International Shipbuilding Progress*, Vol.33, No.379, 1986, pp.40-49
- [5] Nayfeh, A.H. and Khdeir, A.A., 'Nonlinear Rolling of Biased Ships in Regular Beams Waves', *International Shipbuilding Progress*, Vol.33, No.381, 1986, pp.84-93
- [6] Thompson, J.M.T., 'Transient Basins: A New Tool for designing Ships Against Capsize', *Proc. IUTAM Symposium on the Dynamics of Marine Vehicles and Structures in Waves*, London, June 1990, pp.325-331
- [7] Soliman, M.S., Thompson, J.M.T., 'Stochastic Penetration of Smooth and Fractal Basin Boundaries Under Noise Extation', *Dynamics and Stability of Systems*, Vol.5, No.4, 1990.
- [8] Roberts, J.B., 'A Stochastic Theory for Nonlinear Ship Rolling in Irregular Seas', *Journal of Ship Research*, Vol.26, No.4, Dec. 1982, pp.229-24
- [9] Roberts, J.B., 'Roll Motion of a Ship in Random Beam Waves: Comparison Between Theory and Experiment', *Journal of Ship Research*, Vol.29, No.2, Dec. 1985, pp.112-126 *Proc. IUTAM Symposium on the Dynamics of Marine Vehicles and Structures in Waves*, London, June 1990, pp.325-331
- [10] Falzarano, J.M., Shaw, S.W. and Troesch, A.W., 'Application of Global Methods for Analyzing Dynamical Systems to Ship Rolling Motion and Capsizing', *International Journal of Bifurcation and Chaos*, Vol.2, No.1(1992), pp.101-115
- [11] Esparza, I. and Falzarano, J., 'Nonlinear Rolling Motion of a Statically Biased Ship under the Effect of External and Parametric Excitation', *The 14th ASME Vibration Conference*, Sept., 1993
- [12] Hsieh, S.R., Troesch, A.W. and Shaw, S.W., 'A Nonlinear Probabilistic Method for Predicting Vessel Capsizing in Random Seas', *Proc. of the Royal Soccity*, London, Vol. 446, 1994.

- [13] Jiang, C., Troesch, A.W. and Shaw, S.W., 'Highly Nonlinear Rolling Motion Of Biased Ship in Random Seas', submitted to *Journal of Ship Research*, June, 1994
- [14] Beck, F.B. and Troesch, A.W., *Documentation and User's Manual for the Computer Program SHIPMO*, Department of Naval Architecture and Marine Engineering, The University of Michigan, 1990
- [15] Frey, M. and Simiu, E., 'Noise-Induced Chaos and Phase Space Flux', *Physica D 63*, pp.312-340
- [16] Guckenheimer, John and Holmes, Philip, *Nonlinear Oscillations, Dynamical Systems, and Bifurcations of Vector Fields*, Springer-Verlag: New York, Berlin, Heidelberg, Tokyo, 1983
- [17] Wiggins, S., *Introduction to Applied Nonlinear Dynamical Systems and Chaos*, Springer-Verlag: New York, 1990
- [18] Wiggins, S., *Chaotic Transport in Dynamical Systems*, Springer-Verlag: New York, Heidelberg, 1992
- [19] Soong, T.T. and Grigoriu, M., *Random Vibration of Mechanical and Structural Systems*, PTR Prentice Hall: Englewood Cliffs, New Jersey
- [20] Cuong, H.T., Troesch, A.W. and Birdsall, T.G., 'The Generation of Digital Random Time Histories', *Ocean Engineering*, Vol.9, No.6, 1982, pp.581-588

Appendix The Derivation of Phase Flux

To calculate phase flux, the statistics of the oscillatory part $\tilde{M}(t_0)$ of Melnikov function must be determined first. It is obvious that $\tilde{M}(t_0)$ is stationary and Gaussian since the excitation $f(t)$ is stationary and Gaussian. A Gaussian random process is fully defined by its mean and variance. The mean value of $\tilde{M}(t_0)$ is simply

$$E[\tilde{M}(t_0)] = E\left[\int_{-\infty}^{\infty} y_h(t)f(t+t_0)dt\right]$$

$$\begin{aligned}
&= \int_{-\infty}^{\infty} y_h(t) E[f(t + t_0)] dt \\
&= 0
\end{aligned}$$

since $E[f(t + t_0)] = 0$. The Root Mean Square (RMS) value becomes:

$$\begin{aligned}
\sigma_{\tilde{M}}^2 &= E[\tilde{M}^2(t_0)] - (E[\tilde{M}(t_0)])^2 = \int_0^{\infty} S_{\tilde{M}}^+(\Omega) d\Omega \\
&= \int_0^{\infty} (2\pi)^2 |Y_h(\Omega)|^2 |F_{roll}(\Omega)|^2 S_{\zeta}^+(\Omega) d\Omega
\end{aligned}$$

The average rate of phase flux can be calculated through the Melnikov function as follows [15,18]:

$$\begin{aligned}
\Phi &= \lim_{T \rightarrow \infty} \frac{\epsilon}{2T} \int_{-T}^T M^+(t_0) dt_0 \\
&= \lim_{T \rightarrow \infty} \frac{\epsilon}{2T} \int_{-T}^T (\tilde{M}(t_0) - \bar{M})^+ dt_0
\end{aligned} \tag{26}$$

where $M^+(t_0)$ denotes the positive part of the Melnikov function. The ergodicity of $\tilde{M}(t_0)$ enables the time average in Equation (26) to be evaluated by its ensemble average [19], then

$$\Phi = \epsilon E[(\tilde{M}(t_0) - \bar{M})^+] = \epsilon \int_{\bar{M}}^{\infty} (z - \bar{M}) p(z) dz \tag{27}$$

where z is a Gaussian random variable representing the Gaussian random process $\tilde{M}(t_0)$, with mean 0, variance $\sigma_{\tilde{M}}^2$ and probability density function

$$p(z) = \frac{1}{\sqrt{2\pi}\sigma_{\tilde{M}}} \exp\left(-\frac{z^2}{2\sigma_{\tilde{M}}^2}\right) \tag{28}$$

The expression of phase flux can further be simplified by introducing the standard Gaussian probability density function $p_n(z)$ and probability distribution function $P_n(z)$:

$$p_n(z) = \frac{1}{\sqrt{2\pi}} \exp\left(-\frac{z^2}{2}\right) \tag{29}$$

$$P_n(z) = \int_{-\infty}^z p_n(x) dx \tag{30}$$

and Equation (27) is then written as

$$\begin{aligned}
\Phi &= \epsilon \int_{\bar{M}}^{\infty} (z - \bar{M}) \frac{1}{\sqrt{2\pi}\sigma_{\tilde{M}}} \exp\left(-\frac{z^2}{2\sigma_{\tilde{M}}^2}\right) dz \\
&= \epsilon \sigma_{\tilde{M}} \int_{\bar{M}/\sigma_{\tilde{M}}}^{\infty} \frac{1}{\sqrt{2\pi}} \left(x - \frac{\bar{M}}{\sigma_{\tilde{M}}}\right) \exp\left(-\frac{x^2}{2}\right) dx \\
&= \epsilon \left[\sigma_{\tilde{M}} p_n\left(\frac{\bar{M}}{\sigma_{\tilde{M}}}\right) + \bar{M} P_n\left(\frac{\bar{M}}{\sigma_{\tilde{M}}}\right) - \bar{M} \right]
\end{aligned} \tag{31}$$

Because of their linear relationship, the RMS of $\tilde{M}(t_0)$ is proportional to the significant wave height. If we denote σ_0 as the RMS of $\tilde{M}(t_0)$ for unit significant wave height, the rate of phase flux, nondimensionalized by A_h , is

$$\frac{\Phi}{A_h} = \frac{\epsilon}{A_h} \left[H_s \sigma_0 p_n \left(\frac{\tilde{M}}{H_s \sigma_0} \right) + \tilde{M} P_n \left(\frac{\tilde{M}}{H_s \sigma_0} \right) - \tilde{M} \right] \quad (32)$$

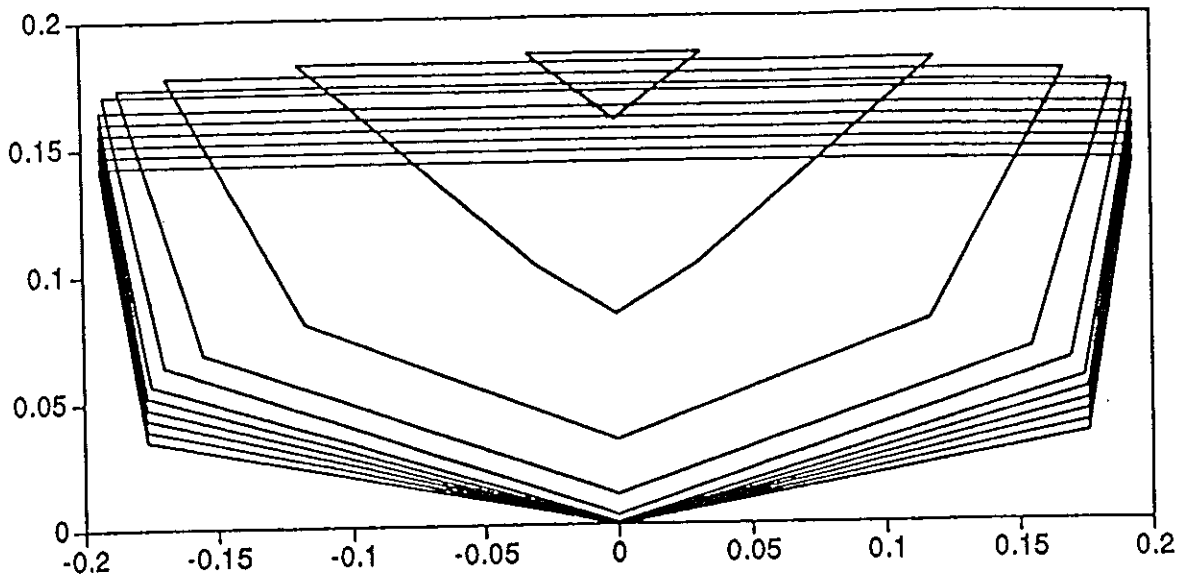


Figure 1 Body plan (nondimensionalized by length, ten equally spaced stations)

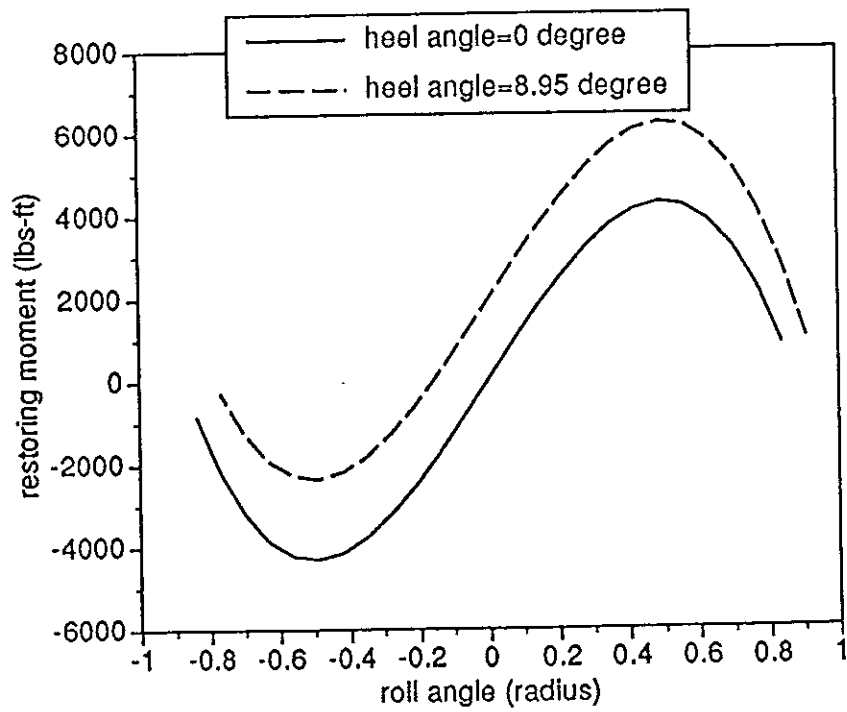


Figure 2 Restoring arm curves

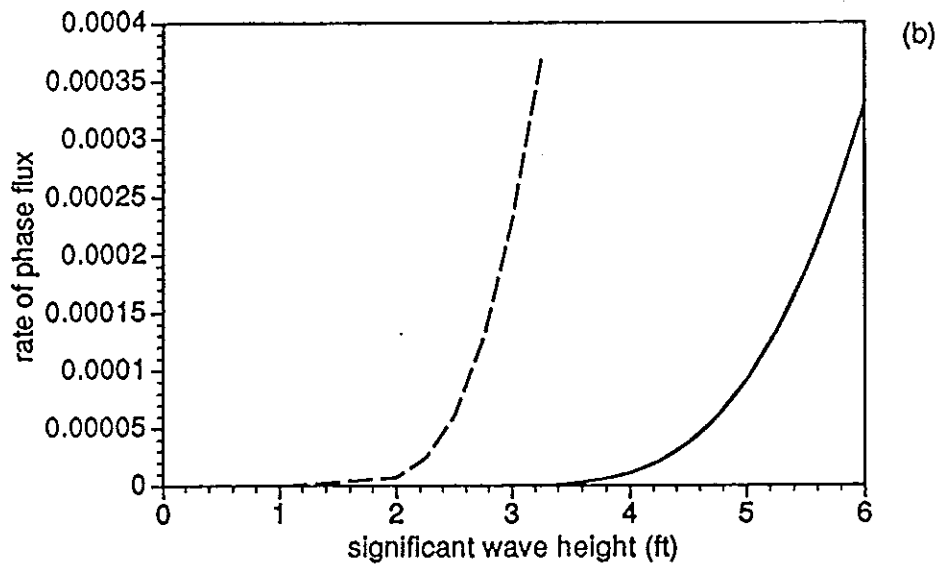
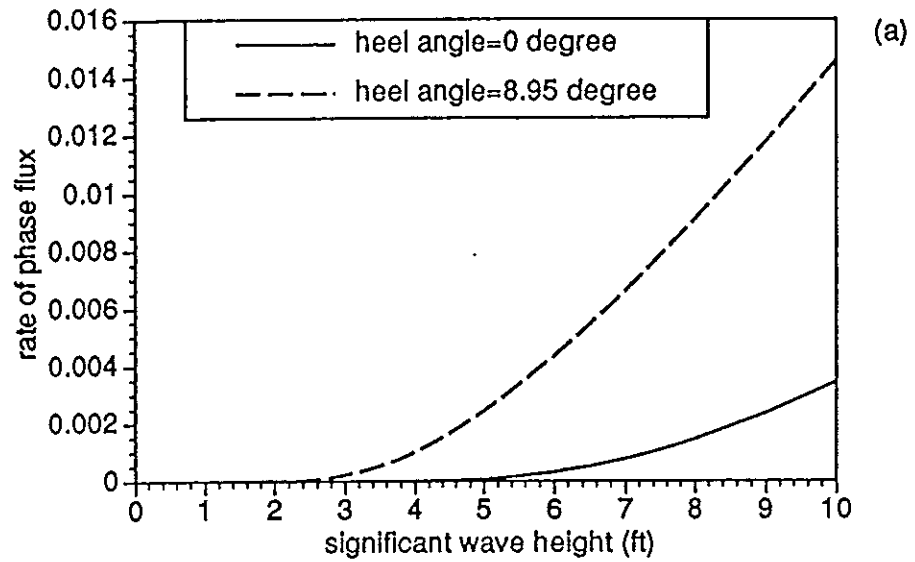


Figure 3 Rate of phase flux at wave period = 4.0 sec. for zero and 8.95 degree heel angle
 (a) Rate of phase flux for a large range of significant wave height
 (b) Expanded view of (a)

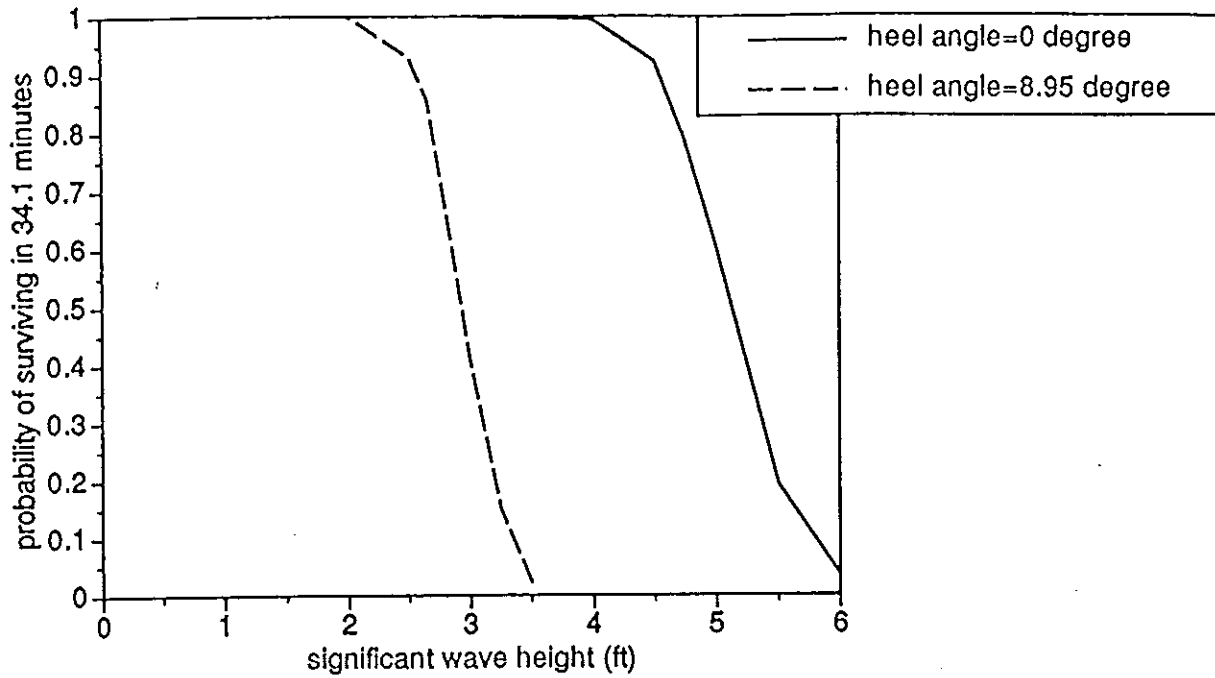


Figure 4 Simulation results. Probability of Survival in 34.1 minutes exposure vs. significant wave height

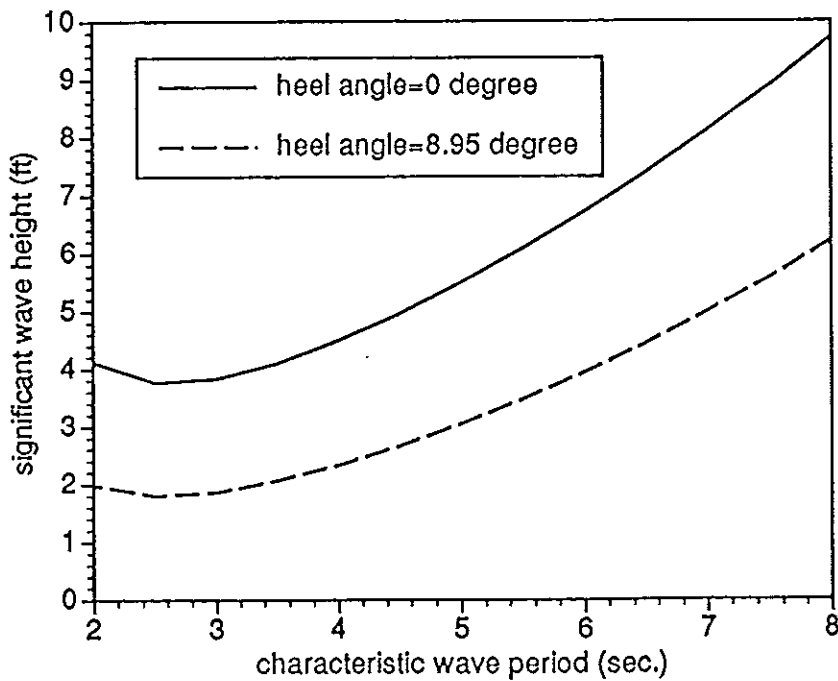


Figure 5 significant wave height vs. wave period at rate of phase flux = 0.000037, the level associated with 5%-8% probability of capsizing

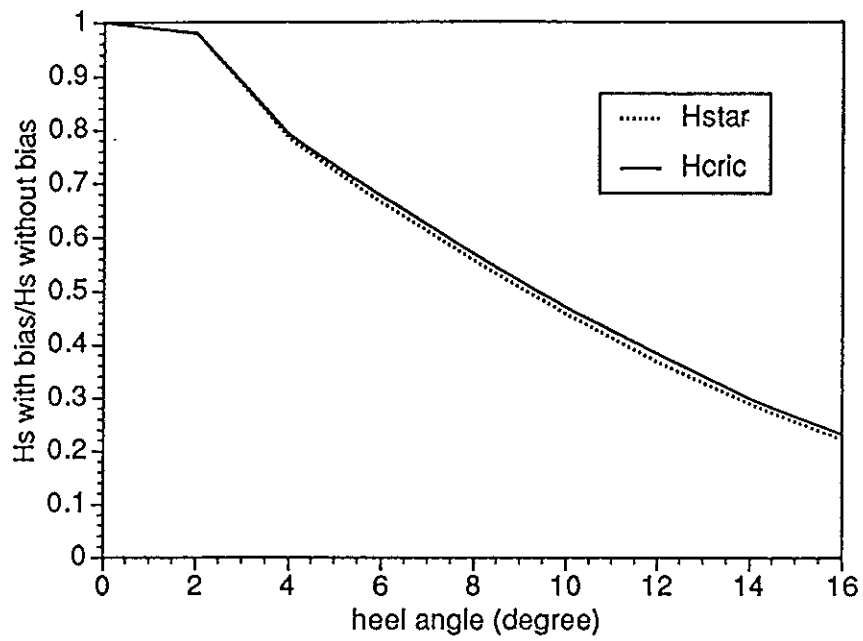


Figure 6 The reduction of significant wave height associated with capsize due to increasing heel angle. Results based on theoretical phase flux concepts.

On the Practical Evaluation of Shallow Water Effect in Large Inclinations for Small Fishing Boats.

Kiyoshi AMAGAI, Nobuo KIMURA and Kimihiko UENO

Abstract

This paper describes the classification of characteristic behavior of shallow water on a ship's deck, based on model tests using an oscillatory rectangular tank physically simulated with sinusoidal motion.

From the viewpoint of transverse stability in small fishing boats, the authors paid attention to two types of complicated behavior, which appeared at near the first and second resonant periods between the shallow water and the ship. These phenomena in large inclinations were simulated by using the Marker-and-Cell(MAC) method and Solution Algorithm for Transient Fluid Flow(SOLA) in order to obtain an equation for the motion of shallow water.

Furthermore, tank tests using a general model of small fishing boats were carried out with shallow water on the deck in beam wave. From the results of rolling motion and transverse force of shallow water, shallow water effect on transverse stability was evaluated practically.

1. Introduction

Small fishing boats in JAPAN have high bulwarks and small-scale scuppers or freeing ports generally. In ordinary circumstances of cruising or fishing operation, these fishing boat structures are useful for an increase in transverse stability. However, when there is shipping water on deck, sea water stays on deck for a long time due to the difficult in expelling the sea water from the freeing ports. For seakeeping qualities of small fishing boats, it's important to estimate correctly the shallow water effect in large inclinations, especially in resonant.

A large number of experimental or numerical studies have been reported about the motion of shallow water on deck. Some of them dealt with the motion of shallow water in an oscillating model tank which simulated physically the motion

of water on deck. But, little has been reported about the characteristics of shallow water when the oscillation period is the first or second resonant period between the water and ship, at a large amplitude rolling motion. Also little attention has been given to the consideration of viscosity when very shallow water is moving across the bottom of the tank at a high velocity.

From the viewpoint of the stability of small fishing boats, the characteristic behaviors of shallow water using an oscillating tank were classified into five categories. Two types of complicated behavior are worthy of attention. In these two behaviors, the movement of the center of gravity could not be estimated by using the conventional static method. Therefore, taking into consideration the above mentioned problem, numerical calculations using the MAC method and SOLA were tried and it was found that they could simulate the behaviors of shallow water.

To clarify rolling motion due to the behavior of shallow water, tank tests were performed by using a ship model i.e. a 19.9GT fishing boat for salmon in beam sea, at near the resonant period. From the experimental results of roll damping and rolling response function, the shallow water effect on transverse stability was evaluated practically.

2 Experiment

2-1 The behavior of shallow water

2-1-1 Experimental method

The rolling system used in the experiment was designed and built by Hiranuama[1] referenced Adee[2]. It consists of a driven mechanism provided with a sinusoidal oscillation to a tank and is as shown in Fig.1. A variable speed A.C. motor was connected to Scotch-Yoke through arm 1 and arm 2, and the Scotch-Yoke ensured sinusoidal motion.

The dimension of the tank used in the experiment was length:10cm, width:50cm, and depth:20cm, respectively. Each combination of the maximum inclining angle of rolling (5.0, 10.0, 15.0, and 20.0 degrees) and water depth (1.0, 2.0, 4.0, and 6.0 cm) were tested in the oscillation period range from 1.1sec to 4.0sec.

2-1-2 Classification of the behavior of shallow water

From the viewpoint of stability, we classified the behavior of the shallow water into five categories (a)~(e) as follows;

(a) The shape of the free surface was kept approximately horizontal[3], and behaved as a standing wave.

(b) As a whole, the behavior of the free surface looked like type (a)'s. However, there were some transient waves resembling bumps on the free surface.

(c) A transient wave arose on the free surface. But at the time when the angle of inclination was maximum, the shape of the free surface was horizontal and as a whole the behavior of the free surface looked like type (a)'s.

(d) A transient wave arose, and the free surface remained nonlinear in shape.

(e) There were two transient waves which proceeded in opposite directions.

Where, we defined the term "transient wave" to refer to a wave which proceeded with its medium, e.g., bore etc.

The classification of characteristic behavior of the shallow water is as shown in Fig.2 (a)-(e).

The authors took notice of the two types of complicated behaviors, (d) and (e), and realized that the movement of the center of gravity could not be estimated using the old static method for transverse stability which assumes that the shape of the free surface is horizontal. Therefore, a numerical simulation became necessary to grasp the shape for these cases. Type (d) appeared close to the first resonant period, and type (e) appeared close to the second resonant period.

2-1-3 The relation between oscillation period and behavior of shallow water

The relation between oscillation frequency and shallow water waves in an oscillating tank has been studied by Yoshioka et al[4]. According to the index S based on the nonlinear theory (refer to Appendix 1), shallow water waves become bore in the domain of $|s| < 1$.

Fig.3 shows the relation between frequency of tank and behavior of shallow water according to this theory[5]. In this figure, $\omega-11$ is the limit frequency that indicates the change from standing wave to bore near the first resonant (in this case $s=-1$), and $\omega+11$ is the limit frequency that indicates the change from bore to standing wave near the second resonant (in this case $s=1$). In this report, the frequency domain that transient wave arises corresponded to the frequency domain that bore arises in Yoshioka's nonlinear theory, and tried to apply this theory for the experimental results. Little is known about the application of this theory to cases where oscillation amplitude is more than 10 degrees.

In cases that oscillation amplitude was larger than 10 degrees, $\omega-11$ indicated the change from standing wave to bore in our experiment. Typical results are as shown in Fig.4(a)-(b). According to this theory, standing wave arose again close to the second resonant frequency. However, in the case shown in Fig.4(b), the domain $|s| < 1$ included the second resonant frequency $2\omega_0$. In other words, $\omega+11$ is larger than $2\omega_0$. Therefore, the application of this theory to this case is impossible. In this case, it was observed that the shallow water wave didn't become a standing wave, and two transient waves proceeded in opposite directions in close to the second resonant frequency (a type (e) wave as defined previously). However, $\omega+11$ is considered to be an important indicator, because $\omega+11$ can indicate the change from type (d) to type (e).

2-1-4 Numerical analysis[6]

As mentioned above, type (d) and (e) showed complicated behavior. Therefore, a numerical simulation became necessary to grasp these behaviors and we tried calculations using the MAC method and SOLA[7-8]. Assuming that the water in the tank is incompressible and viscous, the equations of motion for water in the tank are the Navier-Stokes equations and the mass continuity equation referred to in the Appendix.

Fig.5 shows a comparison of the numerical results with the experimental results in a typical case of type (d) shown in Fig.2(d). In type (d), we sometime observed a phenomenon where a transient wave collided against a side wall of the

tank and just after rolled and collided against the bottom wall of the tank again. Numerical results could grasp this phenomenon.

Numerical and experimental results for type (e) were also in good agreement (see Fig.2(e) and Fig.6). In the case of type (e), the authors observed that two transient waves proceeded in opposite directions. The position where two transient waves collided and the shape of the free surface could be simulated .

2-2 Shallow shipping water effect on ship rolling motion

2-2-1 Tank test

A 2m long ship model of a 19.9GT fishing boat for salmon, reduced in scale by 1/7.6, was used in the experiment. The principal particulars of the model and its body plan are as shown in Table 1 and Fig.7, respectively. The 19.9GT fishing boat is a typical ship form of a small fishing boat in Hokkaido, JAPAN, It has a high bulwark and small scale freeing ports. Loading conditions of the model ship was set to simulate actual full load conditions at the fishing ground. In the state with all free in six degrees of freedom, the model experiments of free roll decay and forced roll motion in regular beam sea were carried out in the experimental towing tank of the Faculty of Fisheries, Hokkaido University. The dimension of the towing tank are length:50m, width:3.5m, and depth of water:1.3m, respectively. Wave conditions used in the experiment are as shown in Table 2. To evaluate the shipping water effect on ship rolling motion, the same tank that was used to experiment using the Scotch-Yoke system was set on the upper deck of the ship model. The width of the tank corresponded to the model ship's breadth and the length corresponded to 1/8 the length of the upper deck, respectively. Considering the bulwark height, water depth on deck was set at in the range of 0.0cm to 4.0cm.

2-2-2 Results of tank test

Fig.8(a)-(e) show the response characteristics of rolling motion on the waves.

Fig.8(a) shows the response function without water. The

response function on small waves is approximately similar to the estimated value by O.S.M (Ordinary Strip Method) in the range of frequency that is more than the natural frequency. Wave size was classified based on the wave slope in Table 2. However, on large waves, the response function at natural frequency is smaller than that on small waves. Although it gives a good effect on ship stability at first sight, there is the danger that the freeing port sinks underwater and shipping water flows into the upper deck from the freeing ports. It was estimated that the overhang of the upper deck had the effect of damping. Generally, the higher the shallow water depth gets, the less the response function of rolling motion becomes. There is little difference in the response function according to wave slope.

Fig.9(a)-(c) shows the typical examples of the relationship between the damping rate of roll angle and water depth in the tank. ϕ_0 is the average amplitude of ship rolling motion without water and ϕ_h is that with water. Therefore, the damping effect on ship rolling motion can be recognized in the case of $\phi_h/\phi_0 < 1$. In Fig.9(a), the damping effect was recognized in all of water depths. This effect of shallow water shows results approximately similar to that of Dillingham [9]. However, this is a characteristic result which was obtained in this study. The closer the rolling frequency of ship gets to the second resonant frequency $2\omega_0$, the less the damping effect on ship rolling motion becomes. In the case where rolling frequency is higher than the second resonant frequency $2\omega_0$, it is sometimes observed that shallow water doesn't act as a damping effect. An example of this case is shown in the case where water depth is 1.0cm, and wave period is 1.3sec, in Fig.9(b). The pattern of behavior in this case is type (e), and that of other behaviors are type (d). Another example is shown where the water depth is 4.0cm, and wave period is 2.2sec, in Fig.9(c), and the pattern of that is type (c). In the experiment, as the behavior of the shallow water is type (d), the damping effect on ship rolling motion was recognized.

4. CONCLUSION

In the above, the authors verified the shallow water effect on ship rolling motion experimentally.

The main points of this study can be summarized as follows:

(1) The damping effect on rolling motion was recognized in the case where the natural frequency ω_0 (first resonant frequency) of shipping water was close to the rolling frequency of the ship.

(2) In the case where the rolling frequency of the ship is near the second resonant frequency $2\omega_0$ of the shipping water, the shallow water sometimes didn't act as a damping effect on rolling motion.

(3) The pattern of behavior of the shallow water on deck is an indicator of the damping effect on rolling motion.

Acknowledgments

The authors would like to thank Mr.A.Yamagishi for help and advice.

References

1. H. Hiranuma et al; An Investigation into the Action of Free Water in Tanks, Bull. of the Faculty of Fisheries, Hokkaido University, 43(1),42-58,1992.
2. B.H.Adee and I.Caglayan; The effects of free on deck on the motions and stability of vessel, Stability'82, 413-426,1982.
3. Alan.F.Jones and A.Hulme; The Hydrodynamics of Water on Deck, Journal of Ship Research, 31(2),125-135,1987.
4. I.Yoshioka et al; On the Shallow Waters in an Oscillating Tank Part 1-3,Journal of the Society of Naval Architects of Japan,123,96-109,1968,128,167-177,1970,129,55-65,1971.
5. T.Morita and K.Shoji; On the Behavior of the Tank Water in Rolling of Ship - I;The Journal of Japan Institute of Navigation, 78,121-128,1988.
6. K.Ueno et al; Experimental and Numerical Studies on the Behavior of Shallow Water in a Large Amplitude Oscillating Tank, The Journal of Japan Institute of Navigation, 90,201-213,1994.
- 7 C.W.Hirt, B.D.Nichols and N.C.Romeo; SOLA-A Numerical

Solution Algorithm for Transient Fluid Flows, Los Alamos Scientific Laboratory Report La-5852, 1975.

8 Francis H. Harlow and J. Eddie Welch; Numerical Calculation of Time-Dependent Viscous Incompressible Flow of Fluid with Free Surface, THE PHYSICS OF FLUID, 8(12), 2182-2189, 1965.

9. J. Dillingham; Motion Studies of a Vessel with Water on Deck, Marine Technology, 18(1), 38-50, 1981.

Appendix

Frequency in relation to wave pattern

$$C_0 = \sqrt{gh} \quad \dots (1)$$

$$\omega_0 = (\pi/B) \cdot \sqrt{gh} \quad \dots (2)$$

$$\varepsilon = \sqrt{(H\omega^2 + g)\phi_0} / (C_0\omega) \quad \dots (3)$$

$$s = \frac{\pi^2 C_0 (\omega - n\omega_0)}{3B\varepsilon\omega_0\omega} \cdot \sqrt{3B / 8C_0} \quad \dots (4)$$

where, C_0 : velocity of shallow water, h : water depth, ω_0 : natural frequency of shallow water, B : breadth of tank, H : distance from center of rotation to surface of still water in tank, ϕ_0 : rolling angle, n : natural number.

Equations of motion for water in tank

The Navier-Stokes equations:

$$\frac{\partial u}{\partial t} + u \frac{\partial u}{\partial x} + v \frac{\partial u}{\partial y} = - \frac{\partial p}{\partial x} + \nu \left(\frac{\partial^2 u}{\partial x^2} + \frac{\partial^2 u}{\partial y^2} \right) + f_x \quad \dots (5)$$

$$\frac{\partial v}{\partial t} + u \frac{\partial v}{\partial x} + v \frac{\partial v}{\partial y} = - \frac{\partial p}{\partial y} + \nu \left(\frac{\partial^2 v}{\partial x^2} + \frac{\partial^2 v}{\partial y^2} \right) + f_y \quad \dots (6)$$

the mass continuity equation

$$\frac{\partial u}{\partial x} + \frac{\partial v}{\partial y} = 0 \quad \dots (7)$$

where u and v are velocity component in coordinate direction (x, y) respectively, p is the ratio of pressure to constant density, f_x and f_y are body accelerations in coordinate direction (x, y) respectively, and ν is the

kinematic viscosity coefficient which is constant[5].

Expressing the roll angle ϕ as

$$\phi = \phi_0 \cos (\omega t + \varepsilon) \quad \dots(8)$$

where ϕ_0 is the oscillation amplitude [deg], ω is the oscillation angular frequency, and ε is the initial phase then f_x and f_y can be written as

$$f_x = -g \sin \phi + x\ddot{\phi} + y\dot{\phi} + 2v\dot{\phi} \quad \dots(9)$$

$$f_y = -g \cos \phi + y\ddot{\phi} - x\dot{\phi} - 2u\dot{\phi} \quad \dots(10)$$

Table.1 The principal particulars

	Model	Full
Lpp (m)	2.000	15.20
B (m)	0.500	3.80
D (m)	0.195	1.48
Disp. (ton)	0.137	59.80
df (m)	0.109	0.827
da (m)	0.242	1.838
dm (m)	0.175	1.332
TRIM (m)	0.133	1.011
GM (m)	0.058	0.443
KG (m)	0.205	1.561
OG (m)	0.174	1.320

Table.2 Wave condition

$\sqrt{L/\lambda}$	$\kappa \zeta a$		
	SMALL	LARGE	EXTRA LARGE
0.52	0.02	0.03	0.04
0.64	0.04	0.06	0.11
0.70	0.03	0.08	0.13
0.77	0.05	0.10	0.17
0.83	0.06	0.11	0.21
0.89	0.07	0.15	
1.02	0.10	0.14	0.26
1.14	0.07	0.17	
1.26	0.16	0.31	

*EXTRA LARGE were only used when depth of water is 3cm.

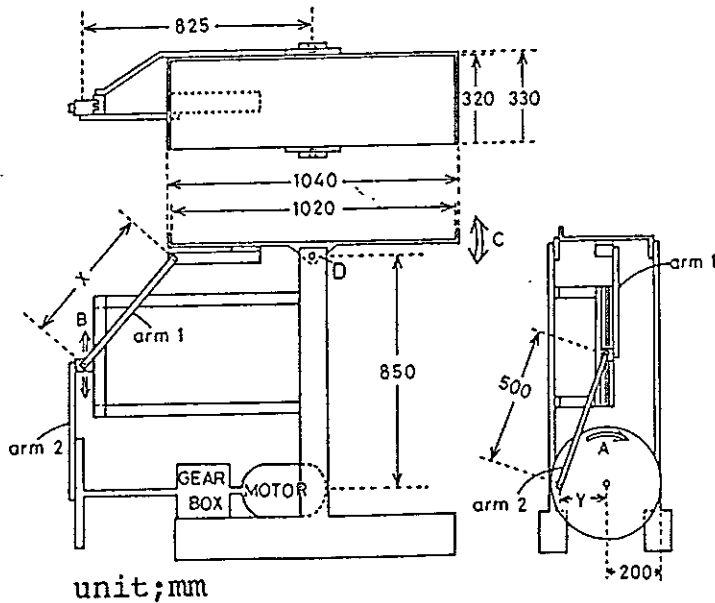


Fig.1 Apparatus

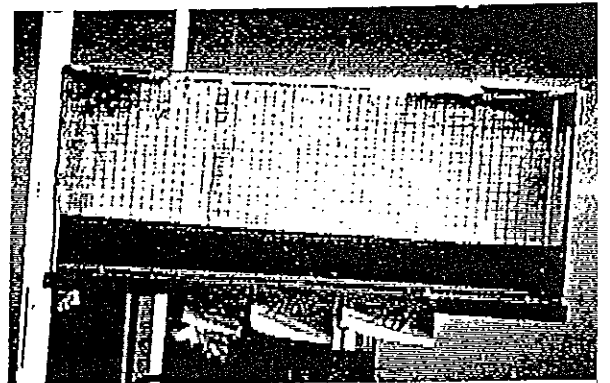
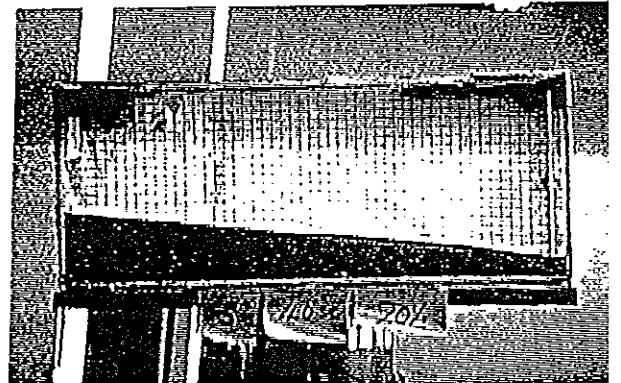
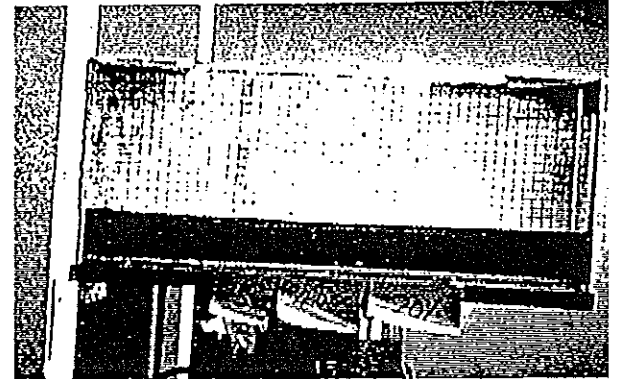
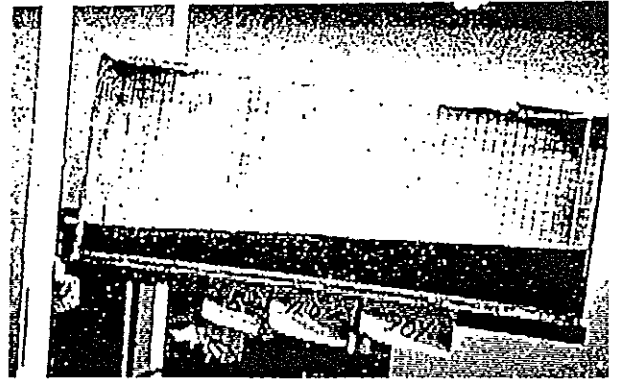


Fig.2(a) The behavior of shallow water, type (a)

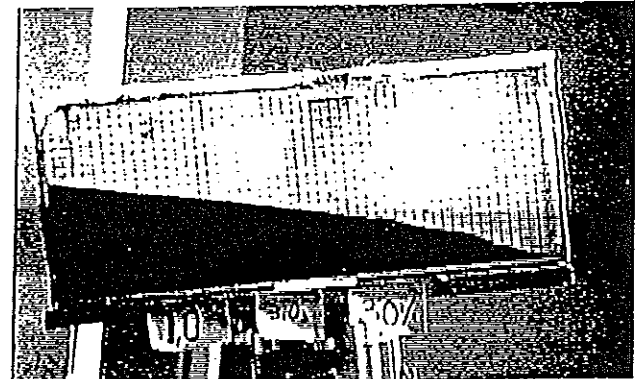
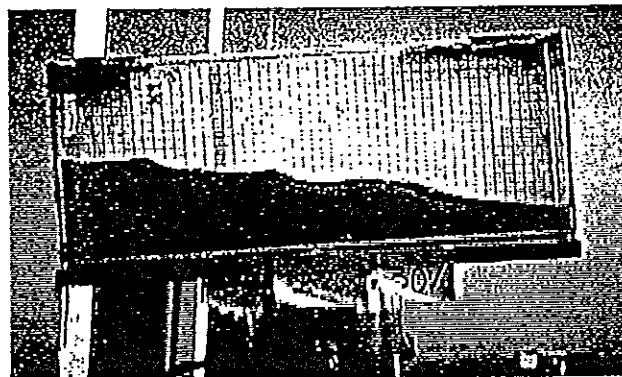
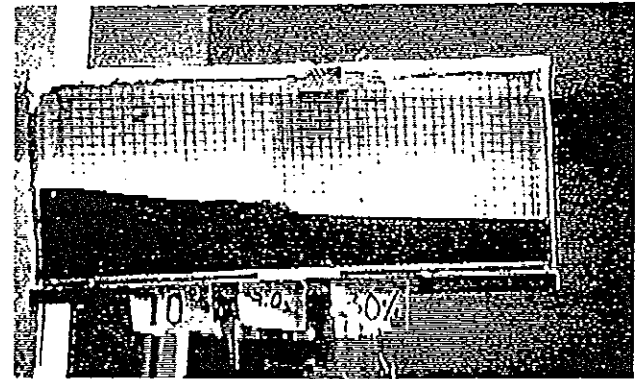
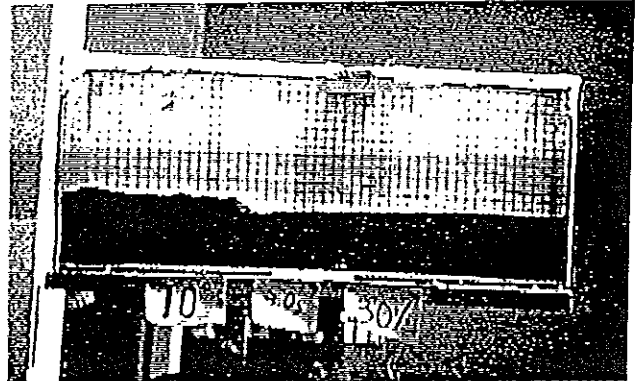
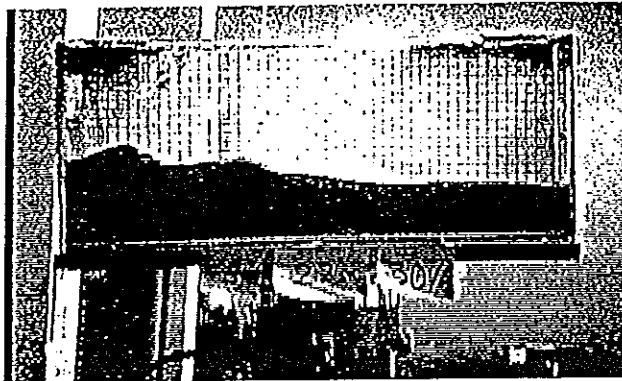
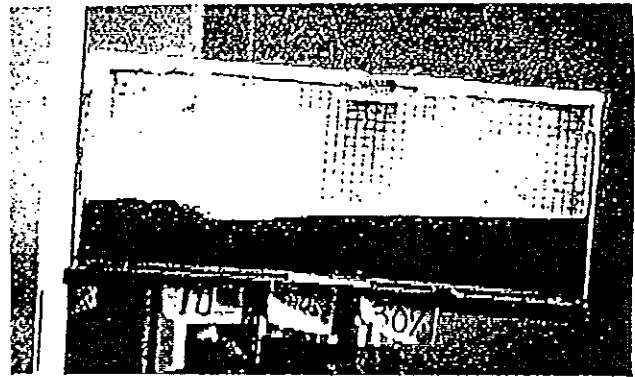
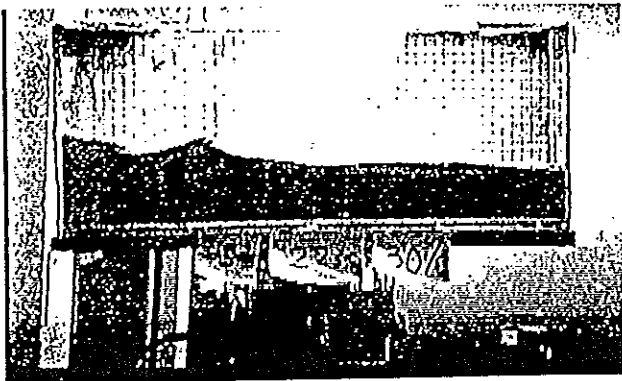


Fig.2(b) Type (b)

Fig.2(c) Type (c)

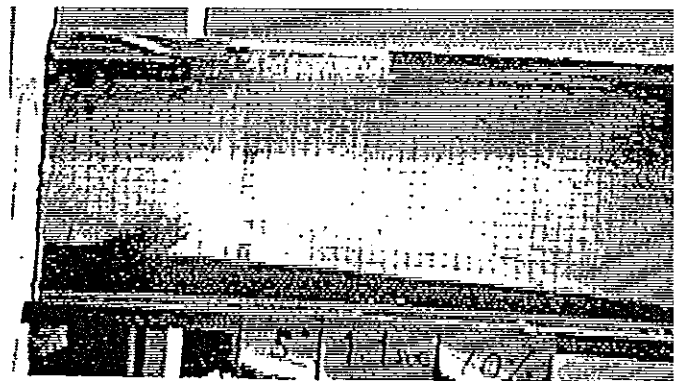
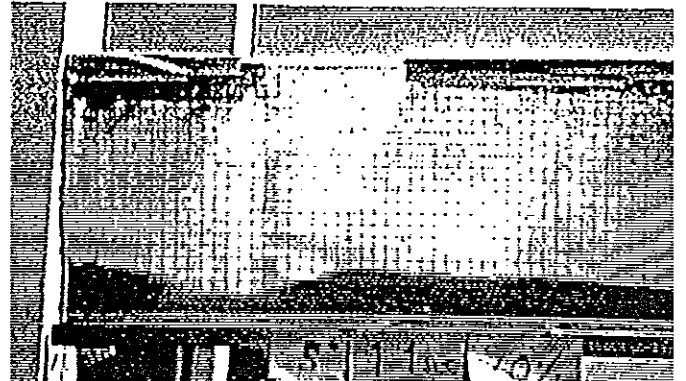
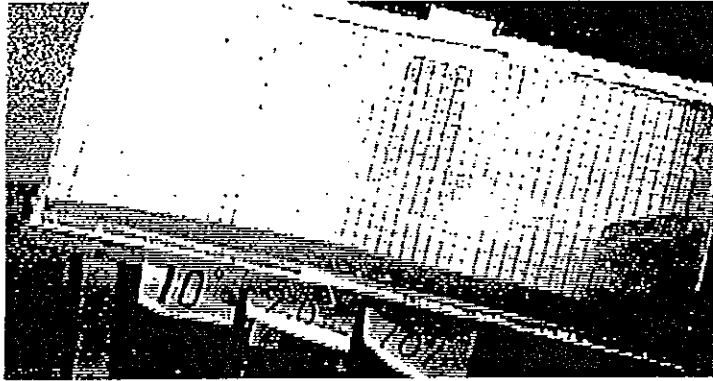
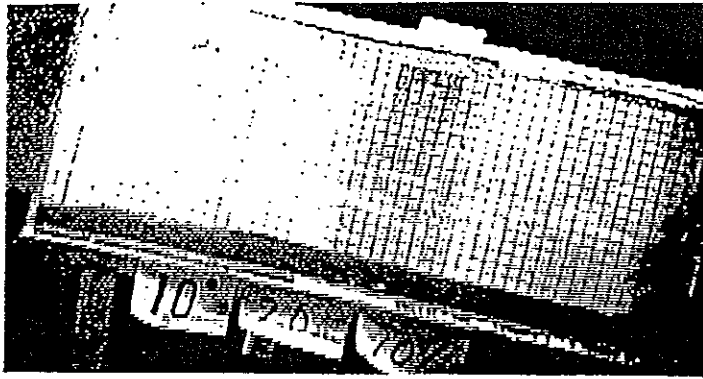


Fig.2(d) Type (d)

Fig.2(e) Type (e)

ω_0 : Natural Frequency

$$\omega_0 = 2\pi / T_0$$

$$\omega_{-11} = 2\pi / T_{-11}$$

$$\omega_{+11} = 2\pi / T_{+11}$$

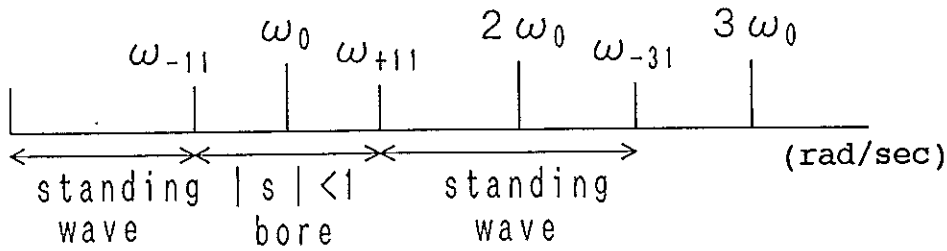


Fig.3 Frequency relation to wave patterns

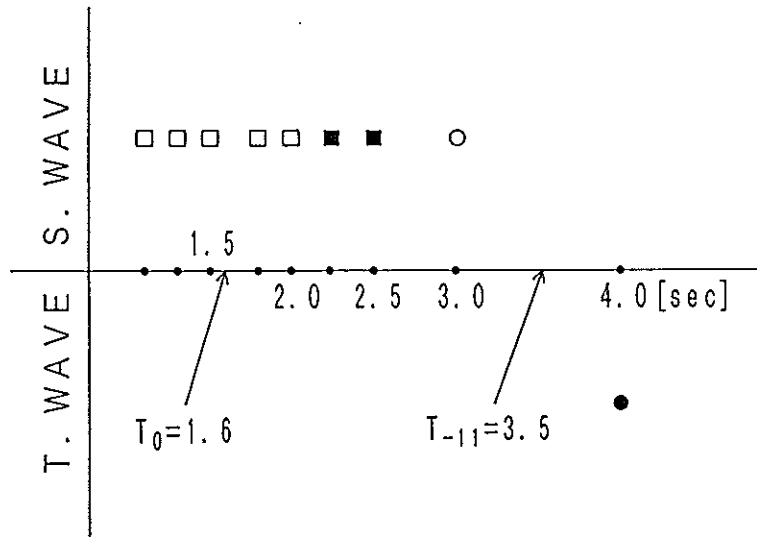


Fig.4(a) Wave patterns, $B=50\text{cm}$, $h=6\text{cm}$, $\phi=10^\circ$

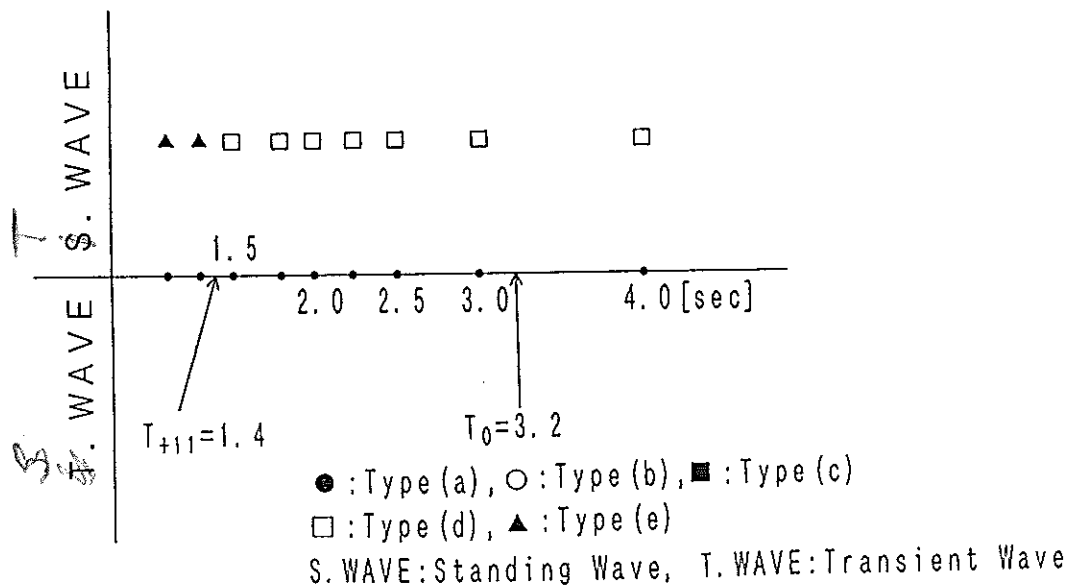


Fig.4(b) Wave patterns, $B=50\text{cm}$, $h=1\text{cm}$, $\phi=5^\circ$

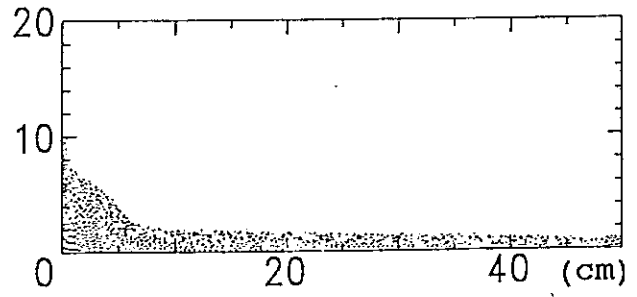
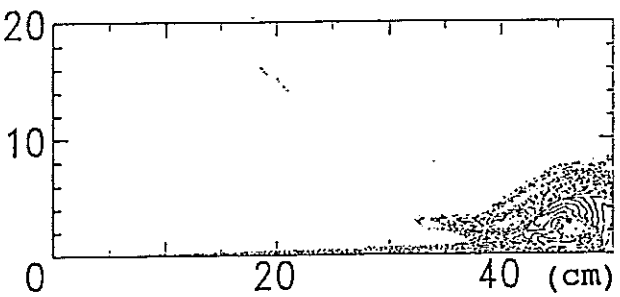
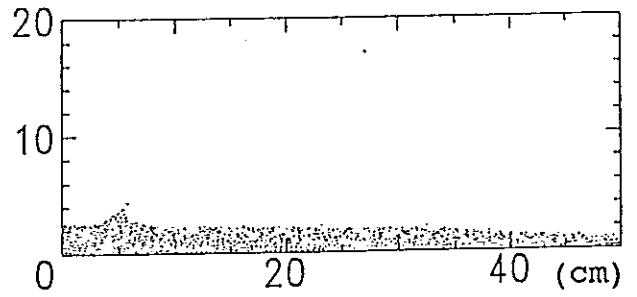
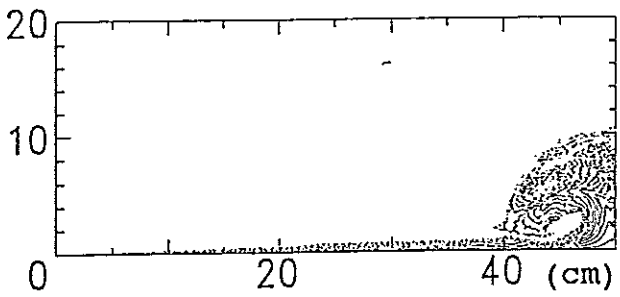
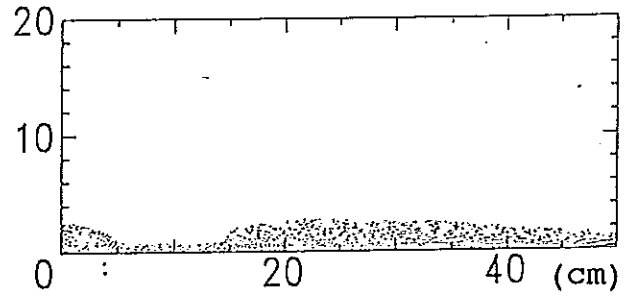
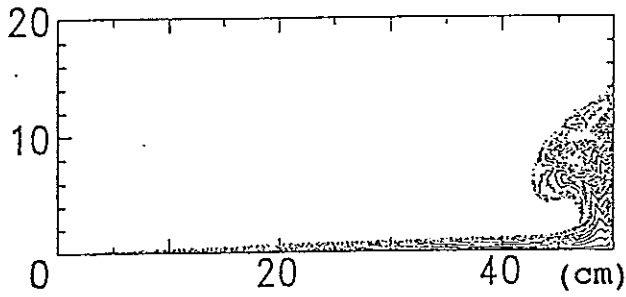
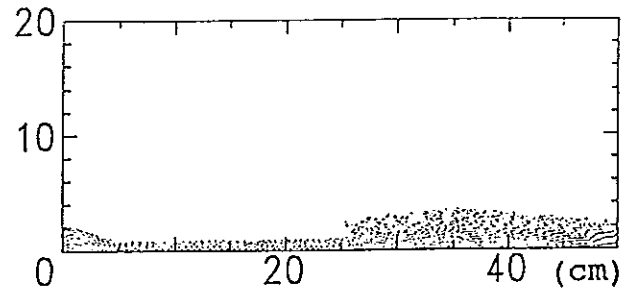
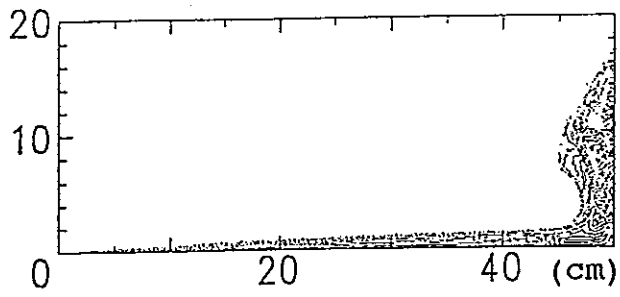


Fig.5 Numerical results, type (d) Fig.6 Numerical results, typ

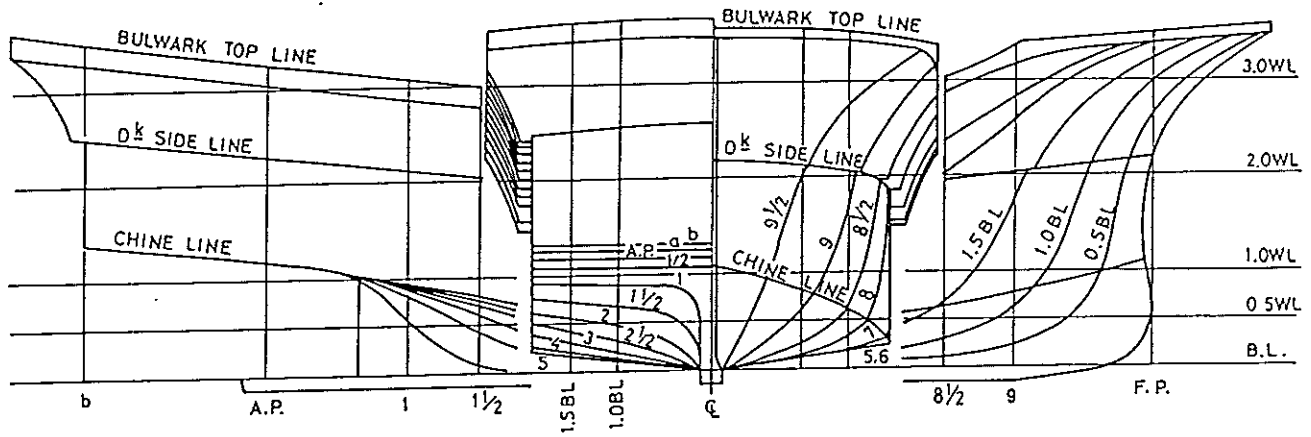


Fig. 7 Body plan

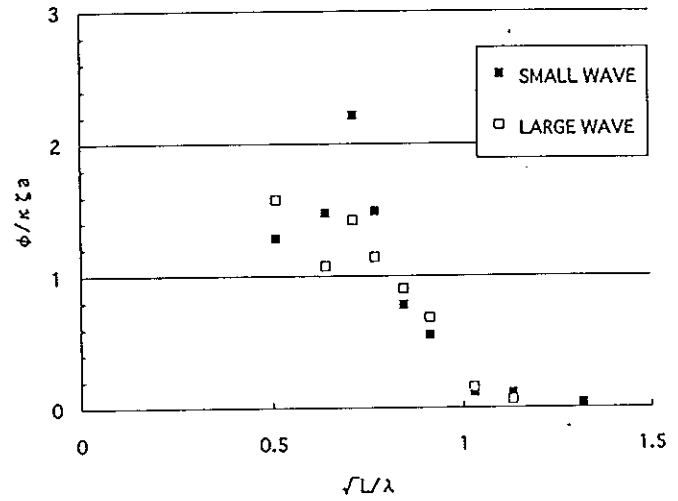
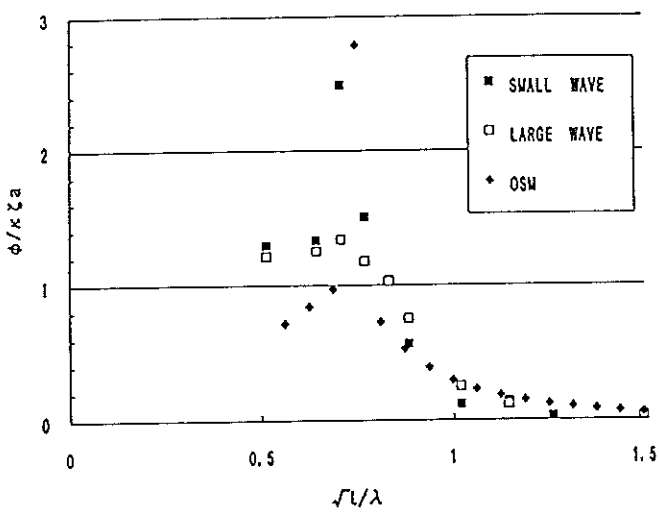


Fig. 8(a) Response characteristics of rolling motion, empty

Fig. 8(b) Response characteristics of rolling motion, water depth 1cm

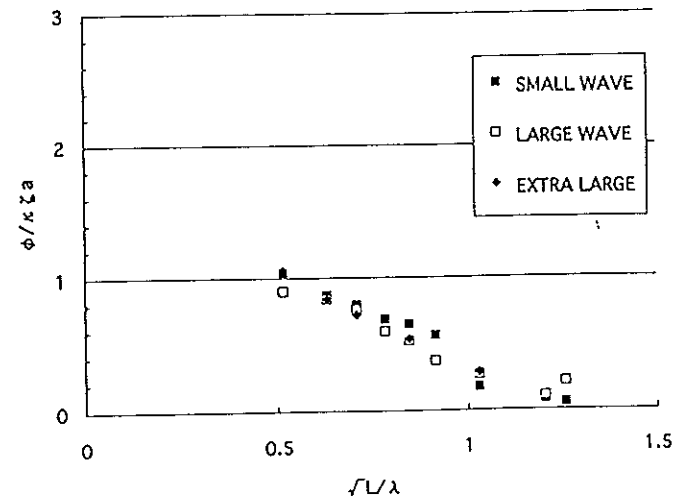
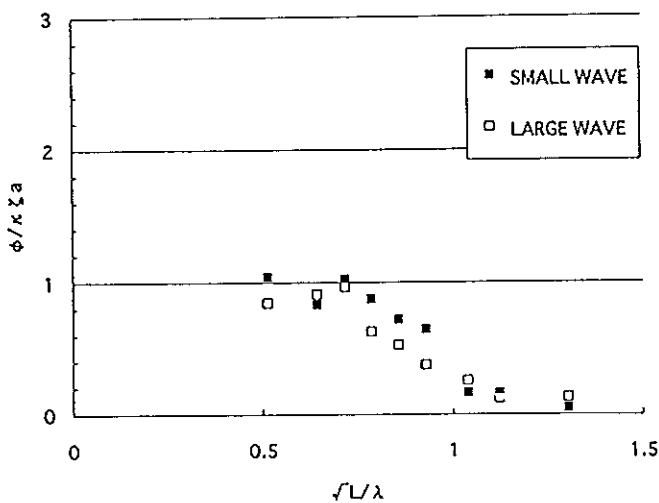


Fig. 8(c) Response characteristics of rolling motion, water depth 2cm

Fig. 8(d) Response characteristics of rolling motion, water depth 3cm

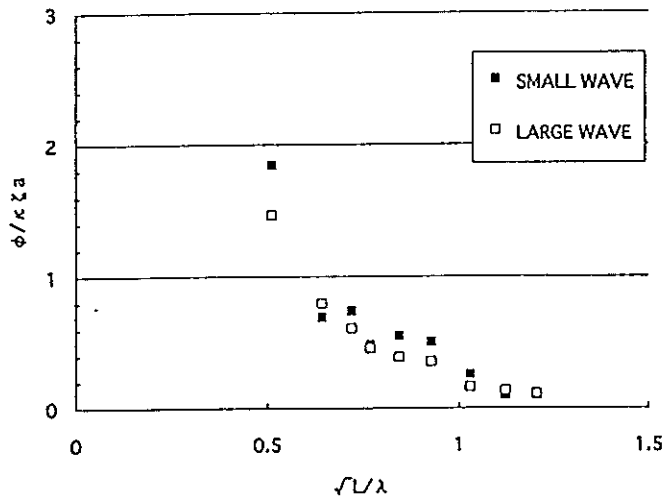


Fig. 8(e) Response characteristics of rolling motion, water depth 4cm

Wave Period = 1.8 [sec] Wave Height = 10.
 $\phi_0 = 15.3$ [deg]

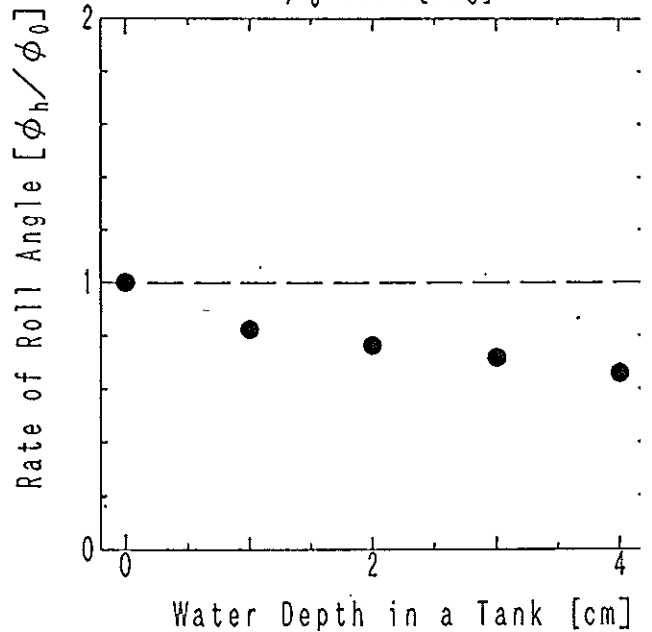


Fig. 9(a) Relationship between the damping rate of roll angle and water depth

Wave Period = 1.3 [sec] Wave Height = 6.0 [cm] $\phi_0 = 11.3$ [deg]
 Wave Period = 2.2 [sec] Wave Height = 8 $\phi_0 = 7.3$ [deg]

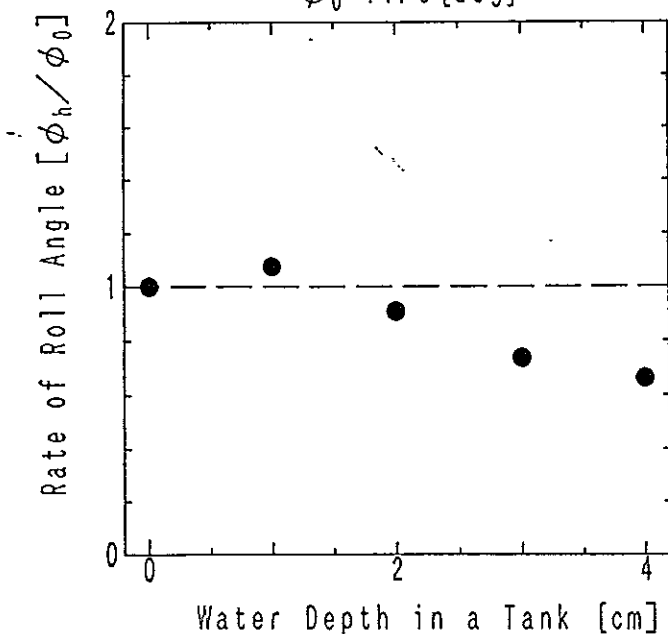


Fig. 9(b) Relationship between the damping rate of roll angle and water depth

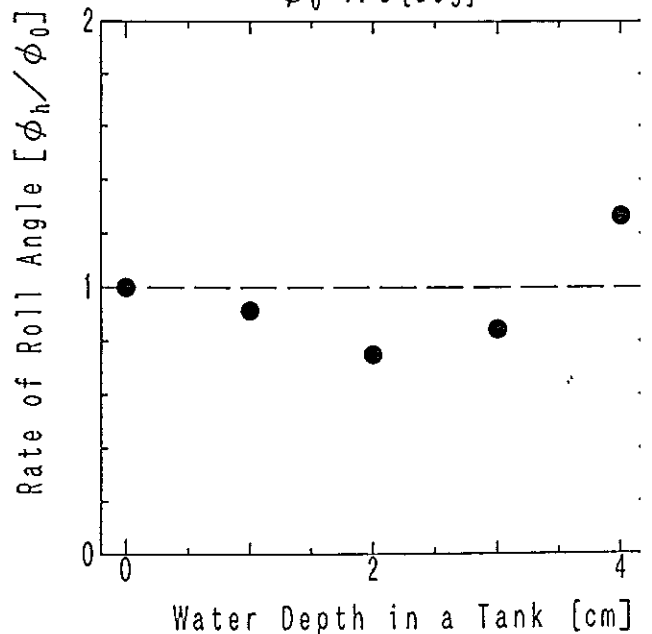


Fig. 9(c) Relationship between the damping rate of roll angle and water depth

SECRETARIAT STAB 94

GENERAL CHAIRMAN	W. A. Cleary, Jr - Adjunct Professor O/E
OCEAN ENGINEERING PROGRAM CHAIRMAN	Professor A. Zborowski, Ph.D.
CENTRAL BAPTIST CHURCH - AUDITORIUM	Dr. Gary Fagan, Pastor
SPECIAL EVENTS - AUXILIARY SERVICES	Ms. Barbara Towers
OFFICE SERVICES - DIRECTOR	Mr. William Hamilton
OFFICE SERVICES - PUBLISHING	Ms. Rosary M. Pedreira
GLEASON AUDITORIUM COORDINATOR	Mr. Gary Allen
OCEAN ENGINEERING STAFF	Ms. Janet Carey Ms. Ann Bergonzoni Ms. Juanita Fennimore Mr. Daryl Slocum
OCEAN ENGINEERING STUDENTS	Ms. Jennifer Clark Mr. Michael Callahan Mr. Damian Hite Mr. Joe Blodgett Mr. Alejandro Gutierrez Mr. Mathew Craven
SOCIETY OF NAVAL ARCHITECTS AND MARINE ENGINEERS FLORIDA TECH STUDENT SECTION	Ms. Allison Link

AND

THE FLORIDA TECH STUDENT SUPPORTING TEAM

STAB 94 COMMITTEES

INTERNATIONAL PROGRAMME

Prof. C. Kuo, University of Strathclyde, Glasgow
Prof. M. Fujino, University of Tokyo
Prof. L. Kobylinski, Tech. Univeristy of Gdansk, Poland
Prof. P. Cassella, University of Naples, Italy
Prof. P. Bogdanov, Ship Hydrodynamics Center, Varna, Bulgaria
Dr. S. Grochowalski, National Research Council, Ottawa, Canada
Prof. P. Blume, Hamburg Ship Model Basin, Germany
Prof. D. Huang, Dalian University, Dalian, China
H. Hormann, Head Marine Safety Germanischer Lloyd
H. Vermeer, Netherlands Shipping Directorate
I. Manum, Norwegian Maritime Directorate
Prof. C. Guedes Soares, Instituto Superior Tech Libson, Portugal
Dr. I. Boroday, Krilov Ship Research Inst., St. Petersburg, Russia
Dr. N. Rachmanin, Krilov Ship Research Institute, Russia
Dr. R. Ozkan, Istanbul, Turkey
Chairman - W. A. Cleary Jr., Florida Institute of Technology

COMMITTEE of the AMERICAS

Prof. B. Adee, University of Washington, Seattle, WA USA
Prof. R. Battacharyya, Annapolis, MD USA
H. P. Cojeen, USCG Headquarters, Washington, DC USA
Prof. R. G. La torre, University of New Orleans, LA USA
Dr. M. A. S. Neves, COOPE/UFRJ, Rio de Janiero, Brazil
Prof. J. R. Paulling Jr., Richmand, CA USA
Prof. N. Perez, University of Chile, Valdiva, Chile
Prof. G. L. Petrie, Webb Institute, New York, NY USA
Prof. C. Sanguinetti, University of Chile, Valdiva, Chile
R. J. Sonnenschein, MARAD, Washington, DC USA
Dr. C. Spadavecchia, Prefectura Navale, Burnos Aires, Argentina
Prof. M. Santarelli, Buenos Aires, Argenina
Dr. J. S. Spencer, ABS AMERICAS, Huston, Texas USA
Prof. R. Yagle, University of Michigan, Ann Arbor, Michigan USA